Therapeutic strategies to promote immune rejection of drug-resistant sub-populations in lung cancer

Mona Julia Tomaschko

Imperial College London
Department: Institute of Clinical Sciences

And

The Francis Crick Institute
PhD Supervisor: Prof. Julian Downward

A thesis submitted for the degree of
Doctor of Philosophy

September 2024

Statement of Originality

I Mona Tomaschko confirm that the work presented in this thesis is my own. Where information has been derived from other sources, I confirm that this has been indicated in the thesis.

Copyright Declaration

‘The copyright of this thesis rests with the author. Unless otherwise indicated, its contents are licensed under a Creative Commons Attribution-Non-Commercial 4.0 International Licence (CC BY-NC).

Under this licence, you may copy and redistribute the material in any medium or format. You may also create and distribute modified versions of the work. This is on the condition that: you credit the author and do not use it, or any derivative works, for a commercial purpose.

When reusing or sharing this work, ensure you make the licence terms clear to others by naming the licence and linking to the licence text. Where a work has been adapted, you should indicate that the work has been changed and describe those changes.

Please seek permission from the copyright holder for uses of this work that are not included in this licence or permitted under UK Copyright Law.’

Abstract

KRAS is the most frequently mutated oncogene in human cancer. Oncogenic KRAS signalling not only instigates aberrant growth in cancer cells but can further inhibit anti-tumour immunity. Hence, recently developed KRAS G12C inhibitors (G12Ci) hold the potential to reshape the treatment landscape for eligible cancer patients. However, rewiring of oncogenic signalling circuits and acquisition of further mutations can lead to rapid development of drug resistance. Indeed, clinical trials for G12Ci Sotorasib in non-small-cell lung cancer revealed a median progression-free survival of only ~7 months, with no overall survival advantage compared to conventional chemotherapy.

In this project, we investigate strategies to combat the development of drug resistance to G12Ci, by fostering an anti-tumour immune response, capable of recognising a pan-cancer-cell archetype and thereby also eliminating drug-resistant cells. First, a preclinical murine model to mimic progression of drug resistance was established by co-engrafting reporter-traced, isogenic G12C- and G12D-mutant lung cancer cells; the latter being inherently G12Ci-incompatible. G12Ci alone can already alleviate mutant-KRAS-driven immune suppression and induce immunogenic cell death in G12Ci-responsive cells. Surprisingly, in our model, employing G12Ci as monotherapy drove therapy resistance by giving the drug-resistant subpopulation a proliferative advantage, which was further investigated through RNA-sequencing.

Next, combination therapies, further supporting immunity through synergy, were investigated. Combining G12Ci with immunotherapy or a SHP2 inhibitor potentiated an adaptive immune response, capable of eliminating both, G12C- and G12D mutant cancer cells and further engendering immune-memory. Underlying mechanisms were investigated by immune-phenotyping of tumours across treatment groups, employing a 36-plex spectral flow cytometry panel. Additional spatial information was obtained through multiplex histopathology. This revealed profound TME remodelling in mice treated with combination therapies.

Here we show that G12Ci resistance could be counteracted though synergistic combinations that enhance immune response and target G12Ci-resistant cells, which could improve employment of therapy rationales.

Acknowledgement

First and foremost, I am very grateful to Professor Julian Downward for providing me with the amazing opportunity to carry out this intriguing research project in his group. His guidance, expertise, and encouragement have been invaluable in shaping my development as a researcher, allowing me to explore new ideas and to grow both professionally and personally.

I would also like to extend my heartfelt gratitude to Miriam, for her compassionate mentorship and unwavering support towards me as well as everyone in our group. I am thankful for our countless brainstorming sessions, your brilliant ideas, keen problem-solving skills, insightful feedback, and for all your patience and warm-hearted support over the last four years.

I would also like to thank all my colleagues and lab members for their kind help, and valuable advice. Our passionate discussions, laughs and friendships have made this PhD a truly inspiring and memorable time. I am especially grateful to Chris, for his mentorship and support with conducting in *vivo* studies, to Claire and Andrea, for their guidance and help with conducting large panel flow cytometric studies and their immunology expertise, to Sareena for all of her indispensable help and for teaching me how to conduct a wide range of experimental assays, to Dave for his abiding support with my myriad study plans, to Alicia for the flow cytometric experiment we ran together, to Sophie for developing a new cell line together, and to Sapta for her help with analysing our spatial tumour microenvironment data and for our many philosophical conversations. I would also like to extend my gratitude to the incredibly bright and kind-hearted students that have contributed to this project, Josephine, Aleks and Isabel, it was inspiring and impressive to see how talented and capable you are so early on in your career! I would further like to thank everyone who contributed to conducting the large-scale experiments in this study, which were only possible thanks to your expertise and amazing teamwork.

Further, I am deeply grateful to our core facilities at the Crick, the Biological Research Facility, Experimental Histopathology Department, Flow Cytometry Core, the High Throughput Screening Laboratory, the Advanced Light Microscopy Platform, Advanced Sequencing Facility, and the Bioinformatics and Biostatistics core (Babs) at the Crick. This project would not have been possible without all of your kind help, support and expertise. I am especially grateful to Dr. James Campbell from Babs for his kind mentorship, profound programming knowledge and for his patience during my work placement and beyond, enabling me to learn statistical analysis and data visualisation in R, which has not only become a valuable skill but also a newfound passion.

I am also thankful to my thesis committee, Dr. Ilaria Malanchi, Dr. Dinis Calado, and Professor Jesus Gil for their constructive suggestions and contributions which were instrumental in refining this study and pushed me to think critically at every step. I would further like to thank my viva examiners, Dr. Luigi Ombrato and Professor Michael Seckl, for your time reading this thesis and for your expertise.

Moreover, I appreciate our collaborators at Novartis and Revolution Medicines for providing the resources and a goal-oriented advice that facilitated the research of this project.

I am deeply grateful to my wonderful partner, KangBo. Not only has he been an incredible help in developing the spatial analysis pipeline for this project, but more importantly, I am profoundly thankful that we have been able to share our entire PhD journey side by side, from day one to the finish line, and for all the adventures that lie ahead. Finally, I would also like to thank my family who have always supported my education and my friends for all of their love and support, I feel truly fortunate for being able to have you in my life.

Table of Contents

Abstract **4**
Acknowledgement **6**
Table of Contents **8**
Table of figures **10**
List of tables **13**
Abbreviations **14**
Chapter 1.Introduction **19**
1.1 An introduction to lung cancer **20**
1.2 Standard of care for NSCLC **21**
1.3 Oncogenic KRAS signalling in NSCLC **23**
1.4 Anti-tumour immune surveillance **27**
1.4.1 Introduction to immune surveillance in solid tumours 27
1.4.2 The arsenal of immunocytes and their role in combatting cancer 28
1.5 Immune evasion in cancer **40**
1.5.1 Immune escape as a hallmark of cancer 40
1.5.2 Oncogenic KRAS mediated immune escape 43
1.6 KRAS inhibitors **47**
1.6.1 The development of KRAS inhibitors 47
1.6.2 Inhibition of oncogenic KRAS signalling can alleviate immune suppression in the TME 50
1.6.3 KRAS G12C inhibitors in the clinic 52
1.7 KRAS G12C inhibition can lead to development of drug resistance **54**
1.8 Overcoming resistance development to KRAS G12C inhibitors **57**
1.9 Project rationale **62**
Chapter 2.Materials & Methods **65**
2.1 Cloning strategy for reporter-encoding plasmids **65**
2.2 Cell culture **68**
2.3 Generation of reporter-traced lines **68**
2.4 In *vitro* assays for screening KPAR1.3 subclones **69**
2.4.1 Viability assays 69
2.4.2 Growth-rate assays 69
2.4.3 In vitro luciferase assays 69
2.5 Time course assays **70**
2.5.1 Western blots 70
2.5.2 qRT-PCRs 71
2.6 In *vivo* techniques **72**
2.7 Bulk-RNA sequencing **74**
2.8 Flow cytometric techniques **75**
2.8.1 Assessing reporter stability of KPAR1.3 subclones in *vitro* 75
2.8.2 Quantifying fraction of KPAR1.3 KRAS G12D cells in *vivo* 76
2.8.3 Multiplex spectral immune phenotyping of therapy-treated tumours 76
2.9 General immunohistochemistry techniques **79**
2.9.1 Immunohistochemistry on frozen tumour sections 79
2.9.2 Immunohistochemistry on FFPE tumour sections 80

Chapter 3.Establishing a model system mimicking the development of drug resistance 83
3.1 Generating reporter-traced cell lines 84
***3.2* Characterising reporter-traced cell lines in *vitro* 88**
***3.3* Characterising reporter-traced cell lines in *vivo* 91**
Chapter 4.Assessing therapy efficacy in combatting drug-resistant tumour sub-populations 94
4.1 Monotherapy with G12Ci Adagrasib accelerates expansion of drug-resistant cancer cells 94
4.2 Assessing efficacy of additional therapy lines as monotherapies ... 98
4.3 Combination therapies can promote immune-rejection of drug-resistant subpopulations 101
4.4 Testing treatment response in subcutaneous model with an alternative KRAS G12Ci-resistant subpopulation 114
Chapter 5.Investigating therapy effects on tumour cell compartment 126
5.1 Investigating cell state of KRASi-resistant tumour cells across treatment groups 126
5.2 bRNA-seq of the entire tumour cell compartment across treatment groups 144
5.3 Investigating cancer cell-intrinsic effects of oncogenic pathway inhibition 159
Chapter 6.Investigating therapy-induced alterations in TME immune cell composition and architecture 167
6.1 Investigating the contribution of the adaptive anti-tumour immunity in elimination of KRASi-resistant sub-populations 168
6.2 Immune phenotyping of the TME and tdLNS 178
6.3 Spatial analysis of the tumour microenvironment 197
Chapter 7.Discussion 209
7.1 A rationale for the investigation of therapy combinations 209
7.2 Therapy-induced alterations in the tumour cell compartment 216
7.3 Contribution of anti-tumour immunity to achieve durable therapy responses 219
7.4 Concluding remarks 230
Reference List 233

Table of figures

Figure 1.1 KRAS signalling. 24
Figure 1.2 Mutation-induced functional impairments of KRAS proteins. 26
Figure 1.3 Anti-tumour immunity. 29
Figure 1.4 Priming of an adaptive anti-tumour immune response. 33
Figure 1.5 Oncogenic KRAS signalling induced immune suppression. 43
Figure 1.6 Schematic of project rationale. 64
Figure 3.1 Generation of reporter-transduced KPAR1.3 cell lines. 87
Figure 3.2 Reporter stability under stress conditions. 89
Figure 3.3 Characterising reporter-traced KPAR1.3 subclones in *vitro*. 90
Figure 3.4 Co-culture assay assessing Adagrasib response over time. 91
Figure 3.5 Assessing growth dynamics of co-engrafted subclones in *vivo*. 93
Figure 4.1 Adagrasib treatment of tumours containing a KRAS G12Ci-resistant sub-population. 97
Figure 4.2 Efficacy of KRASi, a-PD-1, and SHP2i as monotherapy 100
Figure 4.3 Assessing synergistic treatment effects of therapy combinations. 103
Figure 4.4 Additional readouts of dual combination treatments. 106
Figure 4.5 Investigating extended combination treatment regimes. 108
Figure 4.6 Additional readouts of extended combination treatments. 110
Figure 4.7 Investigating treatment-related hepatotoxicity. 112
Figure 4.8 Investigating synergy of SHP2i and a-PD-1 treatment combination. 113
Figure 4.9 Dependency of immune memory on reporter constructs. 114
Figure 4.10 Treatment scheme of generating Adagrasib-resistant tumours. 116
Figure 4.11 Assessing drug response of KPAR1.3 G12C^{res} cell lines. 117
Figure 4.12 Resistance mechanisms in sub-clones of KPAR1.3 G12C^{res} cell line 2. 119
Figure 4.13 Therapy resistance of lines KPAR1.3 G12C$^{res2.1}$ and - G12C$^{res2.2}$ in *vivo*. 121
Figure 4.14 Assessing therapy cross resistance of KPAR1.3 G12C$^{res2.2}$ line. 122

Figure 4.15 KPAR1.3 G12C$^{res2.2}$ line as alternative KRASi-resistant sub-population. 124
Figure 5.1 Schematic of sample acquisition for bRNA-seq. 129
Figure 5.2 Schematic of nf-core pipeline. 130
Figure 5.3 Read count normalisation. 131
Figure 5.4 Dispersion estimates for each gene across samples. 133
Figure 5.5 Principal component analysis of sample distribution. 134
Figure 5.6 Pair-wise gene expression dispersion 135
Figure 5.7 Differential gene expression between treatment groups. 137
Figure 5.8 Abundance of significantly differentially regulated genes between indicated treatment groups. 137
Figure 5.9 Differential gene expression in KRASi- and vehicle samples. 138
Figure 5.10 GSEA of KRASi-treated compared to vehicle samples. 140
Figure 5.11 GSEA of primary treatment effects. 142
Figure 5.12 GSEA of secondary treatment effects. 143
Figure 5.13 Schematic of sample acquisition for bRNA-seq. 145
Figure 5.14 Flow cytometric gating for tumour cell sort 146
Figure 5.15 Read Count normalisation 147
Figure 5.16 Dispersion estimates for each gene across samples. 148
Figure 5.17 Principal component analysis of dataset. 151
Figure 5.18 Differential gene expression between sample groups. 152
Figure 5.19 Individual gene expression by treatment group. 154
Figure 5.20 GSEA of primary treatment effects across genotypes. 156
Figure 5.21 GSEA for secondary treatment effects 157
Figure 5.22 Heatmap of leading-edge genes for E2F gene set KRASi vs vehicle. 158
Figure 5.23 Viability assays of KRAS G12C- and G12D mutant cancer cells. 160
Figure 5.24 Western blots of SHP2i time course assays. 162
Figure 5.25 qPCR analysis of SHP2i time course assays on KRAS signalling transcriptional targets. 163
Figure 5.26 qPCR analysis of SHP2i time course assays on inflammation-associated transcriptional targets. 165

Figure 6.1 Assessing therapy effects in Rag1$^{-/-}$ GH-mice. 170
Figure 6.2 Selective depletion of immune cell populations. 172
Figure 6.3 Immunohistochemical staining of B cells. 174
Figure 6.4 Cancer cell-specific abs in serum from experimental mice. 176
Figure 6.5 Testing for Emv2 specificity in serum antibodies. 177
Figure 6.6 Experimental workflow for immune phenotyping..... 180
Figure 6.7 Overview of cancer cell and immunocyte proportions..... 181
Figure 6.8 Immune sub-type classification by treatment group. 182
Figure 6.9 Proportions of T cell populations by treatment groups. 184
Figure 6.10 Activation status of T cell subpopulations. 186
Figure 6.11 Analysis of non-T cell lymphocytes 187
Figure 6.12 Analysis of tumour-infiltrating macrophage compartment. 189
Figure 6.13 Analysis of tumour-infiltrating dendritic cells. 191
Figure 6.14 Analysis of T cell compartment in tdLNs. 193
Figure 6.15 Analysis of B cell compartment in tdLNs. 194
Figure 6.16 Analysis of GFP^{+} immunocytes in the TME. 196
Figure 6.17 Overview of multiplex EHP workflow..... 198
Figure 6.18 Overview of T cell staining on whole tumour sections. 200
Figure 6.19 High resolution ROIs of T cell infiltration across treatment groups. 201
Figure 6.20 Exemplary images for tumour infiltrating Tregs..... 202
Figure 6.21 Tumour cell populations across treatment groups. 203
Figure 6.22 Exemplary ROI of a proliferating KPAR1.3 KRAS G12D cluster. 204
Figure 6.23 Visualisation of necrotic tumour cores. 205
Figure 6.24 Outline of image analysis pipeline..... 207
Figure 7.1 Combination therapies remodel TME and stimulate anti-tumour immunity. 232

List of tables

Table 2.1 Oligos for site directed mutagenesis. 65
Table 2.2 PCR conditions rolling cycle amplification. 66
Table 2.3 Barcode sequences 66
Table 2.4 Linker oligonucleotide sequences. 67
Table 2.5 Sequencing primers confirming nucleotide substitution. 67
Table 2.6 Western blot antibodies. 71
Table 2.7 qRT-PCR primers. 72
Table 2.8 Drugs employed for in *vivo* therapies. 73
Table 2.9 Spectral flow staining panel 78
Table 2.10 Primary antibodies for staining frozen sections. 80
Table 2.11 Primary antibodies used for IF stainings on FFPE tumour sections. 82
Table 3.1 Predicted MHC-I binding affinities. 88

Abbreviations

Abbreviation	Meaning
AA	Amino acid
Ab	Antibody
ADCC	Antibody-dependent cell-mediated cytotoxicity
ALK	Anaplastic lymphoma kinase
ann	Artificial neural network
APC	Antigen presenting cells
APOBEC	Apolipoprotein B mRNA editing enzyme, catalytic polypeptide-like
bRNA-seq	Bulk RNA sequencing
cDC	Conventional dendritic cell
cDC1	Conventional dendritic cell type 1
cDC2	Conventional dendritic cell type 2
COX2	Cyclooxygenase-2
CPB	Check-point blockers
CPI	Check-point inhibitors
CR	Complete responder
CSFR	Colony stimulating factor receptor
CT	Computerised tomography
ctDNA	Circulating tumour DNA
cTL	Cytotoxic T lymphocytes
DAB	3,3′-Diaminobenzidine
DAMPs	Danger-associated molecular patterns
DCs	Dendritic cells
DGK	Diacylglycerol kinase
DMEM	Dulbecco’s Modified Eagle Medium
DMSO	Dimethyl sulfoxide
eBFP	Enhanced blue fluorescent protein
ECM	Extracellular matrix
eGFP	Enhanced green fluorescent protein
EGFR	Epidermal growth factor receptor
EHP	Experimental Histopathology
EMT	Epithelial to mesenchymal transition

ERVEGP	Endogenous retroviral envelope glycoproteins
FACS	Fluorescence-activated cell sorting
FBS	Fetal bovine serum
FC	Fragment crystallisable
fDCs	Follicular dendritic cells
FFPE	Formalin-Fixed Paraffin-Embedded
FGFR	Fibroblast growth factor receptor
FP	Fluorescent protein
GAPs	GTPase activating proteins
GDP	Guanosine diphosphate
GEF	Guanosine exchange factor
GH	Glowing-head
GRB2	Growth Factor Receptor Bound Protein 2
GSEA	Gene set enrichment analysis
GTP	Guanosine triphosphate
H&E	Haematoxylin and Eosin
HGF receptor	Hepatocyte growth factor receptor
HRP	Horse radish peroxidase
hTL	Helper T lymphocytes
hTL	Helper T lymphocytes
ICB	Immune checkpoint blocker
ICI	Immune checkpoint inhibitors
IEDB	Immune Epitope Data Base
IFN-γ	Interferon gamma
Ig	Immunoglobulin
IL	Interleukin
log2FC	Log 2 Fold Change
IMC	Imaging mass cytometry
iNOS	Nitric oxide synthase
IRF	Interferon-regulatory factors
ISC	Immune suppressive cytokine
IVIS	In vivo imaging system
k.o.	Knock out

KPAR	**K**RAS G12D expression; Tr**p**53 deletion; **A**POBEC expression; **R**ag1 k.o. mouse strain-derived cell line
KRAS	Kirsten rat sarcoma viral oncogene homolog or Kirsten rat sarcoma virus
KRAS G12C(OFF)i	Inactive-state KRAS G12C inhibitors
KRAS G12C(ON)i	Active-state KRAS G12C inhibitors
KRASi	KRAS inhibition/ -inhibitor
LC	Lung cancer
Luc	Luciferase
M1	M1-polarised macrophages
M2	M2-polarised macrophages
MAPK	Mitogen-activated protein kinase
MDSC	Monocyte derived suppressor cell
MFI	Median fluorescence intensity
MHC-I	Major-histocompatibility complex class 1 molecules
MHC-II	Major-histocompatibility complex class 2 molecules
MPs	Macrophages
MRI	Magnetic resonance imaging
N1	Neutrophil type 1
N2	Neutrophil type 2
NBF	Neutral buffered formalin
NETs	Neutrophil extracellular traps
NF-κB	Nuclear factor kappa-light-chain-enhancer of activated B cells
NK	Natural killer cells
NOX2	NADPH oxidase 2
NP	Neutrophil
NSCLC	Non-small cell lung cancer
P/S	Penicillin/Streptomycin
padj	Adjusted p value
PAMPS	Pathogen-associated molecular patterns
PBS	Phosphate-buffered saline

PBS-T	PBS containing 0.05% Tween
PCA	Principal component analysis
PCR	Polymerase chain reaction
PD-1	Programmed cell death protein 1
PD-L1	Programmed death-ligand 1
pDC	Plasmacytoid dendritic cells
pDCs	Plasmacytoid Dendritic cells
PET	Positron emission tomography
PIK3	Phosphoinositide 3-kinases
PRRs	Pattern recognition receptors
qPCR	Quantitative Reverse Transcription PCR
Rag1	Recombination activating gene 1
RNA-seq	RNA sequencing
ROS	Reactive oxygen species
RTK	Receptor tyrosine kinase
SCLC	Small cell lung cancer
SHP2	Src homology-2 domain-containing protein tyrosine phosphatase-2
SHP2i	SHP2 inhibition/ -inhibitor
SIRP1α	Signal regulatory protein 1α
SOS1	SOS Ras/Rac guanine nucleotide exchange factor 1
Tcm	Central memory T cells
TCR	T cell receptor
tdLN	Tumour-draining lymph nodes
tdLNs	Tumour-draining lymph nodes
Tem	Effector memory T cells
Tfh	Follicular helper T cells
Th	T helper cells
TILs	Tumour-infiltrating lymphocytes
TME	Tumour microenvironment
TNFα	Tumour necrosis factor alpha
tr	Technical replicate
Tregs	Regulatory T cells
Trm	Resident memory T cells
Tscm	Stem cell memory T cells
TSG	Tumour suppressor gene

VEGF	Vascular Endothelial Growth Factor

Chapter 1. Introduction

“An honest man, armed with all the knowledge available to us now, could only state that, in some sense, the origin of life appears at the moment to be almost a miracle, so many are the conditions which would have to be satisfied to get it going."

- Francis Crick (1916-2004)

It is truly fascinating how numerous redundancies and safeguards embedded within our cells, in tandem with heedful surveillance by the immune system can prevent unhealthy cells from propagating and developing into malignancies. This sophisticated feat of nature enables humans to reach an amazingly old age, some of us turning 90- or even 100 years old. Tremendous scientific strides and innovations over the last decades have further turned the emergence of cancer from an inviolably fatal malady into a condition with a potential for cure and defiance. Allowing myriad patients a chance of prolonged- and increased quality of life.

Nonetheless, cancer remains the second leading causes of death worldwide with cases on the rise [1-3]. Cancer describes a group of diseases which are characterised by uncontrolled growth- and often spread of aberrant cells, which can eventually lead to the interference of the bodies’ physiological life-sustaining functions. Contracting cancer is statistically associated with an increase in age, which may coincide with an increase in overall life expectancy, indicative of improved control of other causes of death. However, ascended exposure to man-made, potentially carcinogenic compounds, changes in life-style, diet, and other factors could also contribute to this trend.

Because cancer is a vastly complex and ever evolving disease, understanding how cancer cells go awry and how to effectively innovate durable therapy regimes with a curative intent remains imperative.

1.1 An introduction to lung cancer

Lung cancer (LC) is the most commonly diagnosed cancer worldwide with approximately 2.5 million cases in 2022[4]. LC also ranks highest in mortality, with an estimated 1.8 million recorded deaths in the same year[4]. In the USA, lung and bronchus related cancers cause over 100,000 deaths annually, with the death toll being twice that of the next three deadliest cancers, colorectal, breast and prostate cancers taken together[5,6]. Further, the 5-year survival rate of LC patients remains low compared to other cancer types. In the United States of America, the 5-year survival prospects for LC patients is estimated to be only 19% [7]. Although a small increase in 2-year survival of 1.4% annually has recently been observed in patient records with an overall increase of 1.4% annualy[8]. This was mostly attributed to improvement in treatments, wider treatment accessibility as well as an earlier diagnosis on average. In the United Kingdom, the 5-year-survival rate has shown only moderate improvement over the last decades, with an estimated 15% in 2019, compared to 4% in men and 5% in women in 1971-1972[9], according to the CRUK website and the office for national statistics. The most common risk factor to developing LC is smoking of tobacco. However, other contributors such as exposure to asbestos, arsenic, coal smoke, radiation and air pollution, especially particulate matter PM2.5 were also identified [10,11,12,13].

LCs are commonly stratified by their histopathological appearance. The two broader categories being small cell lung cancer (SCLC) and non-small cell lung cancer (NSCLC)[14-16]. SCLC arises from the neuro-endocrine compartment of the lung, is commonly caused by smoking, and makes up approximately 15% - 20% of all diagnosed cases. Non-small cell lung cancer (NSCLC) makes up 80% - 85% of all cases and can be further categorised in subtypes[14]. The main NSCLC subtype is adenocarcinoma, which arises from the epithelial cell compartment in the lung. Followed by squamous cell cancer, large cell carcinoma and other subtypes, such as adenosquamous carcinoma and sarcomatoid carcinoma[13,15,17].

1.2 Standard of care for NSCLC

In addition to the histopathological classification, there are several factors which can contribute to LC patient stratification and disease outcome. Firstly, disease stage has to be taken into account, including tumour size, whether the cancer is contained locally or has metastasised to draining lymph nodes, secondary sites within the lung or other organs. Common distant metastatic sites include the liver, bone marrow, nervous system and adrenal glands[18]. Other factors include the patients age, symptoms, medical history and overall stage of health. Importantly, the driver mutations underlying the disease can play a key role in both, the disease progression and assignment of treatment regimes. Patients diagnosis and disease stage can be assessed through scanning techniques, such as magnetic resonance imaging (MRI)-, computerised tomography (CT)-, or positron emission tomography (PET) -scans, as well as analysing fluid and biopsy samples[16]. Current treatment options for lung cancer patients are often unable to cure the disease. As early disease stages are largely asymptomatic, patients are often diagnosed late, when surgical resection with curative intent is no longer feasible[16]. The standard of care treatment for NSCLC include chemo- or radiation therapy, as well as laser- or photodynamic therapy and electrocautery as well as surgical removal of malignancies if possible[19]. Depending on the disease prognosis and mutational burden, standard of care can also include the prescription of immune- or targeted treatments[19].

A frequent method of immunotherapy in NSCLC is the administration of therapeutic antibodies, such as immune checkpoint blockers (ICB)[20]. Nivolumab being the first ICB approved for NSCLC treatment, followed by Atezolizumab, Pembrolizumab, and Durvalumab[21]. These antibodies can potentiate an anti-tumour immune response, which will be described in more detail in the following sections. A subgroup of NSCLC patients responds well to this treatment with durable treatment responses[21,22]. However, the majority of patients do not respond to ICB, whereat therapy response remains difficult to predict[23].

Targeted therapies usually exploit selective vulnerabilities of cancer cells by inhibiting specific proteins that are essential to cancer cell proliferation and survival[24-26]. Potent targeted inhibitors may target the wild type version of such proteins. One disamenity with such inhibitors is that the therapeutic window, in which the given dose is effective in killing the cancer cells without causing severe side effects, can be difficult to delineate. This is because these proteins usually also play an essential role in the maintenance of other, healthy tissue types. A second group of targeted inhibitors can specifically target the mutant version of a protein in cancer cells, thereby potentially decreasing side effects. For NSCLC, approved targeted therapies include EGFR inhibitors, ALK inhibitors, and, more recently, KRAS G12C inhibitors [27-31]. A potential caveat in the unfunctional nature of employing these drugs is that cancer patients often develop drug resistance and stop responding to therapy within months[25,32,33].

1.3 Oncogenic KRAS signalling in NSCLC

"The notion that genetic changes are important in the genesis of cancer has met strenuous resistance over the years. But now that notion has gained ascendancy."

- J. Michael Bishop

Mutations in the Kirsten rat sarcoma viral oncogene homolog or Kirsten rat sarcoma virus (KRAS) protein are found in approximately 19% of all cancer patients with 3.4 million new annual cases. It is the most frequently mutated oncogene in human cancer[34,35]. KRAS driver mutations occur most commonly in lung (~30%), colorectal (~40-50%) and pancreatic cancers (~80-90%)[36,37].

There are three isoforms of RAS proteins, encoded by KRAS, HRAS, and NRAS genes, their functions varying depending on species, cell type and physiological conditions. In the context of oncology, they are commonly involved in activating signalling pathways associated with proliferation and survival[38] (**Figure 1.1**). Here, RAS proteins act as binary switches, cycling between a guanosine diphosphate (GDP)-bound inactive- and guanosine triphosphate (GTP)-bound active state. The binding of GTP nucleoside leads to a conformational change in two regions in the RAS protein, referred to Switch-I and Switch II, which in turn enables binding of effector proteins[39].

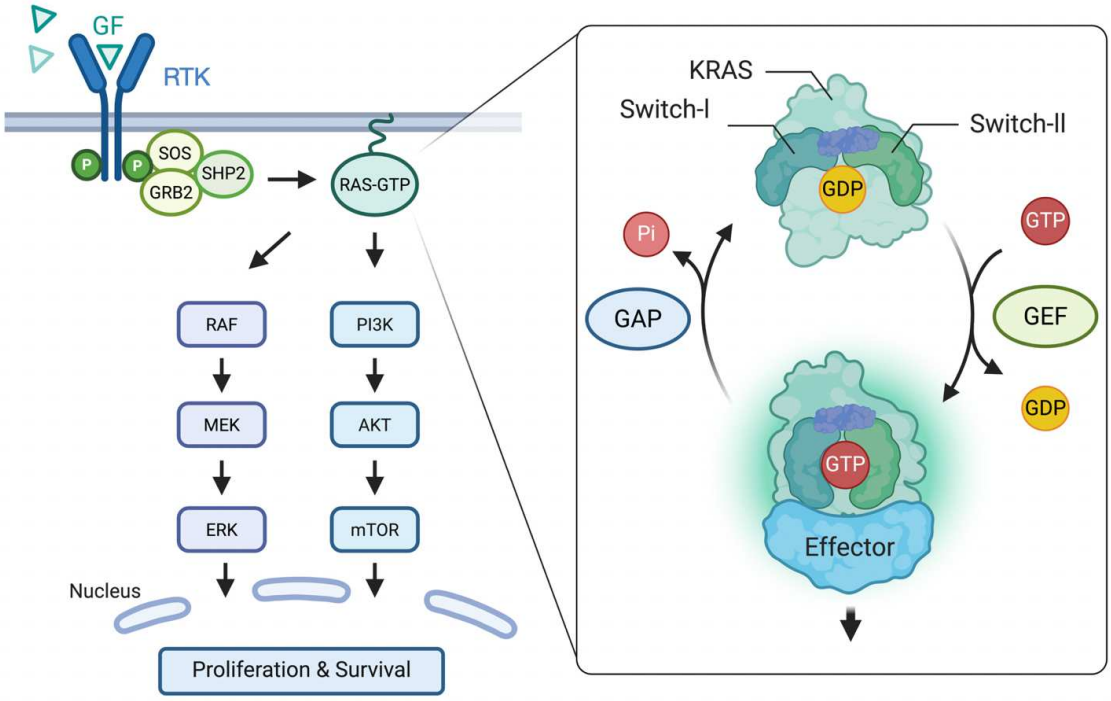


Figure 1.1 KRAS signalling. Extracellular growth factors (GF) bind to receptor tyrosine kinases (RTKs). Receptor activation leads to annealing of scaffold protein complex, including SOS, GRB2, and SHP2, which, in turn induces KRAS activation. This is achieved by exchanging GDP with a GTP nucleoside which, in turn, leads to a conformational change in the switch-I and switch-II domains, allowing for binding of effector proteins. On the other side, GAP-catalysed hydrolytic cleavage of the third phosphate group in GTP reverses KRAS activation. GTP-bound KRAS further activates cytosolic signalling cascades such as RAF/MEK/ERK MAP kinase pathway or PI3K/AKT/mTOR pathway (other downstream pathways not shown here). This transduce signals to nucleus where respective transcription programmes are activated. Image created with BioRender.

In healthy cells, the role of Ras proteins is to transduce external growth- and survival stimuli to the cell interior, activating respective signalling cascades and downstream transcriptional programmes in a precisely controlled manner[40-42]. Ras proteins are commonly localised on the cytosolic side of the plasma membrane, anchored to microdomains of the lipid bilayer through a C-terminal farnesyl tail[43,44]. Ras signalling is activated when growth factors bind to plasma membrane-resident receptor tyrosine kinase (RTK) receptors, such as epidermal growth factor receptor (EGFR). Ligand binding leads to dimerization of the receptors and consequent trans-autophosphorylation of their cytosolic domains. Scaffold proteins such as Growth Factor Receptor Bound Protein 2 (GRB2) and Src homology-2 domain-containing protein tyrosine phosphatase-2 (SHP2) can bind to these phosphorylated sites and, in turn, bind SOS Ras/Rac

guanine nucleotide exchange factor 1 (SOS1), which functions as a guanosine exchange factor (GEF). GEFs can catalyse the exchange of GDP to GTP in membrane resident Ras proteins, thereby aiding their activation[38]. Subsequently, Ras proteins, can activate various downstream signalling cascades. In the context of cancer, the mitogen-activated protein kinase (MAPK) pathway and Phosphoinositide 3-kinases (PIK3) pathway, including Akt and mTOR are widely studied [45]. Respective signals are finally transduced to the nucleus where transcriptional programmes associated with proliferation and survival are activated. Depending on context and cell type, a wide range of processes, spanning metabolism, autophagy, migration, calcium signalling and (de-) differentiation can also be RAS-mediated[46-48].

However, duration and intensity of RAS signalling are, in addition to other negative feedback circuits [49-52], precisely controlled through GTPase activating proteins (GAPs). These catalyse RAS-intrinsic GTPase function, leading to the hydrolytic cleavage of GTP back to GDP. The protein intrinsic GTPase function is relatively slow, with a $t_{1/2}$ of approximately 16 min [53]. However in the presence of GAP proteins, this reaction can be accelerated up to 100,000 fold, depending on GAP concentration and other conditions[54]. Bringing the half-life of active-state KRAS down to seconds or even milliseconds before being switched off and requiring upstream re-activation.

The most common activating mutations in KRAS are found in the amino acids G12, G13, and Q61 and are associated with either impaired GAP-binding, disruption of GTP hydrolysis, or enhanced nucleoside exchange[35,53,55-58]. The five common mutations found in codon 12 result in the original glycine being mutated to KRAS G12C, G12D, G12R, G12S, or G12V[34]. Differences in mutation type can lead to different KRAS activation patterns (**Figure 1.2**) [53,55,59]. For example, G12C mutant KRAS was shown to retain intrinsic GTPase activity, leading to autonomous inactivation with a half-life of approximately 12-25 minutes [53,60,61]. KRAS G12D, on the other hand, was found to have additionally reduced GTPase activity. With less than 20 % of GTP being converted to GDP

after 16 minutes and remaining in an activated state for extended periods of time [53,55,56].

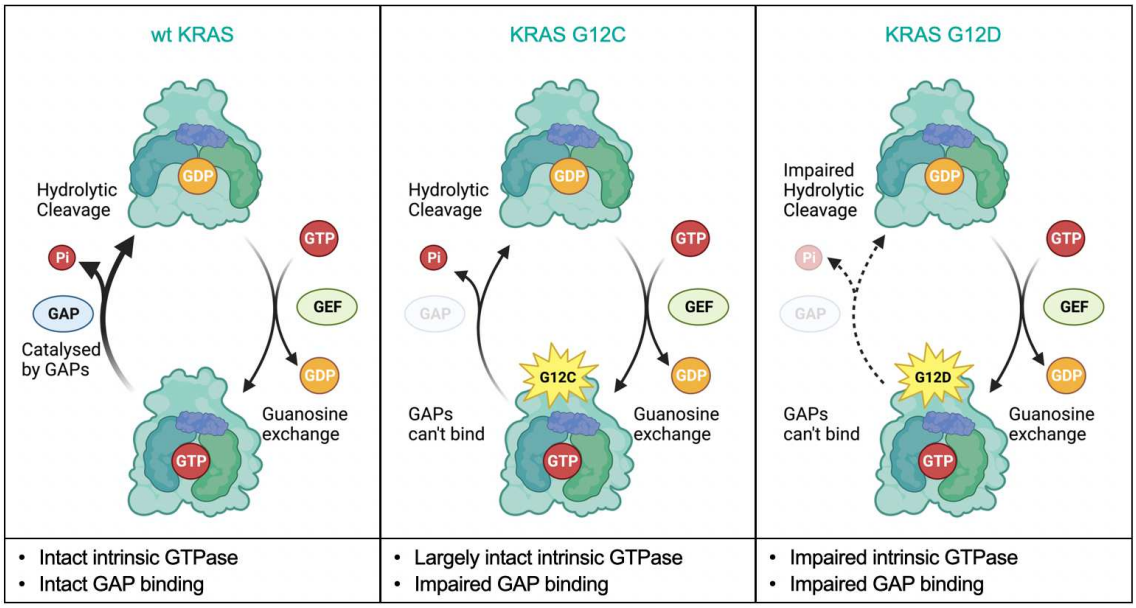


Figure 1.2 Mutation-induced functional impairments of KRAS proteins. Left: Conversion between inactive GDP bound- and active GTP bound state in wt KRAS. Impairments of inactivation in G12C (middle) or G12D (right) mutant KRAS protein.

1.4 Anti-tumour immune surveillance

"Know thy enemy and know thyself; in a hundred battles, you will never be defeated."

– Sun Tsu, The art of war (544–496 BC)

The interplay between the immune system and tumour cells is deeply intriguing. Both being “smart” entities, capable of adapting and overcoming adversities. The immune system often forms a primary line of defence against cancer. In fact, it has been hypothesized that nascent cancerous lesions develop repeatedly throughout our lifetimes but remain undetected as they are either eliminated or remain supressed through natural immunity [62]

1.4.1 Introduction to immune surveillance in solid tumours

The tumour microenvironment (TME) describes the complex entirety of the different cell types as well as extracellular components a tumour mass is comprised of. It can be highly variable between- and even within tumours and can also change and evolve over time and in response to stresses, such as anti-cancer therapies[63]. Cell types commonly found in the TME include fibroblasts, adipose cells, endothelial cells and pericytes, which form tumour vasculature, and, importantly, various types of immune cells [64]. Acellular components include metabolites, extracellular matrix (ECM), as well as small signalling molecules, for example growth factors or interleukins, which immune cells use to communicate [64] [65]. Further, the chemical makeup of a tumour, such as the pH and oxygen availability can also play a role in shaping the TME[66,67].

Immunocytes are especially important in shaping the TME and governing disease control or -progression. Anti-tumour immunity plays a crucial role in detecting and eliminating cancer cells. On the other side, immunocytes,

involved in wound healing-like programmes, and certain regulatory immune populations in the TME may aid tumour growth and survival.

NSCLC patients oftentimes present with a particularly unstable genome and high mutational burden, second only to melanoma[68]. Per se this can facilitate recognition by the immune system, as cancer cells may appear particularly aberrant compared to healthy somatic cells[69]. On the other hand, this can also be associated with a higher genomic flexibility and could accelerate evolution of immune evasive mechanisms[69]. Cancer cells which are easily recognisable and vulnerable to the immune system are likely to be eliminated. Over time, in a dynamic process referred to as immune-editing, this can lead to the positive selection of more resilient cancer cell clones. Eventually, tumours can evolve to evade anti-tumour directed immunity, which can be mediated through a variety of mechanisms.

Depending on the relationship between the immune response and cancer cell compartment, the TME can be categorised into distinct phenotypes[70,71]. Immunologically hot tumours are well infiltrated with anti-tumour directed immune cells that express markers associated with an effective anti-tumour immune response. In contrast, in immunologically cold tumours, the function of anti-tumour-directed immunocytes is often corrupted while immune populations in support of tumour maintenance and growth may be present in greater numbers. A third type of TME is referred to as immune-excluded or immune desert, with overall poor immune cell infiltration. These states of the TME can coexist and vary within and between patients as well as over time.

1.4.2 The arsenal of immunocytes and their role in combatting cancer

Anti-tumour immunity is often a crucial first line of defence in combatting the development and progression of malignancies, through synergism between different types of immunocytes with diverse mechanisms of action (**Figure 1.3**). The immune system can be divided into and innate- and adaptive compartment,

synergistically covering both, immune surveillance through generic recognition of aberrant patterns as well as targeted elimination of unhealthy somatic cells and immune memory. All immunocytes are derived from a common haematopoietic stem cell. From there, they can either further differentiate along the myeloid-trajectory, developing into an innate immune cell, or along the lymphocyte-lineage, which gives rise to an adaptive immune compartment[72]. Leukocytes originate in the bone marrow and may then, in a process referred to as diapedesis, migrate through the lymphatic system, general circulatory or peripheral tissues as they undergo stages of differentiation and exude effector functions.

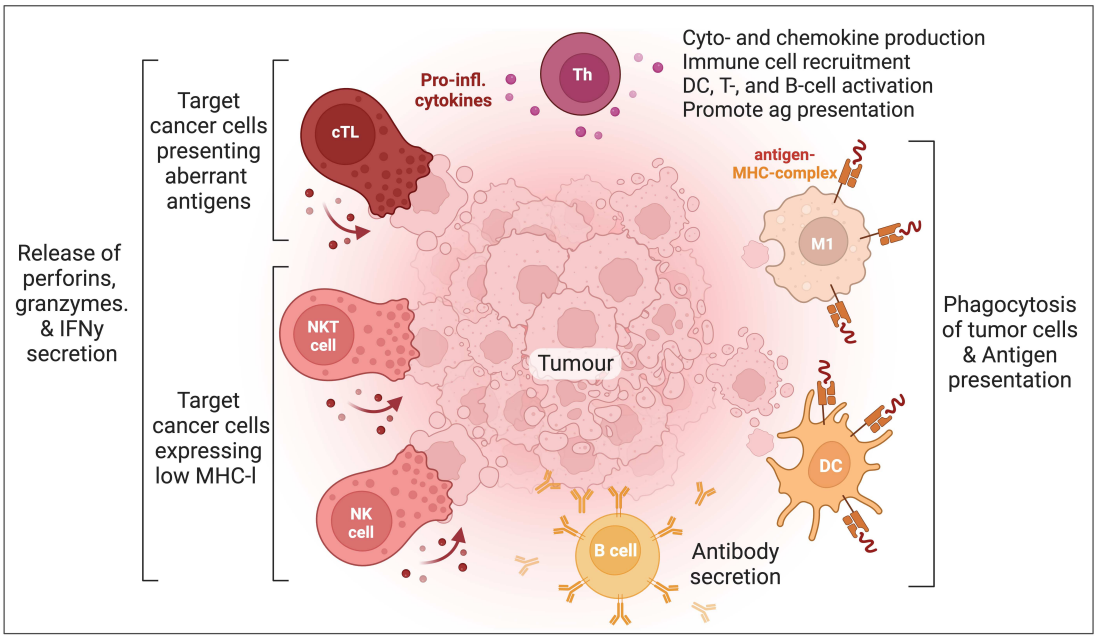


Figure 1.3 Anti-tumour immunity. Schematic of anti-tumour directed immune-cancer cell interactions in the TME. Cell type abbreviations (clockwise): Th: $CD4^+$ T helper cell, M1: M1 polarised macrophage, DC: dendritic cell, NK: natural killer cell, NKT: natural killer T cell, cTL: $CD8^+$ cytotoxic T lymphocyte. Figure was made with BioRender.

1.4.2.1 The innate anti-tumour immune response

The innate anti-cancer immune response is comprised of immune cells which react to generic patterns, hypoxia, the presence of apoptotic cells or an acidic tumour milieu in a pre-determined manner. Most somatic cells, except for

mature erythrocytes, present protein-derived self-peptides on their cell surface via the antigen presenting machinery and trans-membrane major-histocompatibility complex class 1 molecules (MHC-I). Per se, the immune system is rendered immune tolerant towards self-antigens during immune surveillance of somatic cells. However, mutations, genome amplification events, infections, or other harmful events can lead to MHC-I presentation of neoantigens or aberrant patterns of self-peptides which can trigger an anti-tumour immune response[72]. To avoid immune-reconnaissance by the adaptive immune system, cancer cells were found to have downregulated antigen presentation machinery in response[73-75].

However, the innate immune system can counteract this through the employment of natural killer (NK) cells[76,77]. Despite being derived from the lymphoid lineage, NK cells lack antigen specificity. Instead, they recognise the presence or absence of MHC-I molecules on somatic cells via a two-component-circuit[78]. Firstly, NK cells express an NKG2D receptor, which binds to a group of ubiquitously expressed glycoproteins on the target cell. This receptor signals for the NK cell to engage and kill the target cell. However, that circuit is inhibited as long as MHC-I molecules are also detected on the surface of the target cells via the NK cells' killer cell immunoglobulin-like (KIR) receptor. If the inhibitory signalling form MHC-I interaction is absent, the NK cell will engage in killing its target cell. Additionally, NK cells can also be involved in a second line of defence, through detection of cancer cells, opsonised by antibodies [79]. Here, NK cells recognise the Fc-domain of IgG antibodies via their Fc-gamma-Receptor 3A FCyRIIIA (CD16), engaging in antibody-dependent cell-mediated cytotoxicity (ADCC).

Despite being considered part of the innate immune system, NK cells stem from the same lymphoid progenitor cell as B cells or T cells. They kill cancer cells through a similar mechanism to $CD8^+$ T cells, by forming an immune synapse with their target cell and secreting perforins and granzymes, as well as engaging in FAS receptor-ligand interactions. This process can trigger a death

cascade in the target cell, resulting in apoptosis and subsequent release of endogenous cell material, including damage-associated molecular patterns (DAMPs). It can also induce the secretion of tumour necrosis factor alpha (TNF-α) and interferon gamma (IFN-γ) [77,78].This, together with other inflammatory indicators, can attract a range of other immune cells to the tumour site.

Another group of innate immune cells are neutrophils (NPs), which can exert a multifaceted role in anti-tumour immunity as well as immune evasion. They can be subdivided into N1 type NPs, supporting anti-tumour immunity and N2s, which take on an immune suppressive role. N1 functions include degranulation-mediated apoptosis induction in cancer cells, phagocytosis, and antigen presentation. A particular trait of this cell type is the releasing of NPs extracellular traps (NETs), web-like DNA structures that can apprehend cancer cells. However, this mechanism was found to be adept in both, hindering and promoting cancer and metastasis progression [80]. Other innate immunocytes such as mast cells, eosinophils and basophils were shown capable of contributing to both antitumour immunity and promoting cancer progression[81-84]; however, this will not be discussed in detail here.

A further essential regiment of innate anti-tumour immunity are antigen presenting cells (APCs). These APCs fulfil a variety of functions, the first central aspect being the phagocytosis of cancer cells or cancer cell-derived material. Secondly, APCs can thereafter cross-present these tumour-cell-specific antigens to adaptive immune cells, thereby priming a targeted immune response[85,86]. APCs can be attracted to the TME through various stimuli[87,88]. For example, certain chemokines and cytokines such as CCL2, CCL5, CXCL8, CXCL12, IL-1, IL-6, TNF-α, or the presence of Damage-Associated Molecular Patterns (DAMPs) such as extracellular heat shock proteins or ATP, which are indicative of damaged cells in the surrounding[85]. The latter can be recognised by APCs via their pattern recognition receptors (PRRs). Once recruited to the TME, APCs can then internalise cancer cell fragments, or even whole cancer cells. For example, APCs can recognise and engulf apoptotic cancer cells

directly via their MER Tyrosine Kinase (MERTK) receptor, in a process known as efferocytosis. However, it was shown that blocking MERTK can also have anti-tumourigenic effects, through an increased an interferon-mediated stress response due to an accumulation of apoptotic material in the TME[89 90]. Further, if cancer cells are opsonised by antibodies, APCs can also recognise aberrant cells via their Fc receptors [86,91].

The two main groups of contributing innate APCs are M1-polarised macrophages (M1s) and dendritic cells (DCs), which can share a similar role in anti-tumour immunity[72]. Overall, however, M1s seem to fulfil a wider range of functions within the local TME which additionally includes ECM-remodelling, recruitment of various immune cells to the tumour site via cytokine secretion, modulation of vasculature development, and providing continuous stimulation to anti-tumour directed lymphocytes[86,92].

DCs, on the other hand, are the main sentinels of the immune system and take on a major role in the initial priming of an adaptive immune response[85]. They can either activate T cells locally in the TME or migrate to tumour-draining lymph nodes (tdLNs) to prime an adaptive immune response[93]. Three main DC subtypes are conventional DCs (cDCs), plasmacytoid DCs (pDCs), and follicular dendridic cells (fDCs) which differ in origin, marker expression, function, and phenotype [93,94]. cDCs are highly efficient in antigen processing and presentation and can be further subdivided into the types cDC1 and cDC2. cDC1 predominantly present antigens via MHC-I complex to $CD8^+$ T cells while cDC2 cells primarily present antigens to $CD4^+$ T cells via their MHC-II complex. pDCs are less efficient in cross-presentation of antigens but important producers of interferons, TNFα, IL-2, IL-6 and other tumouricidal cytokines [95,96]. Outside of immune-oncology, pDCs play a major role in contending viral infections [97]. fDCs were found to play a crucial role in the formation of germinal centres and coordinate the efficiency of B cell responses as well as B cell memory formation[98]. Additionally, B cells can play a role in phagocytosis and

antigen presentation, however, this is more relevant in the context of B cell activation than tumour clearing or cross presentation to other immune cells.

1.4.2.2 The adaptive anti-tumour immune response

APCs liaise between innate and adaptive immunity through the priming of targeted T cell and, by extension, B cell responses against cancer cells (**Figure 1.4**). APCs can process phagocytosed cancer cell material, breaking down exogenous proteins into smaller peptides. These cancer cell specific antigens can then be cross-presented to different classes T cells via the APCs' MHC-molecules. Having received activation signalling, respective T cells can then become activated, proliferate, and fulfil a range of effector functions.

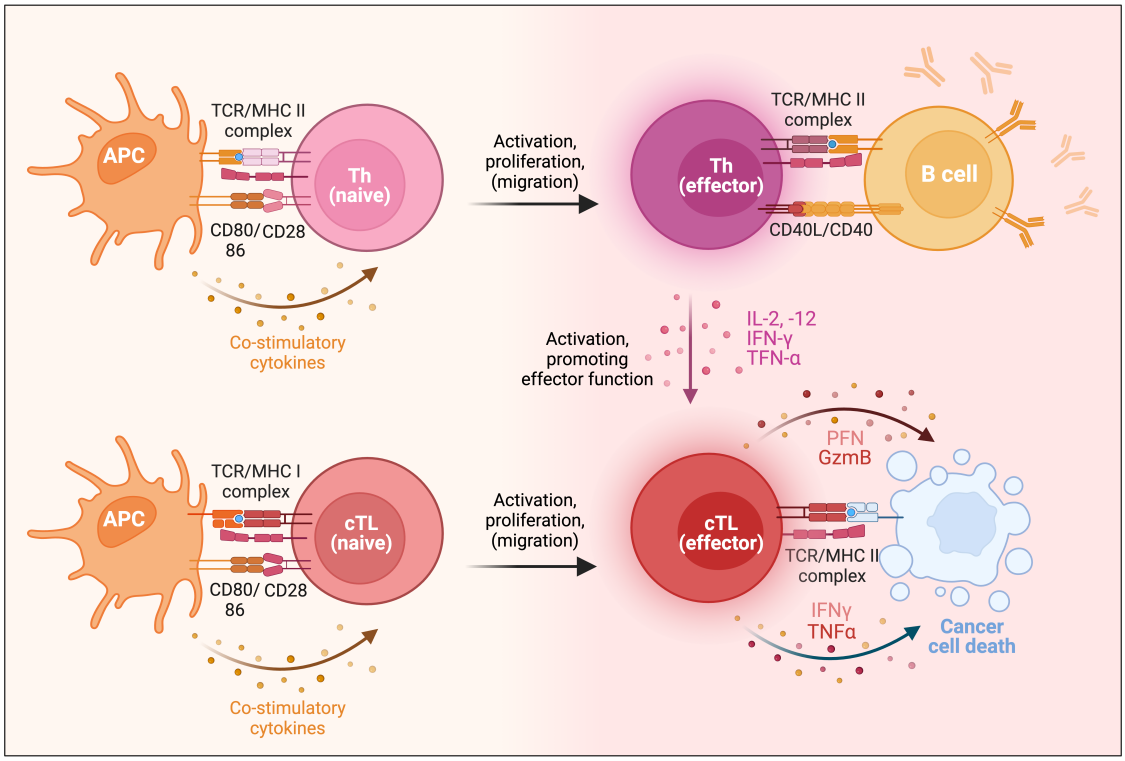


Figure 1.4 Priming of an adaptive anti-tumour immune response. Schematic illustrates mechanisms governing the priming of adaptive anti-tumour immunity. Cell type abbreviations: APC: antigen presenting cell, Th: $CD4^+$ T helper cell,T cell, cTL: $CD8^+$ cytotoxic T lymphocyte. Figure was made with BioRender.

There are several classes of T cells, the most commonly studied being $CD8^+$ and $CD4^+$ T cells. There are also other classes, such as gamma-delta T cells and natural killer T cells, which are situated in the interphase between innate- and adaptive immunity[72]; however, these will not be discussed in detail here. $CD8^+$ and $CD4^+$ T cell precursor cells originate from the bone marrow and migrate to the thymus where T cell receptor (TCR) diversification occurs [72]. This stage of development includes a multistep process, including the genomic re-composition of redundant sequences encoding for TCR fragments, referred to as V(D)J recombination. Subsequently, T cells undergo initial rounds of TCR selection for weak self-antigen recognition, thereby maintaining immune tolerance towards somatic epitopes. Naïve T cells, which pass this threshold then leave the thymus to migrate through the bodies' lymph system. G. Lythe et al. estimated that the human body maintains up to 10^{10} unique TCR-clonotypes [99], suggesting a striking range of T cell plasticity. Naïve T cells can then typically be activated when their TCR has a high affinity towards a neoantigen cross-presented by APCs via their MHC-complexes [72].

The first class of T cells are cytotoxic $CD8^+$ T lymphocytes which take on an active role in cancer cell killing. The CD8 co-receptor recognises an extracellular domain of the MHC-I complex on APC and stabilises the MHC-I-TCR interaction. T cells also express the transmembrane domain CD3, which also engages with the immune synapse and is responsible for transmitting activation signals to their nuclei. Co-stimulation is provided via trans-membrane receptors, such as B7 proteins CD80 or CD86 on APCs binding to CD28 on the T cells. Additionally, APCs secrete activating cytokines, such interleukin (IL)-6 and IL-12 [99,100]. If all the necessary activating signals are present, T cells will then undergo clonal expansion and differentiation into effector cells[72,101].

Peripheral effector $CD8^+$ T cells expressing a specific TCR, can then detect aberrant antigens on cancer cells presented on their MHC-I molecules. For example, several studies of colorectal- and pancreatic cancer demonstrated that KRAS G12D derived peptides presented via MHC-I on cancer cells could

be recognised by $CD8^+$ T cells[102-104]. Upon engagement, $CD8^+$ T cells will create pores in the cancer cell membranes through secretion of perforins and granulysins followed by the secretion of granzymes and other cytotoxins through these openings. Thereby inducing apoptosis through DNA damage, mitochondrial dysfunction, and activating the caspase -cascade pathway, etc. T cell expansion can also be induced after encounter of a cancer-antigen on a target cell[105].

The second major class of T cells is a group of polyfunctional $CD4^+$ T cells. In contrast to $CD8^+$ T cells, $CD4^+$ T cells only recognise- and are activated by antigens presented on MHC class 2 complex (MHC-II), which is mostly expressed on APCs, particularly on DCs[72]. As $CD4^+$ T are MHC-II-restricted, except for certain blood cancers such as lymphomas, $CD4^+$ T cells can not recognise and target cancer cells directly[106]. Instead, they take on a coordinating role in either supporting, or supressing an anti-tumour immune response, depending on subtype and circumstances.

$CD4^+$ T cells can be further divided into different sub-classes, including T helper cells like Th0, Th1, Th2, Th9, Th17, Th22, follicular helper T cells (Tfh) and regulatory T cells (Tregs)[72]. Th1 and Th2 $CD4^+$ T cells support an anti-tumour immune response through various mechanisms[107]. This encompasses recruitment of further APCs to the tumour site and inducing their antigen presentation machinery. They are also involved in activation of antigen-specific B cells, promoting their differentiation into antibody (ab)-producing plasma cells and immunoglobulin IgG class switching $CD4^+$ T cells are also especially important in promoting $CD8^+$ T cell effector functions, through the secretion of high IL-2 and to promote their continued activity and function in the TME. Moreover, they secrete cytokines such as TNFα, and IFN-γ, creating a pro-inflammatory environment, inducing growth arrest in cancer cells and counteracting aberrant tumour vasculature[108,109].

Interestingly, it has become evident in recent years that only a small proportion of T cells in the TME actually recognise cancer-cell-specific antigens via their TCR. The majority of T cells are recruited to the TME as a general site of inflammation and contribute to an anti-tumour immunity through more systemic mechanisms. These include the secretion of pro-inflammatory cytokines, recruiting other immunocytes to the site, TCR cross-reactivity, and cancer cell killing through recognition of stress-induced ligands on cancer cells via innate-like receptors[110-112].

Another group of adaptive immunocyte are B cells, which share a common lymphoid progenitor with NK- and T cells[72] and together make up the fraction of tumour infiltrating lymphocytes (TILS). B cells contribute mainly through a humoral response, by producing and secreting cancer-cell specific antibodies[113]. Opsonisation of cancer cells can facilitate their recognition by innate immunocytes, which bind the antibodies' 'fragment crystalisable' (Fc) domain with their FC-receptors. These are expressed on various innate immune cells, such as APCs, NK cells, eosinophils, basophils, NPs, and mast cells. Further, the FC domain can also activate the complement system and platelets[113].

Similar to T cells, the body also hosts a vast arsenal of ab-producing B cell clonotypes that can respond to a wide range of pathogen-derived or tumour antigens. This clonal diversity is achieved through multi-step processes that starts in the bone marrow, from a lymphoid progenitor cell[72,113]. Rearrangement of redundant genomic segments that create the immunoglobulins (Ig) heavy- and, subsequently, -light chains generates initial clonal diversity. If the recombination resulted in the successful generation of an Ig, the protein will then be expressed as a membrane bound isoform, also referred to as B cell receptor (BCR). If this BCR displays a weak affinity towards self-antigens, implying self-tolerance, the resulting naïve B cells then typically migrate through the lymphatic system and into germinal centers within lymph nodes or the spleen. B cells can be activated through several different mechanisms[113].

Firstly, B cells can bind their target antigen directly via their BRC, although further co-stimulation is usually needed to induce full B cell effector function and memory. Secondly, B cells can present phagocytosed tumour-specific peptides via their MHC-II complex. These can be recognised by the TCR of $CD4^+$ T cells, which, in turn, induce B cell activation through membrane protein interactions as well as cytokine secretion. Thirdly, naïve B cells can also recognise their cognate tumour antigen presented by follicular DCs (fDCs) or $CD169^+$ MPs[114] via their B cell receptor. Once B cells recognise a target antigen and receive co-stimulation, they proliferate while undergoing a process called affinity maturation[113]. Here, somatic hypermutation in the DNA segments coding for the antigen-recognising areas of the Ig creates further variety in the ab arsenal. Activated B cells with a high affinity towards a cancer cell specific neoantigens will then amplify and differentiate. This includes class-switching, changing from a membrane-bound BCR isoform to a secreted IgG thereby becoming functional, ab producing plasma cells [115].

Reports indicate that B- and T cell activation can happen in both, tumour-draining lymph nodes (tdLNs) and directly within TME. Lymph nodes are small, encapsulated, oval shaped organs within the lymphatic system that filter lymphatic fluid and form central hubs in the coordination of adaptive immunity. Here, APCs can migrate from the tumour site to tdLNs and present tumour cell specific antigens to concentrated clusters of T cells. Depending on T cell class and co-stimulation, this can induce proliferation, differentiation and migration in respective T cell clones. Further, $CD4^+$ T cells can support the development of a humoral response through engagement with B cells in an adjacent tdLN zone. Interestingly, within the TME, tertiary lymphoid structures (TLSs) have been identified [116]. These are aggregates of B cells, different subclasses of T cells, as well as smaller populations including antigen presenting cells. These structures appear to vaguely mimic the composition and function of lymph nodes; however, they are not encapsulated and can exist in varying degrees of organisation. TLSs have been associated with a favourable prognosis[117,118] as

well as enhanced responses to immunotherapy, indicating a contribution to anti-tumour immunity[119-122].

Certain cytokines, such as interferon gamma (IFN-γ), can further alert the immune system of the presence of a malignancy[123]. The role of this messenger in modulating the interplay between cancer cells and the immune system is complex and multifaceted. IFN-γ plays an essential role in bolstering immune responses through both, autocrine and paracrine effector pathways. Under the right conditions, both, immunocytes and cancer cells can produce this cytokine. It also plays an essential role in fending off antiviral and -microbial infections. IFN-γ was shown to promote recruitment of pro-inflammatory immunocytes, including TILs and APCs to the TME. It can enhance antigen presentation in APCs as well as increase the intensity and duration of cytotoxic activity of NKs and cytotoxic T lymphocytes (cTLs). In some tumour cells, IFN-γ exposure was shown to inhibit their proliferation and induce upregulation of their antigen presentation machinery, potentially unveiling their aberrancy to the immune system.

1.4.2.3 Immune memory

A significant aspect of an adaptive immunity is the formation of lasting immune memory. In addition to executing a targeted effector response, subgroups of lymphocyte populations remain as long-lived memory cells. If confronted with the same antigen in the future, antigen-specific memory cells were found to expand faster and respond more effectively [72].

The formation of memory B lymphocytes occurs after the germinal centre reaction and affinity maturation[72]. Here, in addition to ab secreting plasma cells, B cells can also develop into B memory cells, if adequate co-stimulatory signals, provided by Tfh cells and/or fDCs, are present. B memory cells can then either continue residing in the germinal center or migrate through the lymph or return to the bone marrow[72].

Memory T cells can exist in different cell states[72,124]. First, stem cell memory T cells (Tscm), are long lived and able to give rise to other progenitor T cells with the same TCR when necessary. Second, central memory T cells (Tcm) travel between the general circulatory and the primary- and secondary lymph tissues. Third, effector memory T cells (Tem), commute between non-lymphoid, somatic tissues as well as the blood-, and lymph system. Lastly, resident memory T cells (Trm), that remain in non-lymphoid tissues. Control of T cell memory populations and their transcension between categories can be achieved through cytokine signalling, including IL-2, IL-7, and IL-15[125].

Further, memory-like NK cells, with an increased magnitude in both, quality and quantity of effector response towards previously encountered stimuli have also been documented [126-128].

1.5 Immune evasion in cancer

"Cancer's life is a recapitulation of the body's life, its existence a pathological mirror of our own."

— Dr. Mukherjee,

The Emperor of All Maladies: A Biography of Cancer

1.5.1 Immune escape as a hallmark of cancer

Cancer cells that are easily recognisable to the immune system are likely to be eliminated. Over time, in a dynamic process referred to as immune editing, this can lead to the positive selection of more resilient cancer cell clones. This "immune-oncological tug-of-war" is complex and can often evolve over decades. Eventually, tumours can evolve to evade an anti-tumour directed immune response, by altering the cell state of immunocytes to become passive or even support tumour growth instead [129,130]. There is a simile of tumour cells co-opting wound-healing programmes of the immune compartment to their avail[131,132].

Firstly, tumour cells can hijack regulatory signalling circuits of the immune system to weaken anti-tumour immunity. Under physiological conditions, controlling the intensity and duration of effector cell responses is intended to avoid hyper-inflammation and auto-immunity-related conditions. However myriad studies found that cancer cells can exploit these regulatory circuits, by aberrantly expressing checkpoint ligands on their own cell surface[133-135]. For example, by exhausting cytotoxic T cells through secretion of immune suppressive cytokines (ISC) and direct cell-to-cell contact [136]. Activated T cells express regulatory checkpoint receptors, such as programmed cell death-1 (PD-1) and CTLA4 on their cell surface. Upon encountering their ligands, programmed death-ligand 1 (PD-L1) and the B7 proteins CD80 and CD86 respectively, the checkpoint receptors can induce a loss of T cell effector

functions, also referred to as T cell exhaustion. These ligands are typically expressed by APCs, Tregs, and myeloid-derived suppressor cells (MDSCs) in a precisely controlled manner[137]. Further transmembrane proteins that can encompass checkpoint-like functions expressed by T cells include LAG-3, TIM3, and TIGIT. In a similar fashion, phagocytic activity of anti-tumour directed APCs can be inhibited through activation of their checkpoint receptor signal regulatory protein alpha (SIRPα). This transmembrane protein interacts with its ligand, CD47, that functions as a “don’t-eat-me” signal [138,139].

Secondly, cancer cell compartment can induce a state of alternate law, inducing the recruitment of immune populations which can either supress an effective anti-tumour immune response or even support tumour growth and progression. This encompasses Tregs which can be demarcated by expression of the transcription factor Foxp3. Under physiological conditions, Tregs are one of the immunocyte populations dedicated to checking the scope of an immune response. However, cancer cells can hijack this immune regulatory mechanism by recruiting T regs to the TME to supress anti-tumour immunity. In addition to expressing checkpoint inhibiting ligands, Tregs also secrete the ISCs IL-10, IL-35 and transforming growth factor-beta (TGF-β) and deplete the TME of pro-inflammatory molecules, such as IL-2 and ATP [140,141]. Another population of immune suppressive cells are myeloid-derived suppressor cells (MDSCs). They describe a heterogeneous group of immature myeloid cells, derived from a common, bone marrow-residing progenitor and often take on a monocyte-like or NP-like morphology. MDSCs express inducible nitric oxide synthase (iNOS) which produces nitric oxide, NADPH oxidase (NOX2) that increases reactive oxygen species (ROS), and arginase-1, which depletes extracellular arginine. All of which can cause impaired APC effector functions and T cell anergy. MDSCs also produce ISCs IL-10 and TGF-β and pro-angiogenic factors such as vascular endothelial growth factor (VEGF). Promoting the development of tumour vasculature that can provide oxygen and nutrients to the tumour but may not facilitate drug delivery, as it is often leaky and underdeveloped. MDSCs can also degrade extracellular matrix through secretion of

metalloproteases which can promote metastasis. Moreover, MDSCs can secrete ISCs and recruit other immune-suppressive immunocytes[142-144]. Alternatively activated M2 macrophages (M2s), can also orchestrate the corruption of antitumour immunity [145,146]. Under physiological conditions, M2 polarised macrophages play an essential role in wound healing, often secreting anti-inflammatory factors as well as promoting angiogenesis. Similar to MDSCs, M2s can secrete ISCs such as IL-4, IL-10, IL-13, and TGF-β, and remodel the TME stroma. In addition, it was reported that M2s can also directly support tumour growth through secretion of EGF [147,148]. Monocytes are also derived from a shared myeloid progenitor; they can differentiate into MDSC or M2s and hence share similar functions in the TME. Although under the right conditions, monocytes can also support antitumour immunity when differentiating into M1s or certain groups of DCs [133]. Another cell type with the potential to subvert antitumour immunity are cDC2s[149,150]. Through their antigen cross presentation to $CD4^+$ T cells via the predominantly expressed MHC-II, they may promote the incitement of Tregs in the TME. They can also produce ISCs and were shown to express high levels of PD-L1 in the TME, attenuating cTL and NK responses. NPs play a bivalent role in anti-tumour immunity and immune evasion. In terms of supporting tumour growth and progression, N2 polarised NPs were found to promote tumour vascularisation through VEGF secretion. They can promote metastasis through destabilisation of the tumour stroma secretion of their Neutrophil extracellular traps (NETs) which can serve as anchorage for circulating cancer cells. N2s can also abrogate a pro-inflammatory response through expression of PD-L1, ISCs, and production of ROS and NO[151,152].

Thirdly, the tumour cell fraction can impose an immune-excluded state in the TME. There are different definitions of what exactly an immune dessert or immune-excluded TME encompasses [153]. However, a common consensus entails that pro-inflammatory immunocytes, particularly TILs are unable to infiltrate the tumour mass and instead are absent or accumulate on the outer perimeter of the tumour. Various factors can contribute to the emergence of this phenotype. Physical barriers such as a capsule comprised of fibroblasts and

extracellular matrix or the lack of tumour infiltrating vasculature could exacerbate immune infiltration. The presence of immune suppressive subpopulations may also discourage pro-inflammatory lymphocytes from entering the TME. Further, the presence of immune suppressive cytokines and -metabolites, as well NO, ROS, hypoxia and an acidic pH in the TME may create unfavourable conditions for TILs [154].

1.5.2 Oncogenic KRAS mediated immune escape

In addition to growth and survival signalling, oncogenic KRAS also plays a key role in thwarting anti-tumour immunity, by manipulating and disrupting myriad processes (**Figure 1.5**) [136].

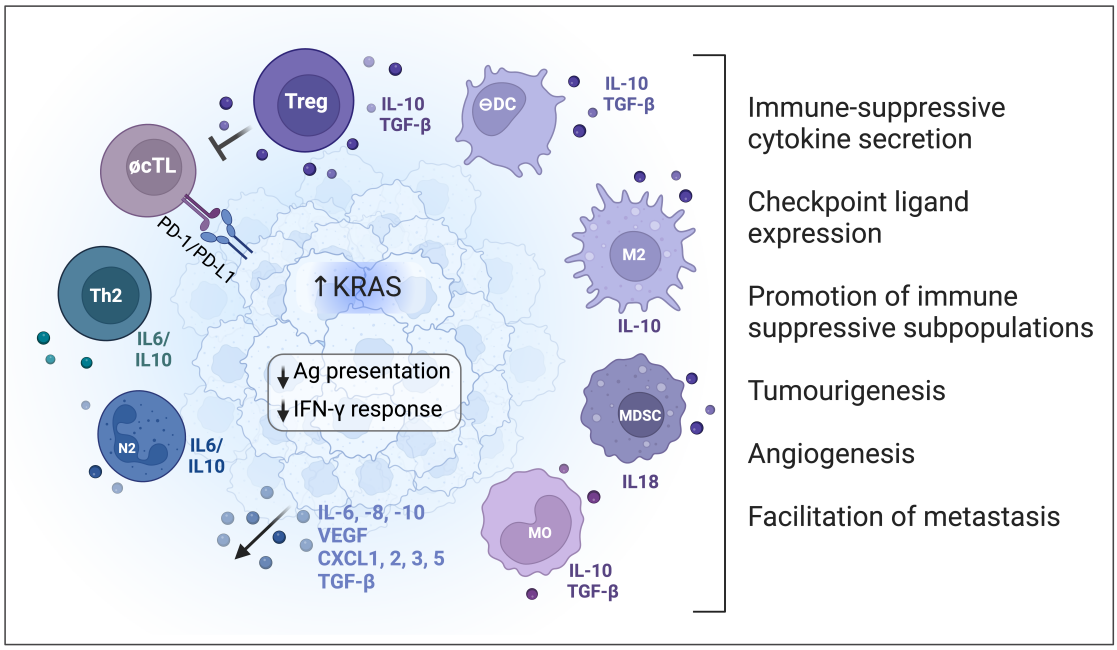


Figure 1.5 Oncogenic KRAS signalling induced immune suppression. Schematic illustrates mechanisms of oncogenic KRAS signalling-induced immune escape. Cell type abbreviations (clockwise): (-)DC: inhibitory subtypes of dendritic cells; M2: M2 polarised macrophage, MDSC: myeloid-derived suppressor cell; MO: Monocyte; N2: type-2 polarised neutrophil; Th2: $CD4^+$ T helper cell with subtype classification 2, ⊘cTL: exhausted $CD8^+$ cytotoxic T lymphocyte, Treg: T regulatory cell. Figure was made with BioRender.

First, mutant KRAS signalling can alter the expression of cancer cell transmembrane proteins that disable immunocytes through direct cell-to-cell contact. Our group was able to demonstrate that oncogenic KRAS signalling is directly responsible for the aberrant stabilisation and expression of PD-L1-encoding mRNA in tumour cells in a preclinical model of NSCLC[155]. Upregulation of PD-L1 has been observed in human KRAS mutant NSCLC samples and was associated with corrupted anti-tumour immunity [156]. Overexpression of oncogenic KRAS in a pre-clinical model of colorectal cancer impaired cytotoxic effector function of T cells and reduced infiltration of cytotoxic T cells[157]. Moreover, PD-1 can also be expressed on other types of immunocytes, including NK cells and MPs and DCs. PD-L1 contact was found to hamper cytotoxicity in NK cells, induce a shift from anti-tumour directed M1 to M2 macrophages, and reduce antigen presentation and cytokine secretion capacity in DCs [158]. Another checkpoint ligand which can be aberrantly expressed in tumour cells in an oncogenic KRAS signalling dependent manner is SIRP1α. It has been verified in both, patient samples and preclinical NSCLC models that interaction with this anti-phagocytotic transmembrane protein with its counterpart CD47 can supress effector function in APCs and granulocytes[159,160].

Second, oncogenic KRAS signalling can induce the aberrant production of ISCs within cancer cells. This includes the chemokines CXCL1, CXCL2, CXCL3, and CXCL5 [161-163]. These, in turn, can bind to their respective chemokine receptors expressed by immune suppressive subpopulations such as monocyte and neutrophils and recruit them to the TME. Employing a murine xenograft model, one study found that mutant Ras-induced CXCL8 or IL-8 was additionally responsible for promoting tumour vascularisation and growth[164]. In a KRAS-mutant preclinical model of pancreatic neoplasia, it was also observed that excessive KRAS signalling lead to cancer cells producing GM-CSF which, in turn led to the recruitment of MDSCs [165]. Several groups found that oncogenic KRAS led to secretion of TGF-β, IL-6 and IL-10 by cancer cells which can induce the conversion in $CD4^+$ T cells to a Treg subtype and hampered anti-

tumour immunity across various cell types of both innate and adaptive immune response[166-169 170]. Elucidating the underlying mechanisms, a study of KRAS mutant lung cancer found that KRAS signalling induced the Nuclear factor kappa-light-chain-enhancer of activated B cells (NF-κB) signalling cascade which in turn contributed to IL-6 production[167]. Another study found that IL-6, IL-10, and TGF-β production was mediated via the MAPK signalling cascade[170]. Moreover, by employing a murine model of lung adenocarcinoma, it was discovered that production of CCL9 and IL-23 instructed an immune excluded TME and abated inflammatory TIL effector functions[171]. Importantly, mutant KRAS signalling can also supress the response to pro-inflammatory cytokines such as IFN-γ[162,172,173]. Multiple studies have demonstrated that oncogene-induced suppression of this cytokine can aid immune evasion. Lower responses to IFN-γ can allow cancer cells to downregulate antigen presentation, thereby exacerbating recognition of neoantigens through cTLs[166]. Lack of IFN-γ stimulation in the TME may also interfere with recruitment- and effector functions of pro-inflammatory immunocytes. Our group, together with others, were able to show that IFN-γ suppression is achieved through cooperation with Myc. This is a key transcription factor, residing downstream of KRAS as well as other cytosolic signalling cascades that can drive various gene expression programmes, including cell cycle progression [172,173]. Although it should be noted that IFN-γ can also hamper anti-tumour immunity through negative feedback loops and promotion of immune suppressive activity [123]. Prolonged IFN-γ exposure can also induce upregulation of PD-L1 in cancer cells which, in turn, can induce T cell exhaustion in the TME[133].

Thirdly, mutant KRAS can also drive immune evasion through metabolic manipulation. For example, oncogenic KRAS induced increase in lactic acid production was also found to impair T cell function in a pre-clinical colorectal cancer mouse model[157]. KRAS can also induce upregulation of CD73, a trans-membrane ecto-5′-nucleotidase, which in turn can increase extracellular adenosine. High adenosine concentrations in the TME were found to impair T cell- and NK cell functions[174,175]. In a KRAS mutant preclinical model of NSCLC,

our group also discovered that excessive KRAS signalling can promote expression of cyclooxygenase-2 (COX2)[176]. This enzyme is involved in the synthesis of the prostaglandin E2 (PGE2) which, when secreted into the TME, can induce immune-suppressive effects when binding its receptor on pro-inflammatory immunocytes[43, 176,177].

It is also worth mentioning that coinciding loss of function of tumour suppressor genes (TSGs) can collude with mutant KRAS signalling to exacerbate immune suppression. The most frequently co-mutated TSGs in KRAS mutant lung cancer are Trp53, STK11, KEAP1[178]. Tp53 is the most commonly mutated oncogene in human cancer as well as NSCLC. Loss of Trp53 (the mouse equivalent) function was shown to inhibit IFN-γ production and increase secretion of IL-17, which can, in turn, promote T cell exhaustion and upregulate expression of PD-L1 and PD-L2. Trp53 loss can further promote the recruitment and activation of immune suppressive subpopulations through various other mechanisms[179]. STK11 mutant NSCLC tumours present with a more immune excluded TME [180]. This was attributed to the suppression of IFN-γ and MHC-II expression[181], recruitment of neutrophils due to increased release of IL-6[182] and silencing of pro-inflammatory STING pathway signalling[183]. Similarly, KEAP1 mutant NSCLC tumours were also reported to have a lymphocyte-excluded phenotype, partially caused through inhibition of interferon response [184,185].

Additionally, in lung cancer, the high degree of genome instability and mutational burden may facilitate immune escape through accelerated cancer cell diversification during cell division. The cause of this increased mutational burden can often be attributed to the aberrant expression of so-called apolipoprotein B mRNA editing enzyme, catalytic polypeptide-like (APOBEC) proteins [186-188]. These are cytidine de-aminases, capable of inducing DNA mutations as well as contributing to genomic instability through non-enzyme-mediated mechanisms[189-192].

1.6 KRAS inhibitors

"Again, the message to experimentalists is: Be sensible but don't be impressed too much by negative arguments. If at all possible, try it and see what turns up. Theorists almost always dislike this sort of approach."

- Dr. Francis Crick (1996-2004)

1.6.1 The development of KRAS inhibitors

Until recently, targeting mutant RAS proteins directly was deemed unfeasible[193]. This is in part due to the globular structure of RAS proteins, as most allosteric inhibitors require binding pockets to interact with a target [39]. Further, the picomolar affinity of RAS proteins towards their natural substrate, GTP/GDP, hampered the development of competitive inhibitors[194].

Previously, targeted therapies for RAS mutant cancer patients instead often aimed for signalling proteins upstream- or downstream of the mutant RAS proteins, such as RTK-, Raf-, MEK-, or Erk inhibitors[36]. However, the lack of cancer cell specificity of these drugs exacerbates the definition of a therapeutic window with tolerable side effects for patients. This is because targeting wild type forms signalling proteins also affects the growth and proliferation signalling in healthy stem- and progenitor cell populations that are required for tissue maintenance. Furthermore, RAS proteins constitute a signalling node with multiple input- and output links. Inhibition of efferent signalling components may allow cancer cells to bypass the inhibitors effects through rewiring their dependency within growth and survival signalling networks[32,36,195]. An additional complication for therapies targeting upstream activation is that mutant RAS proteins are less dependent on upstream re-activation compared to wt RAS proteins which can further impede drug efficacy[55].

However, excitingly, it has recently become possible to inhibit oncogenic KRAS variants directly via mutation-specific small molecule inhibitors. The first functional KRAS G12C inhibitors were pioneered by Kevan Shokat and his team, employing an elegant small molecule tethering screen[61]. Taking advantage of the KRAS G12C-mutant-specific cysteine residue, compounds would covalently bind the mutant protein via a thiol-targeting warhead. Compounds found to inhibit the target protein were then further screened and modified for desired properties. Protein crystallography of these initial hits revealed a previously unidentified, binding pocket in the KRAS G12C mutant protein, referred to as “switch-2 pocket”. The inhibitors would irreversibly bind to KRAS G12C and subsequently anneal into this groove, thereby stabilising the protein in its GDP-bound, inactive confirmation[56,61]. Hence these inhibitors are also referred to as KRAS G12C(OFF)- or inactive-state inhibitors (KRAS G12C(OFF)i). They were shown to prevent KRAS G12C from activating downstream-signalling cascades and decrease the viability in an array of KRAS G12C mutant cancer cell lines in *vitro*[61].

These first-generation inhibitors were then further optimised, by pharmaceutical companies. The two compounds KRAS G12C (OFF)i are MRTX849 (a.k.a. Adagrasib or Krazati), developed by Mirati Therapeutics[196] and AMG-510 (a.k.a. Sotorasib or Lumakras) from Amgen[197], were the first to received fast track FDA approval for NSCLC. However, more than 15 other KRAS G12C inhibitors are currently also undergoing clinical evaluation, some of which have already entered for phase 3 trials[37].

Shortly after the advancement of KRAS G12C(OFF)i, active-state KRAS G12C inhibitors (KRAS G12C(ON)i) were developed, exploiting a different mechanism. These molecular-glue small molecule compounds covalently bind to the surface of a chaperone, Cyclophilin A. Thereby re-modelling its surface and creating a neomorphic interphase with a high binding-affinity towards KRAS G12C in its active, GTP-bound conformation[198]. The resulting, covalently linked, tri-complex then prevents mutant KRAS proteins from interacting with

downstream effectors through steric hinderance. Inhibiting KRAS G12C in its active conformation, may allow for a more rapid and direct disruption of the growth and survival signalling in cancer cells. The first-generation active-state KRAS G12C inhibitor is referred to as RMC-4998 and is the drug used throughout experiments in this project. However, more recently, further optimisation has led to a second-generation inhibitor, referred to RMC-6291, which has also entered early clinical testing [199].

The advantage of covalent, mutant-specific inhibitors is their unique ability to irreversibly stabilise mutant KRAS in a non-functional state. In addition, due to the specificity to the mutant protein, some drugs in this line of therapies may qualify for a higher therapeutic index, as, in theory, healthy cells are left relatively unimpeded. After the initial ground-breaking research of turning G12C mutant KRAS into a druggable target, inhibitors targeting other RAS mutations are currently also in various stages of development and clinical testing [122,200]. This includes similar inhibitors targeting KRAS G12D, -G12R, -G12S and -G12V -, as well as -G13C and -Q61H mutations [201-203]. In addition, a mutant specific, bifunctional protein degrader targeting KRAS with a G12D mutation has also been developed[204].

Another group of compounds, referred to as pan-KRAS inhibitors target both, wt KRAS and a range of mutant KRAS proteins. These non-covalent inhibitors bind preferentially to GDP-bound KRAS and do not inhibit NRAS or HRAS[205]. Another, newer variant of pan-KRAS protein degraders are also being assessed[206]. Furthermore, Revolution Medicines has pioneered a RAS multi(ON) inhibitor, capable of also inhibiting the NRAS and HRAS isoforms, that is now entering clinical testing [207-209]. However, these inhibitors also exert KRAS inhibition in a wide range of healthy somatic cells, which might hamper the therapeutic window for these drugs. Additionally, RAS signalling was found to play an important role in a variety of immune cells, including T- and B cells[210,211]. Pan-RAS inhibitors might hence present an additional caveat of compromising anti-tumour immunity. The advent of targeted therapies capable

of inhibiting mutant KRAS proteins directly opens a new avenue for improving patient care. However, the range of efficacy and mechanism of action of these compounds are still in earlier investigation stages.

1.6.2 Inhibition of oncogenic KRAS signalling can alleviate immune suppression in the TME

Oncogenic KRAS not only drives cancer cell-intrinsic survival- and proliferation signalling, but also has a profound effect on remodelling the TME towards an immune-evasive state. Hence, inhibiting KRAS G12C was found to not only kill tumour cells directly but to further reverse immune suppression in the TME.

When Canon et al. developed the Sotorasib compound, they also performed an array of experiments to evaluate this inhibitors effects on the TME of preclinical mouse models[197]. In respective in *vivo* studies, mice were engrafted with xenografts of human pancreatic or lung cancer cell lines. By administering Sotorasib treatments, some complete responses were generated. After these mice had remained tumour free after the end of treatment period, they were rechallenged by injecting isogenic KRAS G12D mutant cancer cells on the opposite flank. Intriguingly, some mice were able to immune reject these cancer cells, indicating the formation of an immune memory response. When assessing the immune cell composition of the TME from Sotorasib treated mice, the group found an increase in $CD8^+$ T cells and antigen presenting cells, as well as an increase in IFN-γ response in subsequent experiments. Mugarza et al also investigated the effects of KRAS G12C inhibition in a variety of NSCLC mouse models of varying degrees of immunogenicity. It was found that KRAS G12C inhibition restores IFN-γ signalling in cancer cells through the suppression of Myc output. Subsequently, a reduction in several immune suppressive subpopulation, as well as an increase in $CD8^+$ lymphocytes was observed. Additionally, antigen presentation machinery in KRAS G12Ci-treated cancer cells was upregulated[172]. Tumour regression was found to be more pronounced in immune competent mice, compared to immune compromised

animals, further empathising the precedence of restoring oncogenic KRAS-rescinded antitumour immunity[212]. Employing another KRAS mutant murine lung cancer model, treatment with Sotorasib successfully decreased aberrant CD47 expression in tumour cells. Thereby restoring innate anti-immunity through SIRP1α-mediated immune surveillance by macrophages[160]. Another study, utilising human xenograft models as well as KRAS-mutant GEMMs, also observed that Adagrasib treatment resulted in an increase of MHC-I expression on cancer cells, as well as favourable changes in immune cell populations present in the TME. This included a decrease in MDSCs as well as an increase in M1-polarised macrophages, DCs and T cells immunocyte composition after Adagrasib treatment. Further, synergy of Adagrasib- and a-PD-1 treatment in their preclinical mouse models were observed, resulting in durable treatment responses[213]. Further, improvement of anti-tumour immune responses upon KRAS inhibition, coinciding with complete responder mice have been observed in RAS-mutant mouse models of lung-, pancreatic- and colorectal cancer[172,197,212,214,215]. Several other studies conjointly found that KRAS G12Ci treatment can sensitise tumours to immunotherapy [197,212,213,216]. However, the overall state of the TME prior to KRASi may play a role in the efficacy of G12Ci in alleviating immune suppression. For example, one study recently conducted by our group, found that KRAS G12C(ON) inhibitors were able to improve response to immunotherapy in immunologically hot but not cold model[216].

A pivotal aspect in the formation of an inflammatory response is the spatial organisation and distribution of immunocytes throughout the TME. How deep pro-inflammatory lymphocytes can infiltrate into the tumour also seems to play a role in therapy response. Preclinical studies by our group employed imaging mass cytometry (IMC) to explore the alteration KRAS G12C(OFF) inhibitors MRTX1257 and MRTX849[217 218] induced in the tumour microenvironment of 3LL-derived murine lung tumours. They found an increase in antigen-presenting macrophages as well as an increase in the infiltration depth of T cells, which were mostly restricted to the outer tumour perimeter in vehicle treated tumours. Furthermore, neighbourhood analysis revealed an increase in cTLs-DCs-

clusters in the TME of treated samples. Of note, KRAS G12C inhibition was also reported to increase infiltration of Tregs in the TME, pointing to an ambivalent role of the inhibitor in TME remodelling[172,197,218,219]. TME remodelling has also been observed with KRAS G12D inhibitors in mouse models of pancreatic cancer[214,220]. Two studies found that KRAS G12C inhibition increased the number of tertiary lymph node structures (TLSs) [18] in the KPAR1.3 model mouse model [122,212]. TLSs have been identified as a prognostic factor for improved survival and prediction for response to checkpoint inhibitors in solid tumours of preclinical models and cancer patients[113,116,221]. Importantly, the increase of TLSs also indicated an improvement in humoral B cell responses and tumour-binding antibodies [122].

1.6.3 KRAS G12C inhibitors in the clinic

In initial in *vitro* and in *vivo* experiments with the KRAS G12C(OFF)i Adagrasib and Sotorasib, both drugs showed potent inhibition of KRAS-downstream pathways and tumour regression in KRAS mutant cancer mouse models [196,197]. This incentivised clinical testing of these drugs for patients with KRAS mutant cancers. While early clinical testing for KRAS G12C mutant pancreatic [222,223]- and colorectal cancer [224,225] were less successful, several NSCLC patients achieved overall favourable objective response rates at doses with tolerable side effects. Of note, patients from phase 1 and -2 clinical trials had often undergone- and failed on previous rounds of other therapies, possibly having developed increased resilience to KRAS G12Ci through therapy cross-resistance. Nonetheless, propitious results in phase 1 and phase 2 clinical trials for both Sotorasib [197,226 227] and Adagrasib [196 228,229] led to accelerated FDA approval of both drugs for treatment of NSCLC. In the CodeBreak trials, the median progression-free survival interval for NSCLC patients receiving Sotorasib was 6.3 months [227], in the KRYSTAL trials for Adagrasib, it was estimated at 6.5 -7.4 months [223,229,230]. In subsequent phase 3 clinical trials, the majority of NSCLC patients initially responded quite well. However, the recently concluded phase 3 clinical trial for Sotorasib revealed that responses were

often not durable, with no overall survival advantage compared to conventional chemotherapy with Doxatel[231].

As KRAS G12C(ON) inhibitors were developed a few years later, clinical testing hasn't yet advanced as far. However, early clinical data indicates that most patients treated with RMC-6291 show an initial treatment response[199,232]. Intriguingly, this also held true for most patients which had previously been treated with- and developed resistance towards KRAS G12C(OFF) inhibitors [199]. However, long term clinical data on this group of inhibitors has not yet become made available.

1.7 KRAS G12C inhibition can lead to development of drug resistance

"It is not the strongest that survive, nor the most intelligent, but the ones most responsive to change."

- Charles Darwin (1809-1882)

As is often the issue with lines of targeted therapy administered as monotherapy, cancer cells can often bypass inhibitor mechanisms and, rather rapidly, develop drug resistance. This also holds true for KRAS G12Ci, where tumours were found to circumvent the drugs' effects through various mechanisms[33,54,233-235].

First, KRAS G12Ci-resistance can evolve through bypass signalling, via the acquisition of further mutations or genomic re-arrangements. Several independent studies investigated circulating tumour DNA (ctDNA) of NSCLC patients that stopped responding to KRAS G12Ci[236-238]. It was discovered that several patients presented with, sometimes sub-clonal, gain-of-function mutations or amplifications in the genes encoding for other proteins in the KRAS signalling pathways. This included proteins upstream of KRAS G12C, such as the RTKs Anaplastic lymphoma kinase (ALK), fibroblast growth factor receptor **(**FGFR) and Hepatocyte growth factor receptor (HGFR) and rearranged during transfection (RET). Proteins situated parallel to KRAS, such as NRAS, as well as downstream signalling proteins such as BRAF, MAP2K1, RAF could also be mutated. Additional loss of function mutations in the TSGs PTEN and NF1 was also observed. Moreover, further mutations, in the KRAS G12C protein itself were also detected. In some patients the mutant cysteine at amino acid (AA) 12 was converted to a different oncogenic mutation, preventing engagement of the cystein-specific warhead of the KRAS G12C(OFF)i. Interestingly, a few patients had instead acquired a novel secondary mutation in the region of the switch-II pocket at AA H95 or Y96, which prevented the small

molecules from annealing effectively. This was also observed in an in *vitro* screen, where Ba/F3 cells were treated with Adagrasib which resulted in secondary mutation sites in KRAS G12C included G12D/R/V/W, G13D, Q61H, R68S, H95D/Q/R, Y96C[239]. In similar studies with KRAS G12C(OFF) inhibitors, Sotorasib[239] and AZ'8037[240] further mutation sites in mutant Ras proteins as well as on the RAS signalling pathway were found.

A second route of resistance development to KRAS G12Ci appears to be the overexpression of wt- or mutant KRAS itself or overexpression of other pathway components. For example, Xue *et al.* found that in various NSCLC lines KRAS G12C inhibition using KRAS G12C(OFF) inhibitor ARS-1620 lead to upregulation of growth factor EGF within the cancer cell compartment. It was also found that KRAS G12C amplification as well as upregulation of Aurora kinase A can rescue KRAS signalling output[241]. In contrast, Ryan *et al.* found that an RTK-modulated increase in activation of the wt KRAS protein, expressed from the second allele, may play a role in pathway re-activation, as KRAS G12C-inhibitors are mutant specific drugs. This was observed upon KRAS G12Ci with ARS-1620 or AMG510 in their panel of KRAS G12C mutant cell lines[195]. In another study this group discovered that MAPK pathway feedback re-activation could also be achieved through the RTK-mediated activity increase of the NRAS and HRAS isoforms[242]. Several studies also found that upregulation of growth factor receptors upstream of KRAS G12C can lead to a survival advantage in the cancer cell compartment[195,238,243,244]. Since KRAS G12C retains relatively high intrinsic GTPase function, this particular mutation can lead to higher dependency on upstream activation signalling. In addition to an increase in protein activation, amplification of pathway components downstream of KRAS G12C were also observed[236,237,245].

A third group of compensatory mechanisms to evade KRAS G12C inhibitor stems from changes in expression profile of genes not directly related to oncogenic signalling. For example, Adachi *et al.* found that cancer cells can gain resilience to KRAS G12Ci by undergoing epithelial to mesenchymal

transition[246]. A different work demonstrated that tissue factor, a transmembrane glycoprotein which is often overexpressed in NSCLC patients, can aid KRAS G12Ci resistance by promoting epithelial to mesenchymal transition (EMT) as well as hampering anti-tumour immunity[235]. Another study showed that knock-down of KRAS G12C in pancreatic cancer cell lines leads to upregulation of metastasis-associated genes in a subset of viable cells[247]. Further, it was discovered that knock down of KRAS G12C in pancreatic cancer cell lines lead to an increase in focal cell adhesion, as an adaptive strategy[248]. An increase in cell adhesion, via overexpression of the integrin ITGB4 was also observed by Mohanty et al., indirectly aiding bypass signalling via the AKT/mTOR axis. This group further found that chronic Sotorasib treatment induced an aberrant increase in wnt signalling[249]. Several studies also found that increased activity of the YAP signalling pathway can act as a compensatory mechanism in cancer cell to overcome the effects of KRAS G12C inhibition[250-252]. Moreover, Xue *et al*. found that another mechanism of avoiding KRAS G12Ci-induced cell death was for cancer cells to enter a quiescent, but viable state during treatment[241]. Development of resistance to KRAS G12Ci was further associated with immune evasion[244] which might impede the efficacy of certain lines of subsequent therapies. Due to the exceptionally high mutational burden found in NSCLC[68], it is also possible that the resulting genome instability may further accelerate the development of KRAS C12Ci resistance.

1.8 Overcoming resistance development to KRAS G12C inhibitors

"Almost all aspects of life are engineered at the molecular level, and without understanding molecules we can only have a very sketchy understanding of life itself."

- Dr. Francis Crick (1996 – 2004)

Due to a variety of compensatory mechanisms, tumour cells can evolve to become drug-resistant to targeted inhibitors, especially when administered as mono-therapy. There are different strategies to overcome- or prevent the development of drug resistance, one being the combination of treatments to prevent bypass signalling in cancer cells. Combinations can either be designed to reinforce inhibition of the oncogenic signalling[37], or to encroach on cancer cells from different angles, exploiting distinct selective vulnerabilities, such as combining pathway inhibition together with reenforcing anti-tumour immunity or cancer metabolism [253].

Reinforcing inhibition of oncogenic signalling can be achieved via different routes. First, vertical pathway inhibition targets proteins within the same oncogenic signalling axis, situated either upstream or downstream of oncogenic KRAS. One strategy for inhibiting upstream signalling is to target RTKs, especially since it was shown that KRAS inhibition alleviates negative feedback circuits, leading to an upregulation of RTK expression or activity [254]. This strategy has been perused in colorectal cancer, where KRAS G12Ci in combination with EGFR-targeting antibodies has shown overall improved survival compared to standard of care treatment[224,225]. However, the FC region of therapeutic antibodies targeting the EGFR receptor might also contribute to additional immune modulatory effects through opsonisation. A disadvantage of targeting RTKs is their redundancy, as cancer cells may achieve bypass signalling through expression of alternative growth factor receptors.

Another more universal approach for inhibiting upstream signalling is to target the proteins associated with the cytosolic domain of activated RTKs that are directly involved in KRAS activation such as SHP2 and SOS1[255-257]. SHP2 is a bifunctional protein, acting as both, a phosphatase and a scaffold protein involved in the RTK complex-mediated KRAS activation. SHP2 effector functions are regulated via structural conformation of the protein, altering between a more compact, inactive- and more open, functionally active form. The recently developed SHP2 inhibitors stabilise SHP2 in its inactive state, thereby preventing its interaction with the phosphorylated sites on the cytosolic domains of RTKs[258,259]. SHP2 inhibition (SHP2i) was found to inhibit RAS cycling, induce cancer cell killing, and even to resensitise various preclinical tumour models to targeted therapies [255,257,260,261]. Combination of KRASi and SHP2i may also prevent potential overexpression of the wt KRAS isoform and other compensatory feedback loops[195 216]. SHP2 inhibitors as well as SOS1 inhibitors have entered clinical testing[37,261,262], however, early trials are still ongoing. Inhibition of these targets provides the advantage of curbing KRAS reactivation in a more universal manner compared to inhibiting a particular RTK. However, certain versions of oncogenic KRAS proteins are overall less dependent on upstream reactivation, as their mutation entails both, impaired GAP binding and corrupted intrinsic GTPase activity.

To counteract prolonged activation of mutant KRAS proteins as well as compensatory overexpression of wt KRAS from the second allele, another strategy is focal pathway inhibition. This encompasses the combination of KRAS inhibitors with different effector functions, for example, combining KRAS G12C inactive-state inhibitors with KRAS active state or pan Ras inhibitors [207]. However, tumour cells can still achieve bypass signalling by acquisition of additional mutations in proteins downstream of oncogenic KRAS.

Hence, a third route for vertical pathway inhibition is to target signalling proteins situated downstream of mutant KRAS. MEK and ERK inhibitors have already

been tested in combination with KRAS G12C(OFF)i in pre-clinical trials[197]. Another option for combination treatments might be BRAF inhibitors[263], although they have not yet been tested in combination with KRAS inhibitors in the clinic. Further, mTOR inhibitors are also being investigated [196,254,264]. Moreover, the transcription factor Myc, which is downstream of ERK, may provide a target, holding the prerogative of being a central regulator in conveying the output of cytosolic signalling cascades to the nucleus and activating respective transcriptional programmes. In KRAS mutant murine cancer models, it was found that Myc inhibition[265] or degradation[232,233] restrained disease progression.

However, a pivotal caveat of combining two targeted inhibitors is defining a therapeutic window with tolerable toxicity levels. This is especially important for inhibitors not specific to mutant proteins, as these drugs inhibit the proliferation of healthy somatic stem cells, thereby impairing tissue maintenance and function. Further, certain drugs, such as pan-Ras inhibitors may also induce nocuous effects on immunocytes by impeding their Ras-mediated activation signalling required for delivering anti-tumour immunity. Even the first generation of clinically approved KRAS G12C(OFF) inhibitors, which are allegedly mutant-specific, were found to induce high levels of hepatotoxicity in some patients [266,267]. This was speculated to be related to inhibitors also targeting cysteine residues in other proteins as well as increased accumulation of drug conjugated peptides in the liver[37].

A fourth stratagem is the combination of two therapies that target distinct cancer cell intrinsic vulnerabilities. This multi-pronged approach can compound the ontogenesis of bypass signalling, allow for dose reduction of toxicity-prone agents and may even bestow synergistic treatment corollaries. For example, by targeting growth- and survival signalling while also inducing DNA damage via chemo- or radiotherapy. More experimental ideas may include to co-target protein degradation[268], autophagy[268 269,270], cell cycle progression[196,271] or cancer metabolism[268,272].

A fifth avenue for combination treatments with oncogenic KRAS inhibitors is to leverage immunity against cancer. This may be a particularly auspicious accession, because tumours are dynamic entities which can evolve to evade selection pressures. Hence, static therapy regimes may exacerbate treatment responses and increase malignancy over time, ultimately driving patients to a point of terminal disease. However, the immune system likewise comprises a formidable and adaptable regime, capable of contesting an evolving malignancy. Moreover, fostering immune memory may provide long term treatment benefits, preventing disease relapse by combatting persisting residual cancer cells or micro metastasis. One strategy for bolstering the immune system are lines of immunotherapy, where a wide range of treatment lines are being advanced [273-275]. These include cancer vaccines, oncolytic viruses, adoptive immune cell transfer, CAR-T cells, monoclonal antibodies that target cancer cell epitopes, as well as administration of other immune-stimulatory agents, such as interleukins. Another type of immunotherapy are therapeutic antibodies that function as immune check-point blockers (ICB). They bind- and sterically obstruct access to immune-regulatory proteins such as PD-1, PD-L1, or CTLA4, enhancing anti-tumour immunity by preventing immune exhaustion [22,268 276,277]. Unfortunately, only a subset of NSCLC patients respond to ICB when administered as monotherapy with the underlying factors determining therapy response remaining only partially understood [278-282 283]. However, multiple studies across different KRAS G12C mutant preclinical cancer models suggested synergistic treatment benefits of combining KRAS G12Ci with ICB [172,197,212,213,216]. Indeed, combination treatments achieved greater disease control, more complete responders and enhanced immune memory. Another interesting approach for bolstering anti-tumour immunity is by employing the aforementioned SHP2 inhibitors, as SHP2 is a pleiotropic drug target [255,284]. In cancer cells, SHP2i can reinforce inhibition of the oncogenic KRAS signalling pathway. However, SHP2 is also present in the signalling cascades of various immunocytes and other cell types found in the TME. For example, SHP2 is a downstream effector protein of the PD-1 signalling complex in T cells. It was

found that SHP2i in T cells can prevent T cell exhaustion and promote anti-tumour immunity[255]. A shift from M2- to M1 macrophages in the TME upon SHP2i has also been observed [256,284]. Here, SHP2i was found to act in conjunction with the colony stimulating factor receptor (CSFR), as well as SIRPα-, and Siglec-1-mediated signalling cascades. Additionally, a normalisation or reduction of in tumour vasculature has also been reported which may have been induced through SHP2i in the VEGF-signalling pathway of endothelial cells[285,286]. There are currently several ongoing clinical trials, investigating combination treatments with KRAS G12Ci. The two most common drugs currently tested for dual therapies are CPI or SHP2i, but long-term survival data is not yet available [37,287].

1.9 Project rationale

The recently developed lines of therapy targeting mutant KRAS proteins hold the potential to reshape the treatment landscape for many cancer patients with respective driver mutations. The direct and specific inhibition of oncogenic KRAS signalling enables the exploitation of a selective vulnerability within cancer cells while leaving other healthy dividing cells relatively unimpeded; thereby allowing for high treatment efficacy while reducing side effects. However, experimental work as well as evaluation of clinical responses revealed that rewiring of oncogenic signalling circuits and acquisition of further mutations enables these cancers to, often rapidly, develop treatment resistance. For example, clinical data from the recently approved KRAS G12C inhibitor, Sotorasib, showed a median progression free survival in non-small cell lung cancer of approximately 7 months, providing no overall survival advantage compared to conventional chemotherapy [231].

In this project, we want to investigate therapeutic strategies that can combat the development of KRAS G12Ci resistance in lung cancer **(Figure 1.6).** We aim to achieve this by bolstering an anti-tumour immune response, capable of recognising a pan-cancer-cell-archetype, thereby also enabling the elimination of tumour sub-populations that do not respond to targeted therapy directly. Human NSCLC is characterised by an exceptionally high mutational burden compared to other cancer types [68]. On one side the multitude of abnormalities may facilitate immune recognition, while the high degree of genome instability may aid accelerated evolution of immune evasion[288] and drug resistance. A limitation of conventional genetically engineered mouse models (GEMMs) of lung cancer is the oversimplified induction of carcinogenesis. Often achieved via a tissue specific knock out of a TSG, in combination with induced expression of an oncogene. Therefore, traits related to immunogenicity or therapy responses may become distorted in ordinary GEMMs of NSCLC.

To overcome this limitation and provide a clinically relevant setting, we are employing an immunologically hot NSCLC cancer cell line, which was recently established by our group [122]. It was derived from a GEMM that, in addition to inducible **K**RAS G12D expression and **p**53 deletion, further expresses a human **A**POBEC enzyme under the Rosa26 promoter in an immune-compromised **R**ag1 k.o. mouse strain (KPAR). The KPAR1.3 cell line was established from a resulting lung tumour and found to give rise to highly immunogenic tumours when re-engrafted in immune competent mice. Unexpectedly, it was discovered that the immunogenicity of this cell line was mostly contributed to by the aberrant expression of retroviral protein EMV2, rather than APOBEC-induced mutations [122,212]. A further derivative of the initial KPAR1.3 KRAS G12D mutant cell line had been established through Cas9-mediated conversion to a KRAS G12C mutation.

To mimic the emergence of drug resistance in tumours, we developed a model with reporter-traced, co-engrafted isogenic KRAS G12C- and G12D-mutant KPAR1.3 lung cancer cells. In this model the KRAS G12D mutant cells are inherently resistant to G12Ci. Therefore, we imitate one of the resistance mechanisms observed in patients, where, under selection pressure of G12C inhibition, further, sub-clonal mutations in the oncogenic KRAS protein prevent binding of the inhibitor though steric hinderance [231].

Then, first the effects of KRAS G12Ci as monotherapy were tested, assessing induction of cell death and alleviation of immune suppression in the G12C mutant responsive cancer cells. Next, synergistic treatment effects of combining KRAS G12Ci with SHP2i and/or immune-therapeutic antibody a-PD-1 were investigated. Both additional therapies were found to foster an anti-tumour immune response [255,261,284,289-291]. Here, we were able to generate complete responses in mice and assessed the presence of long-term immune memory against cancer cells. The presence of which may indicate benefits contributing to long term survival in patients. Moreover, underlying mechanisms contributing

to immune-mediated recognition and elimination of cancer cells were investigated, employing a multi-omics-based approach.

Understanding how combination treatments can be employed to promote bystander killing of resistant tumour cell sub-populations could contribute to combating the development of therapy resistance in patients.

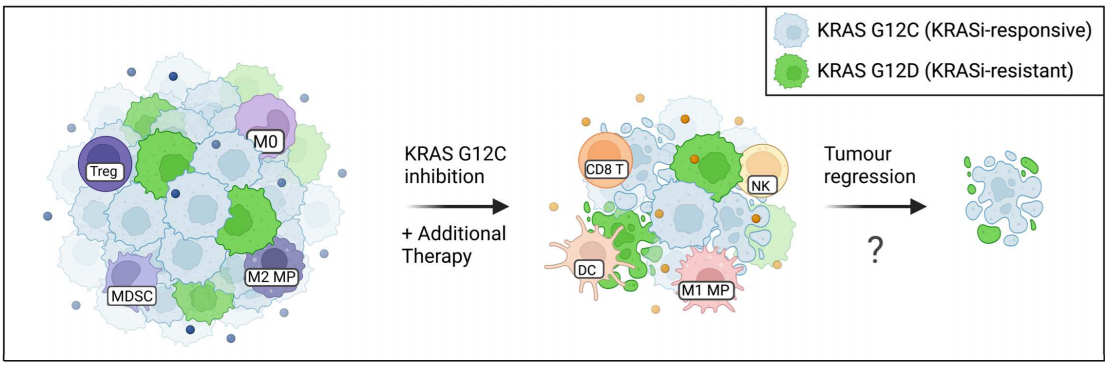


Figure 1.6 Schematic of project rationale. Left: tumour comprised of KRAS G12Ci-responsive KRAS G12C (blue/BFP$^+$)- and KRAS G12Ci-resistant KRAS G12D (green/Luc-eGFP$^+$) mutant KPAR1.3 cells, indicative of a tumour during the development of drug resistance. Purple cells indicate exemplary immune cell populations indicative of an immunologically cold TME in an established tumour: Treg: CD4$^+$ T-regulatory cell, MO: monocyte, M2 MP: macrophage presenting with an alternatively activated type 2 phenotype, MDSC: Myeloid-derived suppressor cells: a heterogeneous collection of, often immature, myeloid cells, capable of supressing anti-tumour directed T cell responses. Middle: Panel indicated therapy-induced cancer cell killing as well as - conversion to an immunologically hot TME. Orange cells indicate exemplary anti-tumour-oriented immune populations: CD8$^+$ T: CD8$^+$ cytotoxic T cell; NK: natural killer cell; M1 MP: macrophage presenting with an anti-tumour directed, pro-inflammatory phenotype, DC: Dendritic cell. Right: Tumour regression achieved through synergistic treatment effects, capable of bolstering an ani-tumour immune response.

Chapter 2. Materials & Methods

2.1 Cloning strategy for reporter-encoding plasmids

Two lentiviral plasmids, pLARRY-eGFP[292] (Plasmid #140025, addgene) and pFUGW-FerH-ffLuc2-eGFP[293] (Plasmid #71393, addgene), were purchased as bacterial stabs, then amplified and purified using the EndoFree Plasmid Maxi Kit (QIAGEN, cat. no. 12362). To convert the enhanced green fluorescent protein eGFP in the pLARRY-plasmid to enhanced blue fluorescent protein (eBFP), two separate nucleotides in the coding sequence were altered by site-directed mutagenesis using the In-Fusion Snap Assembly Master Mix (TaKaRa, cat. no. 638947) kit and protocol together with the custom primers listed below (Synthesised by Sigma Custom DNA Oligo Synthesis;
Table 2.1).

Conversion of AA	Strand	Sequence [5'-3']
Tyr67 to His	Fwd	ccctgacccacggcgtgcagtgcttcag
	Rev	cgccgtgggtcagggtggtcacgagg
Tyr146 to Phe	Fwd	gtacaacttcaacagccacaacgtctatatcatg
	Rev	ctgttgaagttgtactccagcttgtgccc

Table 2.1 Oligos for site directed mutagenesis.

For the PCR rolling cycle amplification step in the protocol provided with the In-Fusion Snap Assembly Master Mix, the following conditions were used **(Table 2.2)**.

Step	PCR cycles	Temp [°C]	Duration [s]
Initial Denaturation	-	95	180
25 cycles	Denaturation	95	30
of PCR amplification	Annealing	66	15
	Elongation	72	45
Final elongation	-	72	300

Table 2.2 PCR conditions rolling cycle amplification.

Edited plasmids were then re-transformed in Stbl2 E. coli using a standard heat-shock protocol. Here, 50 µl of the bacteria suspension was thawed on ice for 10 min, 500 ng of plasmid was added, and bacteria were incubated on ice for another 20 min. Successively, bacteria were heat shocked by incubation at 42°C for 45 s and placed back on ice for another 3 min. Next, 1ml of Lysogeny broth (LB), a common media for growing bacteria, was added, and cultures were incubated in a heat block at 37°C and 200 rpm for 40 min. Colonies containing the plasmid were then selected for by spreading the bacteria suspension agar plates containing 50 µg/ml ampicillin and incubating respective plates at 30°C for 18 h. Resulting colonies were then picked from agar plates into culture tubes containing 4 ml LB-media containing 50 µg/ml ampicillin and amplified in a shaking incubator at 30°C and 200 rpm for 12-16 h. Plasmids were purified for downstream applications using the QIAprep Spin Miniprep Kit (QIAGEN, cat. no. 27104).

Next, a distinct barcode was also cloned into the C-terminal end of the fluorophore-encoding sequence for both pLARRY eGFP and pLARRY eBFP. This was done utilising the Gibson Assembly Cloning Kit (NEB, cat. no. E5510S) with protocol (NEB, E5510) and the following barcode fragments (Synthesised by Sigma Custom DNA Oligo Synthesis; **Table 2.3**).

Barcode (BC)	Strand	Sequence [5'-3']
eGFP_BC	Fwd	gtaaccgttgctaggagagaccataGCGCTCGCGCGATATAACTC
	Rev	GAGACTTAGTACCTAGGTGTtgtctagaggatccgatatcgccac
eGFP_BC	Fwd	gtggcgatatcggatcctctagacaACACCTAGGTACTAAGTCTC
	Rev	GAGTTATATCGCGCGAGCGCtatggtctctcctagcaacggttac

Table 2.3 Barcode sequences.

In the DNA sequences above, lower case letters indicate sequences overlapping with plasmid backbone and capital letters indicate the barcode sequence.

The eGFP-encoding sequence in the pFUGW-FerH-ffLuc2-eGFP plasmid was also cloned out to generate a plasmid encoding only a luciferase reporter. This was achieved via restriction digest with the enzymes Bam-Hl and Xho-l which cut on the 5' and 3' end of the eGFP encoding sequence on the plasmid respectively. To re-ligate the pFUGW-FerH-ffLuc2 plasmid, a short linker sequence was introduced (Synthesised by Sigma Custom DNA Oligo Synthesis; **Table 2.4**), which contains complimentary restriction sites and was also digested with both enzymes.

Oligo-linker	Strand	Sequence [5'-3']
ffLuc-only	fwd	aaaaggatccatagtaaccaactttcttgtacaaagttgtgatgatccaatctcgaggggg
	rev	ccccctcgagattggatcatcacaactttgtacaagaaagttggttactatggatcctttt

Table 2.4 Linker oligonucleotide sequences.

The plasmid backbone and linker fragment were re-ligated at a 1:10 molar ratio using the Quick Ligation™ Kit (NEB, cat. no. M2200S) and protocol (NEB, M2200). Successful alteration of the plasmid sequences at each of the cloning steps was confirmed using the sanger sequencing service at GENEWIZ with the primers listed below (Synthesised by Sigma Custom DNA Oligo Synthesis; **Table 2.5**).

Primer	Sequence [5'-3']
Tyrosine to Histidine confirmation	gcgacgtaaacggccacaagtt
Tyrosine to Phenylalanine confirmation	tccaggagcgcaccatcttctt
Barcode integration confirmation	tgagcaaagaccccaacgag
eGFP deletion confirmation	atgtggccagccaggttacaac

Table 2.5 Sequencing primers confirming nucleotide substitution.

2.2 Cell culture

Cell lines were cultured in Dulbecco's Modified Eagle Medium (DMEM) (Gibco, cat. no. 41966052) with added 10% FCS, 1.5% Glutamine, 1% Penicillin/Streptomycin (P/S). For propagation, cells were dissociated by washing once with DPBS (Gibco, cat. no.14190144) and successively incubating in Trypsin solution (Gibco, cat. no.25200072) for 2-5 min at 37°C. Digestion was stopped by re-suspending cells in culture media.

To establish new primary cell lines from tumours, dissected tumour tissue was either placed directly into a culture dish or tissue was mechanically and enzymatically dissociated prior to culturing using a tumour dissociation kit (Miltenyi Biotec, cat. no. 130-096-730). Resulting cultures were then cultivated using DMEM-F12, supplemented with 10% FCS, 1μM Hydrocortisone, 20 ng/ml EGF, 50 ng/ml GF and 1% PS. In addition, KRAS G12C inhibitor resistant subpopulations were selected continuously culturing respective cultures with a low concentration of the KRAS inhibitors as indicated in respective experiments in the result section.

2.3 Generation of reporter-traced lines

To transduce KPAR1.3 lines[294] with reporter constructs, lentivirus was produced by co-transfecting HEK293T cells with the reporter-encoding lentiviral plasmids pLARRY-eGFP, pLARRY-eBFP, pFUGW-FerH-ffLuc2-eGFP, or pFUGW-FerH-ffLuc2, together with packaging plasmids pCMV-dR8.2 and pCMV-VSV-G using the jetPRIME® transfection kit (Polyplus, cat. no. 101000015). After 48 hours, virus-containing supernatant was collected and filtered using a 0.45 μm filter. KPAR1.3 were infected in 6 well plates via spinning infection (add virus-containing supernatant to 6 well plates with cells, spin plates in centrifuge at 600 rpm for 90 min at RT). Cells expressing the fluorescent reporter proteins were then single cell cloned in 96 well plates using FACS.

2.4 In *vitro* assays for screening KPAR1.3 subclones

For growth-rate-, viability-, and luciferase activity assays, to screen KPAR1.3 sub-clones, cells were plated into cell culture-treated 96 well plates with 1500 cells in 100 μl of standard cell culture media, as described above in cell culture techniques.

2.4.1 Viability assays

For viability assays, the KRAS G12C inhibitor MRTX849 (Mirati Therapeutics), MEK inhibitor Trametinib (Selleckchem), and SHP2 inhibitor RMC-4550 (Revolution Medicines) were added to the wells in the 96 well plate in a serial dilution as indicated in respective experiments. Drug-response was then measured by adding 5 µl CellTiter-Blue® (Promega, G8081) to all wells, incubating plates for 90 min at 37°C, and measuring colour shift using the EnVision® 2105 multimode plate reader (PerkinElmer).

2.4.2 Growth-rate assays

For growth-rate assays, 96 well plates were transferred to an S3 IncuCyte (Satorius) immediately after plating and wells were imaged at 20 x magnification at a 6h interval for upto 5 days or until confluency was reached. Confluency over time was determined using the appurtenant S3 Live-Cell Imaging & Analysis Software (Satorius).

2.4.3 In vitro luciferase assays

In *vitro* luciferase activity of pertinent KPAR1.3 subclones was determined using the Pierce™ Firefly Luciferase Glow Assay Kit (Thermo Fisher, cat.no 16176), following the manufacturers' protocol. Here, bioluminescence was measured employing an EnSight® multimode plate reader and corresponding software (PerkinElmer).

2.5 Time course assays

30,000 KPAR1.3 cells were plated in 6 well plates and treated with inhibitors as indicated in respective experiments. Inhibitors were added to respective wells 48 h, 24 h, or 6 h prior to sample extraction. For the “0 h” time point, DMSO was added as a negative control. Prior to RNA- or protein extraction, plates were sat on ice and wells were washed once with pre-chilled PBS.

2.5.1 Western blots

For protein extraction, cells were lysed using cell lysis buffer (Cell Signalling, cat. no. 9803) supplemented with cOmplete EDTA-free Protease Inhibitor Cocktail (Sigma, cat. no. 4693159001), 25 mM NaF, and 1mM PMSF. Cell lysates were scraped off wells and spun down in a table centrifuge at 15,000 rpm for 15 minutes at 4°C. The protein concentration in the supernatant was then determined using the DC protein assay kit (Bio-Rad, cat. no. 5000111) and normalised across samples. 20 ug of protein were then prepared with 4x NuPAGE LDS Sample Buffer (Thermo Fisher, cat. no. NP0007), separated on NuPAGE 4-12% Bis-Tris protein gels (Thermo Fisher, cat. no. NP0335BOX) and thereafter transferred to PVDF membranes (Merck Millipore, cat. no. IPFL00010). These were incubated with primary antibodies, targeting the proteins of interest **(Table 2.6)**, and successively appropriate HRP-conjugated secondary antibodies. Lastly, protein expression was visualised via bioluminescent signal intensity, using Immobilon Western HRP substrates (Merck, substrates for various chemiluminescence intensities) and Hyperfilms (GE healthcare, cat. no. 28-9068-37).

Target	Company	Cat. no.
Vinculin	Sigma-Aldrich	V9131
AKT	Cell Signalling	2920
pAKT (S473)	Cell Signalling	4060
ERK	Cell Signalling	9107

pERK1/2 (T202/Y204)	Cell Signalling	9101
S6	Cell Signalling	2317
pS6 (Ser235/236)	Cell Signalling	2211

Table 2.6 Western blot antibodies.

2.5.2 qRT-PCRs

For RNA extraction, 350 μl RLT lysis buffer (Qiagen, cat. no. 79216) supplemented with 1:1000 2-Mercaptoethanol (Sigma Aldrich, cat. no. M6250-100ML) was added to each sample and samples were scraped off wells. RNA was then extracted using the RNeasy Mini Kit (Qiagen, cat. no. 74106). RNA concentration was then measured using the NanoDrop 2000 UV Visible Spectrophotometer (Thermo Scientific, cat. no. ND2000CLAPTOP) and normalised across samples. Next, cDNA was synthesised using the iScrip cDNA Synthesis Kit (BioRad, cat. no. 1708890). qPCR reactions were then prepared by combining 5 μl of 2x Fast SYBR Green Master Mix (Applied Biosystems, cat. no. 4385618), 5 ng cDNA, 1 μl of 2μM forward/reverse primer mix **(Table 2.7)** and nuclease-free water (Invitrogen, cat. no. 10609823) was added to a final volume of 10 μl. Relative gene expression was calculated via the △△CT formula, normalising to the average of 2 housekeeping genes.

Gene	Strand	Sequence [5'-3']	Function
Hsp90	Fwd	agattccactaaccgacgcc	Housekeeping gene
	Rev	tgctctttgctctcaccagt	
Sdha	Fwd	tcgacaggggaatggtttgg	Housekeeping gene
	Rev	tcatactcatcgacccgcac	
Gapdh	Fwd	caagctcatttcctggtatgaca	Housekeeping gene
	Rev	ggatagggcctctcttgctc	
Dusp5	Fwd	agtgtggaaagcccgttctc	KRAS downstream target

	Rev	gaaggatttcaaccgggcca	
Dusp6	Fwd	gagccaaaacctgtcccagt	KRAS downstream target
	Rev	gtgacagagcggctgatacc	
Etv4	Fwd	ccatggagagcagtgccttt	KRAS downstream target
	Rev	ctgctgttctgccctggaa	
Etv5	Fwd	tgatgatgagcagtttgtccca	KRAS downstream target
	Rev	tggctacaggacgacaactc	
Stat2	Fwd	ccctggtcgacctattgctg	KRAS downstream target
	Rev	caagaactttgctccagccg	
Myc	Fwd	ccggggagggaatttttgtct	KRAS downstream target
	Rev	gaggggcatcgtcgtgg	

Table 2.7 qRT-PCR primers. All primers target transcript-derived cDNA of the species Mus musculus.

2.6 In *vivo* techniques

All mouse experiments were conducted in congruence with animal welfare guidelines of the Francis Crick Institute as well as national regulations. Study plans were performed in accordance with a project licence approved by the UK Home Office

Unless otherwise indicated, 8- to 12-week-old mice of the glowing-head mouse strain[295] were used for all experiments. For subcutaneous engraftment of cancer cells, 150,000 KPAR1.3 cells were injected into the lower left flank in a volume of 100μl consisting of 50% PBS, 50% Geltrex LDEV-Free Reduced Growth Factor Basement Membrane Matrix (Thermo Fisher, cat. no. A1413202). Throughout experiments, the tumour-engraftment-rate was 100%. Tumour growth was measured twice weekly, via calliper and the tumour volume calculated using the formula *[Length x Width^2]/2*. Mice were treated with lines of anti-cancer drugs when the average diameter of tumours within a cohort reached 150 mm^3 – 160 mm^3.

Drug	Function	Conc. [mg/kg]	Company
MRTX849	KRAS G12C(OFF)i	50 mg/kg	Mirati Therapeutics
RMC-4998	KRAS G12C(ON)i	100 mg/kg	Revolution Medicines
RMC-4550	SHP2i	30 mg/kg	Revolution Medicines
anti-rat PD-1	CPI	10 mg/kg	BioXCell (cat. no. BE0146)

Table 2.8 Drugs employed for in *vivo* therapies. MRTX849 is also known under the commercial names 'Adagrasib' and 'Krazati'.

The oral drugs (MRTX849, RMC-4998, and RMC-4550) were administered via oral gavage. They were prepared in 10% Captisol buffer, which in turn was prepared from 50% of 20% w/v Captisol solution dissolved in H_2O and 50% of 100 mM sodium citrate buffer pH 5. The anti-PD-1 therapeutic ab was prepared in PBS and administered via intraperitoneal injection. The combinations- and duration of treatments will be indicated in respective experiments.

Alternatively, in some experiments RMC-4998 and RMC-4559 were reconstituted in 10% Dimethyl sulfoxide (DMSO) (Sigma, cat. no. D2650), 20% Poly(Ethylene Glycol) average MN 400 (PEG400) (Sigma, cat. no. 202398), 10 % Kolliphor HS 15 (Sigma, cat. no. 42966-1KG), and 60 % of 2% (Hydroxypropyl)methyl cellulose (Sigma, cat. no. 09963-25G) in a 50 mM Sodium Citrate buffer pH 4.

For in *vivo* imaging techniques, mice were first anaesthetised via inhalation of 2% - 2.5% isoflurane, vaporised in O_2. In *vivo* imaging of the Luciferase-eGFP expressing KPAR1.3 KRAS G12D cells was done by intraperitoneal injection of 100 µl 30 µg/ml XenoLight D-Luciferin (PerkinElmer, cat. no. 122799), dissolved in PBS. Mice were then imaged using an In Vivo Imaging System (IVIS) SpectrumCT scanner (PerkinElmer) and resulting data was analysed using the associated Living Image Software (PerkinElmer, versions 4.4 – 4.5). Tumour bearing lungs were imaged using a Quantum GX2 CT scanner (PerkinElmer)

and tumour burden was quantified using the Analyse 12.0 software and a standardised workflow[296].

For studies on subcutaneous tumours, mice were culled using schedule 1 method, when the average diameter of the tumours reached an average diameter reached 1.2 cm, or 1.4 cm when mice were receiving treatments.

Mice that were able to reject their primary subcutaneous tumour and remained tumour free for approximately 4 weeks after the treatment period ended, were considered CRs. These mice were then re-challenged by injecting 150,000 KPAR1.3 Luciferase-eGFP KRAS G12D cells in the opposite flank, and tumour growth was again monitored as previously described.

2.7 Bulk-RNA sequencing

Tumours were engrafted subcutaneously as described above and tumour volume was measured via calliper. Mice were then stratified into therapy groups and treated for the duration indicated by the respective experiments. On the day of sample collection, tumours were extracted, dissociated into a single cell suspension and red blood cells were lysed as described in the flow cytometry section. For the second RNA-seq experiment, an additional processing step was added, where CD45 positive cells were removed, employing a positive selection magnetic pulldown, using the mouse CD45 microbead kit (Miltenyi Biotec, cat. no. 130-052-301). This was done to remove auto-fluorescent immune cells which had previously appeared as false positive events in the $eBFP^+$ sort gate. Thereafter, the cell suspension was filtered through 45 μm cell strainer snap caps (Falcon, cat. no. 352235) into Round-Bottom Polypropylene Test Tubes (Falcon, cat. no. 352063). These were taken to the flow cytometry core facility who kindly helped with sorting the cell populations of interest, as indicated by respective experiments in results section, into chilled 1.5 ml Eppendorf tubes (Eppendorf, cat. no. 0030121503). Samples were immediately spun down at 300g, the supernatant removed and the pellet then snap frozen in

liquid nitrogen. The next day, RNA was purified from each sample individually, using the RNeasy Micro Kit (Qiagen, cat. no. 74004). The yield was determined utilising the NanoDrop 2000 UV Visible Spectrophotometer (Thermo Scientific, cat. no. ND2000CLAPTOP). Samples were then submitted to the advanced sequencing core facility, who kindly performed the library preparation using the Watchmaker RNA Library Prep Kit with Polaris Depletion kit (Watchmaker Genomics, cat. no. 7BK0002-096), as well as NGS sequencing of the samples.

For the analysis of sequencing results, first, sequencing adaptor sequences were removed, reads were aligned to a mouse reference genome and reads for each transcript were counted. For this, samples were run through the nf-core/rnaseq pipeline, version 3.14.0 (https://nf-co.re/rnaseq/3.14.0/). For the aligner, star_rsem was selected and samples were aligned to the mouse reference genome rendition Mus_musculus.GRCm38.95.
The output file was then read into RStudio (2022.07.1 Build 554) where the DESeq2 pipeline (Bioconductor, version published 04/30/2024) was followed to conduct quality controls, assess differential gene expression between treatment groups and perform gene set enrichment analysis (GSEA). For the later, hallmarks gene set collection was sourced from the msigdb website (https://www.gsea-msigdb.org/gsea/msigdb ; gene set ‘H’).

2.8 Flow cytometric techniques

2.8.1 Assessing reporter stability of KPAR1.3 subclones in *vitro*

To assess BPF and GFP reporter stability under stress conditions, 30,000 cells of transduced KPAR1.3 sub-clones were seeded into 6 well plates and grown to over-confluency and until the media had turned acidic, assessed via colour shift of the pH indicator phenol red. Cell lines were then trypsinised as described above, washed once using PBS, resuspended in fluorescence-activated cell sorting (FACS) buffer (PBS with 2% FBS, 1mM EDTA) and filtered through a 45 μm nylon strainer into a FACS tube. DRAQ7 viability dye (Fisher Scientific, cat.

no. D15105) was then added (1:100) and reporter stability was detected using a BD LSRFortessa™ X-20 Cell Analyzer (BD Biosciences) and the corresponding BD FACSDiva™ Software. Subsequent reporter-expression quantification was performed using the BD FlowJo analysis Software (version 10.8.1 - 10.8.3).

2.8.2 Quantifying fraction of KPAR1.3 KRAS G12D cells in *vivo*

The fraction of KRAS G12Ci resistant, Luc-eGFP-expressing KPAR1.3 KRAS G12D cells of tumours resected from mice of different treatment groups was determined via flow cytometry. Here, tumours, cells were first manually cut into small pieces and then enzymatically dissociated using the Tumour Dissociation Kit, mouse (Miltenyi Biotech, cat. no. 130-096-730). Subsequently, the cell suspension was filtered through a 70 μm MACS SmartStrainer (Miltenyi, cat. no. 130-110-916) and red blood cell lysis was then performed by incubating with 5 ml ACK Lysing Buffer (Thermo Fisher Scientific, cat. no. A1049201) for 5 min. Cells were then washed once with FACS buffer, filtered into 45 μm cell strainer snap cap test tubes (Falcon, cat. no. 352235) and DRAQ7 (1:100) was added as viability dye. Sample acquisition was performed as described above.

2.8.3 Multiplex spectral immune phenotyping of therapy-treated tumours

A cell suspension of tumours extracted from therapy-treated mice was prepared as described in **section 2.8.2**. Immune-phenotyping of tumour-draining lymph nodes (tdLNs) was performed as in **section 2.8.3**, but no enzymatic dissociation or ACK lysis were performed. tdLNs were directly pushed through 70 μm MACS SmartStrainers, cell suspension was washed once, and samples were then added to the 96 well plate for staining. A spleen was also collected, for single staining controls. It was also directly pushed through the aforementioned 70 μm MACS SmartStrainer without additional digestion, ACK lysis was performed by adding 7 ml of ACK lysis buffer and incubating for 8 min and cells were washed once with FACS buffer.

Next, all samples were transferred to a low-attachment conical-bottom 96 well plate and pellet sizes were normalised to approximately $1.5*10^6$ cells per well. For staining of the samples, cell suspensions were first prepared by adding 100 µl 1:100 CD16/CD32 FC blocking ab in PBS and incubating for 15 minutes at 4°C. In the meantime, an staining panel master-mix for extracellular staining was prepared in PBS on ice, with the antibodies and viability dye listed in **Table 2.9**. Samples were then stained with 100 µl of the ab master-mix for 20 minutes at RT. Single staining controls of spleen or UltraComp eBeads Compensation Beads (Invitrogen, cat. no. 01-2222-42) were also prepared, however, stained beads were kept in FACS buffer after staining, without the fixation steps, as these would disintegrate the beads. Samples were then washed twice with 170 µl PBS and successively fixed and permeabilised with 110 µl of Foxp3 Fixation/Permeabilization Buffer (Invitrogen, cat. no. 00-5523-00) for 30 min at 4°C. Next, samples were washed once with 110 µl of provided wash Permeabilization Buffer (Invitrogen, cat. no. 00-5523-00) and then stored in the dark at 4°C over night.

The next day, antibodies of the intracellular staining master mix (**Table 2.9**) were prepared in PBS, samples were stained for 20 minutes at RT and thereafter washed 3x with of wash Permeabilization Buffer (invitrogen, cat. no. 00-5523-00). Cells were then resuspended in FACS buffer, transferred to a U-bottom, low-attachment 96 well plate and kept at 4°C until analysis.
For immune-phenotyping, samples were analysed on the Cytek Aurora spectral flow cytometer and initial spectral unmixing was performed using the instrument-associated Cytek SpectroFlow Software. Further compensation and marker expression analysis was then performed using the FlowJo software (versions 10.8.1 – 10.10.1). Analysis was done together with the kind help of Claire Pillsbury.

Target	Fluorophore	Ab clone	Cat. No.	Company
CD107α	BUV395	1D4B	565533	BD Biosciences
B220	BUV496	RA3-6B2	612950	BD Biosciences

CD11c	BUV563	N418	749040	BD Biosciences
Ki-67	BUV615	SolA15	366-5698-82	eBioscience
TIM3	BUV661	RMT2-23	753149	BD Biosciences
CD62L	BUV737	MEL-14	612833	BD Biosciences
CD3	BUV805	17A2	569192	BD Biosciences
CD44	BV421	IM7	103039	BioLegend
CD11b	BV480	M1/70	566117	BD Biosciences
CD69	BV510	H1.2F3	104531	BioLegend
CD19	BV570	6D5	115535	BioLegend
CD103	BV605	2E7	121433	BioLegend
PD-1	BV650	J43	569506	BD Biosciences
Ly6G	BV711	1A8	127643	BioLegend
Ly6C	BV785	HK1.4	128041	BioLegend
CD8α	Spark Blue 550	53-6.7	100779	BioLegend
H-2Kb	NFB610/70S	AF6-88.5.5.3	17836316	Invitrogen
CD45	PerCP	30-F11	103129	BioLegend
CD49b	BB700	DX5	568015	BD Biosciences
MHCII	PerCP-eFluor710	M5/114.15.2	46-5321-82	eBioscience
CD71	RB780	C2	755614	BD Biosciences
LAG3	PerCP/Fire780	C9BV7	125251	BioLegend
PD-L1	PE	10F.9G2	124307	BioLegend
MerTK	PE/Dazzle 594	2B10C42	151523	BioLegend
NK1.1	PE/Cy5	PK136	108715	BioLegend
CD64	PE/Cy7	X54-5/7.1	139313	BioLegend
CTLA-4	PE/Fire810	UC10-4B9	106335	BioLegend
Arginase 1	eFluor450	A1exF5	48-3697-82	eBioscience
FOXP3	eFluor660	FJK-16	50-5773-82	eBioscience
CD86	AF-700	GL-1	105023	BioLegend
Viab. Dye	Zombie NIR	-	423105	Biolegend
SIRPα	APC/Fire750	P84	144029	BioLegend
CD4	APC/Fire 810	GK1.5	100479	BioLegend

Table 2.9 Spectral flow staining panel. Antibodies for intracellular staining are demarcated in bold font.

Analysing the acquired multiplex spectral flow cytometry data, a one-way ANOVA test was performed to assess whether significant differences between vehicle- and treated samples were present. Here, the distribution of individual samples around the sample mean within each treatment group as well as the variation of the standard deviation (SD) between treatment groups were taken

into account to allow for appropriately fitted statistical modelling. If samples within each treatment group followed a normal Gaussian distribution and the range of SD was similar between treatment groups, an ordinary ANOVA test was applied. If sample distribution within each treatment group was unevenly distributed, a non-parametric Kruskal-Wallis ANOVA test was applied. If samples were normally distributed but the range of SD differed between treatment groups, a Brown-Forsythe and Welch ANOVA test was selected.

2.9 General immunohistochemistry techniques

2.9.1 Immunohistochemistry on frozen tumour sections

For immunofluorescent staining of frozen sections, tumours were first prepared by incubation in double distilled H_2O containing 20% sucrose for 20 min and were successively embedded in scaffolds filled with Tissue Tek OCT compound (Labtech, Sakura, cat. no. 16-004004). Tumours were then immediately flash-frozen using liquid nitrogen. 5 μm thick sections were cut from the resulting frozen blocks using an OTF 6000 Cryostat (Bright Instruments) and mounted onto objective slides. Tissue sections were then fixed with 4% Methanol-Free Formaldehyde (Cell Signalling, cat. no. 47746s) for 10 min. Following fixation, sections were washed twice using DPBS (Gibco, cat. no. 14190144) and a third wash was done using PBS containing 0.05% Tween (PBS-T). Sections were next blocked in two successive steps, first 30 min incubation with SuperBlock™ Blocking Buffer (Thermo Scientific, cat. no. 37515), second with DPBS-T containing 1.6% FCS and 1% Mouse BD Fc Block™ (CD16/CD32 ab, BD Biosciences, 553142) for 10 min. Sections were then successively incubated with primary antibodies **(Table 2.10)** for 1h (1:200) as well as appropriate fluorophore conjugated, secondary antibodies for 45 min (1:250).
Next, 20 μl of ProLong™ Gold Antifade Mountant with DAPI (Thermo Fisher, cat. no. P36935) was then applied and the stained tissue section was sealed with a coverslip. Sections were imaged using either an Inverted Zeiss LSM 710 confocal (Zeiss) microscope or a ZEISS Axio Imager 2 (Zeiss) microscope and

ZEN Black software (Zeiss) software. Images were then analysed using the open-source FIJI software (2.1.0/1.53c).

Antigen target	Host-species	Company	Cat. no.
Firefly Luciferase	rabbit	Abcam	ab185923
eGFP and eBFP	goat	Abcam	ab6673

Table 2.10 Primary antibodies for staining frozen sections.

2.9.2 Immunohistochemistry on FFPE tumour sections

Staining of Formalin-Fixed Paraffin-Embedded (FFPE) tissue sections was performed with the kind help of the Experimental Histopathology (EHP) core facility at the Francis Crick Institute. For tissue preparation, subcutaneous tumours or tumour-bearing lungs were fixed in 10 % neutral buffered formalin (NBF) for 48h and successively stored in 70% EtOH. Samples were then embedded in paraffin wax using a Tissue-Tek VIP® 6 AI processor (Sakura) and 3 μm thick sections were cut and mounted onto glass slides. Slides were baked at 60°C for 1 h to adhere tissue sections to slides and melt the wax.

For techniques involving the detection of specific antigens, slides were then transferred to the EHP core facility internal Leica Bond Rx platform (Leica, serial number 3498240). Here, slides were further de-waxed using a ready-to use solution prepared by the core facility. A 0.1% BSA solution for protein blocking and a 3% hydrogen peroxide solution for inhibiting endogenous peroxidases were then applied to prepare the slides for staining.

2.9.2.1 Standard immunofluorescence tissue staining

For immunofluorescent stainings of up to four colours, which did not require the multiplexing approach described in **0**, antigens were stained consecutively by incubating respective HRP-conjugated antibodies with Opals. These are

fluorescent dyes which are permanently deposited onto the tissue section where HRP conjugated antibodies are located. Between each staining of an antigen, slides were exposed to an ab stripping step and antigen retrieval, where slides were heated at 95°C for 20 minutes using either Epitope Retrieval Solution 1 or Epitope Retrieval Solution 2 (Leica, AR9961 or AR9640 respectively). The opals were used in varying combinations across experiments but are all listed in the next section. Finally, nuclei were then stained with DAPI (Thermo Scientific, cat. no. 62248) and cover slips were applied using Prolong Gold Antifade reagent (Invitrogen, cat. no. P36934).

2.9.2.2 Multiplex immunofluorescence tissue staining

When staining more than four markers (including DAPI) on the same slide, a multiplex approach established by the EHP core facility was employed. Here, antigens were again stained consecutively using opals, as described above. To determine the ideal order in which to stain the respective antigens, the STP kindly performed several optimisation runs on test sections. The antibodies are listed in the correct order in **Table 2.11**. For secondary antibodies recognising primary rabbit-derived antibodies, the rabbit bond polymer Novolink Max Polymer (Leica, cat. no. RE7260-CE) was used and for goat-derived antibodies, the ImmPRESS HRP Horse Anti-Goat IgG Polymer Detection Kit (Vector, cat no MP-7405) was utilised. Again, nuclei were then stained with DAPI and slides were mounted using the Prolong Gold Antifade reagent. Slides were scanned on the PhenoImager HT (Akoya, serial number VP2143N2122) in MOTiF scanning mode using the software Vectra Polaris (version 1.0.13) and unmixing of the fluorescent spectra was performed with an appurtenant InForm (version 2.6.0) software.

Position	Ab	Species	Supplier	Cat. no.	Opal	Cat. no.
1	GFP	Rb	Thermo Fisher	A-6455	520	FP1487001KT
2	CD4	Rb	Abcam	ab183685	480	FP1500001KT
3	cCasp3	Rb	Cell Signalling	9579S	750	FP1488001KT

4	CD8	Rb	Abcam	ab217344	690	FP1497001KT
5	Luciferase	Gt	Novus	NB100-1677	620	FP1495001KT
6	Ki67	Rb	Abcam	ab15580	540	FP1494001KT
7	PD-1	Rb	ab214421	EPR20665	780	FP1501001KT

Table 2.11 Primary antibodies used for IF stainings on FFPE tumour sections. All opals were supplied by Akoya.

2.9.2.3 Haematoxylin and Eosin (H&E) tissue staining

Haematoxylin and Eosin (H&E) staining was performed using a Tissue-Tek Prisma automated slide stainer (Sakura, item code: 6132) together with standardised core facility-internal protocols.

Chapter 3. Establishing a model system mimicking the development of drug resistance

In the last decade, it has become evident that the role of oncogenic KRAS signalling exceeds mere mediation of cancer cell-intrinsic growth- and survival signalling. It is further involved in instigating immune suppression in the TME through various mechanisms, which may exacerbate the scope of cancer treatment responses. Cancer therapy with the newly approved KRAS G12C inhibitors holds a unique potential to benefit patients, not only through drug mediated cancer cell killing, but also by sensitising the TME to other lines of immune-related therapies. However, despite initial auspicious treatment responses to KRAS G12Ci in most NSCLC patients, the rapid development of drug resistance hampers the efficacy of the newly developed KRAS G12C inhibitors.

In this project, we aim to develop a mouse model system that allows us to study therapy combinations that can enhance the therapeutic potential of the newly developed KRAS G12C inhibitors and combat the development of treatment resistance. To mimic tumours containing a KRAS G12C inhibitor-resistant subpopulation, isogenic KPAR1.3 cell lines, harbouring either a KRAS G12C- or G12D mutation, are co-engrafted in experimental mice. To allow the distinction of the two KRAS mutant KPAR1.3 cell lines in both, in *vitro* and in *vivo* experiments as well as across different downstream applications, they were transduced with reporter constructs.

As this project aims to study the role of immune-mediated cancer cell killing, it is important to avoid evoking an artificial immune response, targeting exogenous neoantigens, derived from the expressed reporter constructs [293,297]. To counteract this possibility, the immune-competent glowing head (GH)- mouse strain with a C57BL/6J was employed in this project [295]. These mice constitutively express a Luciferase-eGFP fusion protein in the anterior part of the pituitary gland, which is not immune excluded. Thereby increasing immune

tolerance towards this reporter. The GH strain further has an albino coat, due to a homozygous loss-of-function mutation in the tyrosinase gene, which encodes for an enzyme that is responsible for fur pigmentation. This unpigmented fur facilitates “In Vivo Imaging System” (IVIS) IVIS scanning, due to the decrease in photon absorption in white hair.

This first chapter describes the establishment of the model system utilised in this project to study the effects of different treatment schemes on the TME and drug-resistant tumour subpopulations.

3.1 Generating reporter-traced cell lines

Initially, KPAR1.3 cell lines were transduced with an array of reporters which would allow to adapt this model system across experiments as required (**Figure 3.1a**). The newly established cell lines were then screened through various assays to assure their suitability for forthcoming in *vivo* treatment studies. Throughout the forthcoming chapter, exemplary plots for the characterisation of the sub-clonal cell lines, which were ultimately chosen for in *vivo* studies are shown.

The KRAS G12D mutant cancer cells were introduced into tumours as a KRAS G12Ci resistant subpopulation. It was of interest to quantify the fraction of KRASi-resistant cells in various downstream applications as well as to monitor the growth dynamics of this population over time in *vivo*. For this reason, we transduced the KRAS G12D mutant KPAR1.3 cell line with an enhanced green fluorescent protein (eGFP)-Luciferase fusion protein reporter. The eGFP allows for unambiguous segregation of the KRAS G12D population through application such as flow cytometry, especially, as it its fluorescence is relatively bright, compared to other fluorescent proteins (FPs) [298]. Luciferase is an enzyme capable of producing bioluminescence through the breakdown of its substrate, d-luciferin. As only the G12D mutant KPAR1.3 cells express Luciferase, we can

ascertain the role that different therapies play in the emergence or dwindling of drug resistance within the tumour via IVIS scans. In case there were issues with the Luciferase and eGFP being expressed as a fusion protein or it was useful for other applications, the eGFP was also cloned out from our Luc-eGFP reporter construct to obtain a vector encoding for only the luciferase gene.

The Luciferase-eGFP-based reporter constructs were modified from the pFUGW-FerH-Luciferase2-eGFP[293] (Luc-eGFP) plasmid, which was chosen because of its compatibility with the Luciferase-eGFP-tolerant Glowing-Head (GH)-mouse model[295], both established by Chi-Ping Day et al. This GEMM was engineered to expresses the Luciferase-eGFP fusion protein in the anterior part of the pituitary gland, which is not immune excluded, unlike the rest of the brain. Hence, the GH-mice are rendered immune tolerant towards respective reporters, which may minimise an artificial immune response targeting the reporter constructs. The GH-mouse strain we are using is based on the genetic background of C57BL/6 mice, which conventionally have a black fur coat. To facilitate IVIS scanning, the GH-strain has an additional loss-of-function mutation in tyrosinase gene, resulting in an albino fur coat.

To also distinguish the KRAS G12C mutant KPAR1.3 cells from all non-cancer cells in engrafted tumours, this cell line was transduced with an enhanced blue fluorescent protein (eBFP) reporter, which is structurally nearly identical to the eGFP. eBFP was selected, as it was pivotal to find a FP that was structurally similar to eGFP, to avoid evoking an artificial immune response in the GH mice towards cells expressing a divergent reporter. By analysing amino-acid sequences across FPs (not shown) we found that eBFP only differs in 2 AAs, Y67H and Y146F, amounting to an AA sequence homology of 99.2 %. Further structural analysis revealed that these AA reside in the hydrophobic interior of the protein barrel structure and that the two FPs are structurally nearly identical (**Figure 3.1b**); structural modelling performed by KangBo Ng. Moreover, utilising a MHC-I complex affinity modelling algorithm, provided through the ‘Immune Epitope DataBase’ (IEDB), revealed that the eBFP-derived peptides,

containing the two differing AA Y67H and Y146F, were categorised as very weak binding sequences with the lowest artificial neural network (ann)-based IC50 values of 7742.85 and 952.48 respectively (**Table 3.1**)**.** It is hence very unlikely that the two differing AA within eBFP would be presented to immune surveying cells.

To generate an eBFP-encoding reporter, suitable for our system, the eGFP-pLARRY base plasmid[292] was selected because the layout of this plasmid was also highly suitable for various potential sequencing based techniques[292]. This includes single cell sequencing or spatial transcriptomics, which might be employed in future projects. This plasmid encoded the right eGFP isoform for conversion to eBFP which was then achieved by introducing the two required point mutations via rolling circle amplification. Additionally, a unique barcode was introduced on the C-terminal end of the pLARRY-eGFP and -eBFP-based constructs.

Both, KRAS G12C- and G12D KPAR1.3 cells were then virally transduced with all of the above-mentioned reporter constructs, to allow for flexibility with project design in subsequent experiments. We determined that KPAR1.3 cells, expressing the different reporters were clearly distinguishable via flow cytometry (**Figure 3.1c**). Successful detection of the pLARRY-construct-based barcodes in respective KPAR1.3 cells was confirmed via sanger sequencing (**Figure 3.1d**). However, as this barcoding system ultimately was not used, it will not be discussed further here. The successfully transduced cell lines were then single cell subcloned for increased reproducibility of following experiments, as the reporter is integrated into the genome randomly, and 6 sub-clonal cell lines of each cell line were then further characterised.

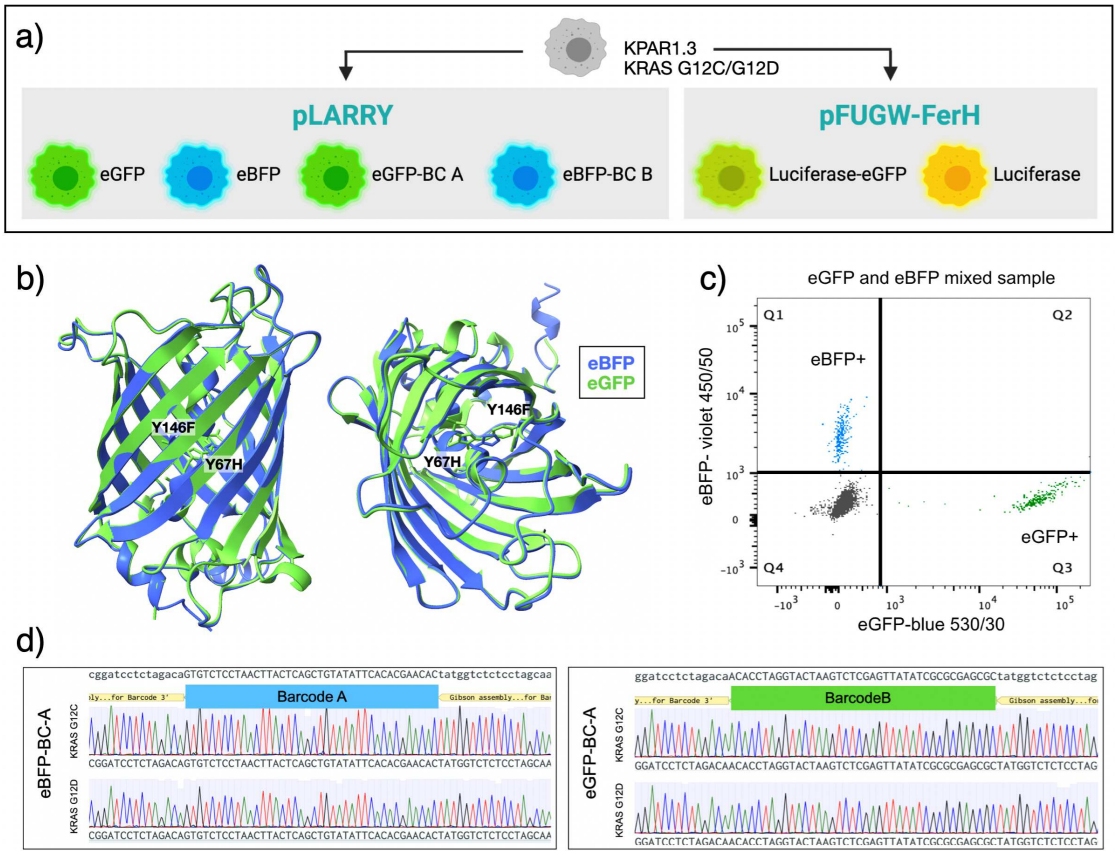


Figure 3.1 Generation of reporter-transduced KPAR1.3 cell lines. a) All reporter-transduced lines were generated and sub-cloned for both, KPAR1.3 KRAS G12C and G12D cell lines. The reporter constructs were modified and adjusted from either the 'pLARRY' or 'pFUGW-FerH' base plasmids. The eGFP-encoding sequence of the 'pLARRY' plasmid was mutated to encode for eBFP and a unique DNA-based barcode (BC) was further inserted at the C-terminal end of the FP sequences. In one variant of the of the 'pFUGW-FerH' plasmid, the eGFP was cloned out. The turquoise square highlights the combination of transduced sub-clonal cell lines which were ultimately chosen for downstream in *vivo* experiments; employing a eBFP-BC-B KRAS G12C- and Luc-eGFP KRAS G12D mutant subclone respectively. Prediction of structural similarity between eBFP and eGFP; eBFP protein structure based on AlphaFold prediction, eGFP protein based on previously solved protein crystal structure (PDB: 4EUL), align based on the Needleman-Wunsch algorithm (together with KangBo Ng). c) Flow cytometric analysis of a mixed sample, containing un-transduced-, as well as eGFP or eBFP expressing KPAR1.3 cells. d) Confirmation that transcribable barcodes can be amplified and correctly sequenced from cDNA of respective samples via Sanger sequencing.

Peptides containing Y67H mutation					
allele	start	end	length	peptide	ann_ic50
H-2-Kb	62	69	8	VTTLT**H**GV	7742.85
H-2-Db	67	76	10	**H**GVQCFSRYP	27951.49
H-2-Kb	63	70	8	TTLT**H**GVQ	26026.48
H-2-Db	63	72	10	TTLT**H**GVQCF	33228.35
H-2-Db	66	75	10	T**H**GVQCFSRY	41515.82
H-2-Kb	61	68	8	LVTTLT**H**G	34313.47
H-2-Db	60	69	10	TLVTTLT**H**GV	30960.01
H-2-Kb	65	72	8	LT**H**GVQCF	27047.65
H-2-Db	61	70	10	LVTTLT**H**GVQ	45032.54
H-2-Kb	67	74	8	**H**GVQCFSR	34708.9
H-2-Kb	66	73	8	T**H**GVQCFS	37290.64
H-2-Db	59	68	10	PTLVTTLT**H**G	44718.85
H-2-Kb	64	71	8	TLT**H**GVQC	34352.11
H-2-Db	64	73	10	TLT**H**GVQCFS	46038.05
H-2-Db	58	67	10	WPTLVTTLT**H**	45902.74
H-2-Db	62	71	10	VTTLT**H**GVQC	45221.47
H-2-Kb	60	67	8	TLVTTLT**H**	36699.04
H-2-Db	65	74	10	LT**H**GVQCFSR	47743.04

Peptides containing Y146F mutation					
allele	start	end	length	peptide	ann_ic50
H-2-Kb	144	151	8	YN**F**NSHNV	952.48
H-2-Db	144	153	10	YN**F**NSHNVYI	4045.8
H-2-Db	146	155	10	**F**NSHNVYIMA	18589.52
H-2-Db	145	154	10	N**F**NSHNVYIM	10562.59
H-2-Db	142	151	10	LEYN**F**NSHNV	21595.95
H-2-Db	140	149	10	HKLEYN**F**NSH	39818.49
H-2-Db	143	152	10	EYN**F**NSHNVY	43582.46
H-2-Db	138	147	10	LGHKLEYN**F**N	40727.86
H-2-Db	141	150	10	KLEYN**F**NSHN	42843.3
H-2-Kb	142	149	8	LEYN**F**NSH	26538.6
H-2-Db	137	146	10	ILGHKLEYN**F**	32346.83
H-2-Kb	140	147	8	HKLEYN**F**N	38359.12
H-2-Kb	141	148	8	KLEYN**F**NS	29873.42
H-2-Kb	139	146	8	GHKLEYN**F**	30312.32
H-2-Kb	145	152	8	N**F**NSHNVY	34272.29
H-2-Db	139	148	10	GHKLEYN**F**NS	48084.14
H-2-Kb	143	150	8	EYN**F**NSHN	39103.78

Table 3.1 Predicted MHC-I binding affinities. Analysis of eBFP-derived peptides containing the two altered AA residues. Artificial neuronal network (ann) IC_{50} scores of ≤ 50 indicate a strong predicted binding affinity, ≤ 500 indicates a medium-strength binding affinity, and ≥ 500 indicate a weak binding affinity.

3.2 Characterising reporter-traced cell lines in *vitro*

Before moving to an in *vivo* model system of tumours containing a drug-resistant subpopulation, transduced, all sub-clonal cell lines were first characterised in culture to verify their retained phenotypical comparability to the parental KPAR1.3 lines. In this chapter, exemplary results of the sub-clonal cell lines, ultimately chosen for following in *vivo* experiments, are shown.

It was previously shown that reporter expression stability can be compromised under stress conditions[293]. To mimic some of the stresses which may be exerted on cancer cells by the TME [299], sub-clonal cell line cultures were grown to over-confluency without replenishing the culture media, resulting in acidic- and nutrient-depleted conditions (**Figure 3.2a**). Flow cytometric analysis was then performed on resulting cultures for all FP-traced sub-clonal cell lines. An example of a subclone with unstable reporter expression after cell stress (**Figure 3.2b**), as well as the two subclones which were ultimately chosen for forthcoming in *vivo* experiments, KPAR1.3 KRAS G12D Luc-eGFP clone 6

(**Figure 3.2c**) and KPAR1.3 KRAS G12C eBFP clone 2 (**Figure 3.2d**), are shown. Compared to eGFP, eBFP inherently harbours a chromophore with dimmer fluorescence emission [298].

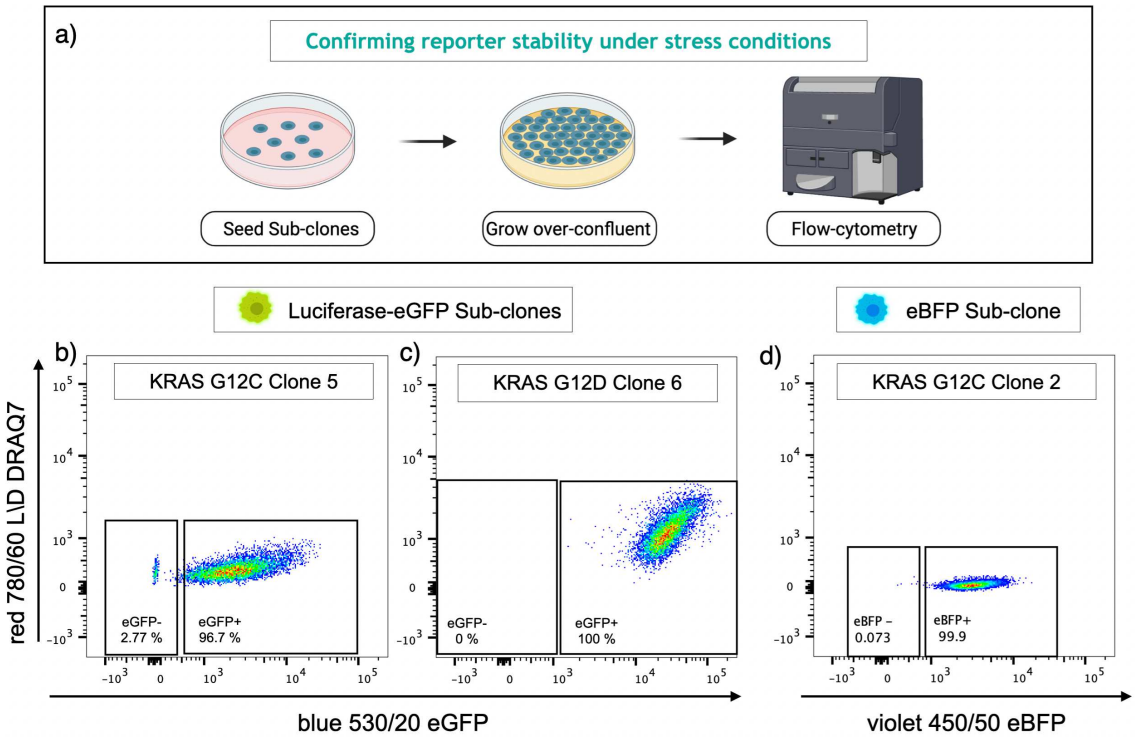


Figure 3.2 Reporter stability under stress conditions. a) Schematic of experimental setup; experiment was repeated with n=3 for all cell lines. b) Representative plot of a sub-clone that displayed unstable reporter expression under induced cell stress condition; 6 sub-clones were tested for each reporter-transduced cell line. c) Representative plot of the KPAR1.3 KRAS G12D sub-clonal cell line which was chosen for mimicking the KRAS G12Ci-resistant subpopulation forthcoming experiments. d) Representative plot of the KPAR1.3 KRAS G12C sub-clonal cell line, chosen to represent the KRAS G12Ci responsive tumour cells for forthcoming experiments; eBFP is inherently a dimmer fluorophore and hence closer to the eBFP- gate across all respective subclones.

The three clones for each reporter construct which retained most stable reporter expression were then selected for further downstream analysis. This included confirming that the growth rate of selected cell lines remained unaltered compared to the parental KPAR1.3 cell lines, which was tested via IncuCyte live confluency imaging (**Figure 3.3a**). Unaltered response to the KRAS G12C(OFF)i Adagrasib (**Figure 3.3b**) and MEK inhibitor Trametinib (**Figure 3.3c**) were also tested through viability assays. As expected, it was found that KPAR1.3 KRAS G12D-derived cell lines did not significantly respond to

Adagrasib at physiological doses. While both, KRAS G12C and G12D- derived cell lines presented with decreased viability upon MEK inhibition. For all sub-clonal lines expressing either a Luc-eGFP fusion construct or luciferase alone, enzymatic activity was confirmed via an in *vitro* luciferase imaging assay, exemplary plot for selected Luc-eGFP KRAS G12D sub-clones is shown (**Figure 3.3d**).

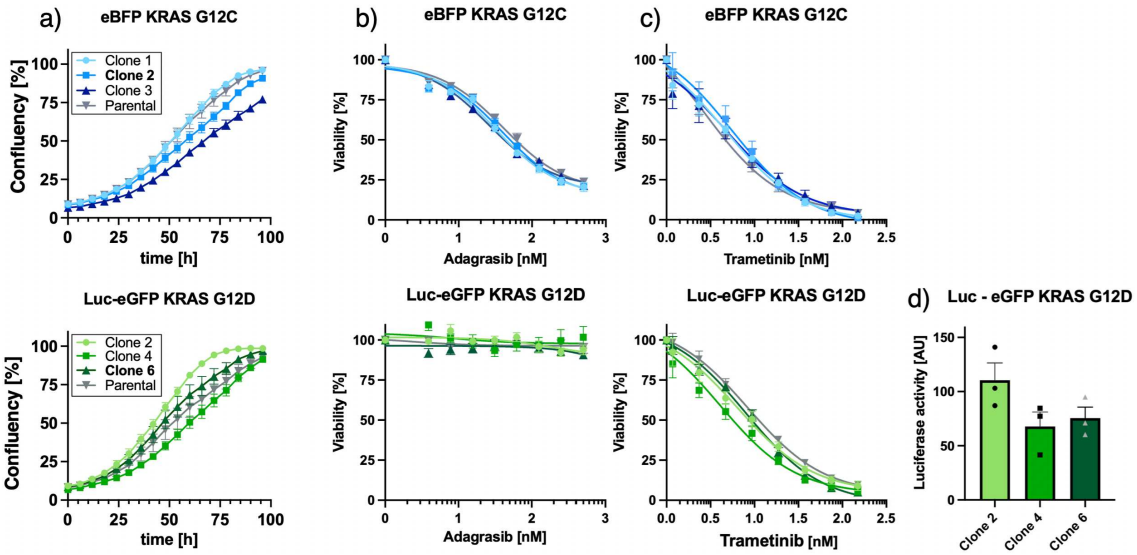


Figure 3.3 Characterising reporter-traced KPAR1.3 subclones in *vitro*.a) Exemplary plots of selected sub-clones, showing proliferation rates over time, assessed via IncuCyte live imaging . Upper panel: eBFP KRAS G12C (blue), lower panel Luc-eGFP-G12D (green), compared to respective parental KPAR1.3 cell lines (grey). Clones which were chosen for forthcoming in vivo experiments are indicated in bold fond. Experiments were repeated with biological replicates (n) = 3 and technical replicates (tr) within each experiment tr(n) = 5-6; error bars indicate SEM. b-c) Viability assays of selected subclones upper panel: eBFP KRAS G12C (blue), lower panel Luc-eGFP-G12D (green) are shown for Adagrasib (b) or Trametinib (c) with n = 3, tr(n) = 3, SEM. d) Exemplary plots of KPAR1.3 KRAS G12D Luc-eGFP sub-clonal cell lines, testing for in *vitro* luciferase activity by luminescence imaging; n=3, tr(n) = 3, error bars indicate mean + SEM.

After this initial screening, a suitable sub-clone from the eBFP-transduced KPAR1.3 KRAS G12C cell lines as well as a subclone of Luc-eGFP transduced KRAS G12D cell lines were selected. It was decided that, for future experiments, only the KRAS G12D mutant cell line should carry a luciferase reporter, as this allows to track the drug-resistant subpopulation over time in *vivo*, via IVIS scanning.

Before testing the selected cell lines in *vivo*, we wanted to determine a suitable ratio for co-engrafting the reporter-traced KPAR1.3 G12C and KPAR1.3 G12D cell lines for mimicking tumours containing a drug-resistant subpopulation. Therefore, the aforementioned cell lines were set up in co-cultures at the ratios 90:10, 95:5, and 99:1. Population dynamics during continuous treatment with 250 nM Adagrasib were then monitored over time via flow cytometric analysis (**Figure 3.4**). In contrast to DMSO-treated control co-cultures, the fraction of KPAR1.3 KRAS G12C cells in Adagrasib-treated samples was converging towards zero in the given time, even with a starting fraction of only 1% G12D cells.

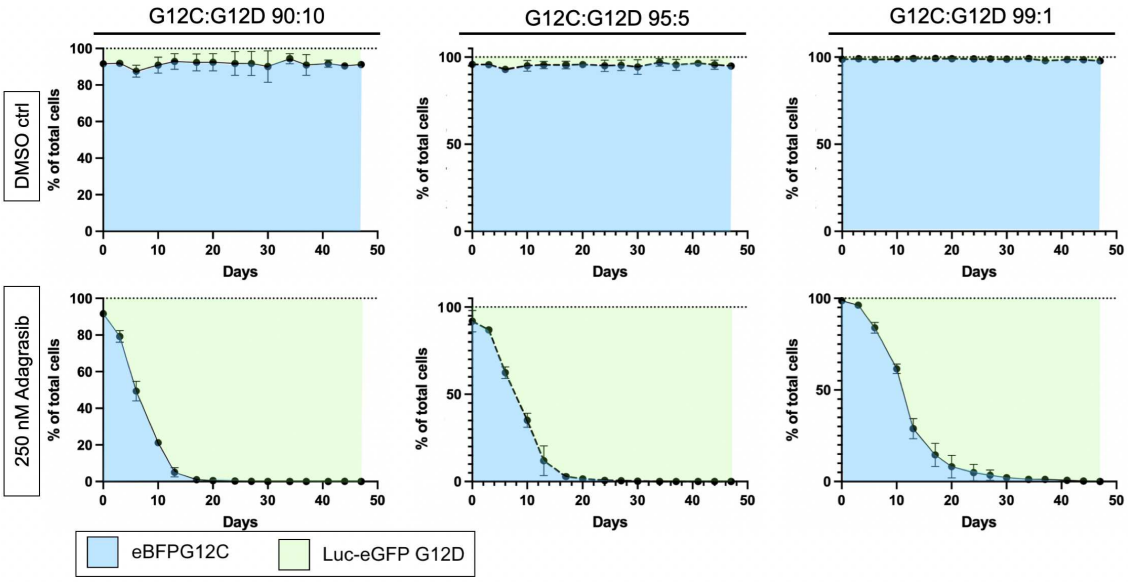


Figure 3.4 Co-culture assay assessing Adagrasib response over time. Blue and green areas on graphs depict the fractions of KPAR1.3 KRAS G12C or G12D populations respectively over time. DMSO was used as vehicle to dissolve Adagrasib in this assay. Experiment was repeated with biological replicates n = 3, each with technical replicates tr(n) = 3 until day 37, as experiments were started in 1-week intervals. Error bars indicate SD.

3.3 Characterising reporter-traced cell lines in *vivo*

To assess whether, without the addition of any cancer treatments, the selected subclones proliferated at equal rates in *vivo*, the aforementioned reporter-traced KRAS G12C/-G12D mutant cell lines were co-engrafted subcutaneously at a

50:50 ratio, 75,000 cells of each type, in GH-mice. After 14 days, resulting tumours were analysed by flow cytometry, which revealed that the fractions of the engrafted cell lines remained largely unaltered over time; this was confirmed in two independent experiments (**Figure 3.5a**). Three tumours were also submitted for histopathological analysis to visualise the spatial distribution of the KRAS G12C- and G12D-mutant cancer cells within the tumour. Because of the high structural similarity between eBFP and eGFP, it is possible to demarcate all tumour cells using a single anti-eBFP/eGFP ab as a pan-cancer cell marker. By adding an additional anti-luciferase ab to the staining panel, the KRAS G12D mutant cells can be discerned, as they will appear double positive for both markers. KRAS G12C and G12D mutant cancer cells grew largely in an interspersed pattern (**Figure 3.5b,c**). Although some areas within the tissue section where the presence of KRAS G12C or-G12D mutant tumour cells were more predominant were also observed (**Figure 3.5d**). Of note, eBFP inherently possesses a dimmer chromophore compared to eGFP [298]. Hence, a viral promoter was chosen for the eBFP reporter construct [292] to increase FP expression, while the Luc-eGFP construct reporter is expressed under a housekeeping reporter gene to prevent silencing of the much larger reporter in vivo[293]. This may explain why the eBFP-expressing KPAR1.3 KRAS G12C tumour cells appear brighter in the anti-eGFP/eBFP staining compared to the KPAR1.3 KRAS G12D cells.

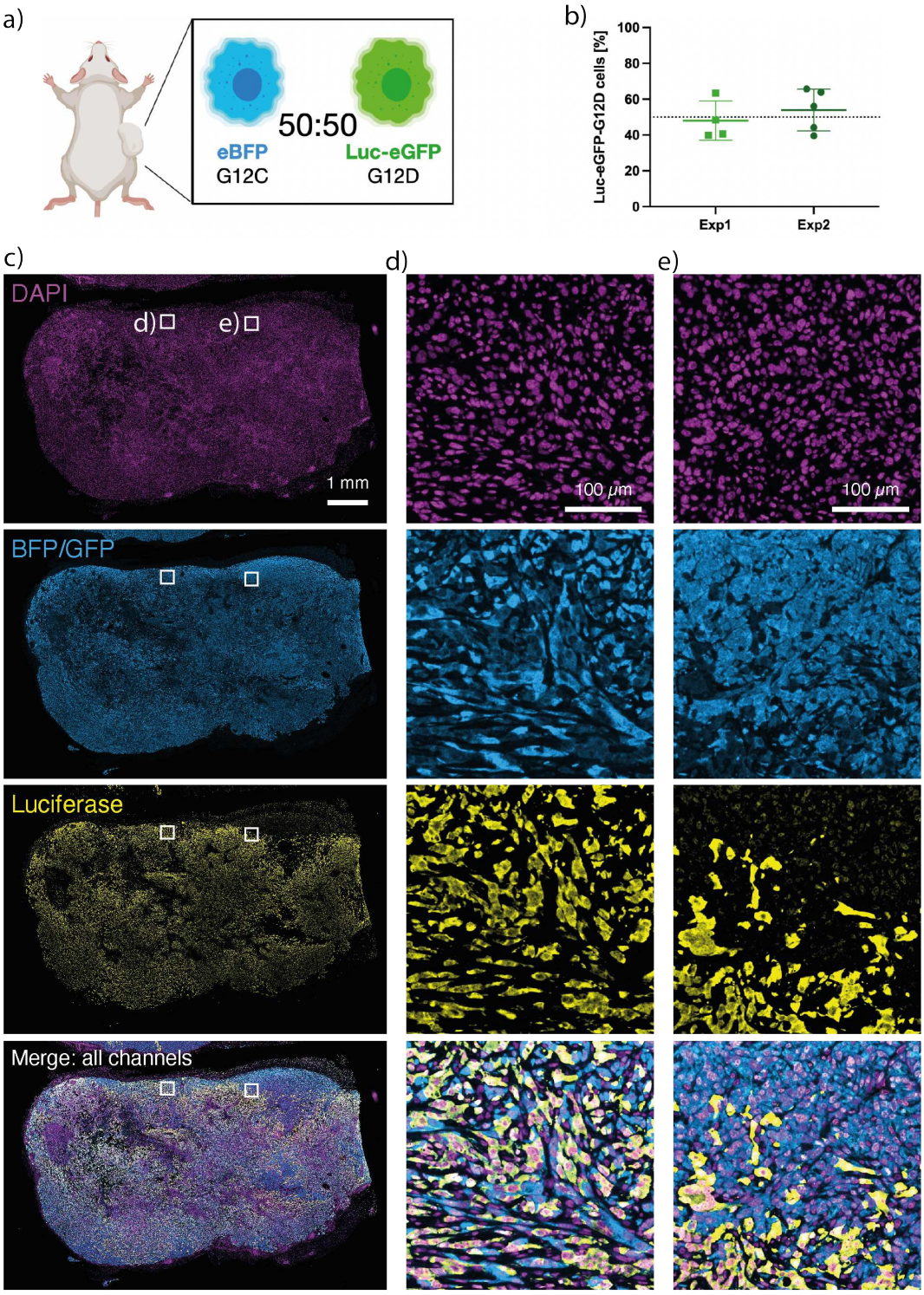


Figure 3.5 Assessing growth dynamics of co-engrafted subclones in *vivo*. Luc-eGFP KRAS G12D clone 6 and eBFP KRAS G12C clone 2 were co-engrafted subcutaneously in GH- mice at a 50:50 ratio in 2 independent experiments. a) Schematic of experiment. b) Graph depicts fraction of Luc-eGFP KRAS G12D clone 6 tumour cells within all live cancer cells; flow cytometric analysis was performed 14 days after engraftment of tumours; dots depict individual tumours, each derived from 1 mouse; for each experiment: n = 5, error bars depict mean + SD. c-e) Representative immunohistochemistry staining of tissue sections derived from tumours that were engrafted under the same conditions. eBFP/eGFP: blue, luciferase: yellow, DAPI: magenta; scale bars as indicated on individual images.

Chapter 4. Assessing therapy efficacy in combatting drug-resistant tumour sub-populations

In the last decade, it has become evident that the role of oncogenic KRAS signalling exceeds mere mediation of cancer cell-intrinsic growth and survival signalling. Moreover, it is involved in instigating immune suppression in the TME through various mechanisms, which may exacerbate the scope of cancer treatment responses.

Combatting the development of drug resistance towards lines of targeted cancer therapies remains challenging. Although patients may present with initial tumour regression, responses to such treatments are often not durable and tumours can relapse in a matter of months. This observation has also been made in clinical trials of the newly developed KRAS G12C inhibitors Sotorasib and Adagrasib [236,239] [231]. Furthermore, the mechanisms of resistance can vary, from achieving bypass signalling through acquisition of further mutations or increased expression of relevant signalling proteins, to genome-wide expression changes to enter a state of quiescence or undergo EMT[233,244]. In this chapter, we investigated therapeutic strategies with the potential to promote an anti-tumour immune response, capable of also eradicating the cancer cells which do not respond to KRAS G12Ci directly. We further test whether complete responses and durable immune-memory towards drug resistant tumour cells can be achieved with respective therapy schemes.

4.1 Monotherapy with G12Ci Adagrasib accelerates expansion of drug-resistant cancer cells

First, the effects of using the KRAS G12C(OFF)i Adagrasib as monotherapy on tumours containing a drug-resistant subpopulation were assessed (**Figure 4.1a**). This was to test whether drug-induced cancer cell killing and alleviation of

immune suppression in the KRAS G12Ci-responsive cells was already sufficient to re-enforce an immune response which could also target the KRAS G12D cells in the tumour. Here, consecutive in *vivo* experiments were performed, testing 4 different engraftment ratios of eBFP KRAS G12C and Luc-eGFP KRAS G12D cells in a subcutaneous setting. Tumour growth over time was measured via calliper (**Figure 4.1b**)**.** The relative change in G12D cells over time was assessed via IVIS scans, which detect luminescence based on the luciferase reporter activity, which is only present in the KRAS G12D mutant tumour cells (**Figure 4.1c**). At endpoint, tumours were harvested and the fraction of KRAS G12D mutant cancer cells out of all live cancer cells was determined via flow cytometry (**Figure 4.1d**), as described in the previous experiment (**Figure 3.5b**).

The two isogenic cancer cell lines were initially engrafted at a 50:50 ratio, to assess the impact of Adagrasib on the proliferation or regression rate on the respective sub-populations. In this experiment, the tumour size of the mice receiving Adagrasib continued to increase, even while on treatment. Here, IVIS scans implied that, during treatment, the luminescent signal emitted by luciferase-expressing KRAS G12D cells steeply increased, compared to vehicle-receiving mice. Flow cytometry at the experimental endpoint revealed that, while in vehicle mice the ratio of KRAS G12C:G12D cells was still approximately equal, the treated tumours were now mostly comprised of KRAS G12Ci-resistant tumour cells.

At this point, it was hypothesised that engrafting tumours where 50% of the engrafted tumour is already inherently unresponsive to treatment may have counteracted the development of an efficient anti-tumour immune response. Further, this may also not be an accurate depiction of patients' clinical physiology, where tumours are initially treatment responsive, and resistance likely emerges small sub-clonal populations which have acquired treatment resilience under selection pressure. Hence, next, the effect of KRAS G12Ci as monotherapy was tested on tumours containing a smaller fraction of KRAS

G12D cells. The engrafted fraction of KRAS G12D mutant cells decreasing from 1%, to 0.05% and even 0.01%. At the lowest ratio, when engrafting a total of 150,000 cancer cells, only 15 cells would harbour a G12D mutation. However, even at this lowest ratio, it was observed that after just 12 days of treatment, the majority of tumours were mostly comprised of KRAS G12D cancer cells.

Thus, we concluded that treating tumours which already contain a KRAS G12Ci-resistant subpopulation with KRAS G12Ci as monotherapy is not sufficient by itself to trigger an immune response to the resistant cells, but rather actually provides the drug-resistant KRAS G12D cells with a proliferative advantage and exacerbates disease progression (**Figure 4.1e**).

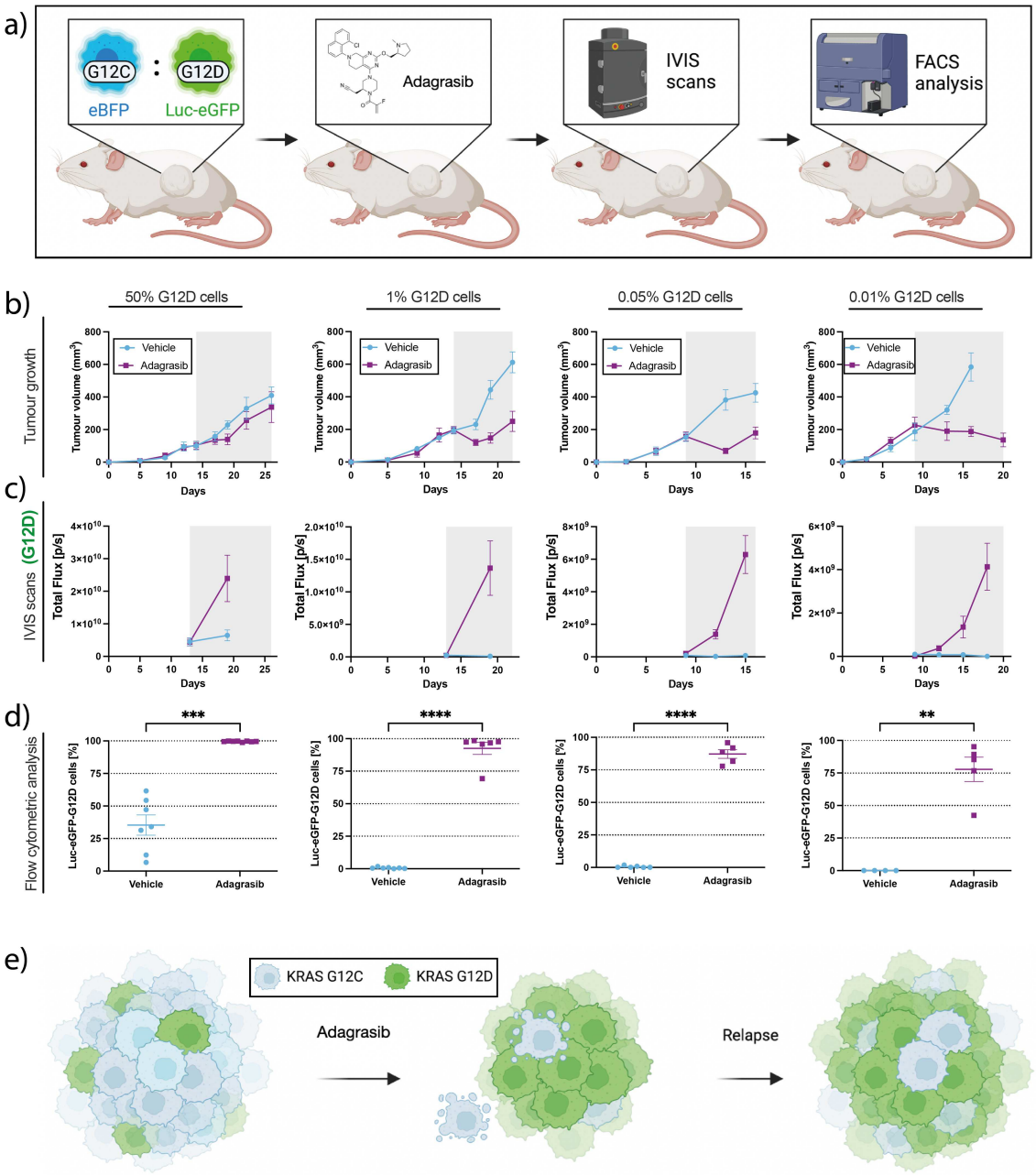


Figure 4.1 Adagrasib treatment of tumours containing a KRAS G12Ci-resistant sub-population. a) Schematic of experimental setup. Mice treated with Adagrasib were dosed daily with 50 mg/kg, indicated by grey area on plots. b) Grouped tumour growth over time. c) In *vivo* IVIS scans over time, detecting luminescent signal emitted by luciferase-expressing KPAR1.3 KRAS G12D tumour cells. d) Flow cytometric analysis of Luc-eGFP KRAS G12D cancer cells of all live cancer cells. Experimental mice from left to right panel: (i) n(vehicle) = 7 , n(Adagrasib) = 8; (ii) n(vehicle) = 7 , n (Adagrasib) = 6; (iii) n(vehicle) = 6 , n(Adagrasib) = 6; (iiii) n(vehicle) = 6 (2 mice had to be culled before flow cytometric analysis due to tumour ulceration), n(Adagrasib) = 6 (one sample excluded from flow cytometric analysis due to recording issue); Error bars for all graphs display mean + SEM; statistics indicate pair-end students t-test with Welch's correction for varying standard deviation between treatment groups. e) Schematic indicating the observed changes in KPAR1.3 tumour cell subpopulations induced by Adagrasib treatment.

4.2 Assessing efficacy of additional therapy lines as monotherapies

Adagrasib treatment, administered as monotherapy, was insufficient for tumour control in our heterogenous model system and even accelerated the emergence of KRAS G12Ci-resistance. Hence, two additional lines of anti-cancer drugs, shown to potentiate beneficial effects on anti-tumour immunity, were introduced. This included a line of immunotherapy, an anti-PD-1 therapeutic ab, as well as the SHP2 inhibitor (SHP2i) RMC-4550. It was also decided to switch from the KRAS G12C(OFF)i Adagrasib to the newly available KRAS G12C(ON)i RMC-4998. Our group found that the latter inhibitor was more effective in decreasing viability in KRAS G12C KPAR1.3 cells compared to inactive state KRAS inhibition [216].

Before introducing these inhibitors as combination therapies in our model system of tumours containing drug resistant subpopulations, their effect on KRAS G12C- or G12D-derived tumours was assessed individually **(Figure 4.2a)**. It was first confirmed that KRAS G12C(ON)i RMC-4998 was able to induce tumour regression in KRAS G12C-derived tumours **(Figure 4.2b)**. In this experiment, 3/8 complete responders (CRs) were also generated, that remained tumour free for a month after treatment period ended.

Treatment with a-PD-1 as monotherapy seemed to have no visible impact on the growth of G12D-derived tumours compared to the IgG isotype control-treated mice **(Figure 4.2c)**. This is in agreement with previously published results, where the parental, non-reporter-traced equivalent of the KPAR1.3 cell line was used[294]. a-PD-1 appeared to induce moderate inhibition on KRAS G12C derived tumours, unable, however, to check tumour growth during treatment **(Figure 4.2d)**. This difference in response between the two isogenic cell lines may be related to their origin. The original cell line, established from a KPAR ($KRAS^{LSL\text{-}G12D/+;}$ $Trp53^{fl/fl}$; $Rosa26^{A3Bi}$; $Rag1^{-/-}$) tumour, harboured a KRAS G12D mutation while the alteration to the KRAS G12C mutant isogenic cancer

cell line required further Cas9-mediated genomic modification. It was previously observed by our group that, at least in an orthotopic setting, the KRAS G12D mutant cell line appeared encompass an enhanced ability to engraft robustly or may inherently retain a higher oncogenic capacity.

On a conceptual level, the SHP2i RMC-4550 can constrain oncogenic KRAS signalling by inhibiting upstream-reactivation of KRAS proteins. G12C mutant KRAS proteins, despite impaired GAP binding, still largely retain their inherent GTP-GDP-cycling ability. In G12D mutant KRAS, on the other hand, the protein intrinsic GTPase activity is also impaired, thereby lessening dependency on upstream RTK-mediated reactivation **(Figure 1.2)**. Hence, we hypothesised that KRAS G12C mutant cancer cells may have a stronger response to SHP2i, compared to KRAS G12D mutant KPAR1.3 cells. Indeed, it was observed that mice harbouring KRAS G12D-derived tumours, again, presented no significant therapy response to SHP2 inhibition **(Figure 4.2e)**. On the other hand, growth of KRAS G12C-derived tumours was inhibited during the treatment period, although all tumours grew back after treatment and no CRs were observed **(Figure 4.2f).**

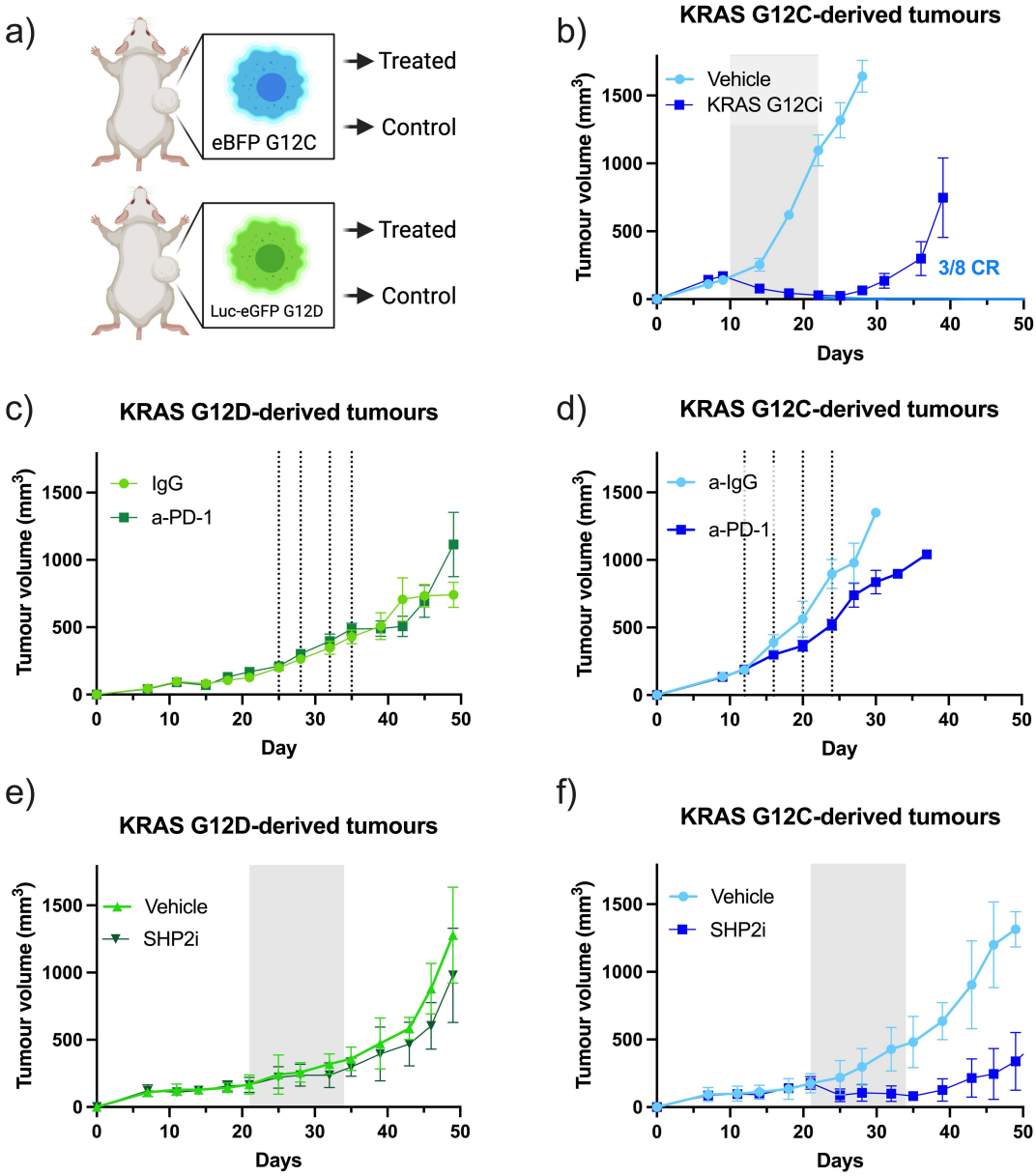


Figure 4.2 Efficacy of KRASi, a-PD-1, and SHP2i as monotherapy. Error bars indicate mean +/- SEM; measurements shown in blue represent KRAS G12C-derived tumours, measurements in green -G21D-derived tumours. Treatment period for all experiments was two weeks, whereat either 12 doses of the oral drugs KRAS G12C(ON)I RMC-4998 (100 mg/kg; indicated as KRASi) or SHP2 inhibitor RMC-4550 (30 mg/kg; indicated as SHP2i) were administered (grey area on plots) or 4 doses of antibody injections (10 mg/kg), as indicated by vertical dotted lines. To standardise plots, data was cut off after day 50, if any mice remained after this timepoint. a) Schematic of general experimental design; b) Mice harbouring KRAS G12C-derived tumours were treated with either vehicle (n=6) or RMC-4998 (n=8); From the end of treatment, the 3 complete responders are indicated as separate tumours on the plot. c) Mice harbouring KRAS G12D-derived tumours were treated with either IgG (n=6) isotype control or a-PD-1(n=7). d) KRAS G12C-derived tumours treated with either IgG (n=7) isotype control or a-PD-1(n=8). e) KRAS G12D-derived tumours treated with either vehicle (n=7) or RMC-4550 (n=8). f) KRAS G12C-derived tumours were treated with vehicle (n=8) or RMC-4550 (n=8).

From this series of experiments, it was concluded that RMC-4998 was able to, as expected, inhibit tumour growth in KRAS G12C-derived tumours. However, although neither a-PD-1, nor RMC-4550 were sufficient to eradicate KRAS G12D- or - G12C-derived tumours when administered as monotherapy, KRAS G12C tumours showed higher sensitivity to these therapies.

4.3 Combination therapies can promote immune-rejection of drug-resistant subpopulations

Treating tumours derived from KRAS G12C or -G12D mutant KPAR1.3 cancer cells allowed to disentangle the individual treatment contributions of RMC-4550 and a-PD-1. In this next section, it was investigated whether combining KRAS G12Ci with these additional therapy lines can achieve tumour control through treatment synergy.

Based on the previous experiments testing different G12C:G12D ratios (**Figure 4.1**), it was decided to engraft 150,000 cancer cells, in total, containing 99.96% KRAS G12C and 0.04% KRAS G12D cells. This ratio was selected because, on one hand, engrafting this small fraction of G12D cells (~60 cells) was already sufficient to generate drug-resistant tumours within two weeks of treatment when treating with Adagrasib as monotherapy. On the other hand, reducing the fraction of KRAS G12D mutant cancer cells any further might compromise the detection of luminescence in the baseline IVIS imaging before treatment. Therapy response was then monitored by measuring tumour size (**Figure 4.3a**) and tracking the KRAS G12D subpopulation over time via IVIS scans (**Figure 4.3b**). As in previous experiments, the KRAS G12D mutant KPAR1.3 cell population did not proliferate at an accelerated rate in vehicle-treated mice, measured by reduced luminescence signal. Similarly, G12D cells would also not proliferate at an accelerated rate when treated with a-PD-1 or RMC-4550 as monotherapy. However, in tumours treated with RMC-4998, IVIS data indicated

that the G12D fraction expanded significantly more compared to vehicle-treated mice, similar to the previous experiments conducted with Adagrasib (**Figure 4.1**). However, in contrast with Adagrasib, treating mice with RMC-4998 as monotherapy yielded one CR mouse.

The dual combination treatments of KRAS G12Ci RMC-4998 with either SHP2i RMC-4550 or a-PD-1, were able to generate 7/14 or 6/12 CRs respectively, even though the KRAS G12D tumours are not sensitive to any of the individual therapies used. For the combination treatment groups, the IVIS scans showed different patterns for individual mice. Although no luminescence signal was detected on treatment, the G12D population expanded over time in mice that would relapse after the treatment period. Contrarily, the G12D population remained checked in mice which would later become CRs.

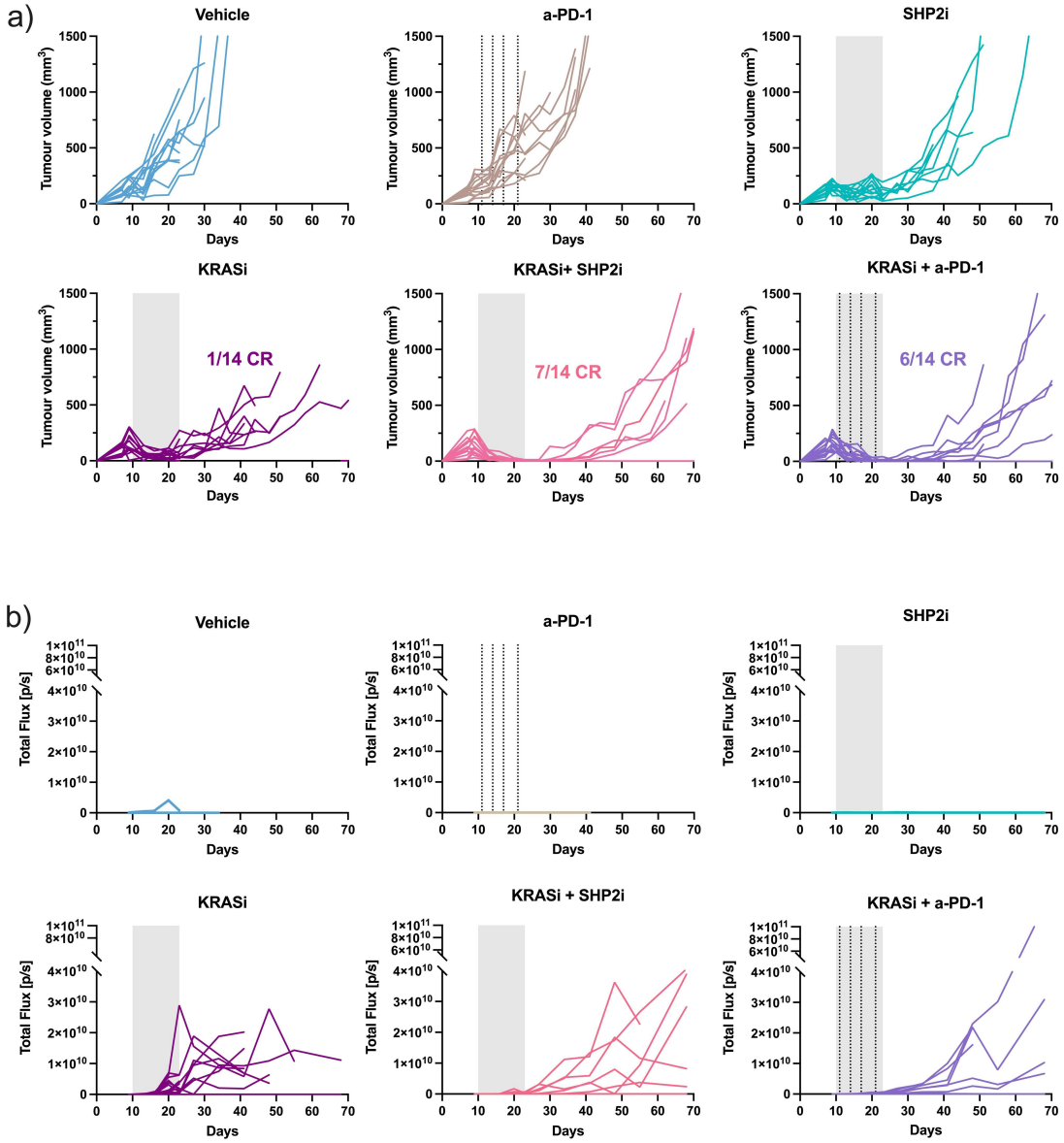


Figure 4.3 Assessing synergistic treatment effects of therapy combinations. Mice received treatments for 2 weeks, whereat 12 doses of the oral drugs KRAS G12C(ON)I RMC-4998 (100 mg/kg; indicated as KRASi) or SHP2 inhibitor RMC-4550 (30 mg/kg; indicated as SHP2i) were administered (grey area on plots) or 4 doses of a-PD-1 injections (10 mg/kg), as indicated by vertical dotted lines. a) Tumour volume over time of individual tumours by treatment group. b) Bioluminescence signal, photon flux detected per second, measured via IVIS scans, indicative of the abundance of KPAR1.3 KRAS G12D cells over time.

As an additional readout, flow cytometric analysis was performed by selecting 4-5 palpable tumours from each treatment group at the end of the treatment period (**Figure 4.4a**). Here, tumours were selected to reflect the overall variance in tumour sizes within each treatment group and to represent the

overall mean and median of tumour sizes and IVIS signal as well as possible. No samples from the combination treatment groups were harvested, as the respective tumours were too small to be isolated at this point. Quantifying the Luc-eGFP-traced KPAR1.3 KRAS G12D tumour cell population over all live cancer cells reflected the trends indicated by the combination of tumour growth and IVIS scans in this experiment (**Figure 4.3**). This data is in congruence with the findings from treating KRAS G12C:G12D mixed tumours with Adagrasib as monotherapy (**Figure 4.1**). It appears that Adagrasib, as well as RMC-4998, which can induce efficient cancer cell killing in KRAS G12C cells, also induce increased proliferation in KRAS G12D cells, while SHP2i and a-PD-1 treatments when administered as monotherapy do not trigger this effect and therefore most tumours at the end of the treatment contain mainly KRAS G12C cells. In addition to performing flow cytometric analysis of selected tumours at the end of treatment, tumours were also isolated whenever mice reached a defined experimental endpoint (**Figure 4.4b**). This revealed that cancer cells from tumours of the vehicle, a-PD-1, and RMC-4550 treatment groups were still mostly comprised of KRAS G12C mutant cancer cells, continuing onward from the treatment endpoint. On the other hand, in KRAS G12Ci- or combination-treated tumours the fraction of G12D mutant tumour cells within all live cancer cells varied. In some tumours, the regrowth was mainly driven by KRAS G12D mutant cells, while, in other tumours, growth was driven by remaining KRAS G12C mutant tumour cells. It has previously been reported that drug-resistant cancer cells can form a protective niche, allowing treatment responsive cells to persist during therapy[300]. This may have come into play for relapsed tumours with their main bulk comprised of KRAS G12C mutant cancer cells. For most individual tumours, the final composition of KRAS G12C vs G12D mutant fractions at endpoint correlated with the respective combination of tumour growth and IVIS data in **Figure 4.3**.

Further plotting the survival probabilities across treatment groups visualised a clear survival advantage of combination treated tumours (**Figure 4.4c**), with the generation of complete responses in half of the mice. To investigate whether an

anti-tumour immune response contributed to the bystander killing of the KRAS G12Ci resistant KRAS G12D cells and to test for immune memory in CRs, a re-challenge experiment was performed. For this, mice which remained tumour free for one month after the treatment period had ended, were injected with 150,000 KRAS G12D mutant cancer cells in the opposite flank (**Figure 4.4d,e**). If mice were able to reject the engraftment of a secondary tumour without any further treatment, this would indicate the successful formation of an immune-memory-based anti-tumour response. A group of age-matched mice, that had not previously been exposed to cancer cells, were also included as a negative control and referred to as naïve mice. The mouse from the KRASi treatment group, as well as 3/7 mice from the KRASi + SHP2i group and 3/6 mice from the KRASi + a-PD-1 group were able to immune-reject the newly injected cancer cells. In non-immune-rejected tumours, the secondary tumours would often grow back at a slower rate, compared to a control group of naïve mice, which may indicate that some anti-cancer immunity was present in these mice as well.

.

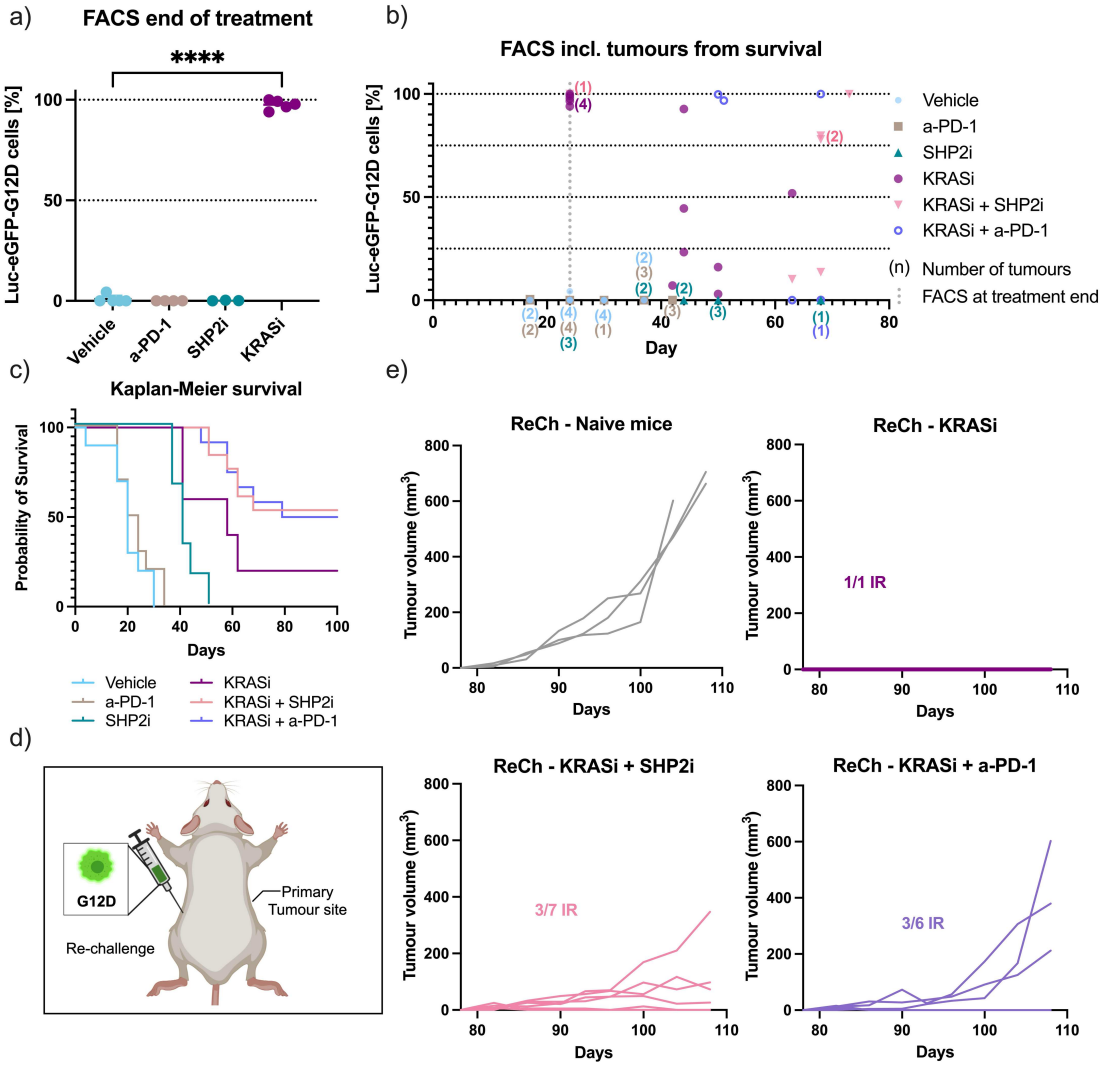


Figure 4.4 Additional readouts of dual combination treatments. KRASi refers to the KRAS G12C(ON)i RMC-4998; SHP2i refers to the drug RMC-4550. a) Representative tumours were isolated from vehicle and single-therapy treatment groups and fraction of live KPAR1.3 KRAS G12D cells within all cancer cells was determined via flow cytometry; each dot represents one tumour, within each treatment group, mean together with SEM are plotted; statistics indicate one-way ANOVA test, comparing each of the treatment groups to the vehicle, only significant comparisons are shown. b) Fraction of live KPAR1.3 KRAS G12D cells of all live cancer cells is plotted over time. The vertical grey line at day 24 represents the flow cytometry performed at treatment endpoint, visualised in (a); each dot represents one tumour, if dots overlapped in plot, number of individual tumours is indicated for respective days in matching colours. c) Survival probability across different treatment groups; tumours taken out for flow cytometry at endpoint were excluded; cut-off value was 500 mm^3. d) Schematic of re-challenge experiment. e) Tumour growth over time of re-challenge (ReCh) tumours in naïve mice or CRs; mice which were able to immune reject (IR) the re-injected cancer cells out of all mice are indicated for applicable graphs.

We next wanted to investigate whether extending the treatment period from two- to three weeks might provide an additional survival advantage to tumour-

bearing mice. In addition, as mice had tolerated dual-combination treatments well, it was decided to also include a triple-combination branch, to probe the underlying mechanisms of treatment synergy. The triple combination therapy scheme between KRAS G12Ci, SHP2i, and a-PD-1 will most likely not become feasible as a therapeutic combination for cancer patients. However, it could still provide meaningful insights into fundamental mechanism through which different lines of therapy are able to synergise with each other and restructure TME architecture.

For this, subcutaneous tumours were again engrafted in GH-mice with the same parameters as in the previous experiment (**Figure 4.3, Figure 4.4**). Tumour growth was monitored (**Figure 4.5a**) and the fraction of KRAS G12D mutant cancer cells tracked via IVIS scans (**Figure 4.5b**). Surprisingly, despite the extended treatment period, less CRs were observed in the dual combination treatment groups with 3/15 CRs in the KRAS G12Ci + SHP2i combination group and 2/12 CRs in the KRASi + a-PD-1 group. When revising the baseline IVIS scan and tumour volume before treatment, it was observed that the average tumour volume before treatment was 177 mm^3 in this experiment compared to 157 mm^3 in the previous combination treatment experiment. Further, the intensity of the bioluminescent signal detected via IVIS signal was measured at $9.61*10^6$ $p/s/cm^2$, compared to $5.41*10^6$ $p/s/cm^2$ in the previous experiment. The latter indicating that there were nearly twice as many KRAS G12D cells present in this second experiment at the day before treatment start. It is possible that the difference in overall tumour volume and/or the increase in the KRAS G12D fraction may have influenced treatment response. However, despite having less CRs in the dual combination treatment groups compared to the previous experiment, with the triple treatment combination of KRAS G12Ci, SHP2i, and a-PD-1, 12/14 mice were CRs.

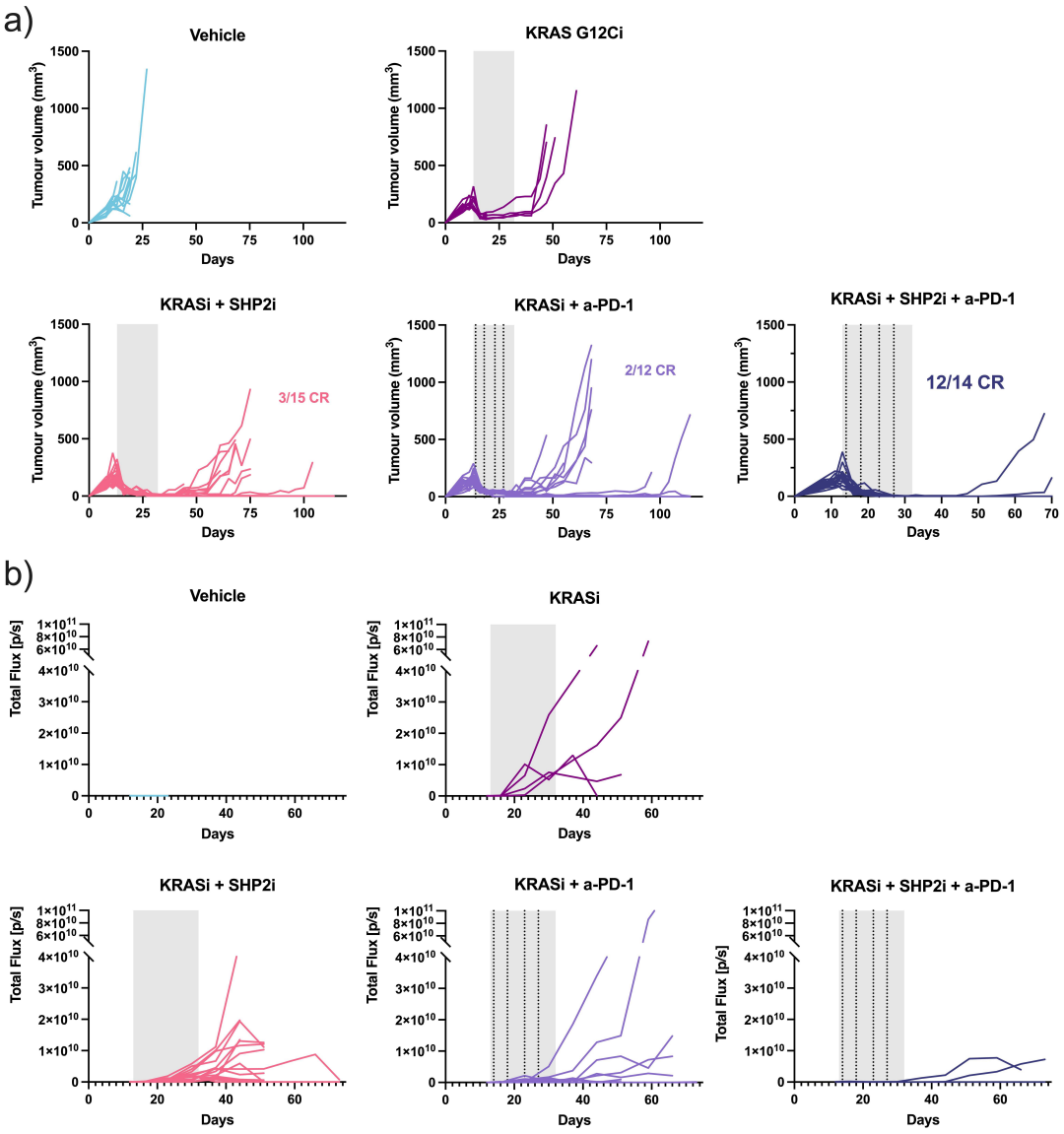


Figure 4.5 Investigating extended combination treatment regimes. Mice were treated for 3 weeks, whereat 18 doses of the oral drugs KRAS G12C(ON)i RMC-4998 (100 mg/kg; indicated as KRASi) or the SHP2 inhibitor RMC-4550 (30 mg/kg; indicated as SHP2i) were administered (grey area on plots); or 4 doses of a-PD-1 injections (10 mg/kg), as indicated by vertical dotted lines. a) Tumour volume over time of individual tumours by treatment group. b) Bioluminescence signal, photon flux detected per second, measured via IVIS scans, indicative of the abundance of KPAR1.3 KRAS G12D cells over time.

This triple combination also clearly provided a survival advantage over the dual treatment combinations (**Figure 4.6a**). Again, tumours from each treatment group were isolated to assess effect of inhibitors on the KPAR1.3 KRAS G12D subpopulation (**Figure 4.6b**). However, to obtain enough sample to also

investigate combination treatment groups, representative tumours for each group were isolated after only 7 days of treatment. In this experiment, it was, again, observed that the fraction of KRAS G12D mutant cells increased when mice were treated with the KRAS G12C(ON)i. This was more pronounced when KRAS G12Ci was employed as monotherapy compared to the combination treatments. Further the addition of a-PD-1 therapeutic ab appeared to curb the proliferation of KRAS G12D mutant cells. The fact that the outgrowth of KRAS G12D mutant cells was less pronounced compared to the previous experiment (**Figure 4.4a**), might relate to the shorter treatment period before sample isolation in this study. Flow cytometric analysis of tumours isolated from mice that had reached an experimental endpoint (**Figure 4.6c**) coincide with the findings of the previous experiment (**Figure 4.4a**). Both tumours from the non-responders of the triple-combination treatment group were mostly comprised of KRAS G12D mutant cancer cells at endpoint, however, as only two tumours were available for analysis in this group, this information remains inconclusive. Re-challenge of the CRs mice resulted in 1/3 IRs in the KRAS G12Ci + SHP2i treatment group, 2/4 IRs in the KRAS G12Ci + a-PD-1 group and 6/12 IRs in the triple combination group (**Figure 4.6d**).

Although in mice the triple treatment combination induced little to no side effects, this triple combination treatment may not be as well tolerated in human cancer patients. However, for investigating the underlying mechanisms of remodelling the tumour microenvironment and training an anti-tumour directed immune response, it is providing valuable insights.

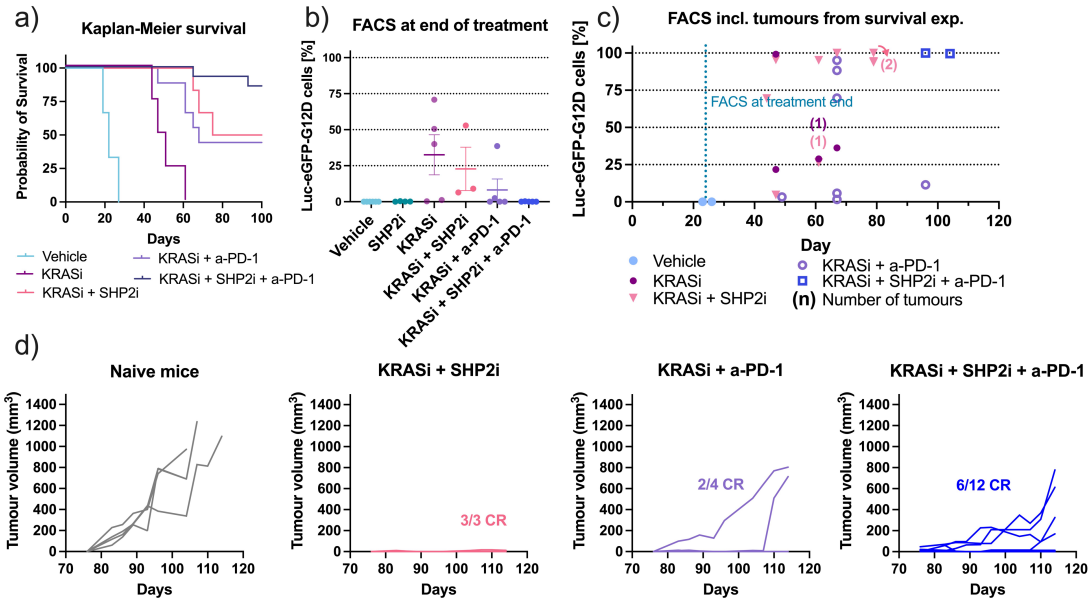


Figure 4.6 Additional readouts of extended combination treatments. KRASi refers to the KRAS G12C(ON)i RMC-4998; SHP2i refers to the drug RMC-4550. a) cutoff volume for survival plot was 460 mm^3; SHP2i only group not plotted because mice for this treatment group were only included for flow cytometric analysis after 7 days treatment; fewer mice are plotted for vehicle group, as majority of mice were culled for flow cytometric analysis. b) After 7 doses of treatment, the fraction of KRAS G12D tumour cells within all live tumour cells, determined via flow cytometry; each dot represents one individual tumour, plotted together with mean + SEM for each treatment group; one-way ANOVA test was applied to this graph, however none of the comparisons were significant when comparing (I) all treatment groups to the vehicle or (II comparing every mean to every other mean, hence no statistics are shown here. c) Fraction of live KPAR1.3 KRAS G12D cells of all live cancer cells is plotted over time; the vertical grey line at day 24 represents the flow cytometry performed at treatment endpoint, visualised in (b) (data not shown in this graph). d) Individual tumours of mice from re-challenge of complete responders. Mice which were able to immune-reject (IR) secondary tumours are highlighted in respective graphs.

In patients, it was observed that combination treatments with Sotorasib can induce side effects, oftentimes manifesting as hepatotoxicity related conditions[199,228,266,267,301].Even in the triple combination experiment, mice did not present with obvious symptoms of side effects or signs of discomfort. Nonetheless, we wanted to investigate whether the combination treatments caused liver toxicity in the GH-mice. Hence, when tumours had been isolated for flow cytometric analysis after 7 days of treatment (**Figure 4.6c**), serum was also collected from respective mice. Serum levels of the enzymes aspartate aminotransferase (AST) and alanine transaminase (ALT) were then measured (**Figure 4.7)**. Quantifying the activity of these enzymes in serum samples can

be used as indicators of increased liver inflammation in the clinic. However, for this line of mouse experiments, there are few comparable results to determine what would comprise high levels of liver inflammation. Possible reference levels come from a study comparing liver toxicity in mice on a normal- compared to a high-fat diet[302]. Here, healthy serum activity levels in mice were estimated around 23.7 ± 2.3 units per litre (U/L) for ALT and 32.4 ± 2.2 U/L for AST. We also included an internal negative control in form of serum isolated from a naïve mouse. The results indicate that most mice presented with elevated levels of hepato-toxicity as a trend, especially if the SHP2 inhibitor was included in the treatment, although this condition was largely asymptomatic. One mouse in the KRASi + SHP2i combination group presented with particularly elevated levels for both of the aforementioned enzyme activities. However, when tracing back notes the health condition and weight measurements for this mouse, this toxicity appeared to have been largely asymptomatic as well, since the mouse had neither lost weight nor shown signs of discomfort. It was also surprising that two mice in the dual KRASi + SHP2i combination group presented higher toxicity levels compared to mice in the triple combination group. Following up on this did not warrant any clear explanations. Since mice in this experiment had only been treated for one week before being sacrificed for the flow cytometric analysis of tumours it is also possible that liver toxicity may have increased if mice had remained on treatment for a longer time.

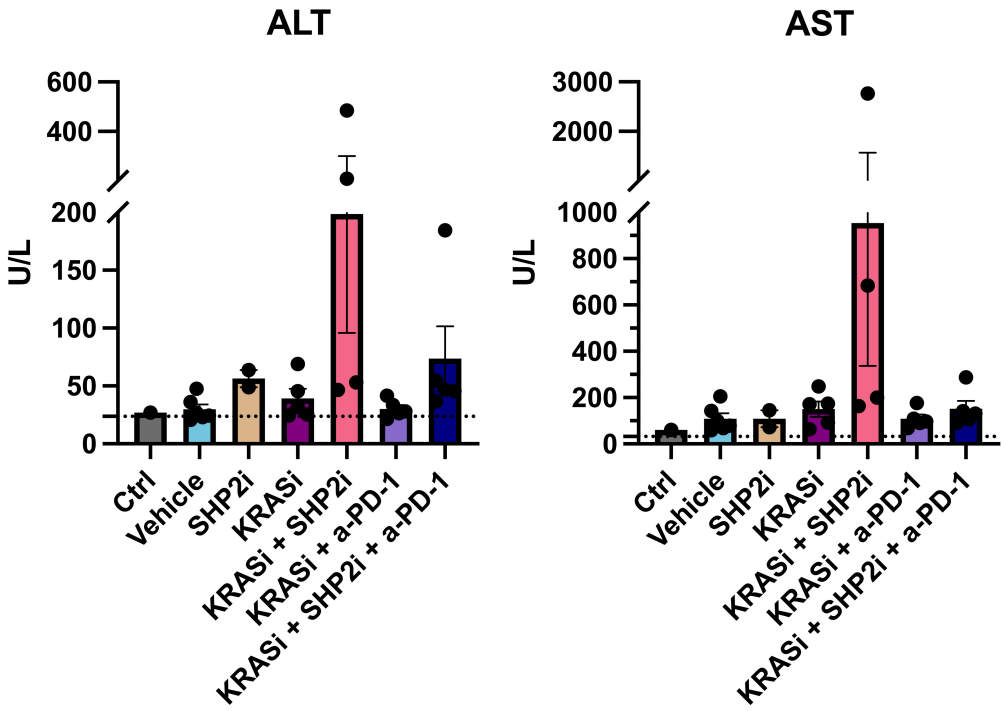


Figure 4.7 Investigating treatment-related hepatotoxicity. ALT and AST Enzyme activity was tested in serum isolated from indicated treatment groups, each dot is representative of serum isolated from 1 mouse; measurements are plotted as units/litre (U/L). At the point of sample collection, mice had been treated for 7 days, with SHP2i RMC-4550 being administered at 30 mg/kg, KRASi RMC-4998 being administered at 100 mg/kg and 2 doses of a-PD-1 being administered at 10 mg/kg. Error bars indicate mean + SEM, a one-way ANOVA test between all treatment groups and vehicle was performed, however, none of the changes were significant in respective plots. Additionally, healthy serum levels for respective enzyme activities in mice, based on literature research, 23.7 (± 2.3) U/L for ALT and 32.4 (± 2.2) U/L for AST, are indicated by the dotted horizontal line. This experiment was performed with the kind help of Sapta Mukherjee from our group.

Next, the dual treatment combination of SHP2i + a-PD-1 was tested for synergistic treatment effects on KRAS G12C or KRAS G12D tumours (**Figure 4.8a**). This control was performed to isolate the contribution of this dual treatment combination on eliminating respective tumour cell populations. Surprisingly, although KRAS G12D cells did not response to single therapies (**Figure 4.2**), this treatment combination was able to achieve tumour regression in both, KRAS G12C- and G12D-derived tumours (**Figure 4.8b,c**), with one CR mouse engrafted with a KRAS G12D-derived tumour. This experiment indicates that additional treatment synergy between SHP2i + a-PD-1 may have contributed to the increased number of complete responders in the triple-

combination treatment group of the previous experiment (**Figure 4.5**). Of note, mice in this experiment were treated for three weeks to match the treatment schedule of the triple-combination experiment while the single therapies had previously only been administered for two weeks.

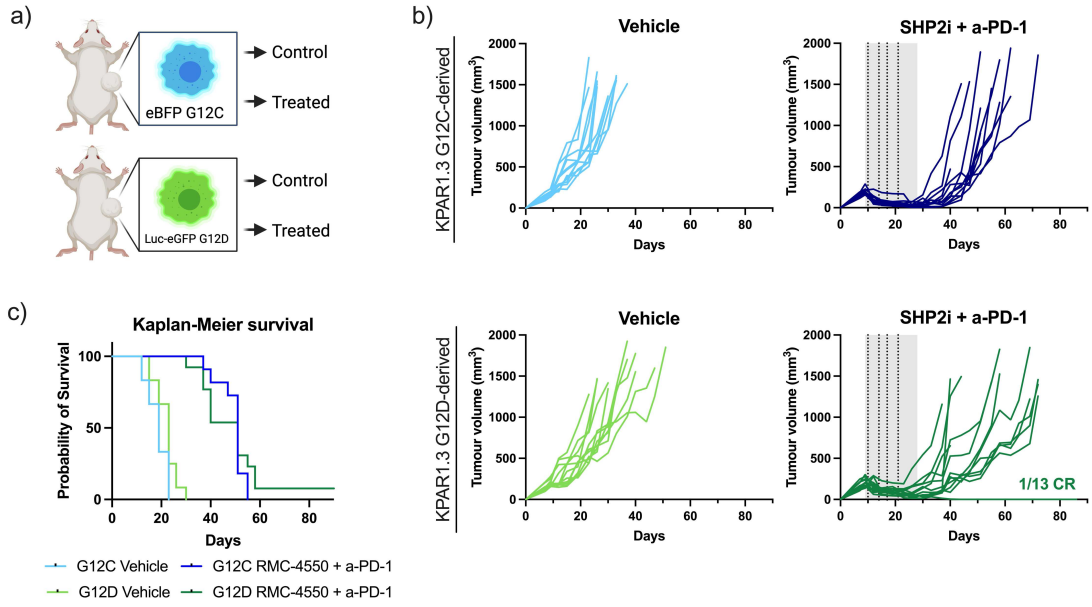


Figure 4.8 Investigating synergy of SHP2i and a-PD-1 treatment combination. a) Schematic of experiment. b) Individual tumour growth of eBFP KPAR1.3 KRAS G12C (blue) or Luc-eGFP KPAR1.3 KRAS G12D (green) derived tumours by treatment group; SHP2i RMC-4550 was administered as oral gavage at 30 mg/kg for 3 weeks, whereat 18 doses were administered (grey area on respective plots) and 4 doses of a-PD-1 were given via IP injection at 10 mg/kg, indicated by vertical dotted lines. c) Survival probability of all treatment groups, cut off value selected was a tumour volume of 500 mm^3.

Lastly, we also wanted to test whether the therapy-enhanced formation of immune memory was independent of reporter construct expression. Therefore, we selected the CRs from two experiments, and engrafted untraced, parental KPAR1.3 cells for the re-challenge branch of the respective experiments. This included the CR from the previous experiment (**Figure 4.8**), as well as the CRs from the experiment where mice had been engrafted with eBFP+ KPAR1.3 KRAS G12C tumours and were then treated with KRASi (**Figure 4.2b**). Although the number of CRs utilised to test this hypothesis was small and further validation would be necessary to draw any definite conclusions, one CR of each experiment was able to immune reject the untraced KPAR1.3 cells

during the re-challenge, hinting that an immune response had formed independently of reporter construct expression (**Figure 4.9**).

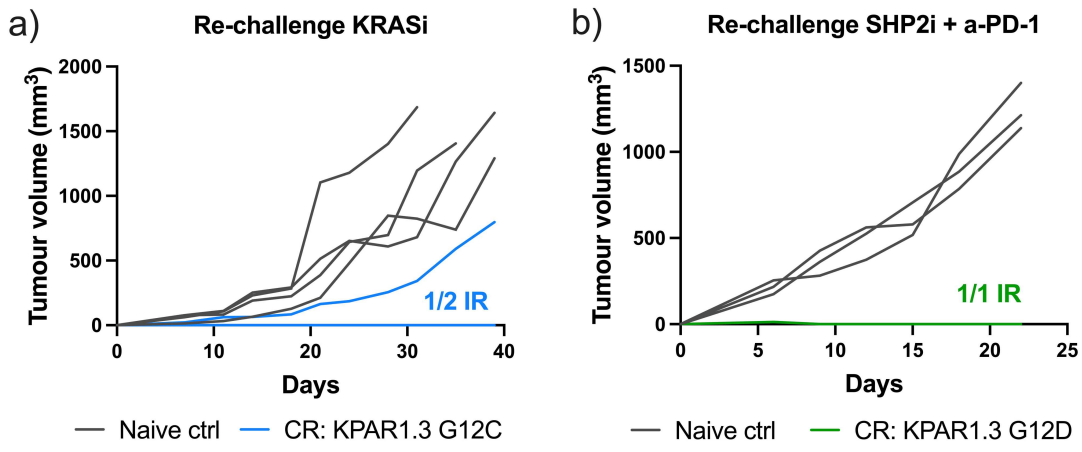


Figure 4.9 Dependency of immune memory on reporter constructs. IR: mice which successfully immune-rejected the cancer cells engrafted on the opposite flank; naïve mice for each re-challenge experiment were age and gender matched to CRs a) Re-challenge of CRs from **Figure 4.2b**; mice were engrafted on the opposite flank with 150,000 untraced, KPAR1.3 KRAS G12D cells. b) Re-challenge of CR from **Figure 4.8**; mice were engrafted on the opposite flank with 150,000 untraced, KPAR1.3 KRAS G12C cells.

Overall, in this line of experiments, we found that combination therapies can generate a durable, immune-mediated rejection of tumours containing a KRAS G12Ci-resistant sub-population. Resistant cells were not sensitive to SHP2i or aPD-1 therapies, which would indicate that double therapy treatments resulted in the bystander killing of the resistance KRAS G12D cells. Further, indications of immune memory towards KPAR1.3 cancer cells was found.

4.4 Testing treatment response in subcutaneous model with an alternative KRAS G12Ci-resistant subpopulation

Mechanisms of KRAS G12Ci resistance development have been studied in both patient samples and pre-clinical model systems. These studies have revealed that tumour cells can evolve in myriad ways to circumvent KRAS

G12C inhibition, one occurrence being acquisition of further mutations in the KRAS G12C mutant protein itself, which hinders the interaction of respective small molecule inhibitors[239 235 236,237]. By introducing a KRAS G12D mutant subpopulation to engrafted tumours, we model one of these mechanisms. However, we wanted to assess whether our combination therapy strategy might also encompass wider clinical implications. Therefore, it was investigated whether bolstering anti-tumour immunity to reject KRAS G12Ci-resistant sub-populations would also be effective when introducing a subpopulation with a different type of resistance mechanism. Here, KPAR1.3 cell lines retaining their KRAS G12C mutation, but presenting with increased resistance to Adagrasib were employed, here referred to as KPAR1.3 G12C^{Res} cell lines. This was done in a collaborative project together with Sareena Rana and Sophie de Carné.

For the establishment of KPAR1.3 G12C^{Res} cell lines, Sophie de Carné injected original KPAR1.3 KRAS G12C cell line via tail vein in immune competent C57BL/6J mice. Mice were then monitored via weekly micro-CT scans and, once tumours were established, mice were treated with 50 mg/kg Adagrasib as indicated in (**Figure 4.10**). Here, tumour bearing mice were given a treatment break when tumours regressed and were subsequently put back on treatment when tumours grew back. This intermittent pattern was repeated until mice no longer responded to KRAS G12Ci. Next, a total of 5 tumours were isolated from the lungs of the two mice from which five cell lines were established. Here one batch of each line was continuously cultured in Adagrasib-supplemented media while the other culture was maintained without the addition of this inhibitor. The addition of Adagrasib to the media would ensure the continuous selection of drug-resistant tumour cell subclones, in case tumours also harboured remaining treatment responsive cells. On the other hand, the batch of cells cultivated without the addition of further KRAS G12Ci would help to discern whether resistance development had likely taken place in *vivo* or only after culturing the cells with Adagrasib. Ex *vivo* cultures were passaged five times to purify cancer cell lines from immunocytes and other remnants of the TME, which are short lived in the culture conditions applied to select for epithelial cells.

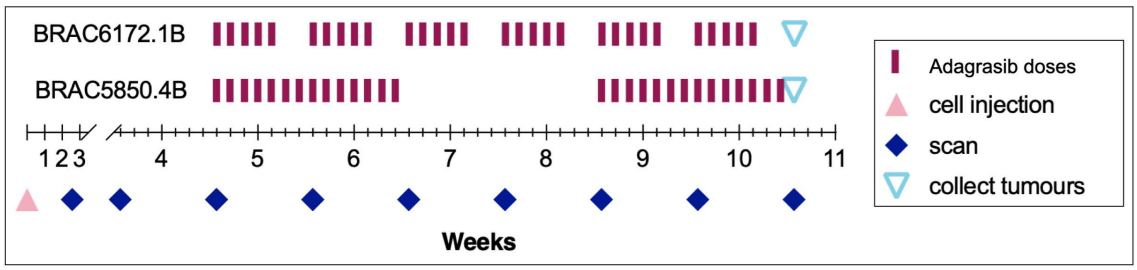


Figure 4.10 Treatment scheme of generating Adagrasib-resistant tumours. This figure was adapted from an illustration made by Sophie de Carne (unpublished). The light red triangle on the left side of the x-axis indicates the beginning of the in *vivo* experiment, when KPAR1.3 cells were injected via tail vein; the individual doses of Adagrasib (50 mg/kg) are indicated by the red lines for the two C57BL/6J mice: the blue rhombuses below the x-axis indicate the weekly of micro-CT scans; the inverted light blue triangles indicate the point of tumour isolation.

Next, viability assays were ran to evaluate the degree of drug resistance to Adagrasib (**Figure 4.11a**) as well as the MEK inhibitor Trametinib (**Figure 4.11b**). The latter inhibitor was included to assess the efficacy of KRAS G12Ci on downstream signalling activity. Out of the five tested KPAR1.3 G12C^{Res} cell lines, the cell line 2 (KPAR1.3 G12C^{Res2}) was most resistant to Adagrasib, although it did not display complete resistance, compared to the control of the original KPAR1.3 KRAS G12D cell line. Interestingly, however, line KPAR1.3 G12C^{Res2} was significantly more resistant to Trametinib, compared to both the other KPAR1.3 G12C^{Res} cell lines as well as the parental control KPAR1.3 cell lines.

Additionally, in these viability assays only moderate differences were observed between the KPAR1.3 G12C^{Res} lines that were cultured either with- or without Adagrasib supplementation to the culture media. This could indicate that KRAS G12Ci resistance had already developed in *vivo*, prior to cell line establishment. This might indicate that KRAS G12Ci resistance mechanisms were not based on a transient change in gene expression but may rather be indicative of a more permanent alteration.

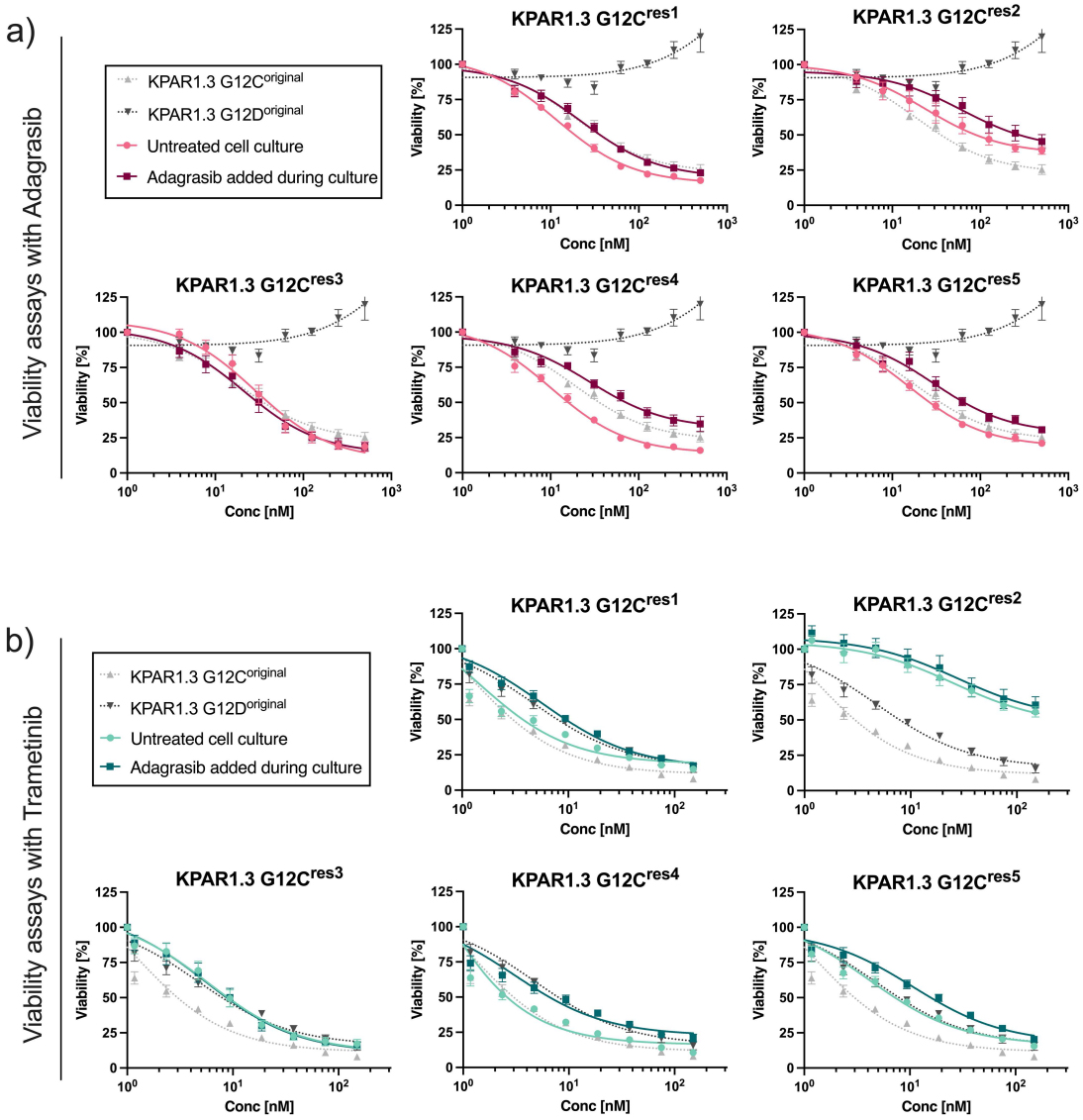


Figure 4.11 Assessing drug response of KPAR1.3 G12C^{res} cell lines. Viability assays for newly established cell lines, which had previously been propagated in in presence or absence of Adagrasib, as indicated in respective legends. Additionally, the viability assays were also conducted on the original KPAR1.3 KRAS G12C or G12D cell lines as controls; these are plotted alongside each of the newly established cell lines as reference. Viability assays were performed using a) Adagrasib or b) Trametinib, with the respective concentration gradients being indicated on the x-axis. Experiments are comprised of 3 independent biological replicates with 3 technical replicates each, plot points indicate mean + SEM, connecting lines were fitted using a non-linear transformation.

We suspected that the partial response to Adagrasib and possibly also Trametinib in KPAR1.3 G12C^{Res2} may be related to a certain degree of heterogeneity within this bulk cancer cell population. To further disentangle the resistance mechanism(s), present in the KPAR1.3 G12C^{Res2} cells, this line was

further single-cell sub-cloned and several emerging clones were selected for further analysis. Here the KPAR1.3 G12C^{Res2} which had been propagated without Adagrasib supplemented to the culture media was selected.

Sareena Rana from our research group then performed further characterisation of the selected clones, including viability assays, qPCRs and western blots. Because this part of the collaboration was performed by another lab member, it will not be discussed in detail here. However, an exemplary western blot is included, which indicates a shift in RTK expression, from EGFR in the parental KPAR1.3 cell line to the fibroblast growth factor receptor (FGFR) in the resistant clones. A loss of E-cadherin in resistant clones was also observed (**Figure 4.12a**). Together, this might indicate a transition from an epithelial to mesenchymal phenotype leading to drug resistance. Viability assays with the KRAS G12C(OFF) inhibitor Adagrasib and KRAS G12C(ON) inhibitor RMC-4998 indicate a significant increase in resistance for both KPAR1.3 G12C^{Res2} sub-clonal cell lines towards both drugs compared to the original KPAR1.3 cell line. Further, both subclones displayed a significantly increased resistance to trametinib, compared to the parental KPAR1.3 KRAS G12C cell line, indicating that the lines with increased resistance might share a common origin (**Figure 4.12b**). Other potential contributions to the increased resistance to KRAS G12Ci were also assessed, via time course or viability assays. However, so far no clear other resistance signature has been identified. Recently, an RNA-sequencing experiment was also initiated to investigate this, but results are not yet available.

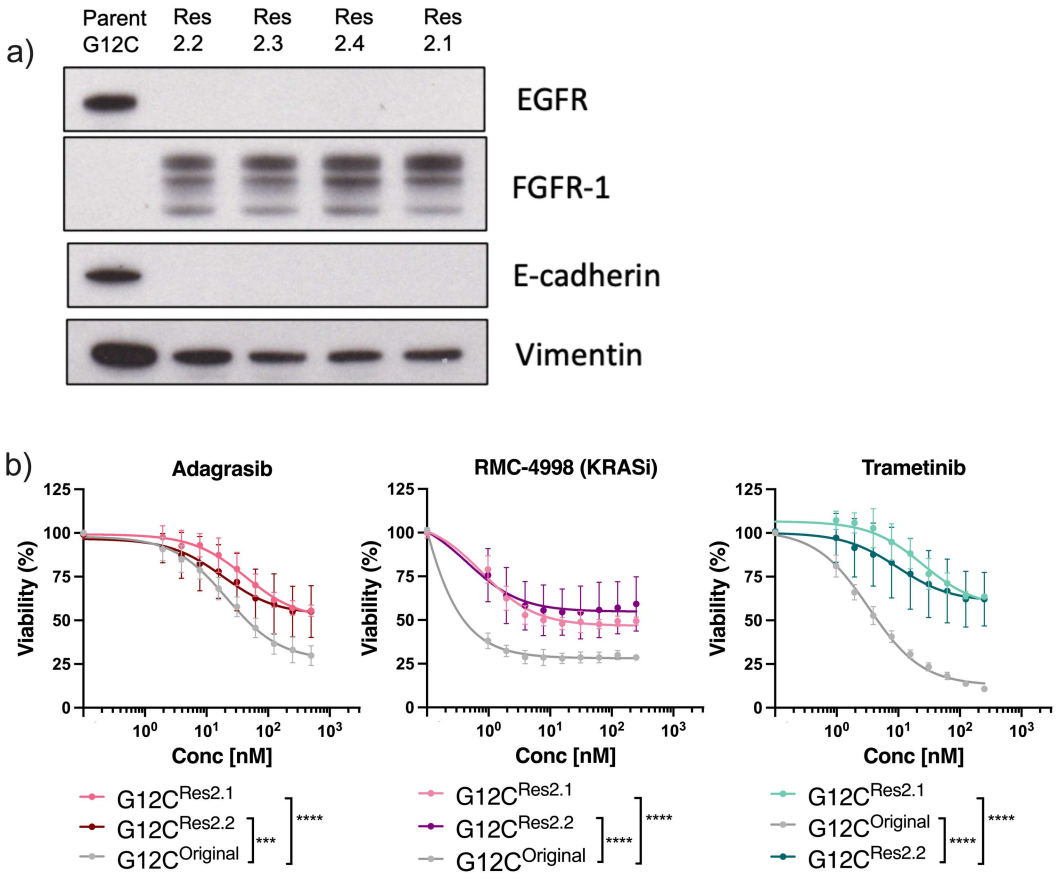


Figure 4.12 Resistance mechanisms in sub-clones of KPAR1.3 G12C^{res} cell line 2. a) Representative Western blot showing protein expression of parental KPAR1.3 G12C (Parent G12C), as well as KPAR1.3 G12C^{Res2} sub-clones (written as Res$^{2.x}$). Vimentin is included as loading control. b) Viability assays with indicated cell lines for the inhibitors (left to right) Adagrasib, RMC-4998, and Trametinib; data is representative of 3 independent experiments, each performed with three technical replicates, error bars indicate SEM. A two-way ANOVA test was performed to assess cell line related differences in drug response, comparisons between the parental KPAR1.3 cell line and KPAR1.3 ^{Res2} sub-clonal lines are indicated. Western blot and viability assays done by Sareena Rana.

Based on this initial in *vitro* analysis, two of the sub-clonal cell lines were selected for further in *vivo* characterisation, where they were engrafted subcutaneously in immune-competent mice. This experiment tested whether, compared to the original KPAR1.3 KRAS G12C cell line (**Figure 4.13a**), the two selected clones, KPAR1.3 G12C$^{res2.1}$ (**Figure 4.13b**), and KPAR1.3 G12C$^{res2.2}$ (**Figure 4.13c**) retained their resistance to Adagrasib when re-engrafted in mice. Here, mice were treated for two weeks, once an average tumour volume of ~200 mm^3 was reached. Compared to the parental cell line, tumours derived from both, KPAR1.3 G12C$^{res2.1}$ and KPAR1.3 G12C$^{res2.2}$ displayed an increased

resistance to Adagrasib in *vivo*. Tumours established from the parental cell line regressed on treatment and one CR was generated. On the other hand, the growth rate of KPAR1.3 G12C$^{res2.1}$-derived tumours decreased somewhat initially during Adagrasib treatment, however, most tumours relapsed on-treatment. KPAR1.3 G12C$^{res2.2}$ seemed the most resistant to Adagrasib, as tumours continued to grow during treatment, although at a slightly lower rate compared to the vehicle tumours.

Additionally, the two selected subclones also grew at a faster baseline rate compared to the original KPAR1.3 KRAS G12C cell line, as visualised in **Figure 4.13d**. Here, the grouped growth rates over time within each cell line may look inconstant, especially in the vehicle group. However, this is due to mice with tumours reaching the defined size endpoint being culled after each measurement, thereby possibly decreasing the average tumour volume of the consecutive measurement. As a consequence to the difference in basal growth rate, mice with tumours derived from the resistant cell lines were put on treatment earlier after engraftment (**Figure 4.13e**). Nonetheless, the two resistant cell lines responded less to Adagrasib treatment compared to the original KPAR1.3 G12C cell line, particularly the line KPAR1.3 G12C$^{res2.2}$. This trend was also seen when comparing the survival probabilities of Adagrasib treated mice (**Figure 4.13f**).

KPAR1.3 G12C$^{res2.2}$ line appeared to be more resistant to KRAS G12Ci in *vivo*, compared to KPAR1.3 G12C$^{res2.1}$ line. Therefore, out of the two cell lines, the KPAR1.3 G12C$^{res2.2}$ line was selected for further investigation.

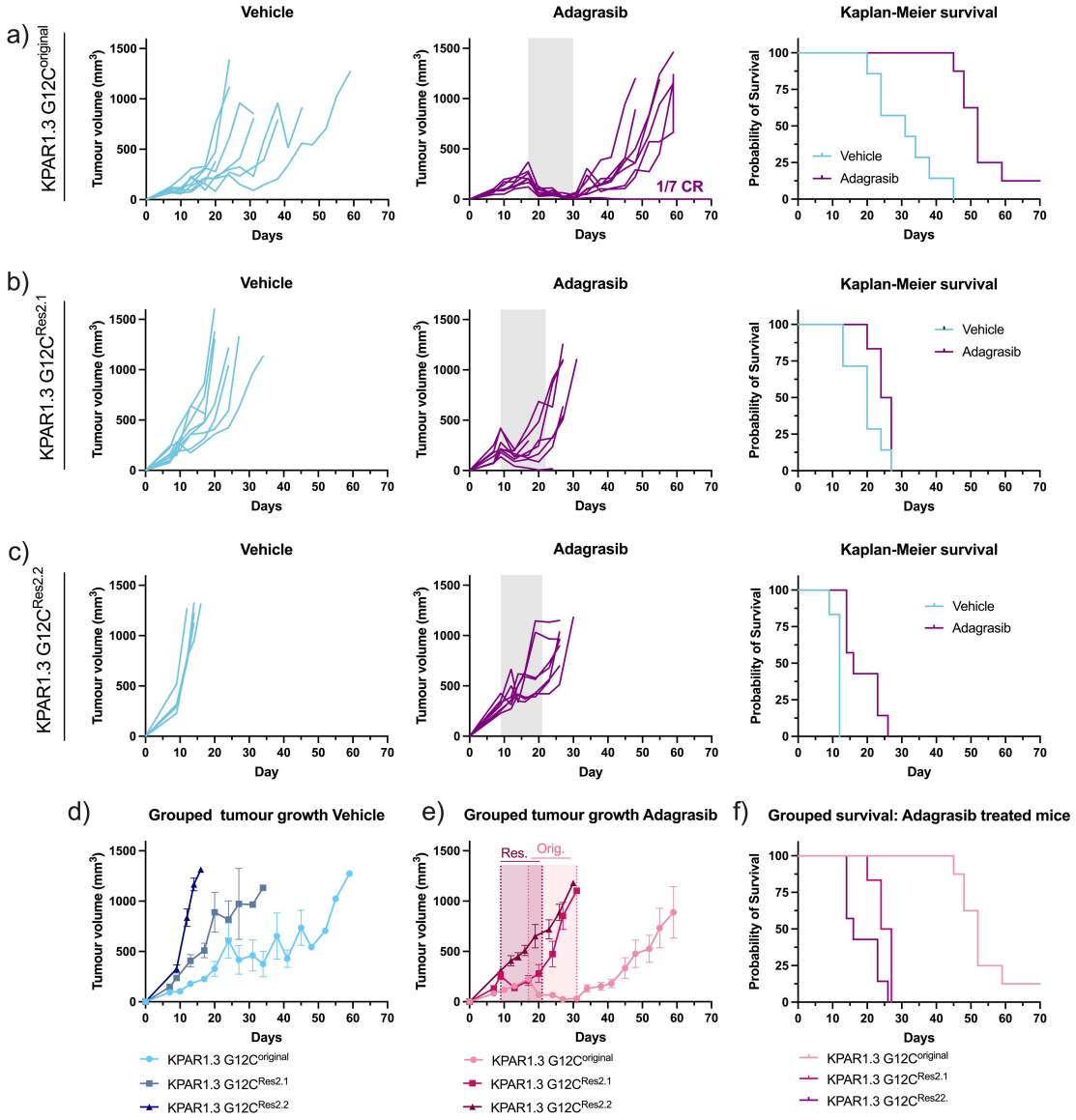


Figure 4.13 Therapy resistance of lines KPAR1.3 G12C$^{res2.1}$ and - G12C$^{res2.2}$ in *vivo*. Growth of subcutaneous tumours derived from a) KPAR1.3 G12C^{original}, b) KPAR1.3 G12C$^{res2.1}$, and c) KPAR1.3 G12C$^{res2.2}$ cell lines was measured. Each line is representative of a single tumour. Mice were stratified into either Vehicle- or Adagrasib treatment group when average tumour volume had reached ~200 mm^3. Treated mice received 12 doses of 100 mg/kg Adagrasib within 2 weeks. For Kaplan-Meier survival plots in the right panel, a tumour volume of 500 mm^3 was selected as cutoff value. Tumour growth of d) vehicle mice, and e) Adagrasib-treated mice are shown, grouped by cell line and plotted as mean + SEM. For the latter plot, KPAR1.3 G12C$^{res2.1}$, and KPAR1.3 G12C$^{res2.2}$ tumour-bearing mice were treated from day 9 to day 21, while KPAR1.3 G12C^{orig} mice were put on treatment from day 17 to day 31; respective treatment periods are indicated through highlighted areas. f) Visualisation of survival probability of all Adagrasib treated mice by treatment group; 500 mm^3 was selected as cutoff value.

We next wanted to test whether the KPAR1.3 G12C$^{res2.2}$ cell line, might also have developed a degree of cross-resistance towards other therapy lines.

Therefore, we engrafted KPAR1.3 G12C$^{res2.2}$ -derived subcutaneous tumours to assess drug response towards the KRAS G12C(ON)i RMC-4998 and the SHP2i RMC-4550. This was tested either as monotherapies (**Figure** 4.14**a**) or as dual therapies (**Figure** 4.14**b**), where the combination of RMC-4998 and a-PD-1 was also included. We indeed found that tumours presented with increased resistance of the respective therapy lines. For example, 5/7 KPAR1.3 G12C$^{res2.2}$ derived tumours progressed on RMC-4998 treatment. Further, no CRs were generated, with all primary tumours growing back after treatment. Plotting survival probabilities indicated moderate efficacy of treatments, with tumours of mice treated with combination therapies responding slightly better compared to monotherapy (**Figure** 4.14**c**).

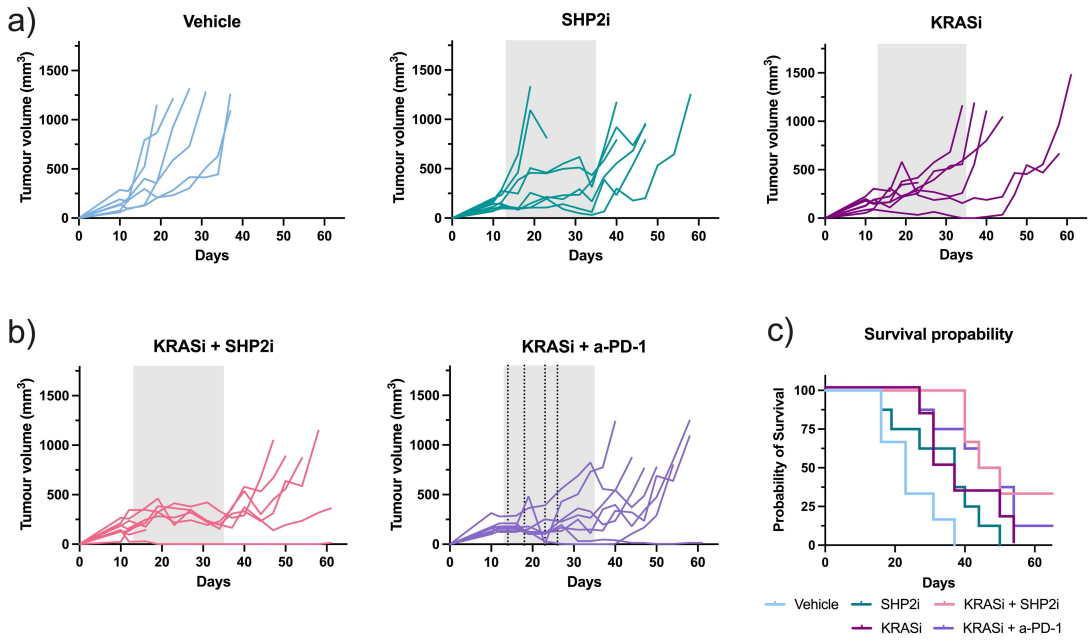


Figure 4.14 Assessing therapy cross resistance of KPAR1.3 G12C$^{res2.2}$ line. Mice were engrafted with KPAR1.3 G12C$^{res2.2}$-derived subcutaneous tumours. SHP2i: RMC-4550, administered at 30 mg/kg; KRASi: RMC-4998, administered at 100 mg/kg; a-PD-1 was administered at 10 mg/kg. Mice were treated for three weeks, in which respective treatment groups received 18 doses of oral gavages and 4 doses of a-PD-1; treatment period for oral gavages are indicated by grey areas in respective plots and a-PD-1 doses by vertical dotted black lines. a) Tumour growth for individual mice of vehicle or monotherapy treated mice. b) Tumour growth for mice receiving therapy combinations; c) Survival probabilities plotted by treatment group.

Now that the KPAR1.3 G12C$^{res2.2}$ cell line had been characterised through both, in *vitro* and in *vivo* experiments, we wanted to introduce this line as an alternative drug-resistant subpopulation. This was to test whether our therapy combination strategy would also be applicable in a larger context to target the development of drug resistance. To clearly distinguish the KPAR1.3 G12C$^{res2.2}$ cell line in tumours comprised of mixed cancer cells, it was also transduced with the Luc-eGFP reporter with the kind help of Sareena Rana and a visiting student, Isabel Rafalin.

Subsequently, tumours comprised of 99.96% eBFP KRAS G12C cells and 0.04% Luc-eGFP KPAR1.3 G12C$^{res2.2}$ cells were engrafted subcutaneously in GH mice. Tumour size was measured via calliper and the relative fraction of Luc-eGFP KPAR1.3 G12C$^{res2.2}$ cells over time was assessed via IVIS scans. In the first pilot experiment **(Figure 4.15a**), we wanted to test how the KPAR1.3 G12C$^{res2.2}$ subpopulation would respond to KRAS G12Ci. As the KPAR1.3 KRAS G12D-based subpopulation in previous studies was found to be proliferating at an accelerated rate compared to the vehicle control (**Figure 4.1, Figure 4.3**). Here, IVIS scans indicated that the Luc-eGFP KPAR1.3 G12C$^{res2.2}$ cells did not increase in proliferation in this experiment. This may be related to this cell line still retaining a partial response to KRAS G12Ci (**Figure 4.15a**).

After this initial test **(Figure 4.15b**), we wanted to test whether CRs could be generated with the triple-combination treatment scheme when employing this alternative subpopulation with increased KRASi resistance. Here, we engrafted tumours and defined treatment parameters to match the triple-combination treatment experiment with the Luc-eGFP KPAR1.3 KRAS G12D subpopulation, to assess if CRs could be generated (**Figure 4.5**). We again injected 1.5 *10^5 cancer cells comprised of 99.96% eBFP-transduced KPAR1.3 KRAS G12C cells and 0.04% Luc-eGFP KPAR1.3 G12C$^{res2.2}$ cells. In one of the IVIS scans, a signal peak was observed for one of the vehicle tumours with a magnitude of

2.68e+009 photons/s/cm^2. This spike may be related to a dual injection of d-luciferin, as the signal had returned to a lower value in the subsequent scan.

Treatment with the triple combination was able to generate 6/11 CRs. An additional mouse had also remained tumour free for 2.5 weeks post treatment but had to be culled early due to health concerns and was hence not counted as CR. The volume of 2/4 tumours that did grow back after treatment was still below 50 mm^3 30 days after the treatment had ended, indicating immune-mediated tumour control may still have been generated. The number of CRs in this experiment was lower than the 10/12 CRs obtained when a KRAS G12D mutant cell line was used as a drug-resistant population (**Figure 4.5**). This could have been related to the faster proliferative rate of this cell line. However, overall, these results indicate that the combinations proposed might also target other mechanisms of resistance.

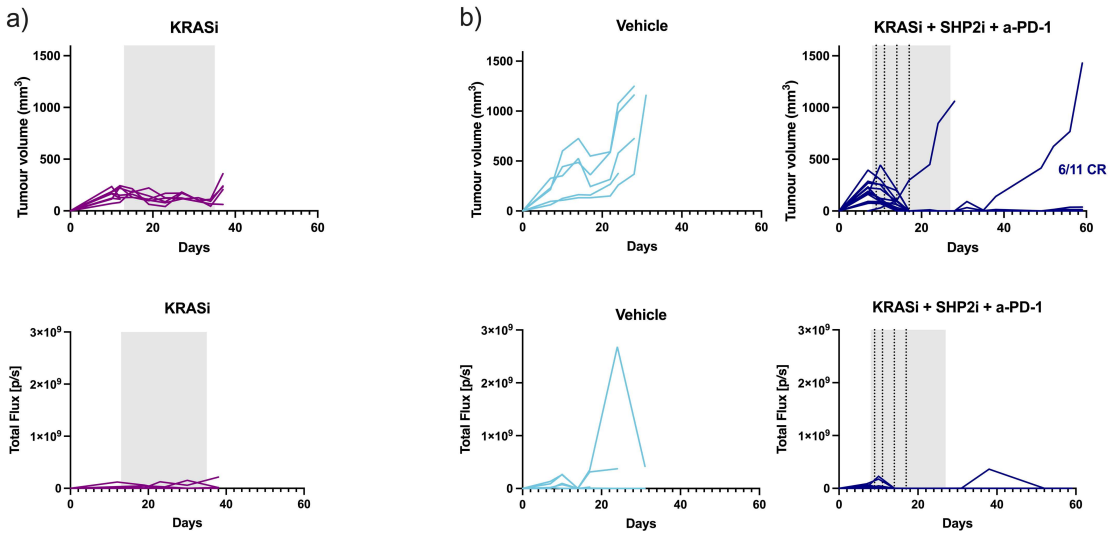


Figure 4.15 KPAR1.3 G12C$^{res2.2}$ line as alternative KRASi-resistant sub-population. Mice were engrafted with subcutaneous tumours comprised of 99.96% eBFP-transduced KPAR1.3 KRAS G12C cells and 0.04% Luc-eGFP KPAR1.3 G12C$^{res2.2}$ cells. KRASi: RMC-4998, administered at 100 mg/kg; SHP2i: RMC-4550, administered at 30 mg/kg; a-PD-1 was administered at 10 mg/kg. Mice were treated for three weeks, in which respective treatment groups received 18 doses of oral gavages and 4 doses of a-PD-1; treatment period for oral gavages are indicated by grey areas in respective plots and a-PD-1 doses by vertical dotted black lines. a) Upper panel: Tumour growth and lower panel: IVIS scans for individual mice of KRASi treated mice. b) Upper panel: Tumour growth and lower panel: IVIS scans for individual mice for Vehicle and triple combination treated mice.

Overall, in our preclinical murine model system, we were able to show that the proposed combination therapy schemes were able to enhance the rejection of tumours containing a treatment-resistant subpopulations. Further investigation indicated that this was achieved by fostering anti-tumour immunity, possibly capable of recognising a pan-cancer-cell archetype and thereby also eliminating drug-resistant sub-populations. Complete responder mice further presented with enhanced immune memory.

The next two chapters explore the underlying mechanisms governing therapy-induced TME re-composition and promoting anti-tumour immunity. Specifically, **Chapter 5** focuses on understanding how drug-sensitive or -resistant tumour cells respond to exposure to different anti-cancer drugs and anti-tumour immunity. **Chapter 6** examines how the different anti-cancer drugs contribute to fostering an effective immune-response and the development of immune memory. This was achieved through a combination of in *vivo* studies, immune-phenotyping and the exploration of spatial TME organisation.

Chapter 5. Investigating therapy effects on tumour cell compartment

We have discovered that employing KRAS G12Ci as monotherapy on tumours containing a fraction of KRAS G12D cells had accelerated the development of drug resistance. This was not observed with the KPAR1.3 G12C$^{res2.2}$ cell line which may be due to it still being partially responsive to this inhibitor. On the other hand, combination therapies were able to achieve complete rejection of tumours containing drug resistant cells in some animals and further provided a survival advantage for the majority of treated mice. To understand how therapy combinations could be employed most effectively in the clinic, the underlying mechanisms governing treatment- and/or immune mediated tumour cell elimination or outgrowth were further investigated. For this, the cell state of KPAR1.3 tumour cell fractions across treatment groups were analysed via bulk RNA sequencing (bRNA-seq) in two successive experiments. Additionally, to further disentangle cancer cell intrinsic and immune mediated influences on the tumour cell compartment, an array of further in *vitro* assays was performed.

5.1 Investigating cell state of KRASi-resistant tumour cells across treatment groups

For the first bRNA-seq experiment, we investigated how the cell state of the KRASi-resistant KPAR1.3 KRAS G12D tumour cell subpopulation would change when exposed to either KRASi alone, or in dual combination therapies with either a-PD-1 or SHP2i. Here, immune competent GH mice were engrafted subcutaneously, with the isogenic KPAR1.3 KRAS G12C and G12D mutant cancer cell lines at the ratios indicated in **Figure 5.1a**. In this experiment, for mice in the treatment groups a 99.5:0.5 ratio for the KRAS G12C : KRAS G12D mutant KPAR1.3 cells was chosen, while in the vehicle group a 50:50 ratio for the KRAS G12C : KRAS G12D mutant KPAR1.3 cells was chosen. This was

based on the previous observation that the KRAS G12D mutant tumour cells would proliferate less in vehicle-treated tumours compared to KRASi treated tumours, hence it might not be possible to obtain enough sample to perform bRNA-seq if only a small subpopulation was engrafted. On one hand, this posed a limitation for comparing between treatment groups, however, it enabled the establishment of a baseline for the cancer cell state of KRAS G12D mutant tumour cells when no treatment pressures were exuded on tumours. To allow for accurate flow cytometric sorting of the target cell populations, additional mice were engrafted with tumour cells which either expressed no FPs or only BFP or GFP.

When tumours reached a size of ~500 mm^3, mice which had not been assigned to the vehicle group at the start of the experiment, were stratified into treatment groups. Tumours were grown to a larger volume before the start of treatment, compared to previous survival experiments to allow for enough material to remain for bRNA-seq after the treatment period. In this experiment, mice were treated with oral drugs for 6 successive days, whereat 2 doses of a-PD-1 were also administered to mice in the respective treatment group. Subsequently, tumours were harvested, dissociated into a single cell suspension and the auto fluorescent red blood cells were lysed. A viability dye was then added to each sample for gating out dead or apoptotic cells which may also display increased autofluorescence and show up as false positive events in the sorting gates. Tumour cells were then flow cytometrically sorted via their FP expression and snap frozen (**Figure 5.1b**). RNA was then isolated from the collected KPAR1.3 KRAS G12D tumour cell fractions and submitted to the advanced sequencing facility at the Crick, who kindly created the cDNA libraries and performed NGS sequencing.

Initially, in this experiment we had aimed to sort both, the eBFP G12C and Luc-eBFP G12D tumour cell fraction. However, when running the negative control of a tumour sample established from untraced KPAR1.3 cells to set the sorting gates, it was discovered that a population of highly auto fluorescent cells were

present in the eBFP$^+$ gate. Since eBFP is inherently a dimmer fluorophore, the distance of the eBFP positive population to the gate is relatively small, thereby exacerbating segregation from cell populations with a high autofluorescence profile. Back gating on the forward and side scatter implied that these false positive events likely stemmed from immunocytes. Treatments might also influence the quantity of CD45$^+$ cells present in different treatment groups, which could further alter the fraction of immune cell contamination present in the eBFP$^+$ gate. Because of this, it was decided to only proceed with the Luc-eGFP KRAS G12D tumour cell fraction in this experiment which had been clearly distinguishable. Another caveat of this first bRNA-seq experiment was that samples of the treatment combination groups of KRASi + SHP2i and KRASi + a-PD-1 cells from individual tumours had to be pooled in groups of three to four tumours per sample to obtain sufficient material. This could increase the variability of gene expression within these samples compared to unpooled samples, which had to be taken into account in the subsequent analysis. Of note, all of the aforementioned experimental limitations were resolved in the second bRNA-seq experiment.

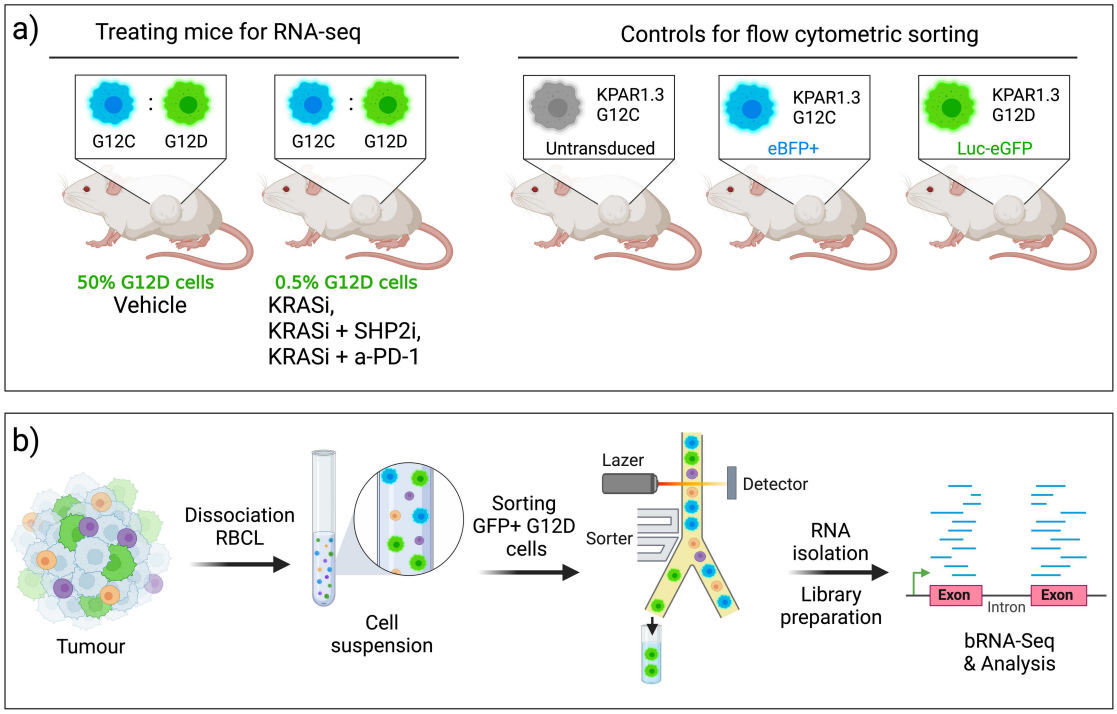


Figure 5.1 Schematic of sample acquisition for bRNA-seq. Overview of in *vivo* part for bRNA-seq experiment; left: 2 tumours for each control group, with or without single FPs were engrafted, to allow for accurate gating during cell sort; right: Tumours engrafted for bRNA-seq sample acquisition, fraction of Luc-eGFP G12D cells of all engrafted cancer cells indicated for respective treatment group. Mice were put on treatment when average volume of 500 mm^3 was reached, mice were treated with 6 doses of oral gavages for KRASi RMC-4998 at 100 mg/kg, SHP2i RMC-4550 at 30 mg/kg, and 2 doses of a-PD-1 were administered to respective mice at 10 mg/kg. b) Harvested tumours were dissociated into a single cell suspension and red blood cell lysis (RBCL) was performed; Luc-eGFP G12D cells were then collected via flow cytometric sorting, subsequently, RNA was isolated, libraries were generated from samples and NGS sequencing was performed. Image was created with BioRender.

Thanks to the kind mentorship of Dr. James Campbell, the bioinformatics training officer at the Crick, I was able to analyse the sequencing data for the bRNA-seq experiments in this project.

The raw sequencing data obtained from advanced sequencing facility was first run through the nf-core pipeline[303], which performs a streamlined pre-processing (**Figure 5.2**). In brief, poly-A tail capture probe and sequencing adapter sequences were removed, reads were aligned to a pre-selected mouse reference genome (Mus_musculus.GRCm38.95) and allocated to corresponding genes and isoforms. The reads for each transcript across all

samples were then quantified and a multi sample read count tsv output file was created.

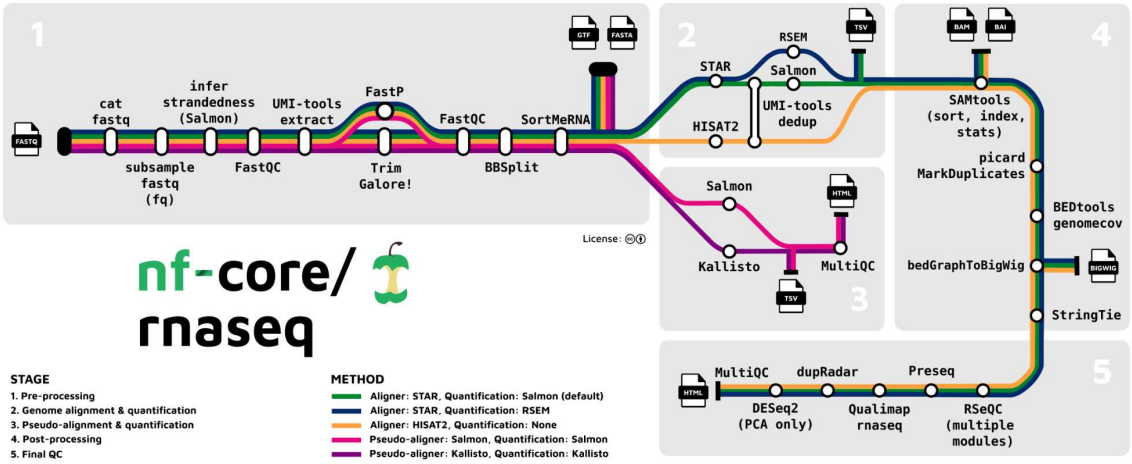


Figure 5.2 Schematic of nf-core pipeline. Visual map of bRNA-seq sample pre-processing pipeline; version 3.14.0 was employed for analysis, STAR-RSEM was chosen as aligner; instead of selecting the branch terminating in section 3, pipeline was followed through section 4 and 5, thereby including internal quality controls. Image was sourced from the nf-core website: https://nf-co.re/rnaseq/3.14.0/.

The read counts were then read into R, where sequencing quality controls were performed and the preliminary expression data was further normalised which, in large parts followed the DESeq2 vignette[304], also referenced in **methods section 2.7**. First, an experimental model was designed and encoded where biologically relevant comparisons between treatment groups were defined, while also taking potential batch effects into account.

Several sample normalisation steps were then performed. For example, the differences in total read counts between each sample during sequencing had to be taken into account. The raw read counts for each sample are visualised in (**Figure 5.3a**). Next, a size factor was calculated for each sample to allow for normalisation (**Figure 5.3b**). The respective size factors were then applied to the respective samples to normalise expression counts for each gene accordingly (**Figure 5.3c**). The reason the bars for normalised counts for different samples are not exactly at the same hight after normalisation is related to true changes in gene expression between samples.

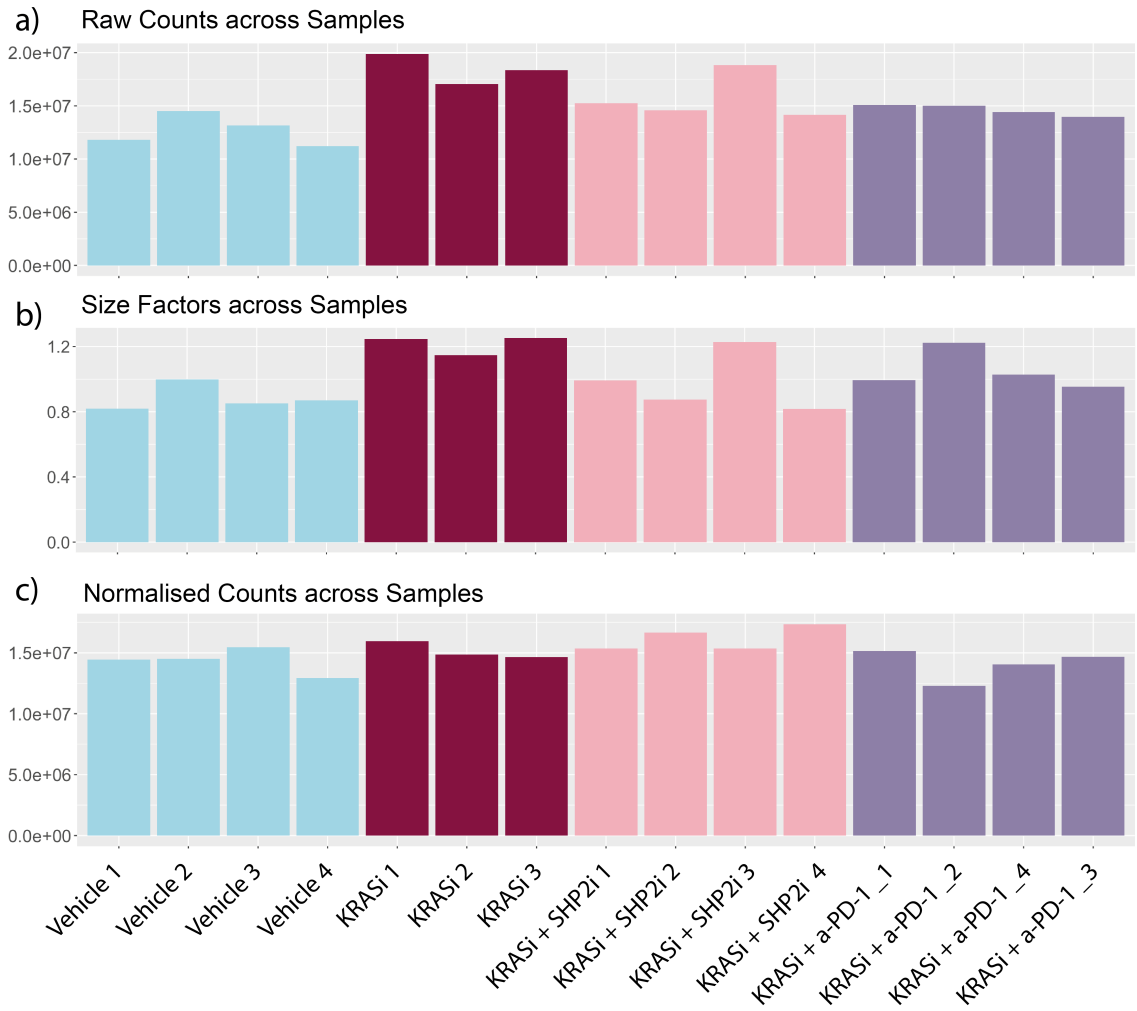


Figure 5.3 Read count normalisation. a) Total raw counts for each sample. b) Calculated size factor for each sample, used for read count normalisation. c) Total read counts after normalisation.

Additionally, the data was log-transformed, whereat the gene expression variance for genes with low read counts was assigned a lower weight. The later was done to determine meaningful gene expression changes in throughout the data set. For example, if ‘Sample 1’ has 500 reads for ‘gene A’, while ‘Sample 2’ has 2000 reads, this likely represents a meaningful alteration in gene expression, encompassing a dual log fold change. On the other hand, if ‘Sample 1’ has 2 reads while in ‘Sample 2’ 8 reads were captured, this equally represents a dual log fold change. It may, however, not represent a meaningful

change in gene expression, as read numbers in this low range may be subject to coincidental capture of RNAs with low presence.

To understand the gene-wise expression variability across all samples, the calculated gene-wise dispersion estimates for all genes across all treatment groups were plotted (**Figure 5.4**). This is an important diagnostic visualisation approach to probe the quality of the RNA-sequencing data set. Diversions from a standard pattern on this plot could indicate insufficient sample numbers, technical issues with sample quality or library preparation, insufficient sequencing depth, etc. For an expected dispersion regression, the information published by the DESeq2 vignette on bioconductor.org, as well as the underlying mathematical modelling[304] were taken as reference. In brief, for this data set, the dispersion estimations indicate high data quality and an appropriately fitted experimental design.

To further elaborate on the concept of this visualisation, due to the relatively low number of samples within each treatment group, the respective variation of expression for individual genes may be unreliable. The initial dispersion estimates for each gene are visualised as black dots in the plot below (**Figure 5.4**). The DESeq2 workflow will then estimate a mean for the expected dispersion value for genes of a given expression strength, through information sharing across all genes. The resulting mean is indicated by the red line in the dispersion plot. The initial dispersion estimated for each gene will then be regressed towards the respective predicted mean, assuming a negative binomial distribution. Here, genes with a dispersion value lower than the estimated mean are shrunk towards the red curve, genes with a dispersion estimate slightly above the estimated average are also regressed towards the estimated mean. These are represented as blue dots on the plot. However, genes displaying an exceptionally high dispersion estimate for their respective abundance, will not be regressed towards the mean. This is because the high dispersion is assumed to be indicative of a biologically meaningful change in

gene expression. These genes are highlighted as black dots surrounded by a blue circle and are not shrunk towards the predicted mean trend line.

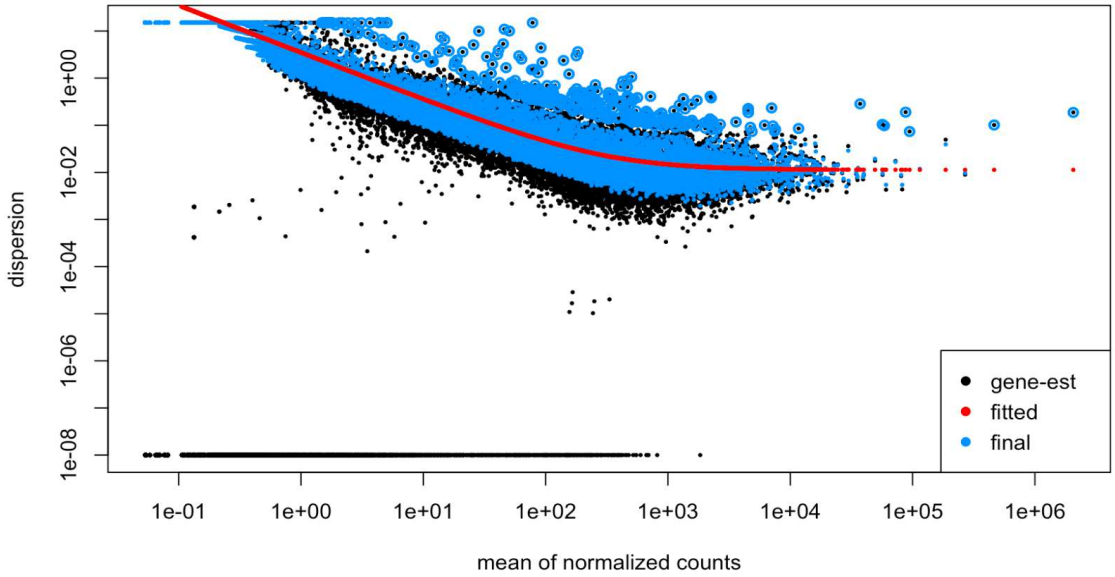


Figure 5.4 Dispersion estimates for each gene across samples. The dispersion of gene expression (y-axis) is plotted over the mean of normalised gene counts (x-axis). Each point in the plot is representative of one gene; the black dots indicate the initial maximum likelihood dispersion estimate. The red line is fitted as an estimated mean for the expected dispersion for genes with a certain number of read counts. Blue dots indicate adjusted dispersion values for individual genes. Genes with extremely high dispersion values, which are not regressed towards the mean are indicated as black dots surrounded by blue circles.

Next, a simple principal component analysis (PCA) was performed across all samples, to assess how tumour cell samples would cluster together (**Figure 5.5**). This revealed that vehicle samples clustered separately from treated samples but were closer to the groups of samples treated with KRASi, or KRASi + a-PD-1, compared to the combination treated samples in the KRASi + SHP2i group. Since KRAS G12C inhibitor RMC-4998 does not inhibit KRAS signalling in the KRAS G12D mutant tumour cells, it would be reasonable that KRASi, or KRASi + a-PD-1 cells may cluster closer together. The vehicle samples may be more distant to treated samples, due to the increased proliferation rate in the KPAR1.3 KRAS G12D mutant subpopulation in KRAS treated tumours. SHP2i, on the other hand was found to generate a moderate inhibition in the KRAS G12D-mutant cancer cell compartment. Hence it could explain why samples

treated with this combination cluster separately from the other treatment groups.

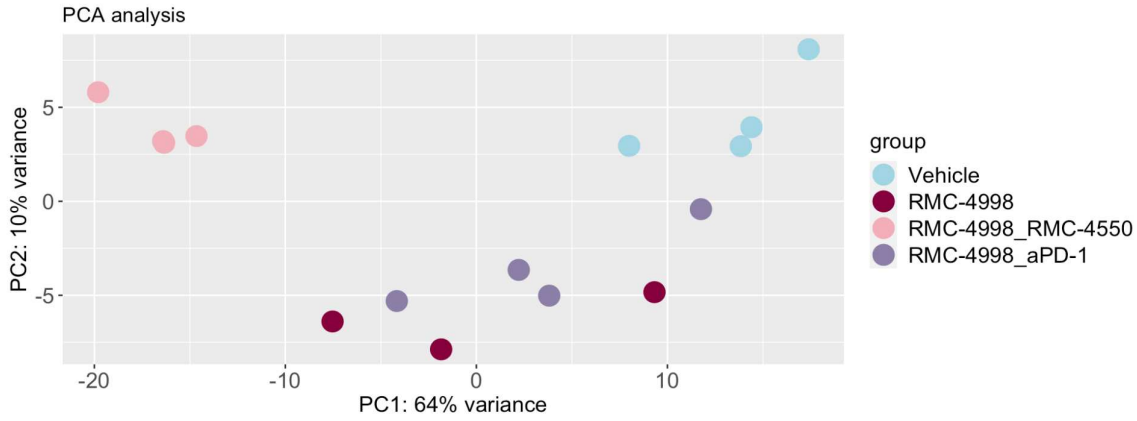


Figure 5.5 Principal component analysis of sample distribution. PCA plot visualising the sample distribution along the first two principal components. Samples are coloured by treatment group.

As mentioned above, for the combination treatment groups, sorted tumour cells from several individual tumours were pooled to obtain enough material, however, samples were not pooled for vehicle and KRASi-only treatment groups. Hence, it was assessed whether this experimental step had introduced differences in the gene expression dispersion between pooled and un-pooled samples. Plotting gene expression variability in a pairwise manner, revealed that the dispersion rate was similar between pooled and individual samples. Implying that heterogeneity in samples within one treatment group was likely small and did hence not obscure findings in pooled samples, although this analysis is not fully sufficient to interrogate this potential quarry. Exemplary plots are shown for each treatment group are shown in (**Figure 5.6a-e**).

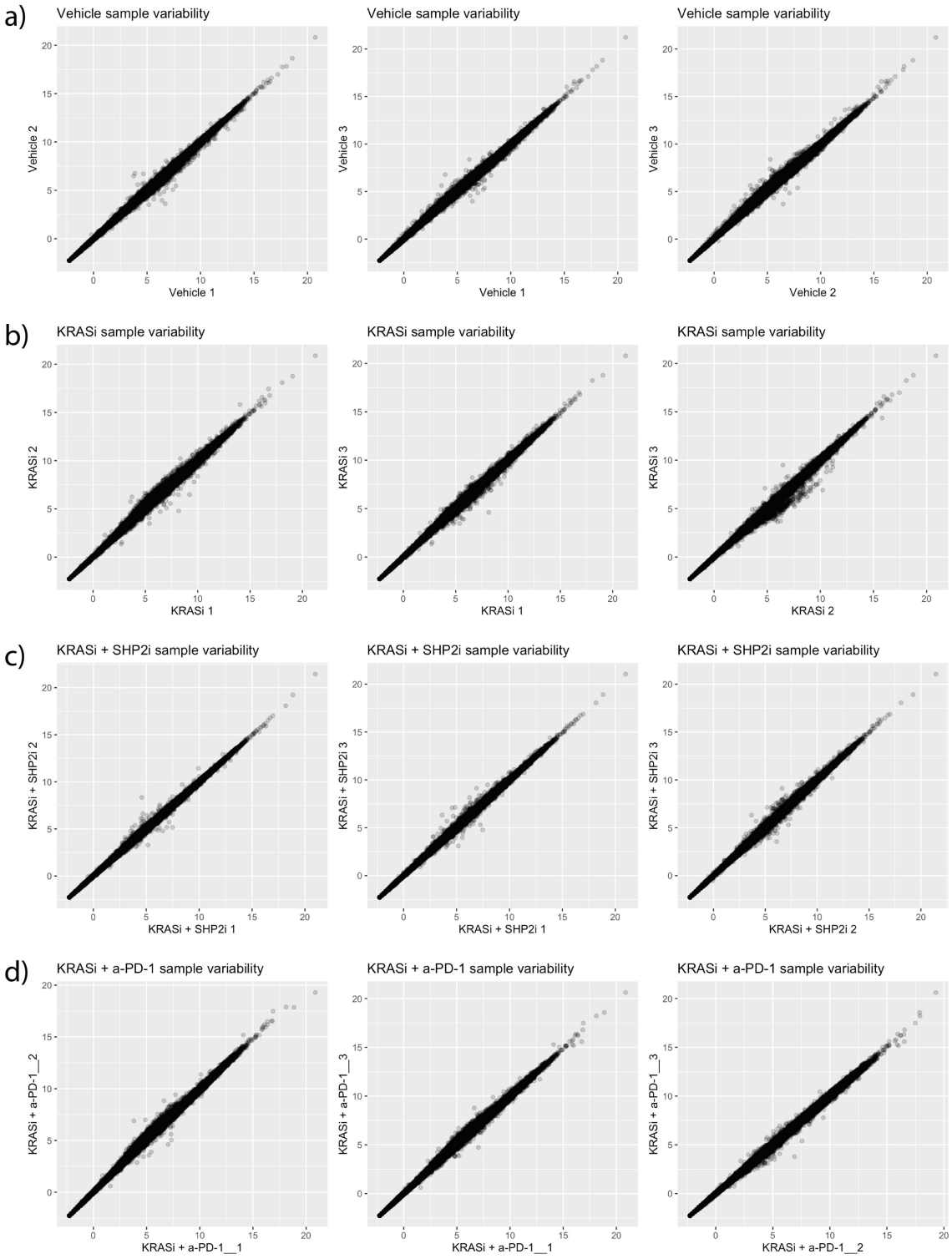


Figure 5.6 Pair-wise gene expression dispersion. Pairwise gene expression dispersion plots by treatment group, each dot is representative of one gene, x- and y-axis scales indicate normalised, log-transformed gene expression values. a) Vehicle, b) KRASi (RMC-4998), c) KRASi + SHP2i (RMC-4550), d) KRASi + a-PD-1.

To understand the scope of treatment-induced changes in gene expression, differential gene expression between treatment groups was also visualised in form of MA plots (**Figure 5.7**). In this scatter plot, the log2 fold change (log2FC) between 2 treatment condition is displayed on the y-axis (M), and the average of log-transformed counts across all samples (A) is displayed on the x-axis. This visualisation implied that the presence of KRAS G12Ci as monotherapy in the mixed tumours induced significant changes in gene expression in the KPAR1.3 KRAS G12D tumour cell compartment. Since KRASi does not directly inhibit oncogenic KRAS signalling in these tumour cells, the observed changes in gene expression were likely the result of other treatment-induced changes, such as alterations in immune cell composition and activation states in the TME. The highest number of differentially regulated genes with a log2FC > 3 was observed between samples of vehicle and KRASi + SHP2i treated mice. Assessing secondary treatment effects, the addition of a-PD-1, compared to treatment with KRAS G12Ci as monotherapy appeared to induce the least additional effects on the KRAS-G12D mutant tumour cell compartment. These findings are consistent with the sample dispersion in the PCA analysis (**Figure 5.5**).

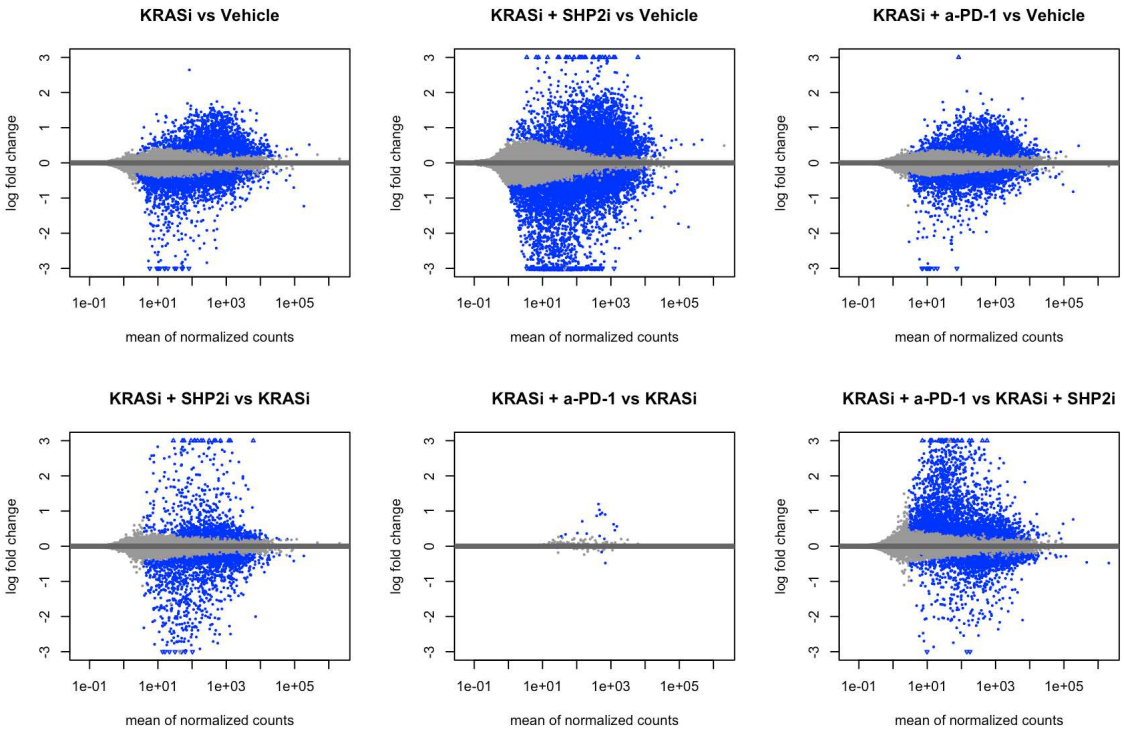


Figure 5.7 Differential gene expression between treatment groups. MA-plots visualising the log2 fold changes over the mean expression of normalised gene counts. The later term in the respective plot titles is considered as "baseline" (set as 0 on x-axis). Top panel shows primary treatment effects, comparing samples from treated mice to vehicle samples, set as baseline. The bottom panel visualises secondary treatment effects. If padj ≤ 0.1, data points on plot are coloured blue, data points which fall out of the range of the defined y-axis are plotted as triangles. KRASi (RMC-4998), SHP2i (RMC-4550).

To further visualise the quantity of differentially regulated genes, for each of the comparisons, their abundance over respective adjusted p values (padj) was plotted (**Figure 5.8**). This showed that KRASi + SHP2i treated tumours had the most significantly differentially regulated genes with small padj values. On the other hand, there were fewer significantly differentially expressed genes between KRASi as monotherapy and KRASi + a-PD-1, again, implying that the addition of immunotherapy to KRASi treatment may not have exerted much additional effects on the KRAS G12D mutant tumour cell population.

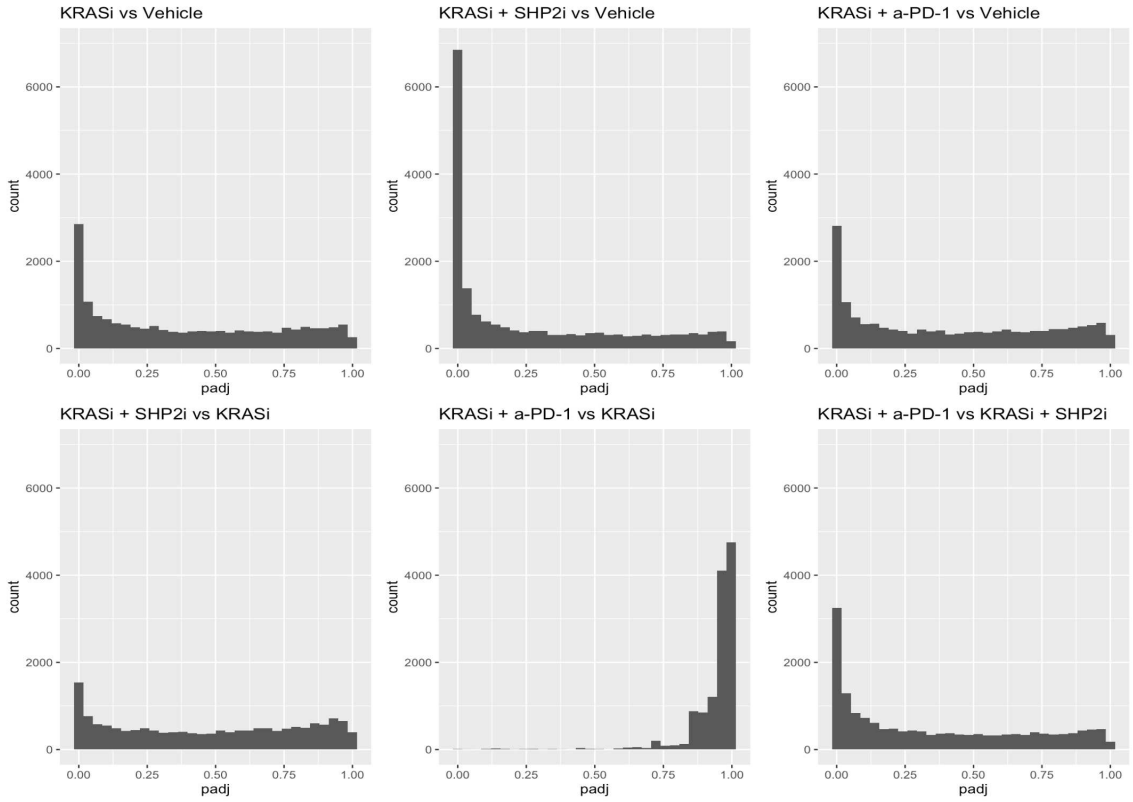


Figure 5.8 Abundance of significantly differentially regulated genes between indicated treatment groups. Pairwise treatment group comparisons as indicated by plot title, the later term being set as baseline. Number of genes ('Counts') plotted over their corresponding padj

values. Plots in top panel compare indicated treatments to vehicle, bottom panel compares samples from different treatment groups to each other.

As the plotting tools above do not provide insights into the identity of genes that are differentially regulated, pairwise treatment comparisons were also visualised as volcano plots. As an example, differential gene expression between vehicle and KRASi treated samples is shown below (**Figure 5.9**). This revealed that some of the most upregulated transcripts in treated samples are related to proliferation and cell cycle progression. This included Ccna2, which encodes for a cyclin-dependent kinase, E2f7, which encodes the E2F transcription factor7 that is involved in promoting survival and proliferation, and Mik67 which is the transcript for the proliferation marker Ki67. On the other hand, several down regulated genes are related to interferon signalling, such as Irf7, Isg15, Cx3cr1 as well as TSGs, such as Ptpn13 and Trib3.

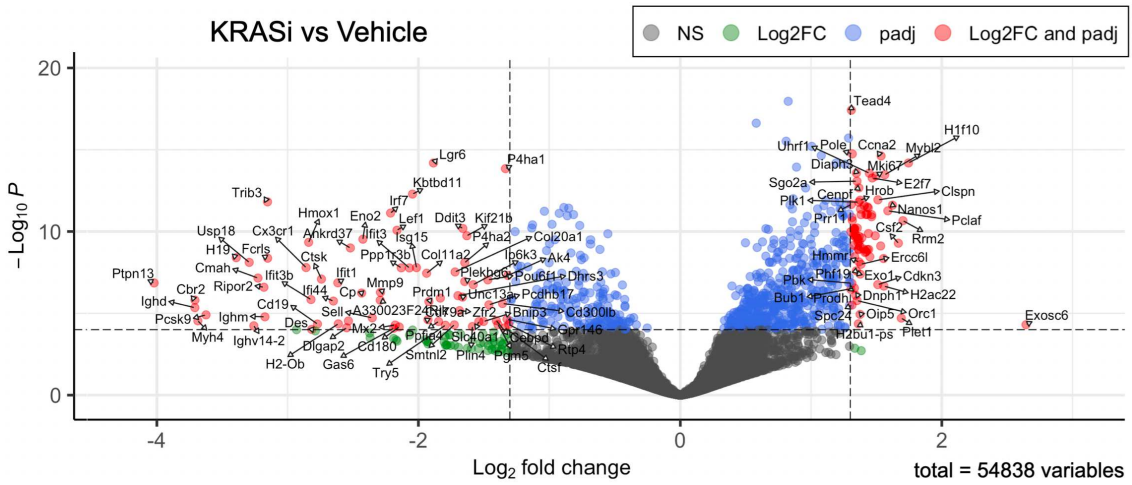


Figure 5.9 Differential gene expression in KRASi- and vehicle samples. Volcano plot showing the differential gene expression between vehicle (baseline) and KRASi (RMC-4998) treated samples. Dots indicate individual genes, the negative Log10 of adjusted p values (y-axis) is plotted vs Log2FC for respective genes (x-axis). With dotted lines indicating cutoff ranges for $Log_2FC \leq (-1)$ or ≥ 1 and $-Log_{10}P \leq 10^{-13}$.

To gain deeper insights into systemic expression changes within the KRAS G12D mutant cancer cells, rather than looking at individual genes, gene set enrichment analysis (GSEA) was performed. An example for individual GSEA

plots for the comparison between Vehicle- and KRASi treated samples is shown for the top 4 hits for positive- (**Figure 5.10a**) and negative (**Figure 5.10b**) enrichment scores. The 4 gene sets associated with a strong positive enrichment score were all associated with proliferation and cell cycle progression, while the top 4 hits with a negative enrichment score were associated with a downregulation in inflammatory signalling and hypoxia.

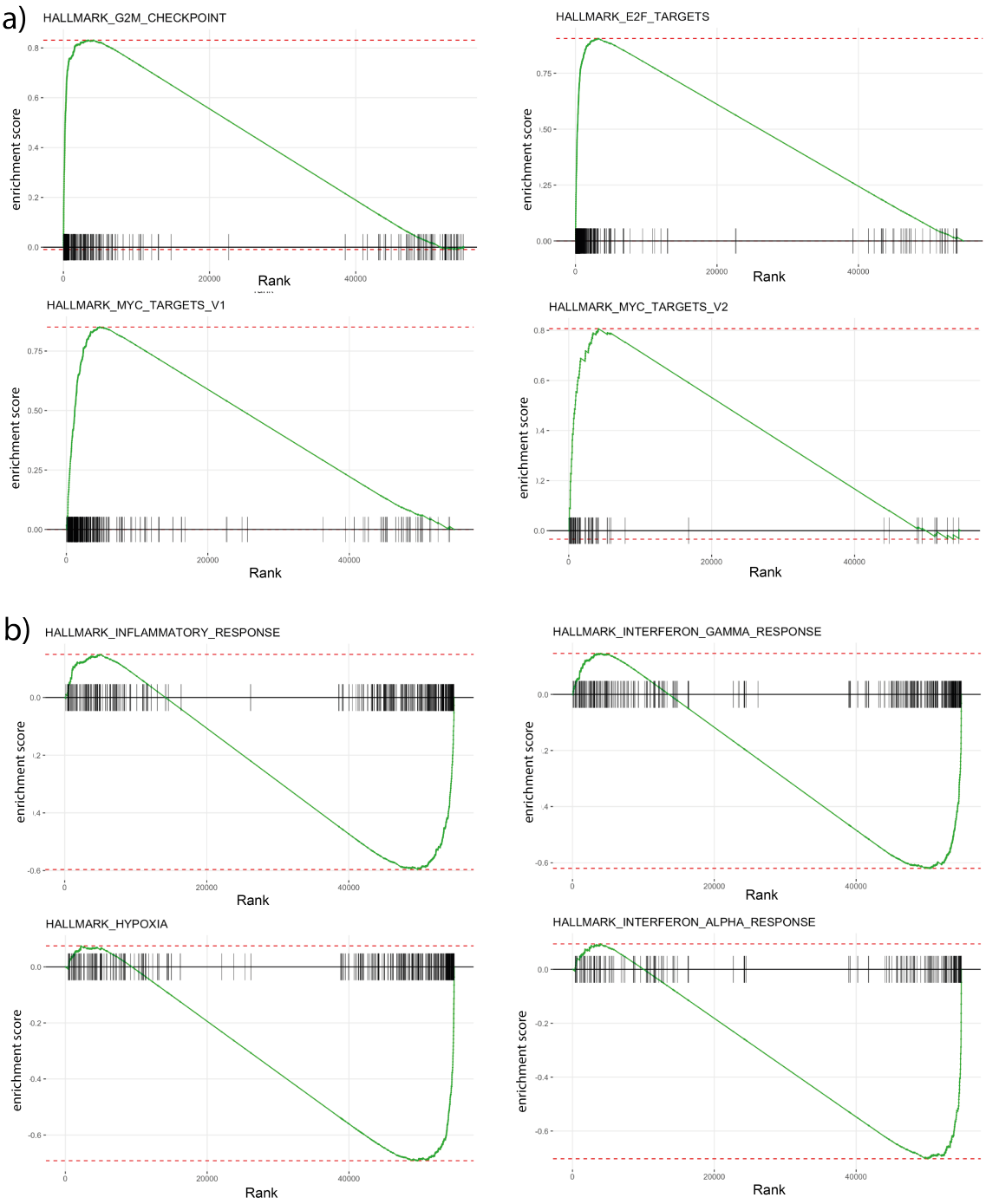


Figure 5.10 GSEA of KRASi-treated compared to vehicle samples. GSEA plots for a) top 4 upregulated and b) downregulated gene sets in the comparison between vehicle and KRASi (RMC-4998) treated samples. Individual ranked genes in respective gene set collections are shown on x-axis as individual dashes, plotted over their respective enrichment score (y-axis).

To visualise an overview of differentially regulated gene sets across treatment groups, point graphs displaying all significantly differentially regulated gene sets with a padj ≤ 0.05 were created. Here, primary treatment effects on the

KPAR1.3 KRAS G12D tumour cells compared to vehicle samples were analysed first (**Figure 5.11**). This visualised that several gene sets related to proliferation and cell cycle progression, such as E2F and MYC target sets, were upregulated when the KRAS G12C inhibitor was administered. Intriguingly, this was also true for RNA samples isolated from combination treated tumours, despite the signature for KRAS signalling being slightly downregulated in the KRASi + SHP2i combination treated samples. On the other hand, several signatures related to interferon signalling and inflammation appeared to be downregulated in samples treated with KRASi as monotherapy or in combination with a-PD-1 treatment, compared to vehicle. The addition of SHP2i, however, appeared to increase IFN-α and IFN-ɣ related signatures.

The increase in proliferation signatures is consistent with the observations made in previous experiments, based on IVIS scan and flow cytometric readouts. These showed that treating tumours comprised of mixed KRAS G12C and G12D mutant cancer cells with a KRAS G12Ci will give the KRASi-resistant subpopulation a proliferative advantage. Intriguingly, this proliferation signature was also maintained in combination-treated samples. Being able to generate complete responders with combination therapies despite this increased proliferation signature might imply a significant contribution of adaptive antitumour immunity in eliminating these cancer cells.

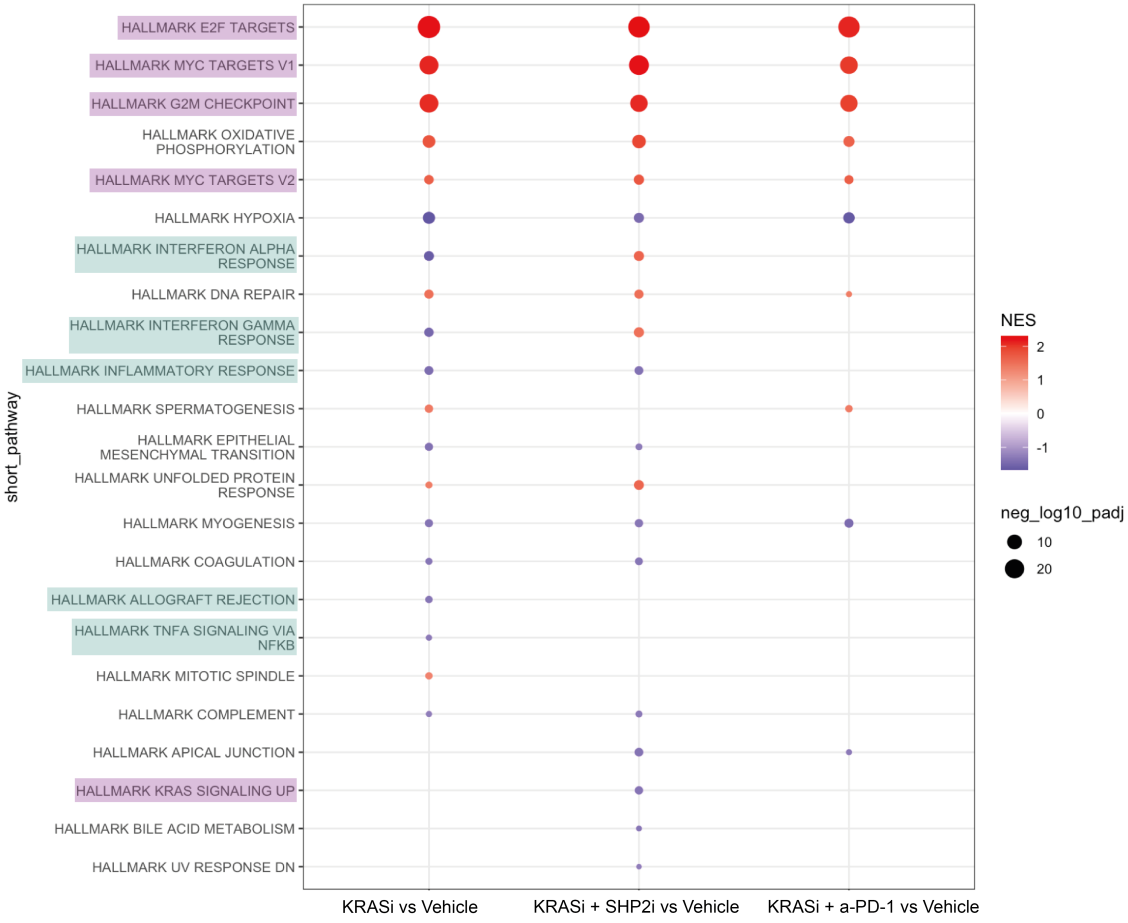


Figure 5.11 GSEA of primary treatment effects. Overview of enriched gene sets in the KPAR1.3 KRAS G12D tumour cell compartment across treatment groups, with normalised enrichment scores (NES) indicated by colour of respective dots and respective adjusted p-values indicated by size of respective dots. For all comparisons, the vehicle group is set as baseline and differentially enriched gene sets in treatment groups are displayed. Only gene sets which had a padj of ≤ 0.05 in at least one of the compared treatment groups are shown. Along the y-axis, proliferation and/or cell cycle progression associated signatures are highlighted in mauve, inflammation associated signatures in green. KRASi: RMC-4998, SHP2i: RMC-4550.

GSEA was also performed to investigate synergistic effects between treatment groups (**Figure 5.12**). This indicated that there were no profound differences in cancer cell state of the KPAR1.3 KRAS G12D compartment between KRASi as monotherapy and KRASi with the addition of immune therapy. Interestingly, in this experiment, addition of the SHP2 inhibitor overall further increased the enrichment score for proliferation-related signatures, when compared to KRAS G12Ci as monotherapy or in combination with a-PD-1, despite KRAS signalling gene set displaying a negative enrichment score. Simultaneously, inflammation

associated signatures also appeared to be upregulated in the presence of the SHP2i.

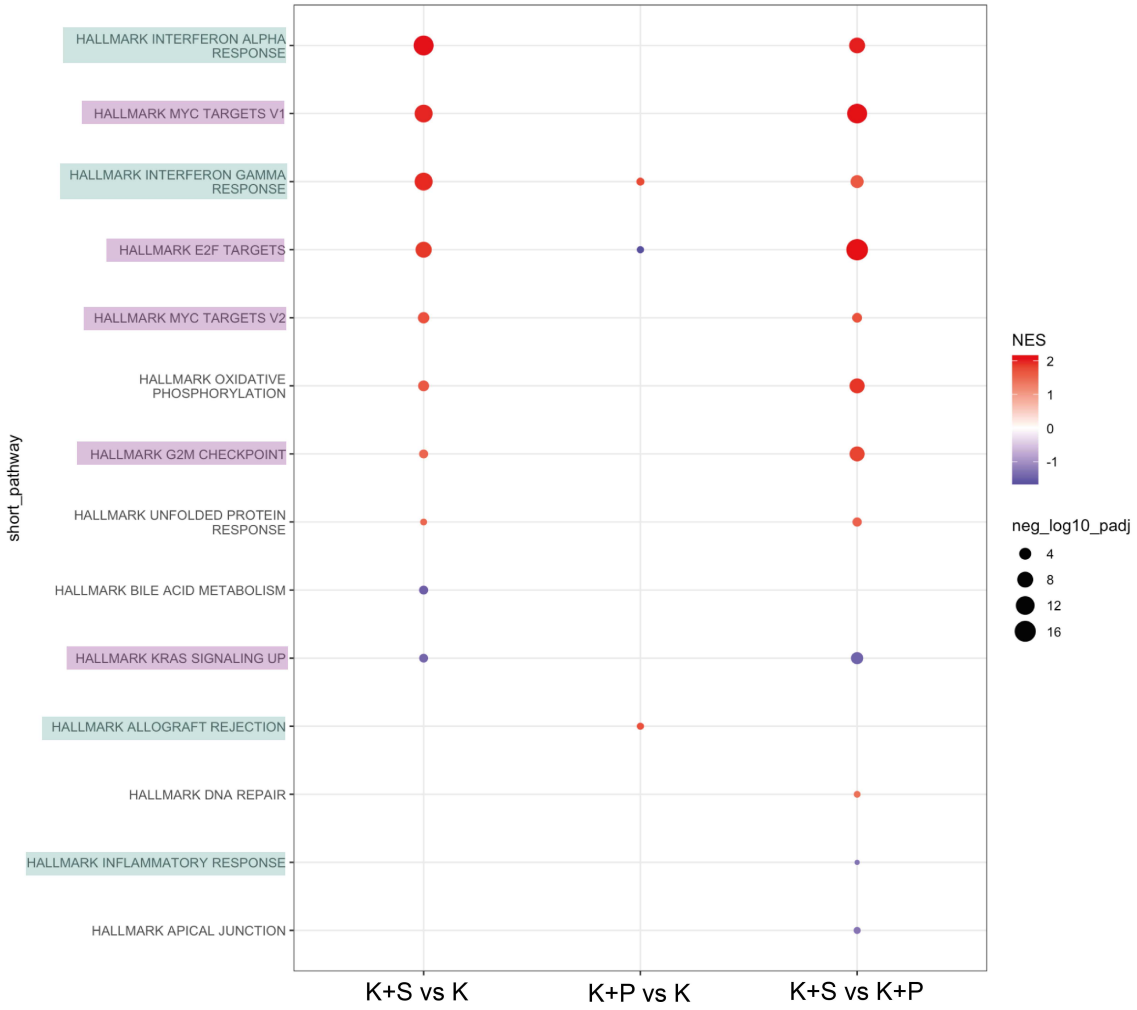


Figure 5.12 GSEA of secondary treatment effects. Overview of enriched gene sets in the KPAR1.3 KRAS G12D tumour cell compartment comparing between treatment groups, with normalised enrichment scores (NES) indicated by colour of respective dots and with respective adjusted p-values indicated by size of respective dots. For all comparisons, the later term in the tile of the x-axis was set as baseline and differentially enriched gene sets are displayed on the plot. Only gene sets which had a padj of ≤ 0.05 in at least one of the compared treatment groups are shown. Along the y-axis, proliferation and/or cell cycle progression associated signatures are highlighted in mauve, inflammation associated signatures in green. Abbreviations on x-axis of graph: Vehicle (V), SHP2 inhibitor RMC-4550 (S), KRAS G12C inhibitor RMC-4998 (K), a-PD-1 (P).

This first RNA sequencing experiment had several limitations. First, vehicle tumours were engrafted with a different ratio of KRAS G12D mutant cancer cells than the tumours for the different treatment groups. Secondly, samples

from combination treated tumours, were pooled to generate enough material for RNA-seq. Thirdly, we were unable to analyse the KRAS G12C tumour cells in this experiment due to highly auto fluorescent immune cells appearing in the BFP^+ gate. Moreover, SHP2 inhibition appeared to exert inhibitory effects in the KRAS G12D cancer cell compartment directly, however, it was not possible to disentangle the overall contribution of KRAS G12C inhibition and SHP2 inhibition in the dual therapy combination group. However, this experiment was able to demonstrate that multiple proliferation-associated signalling pathways were upregulated in the KPAR1.3 KRAS G12D compartment, in the presence of KRASi treatment and that this signature was maintained even in combination treated tumours.

5.2 bRNA-seq of the entire tumour cell compartment across treatment groups

To address the open questions from the previous experiment, a second RNA sequencing study was conducted. The first bRNA-seq study, suggested that the addition of SHP2 inhibition appeared to produce stronger synergistic effects in the KRAS G12D mutant tumour compartment. Hence, further disentangling the contributions of the two targeted inhibitors was prioritised in this experiment. The fraction of the Luc-eGFP KPAR1.3 KRAS G12D cell subpopulation was also standardised across all treatment groups in this experiment and adjusted based on the previous experiment, so that no samples had to be pooled for RNA-seq.

Subcutaneous tumours were again engrafted in immune competent GH-mice (**Figure 5.13a**). Again, tumours engrafted from single FP KPAR1.3 cell suspensions or untransduced KPAR1.3 cells, were included to enable accurate gating during flow cytometric sorting. In this experiment, the number of tumour cell populations obtained from different treatment groups in the previous run were taken into account. Based on these counts, it was calculated that

engrafting a fraction of 7.5% G12D cells across all treatment groups would enable sorting both KRAS G12C- and G12D derived populations in sufficient numbers from individual samples. Tumours were again dissociated into a single cell suspension and red blood cell lysis was performed (**Figure 5.13a**). To eliminate the highly auto fluorescent immune cells which had previously shown up as false positive events in the eBFP sorting gate, an additional sample processing step was performed. This comprised a positive magnetic pulldown of $CD45^+$ cells, to remove all immunocytes from the samples. BFP^+ and GFP^+ tumour cells were then sorted as in the previous experiment; RNA was isolated and samples were submitted for library preparation and NGS sequencing (**Figure 5.13b**).

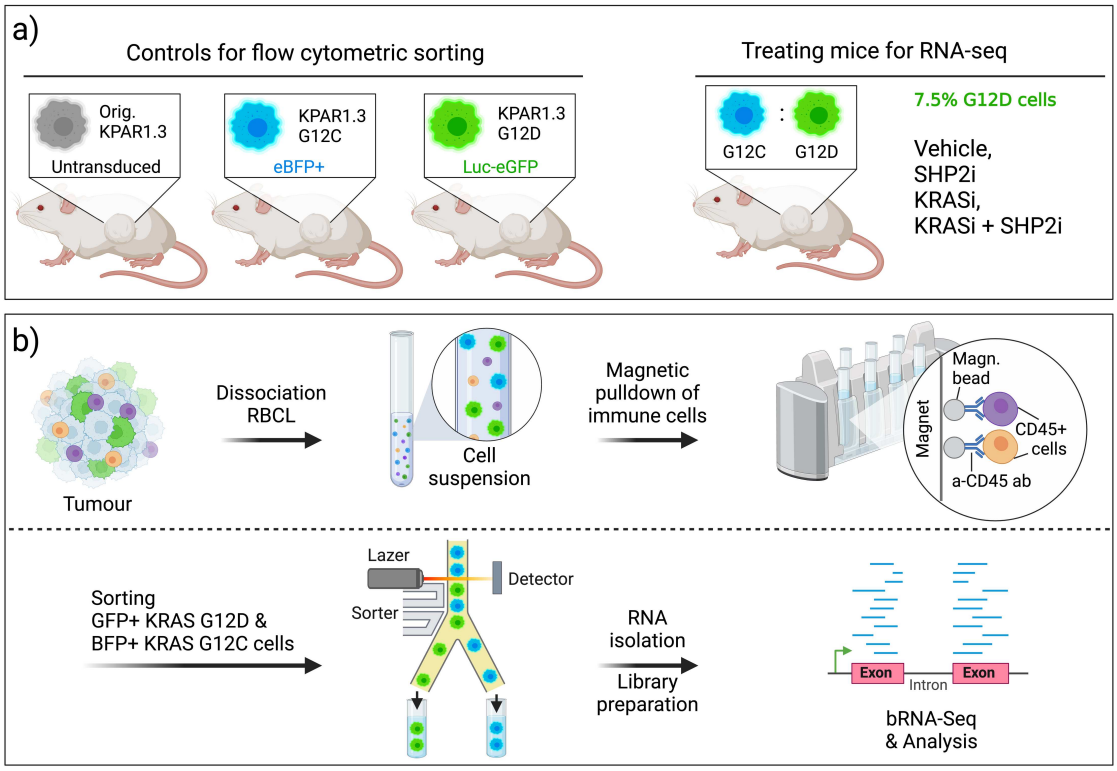


Figure 5.13 Schematic of sample acquisition for bRNA-seq. a) Engraftment of tumours for experiment; left: KPAR1.3 derived tumours utilised setting up flow cytometric gates, right: Tumours engrafted for bRNA-seq sample acquisition, with a fraction of 7.5% KPAR1.3 KRAS G12D cells for all treatment groups. Mice were put on treatment when average volume of ~580 mm3 was reached, mice were treated with 5 doses of oral gavages for KRASi RMC-4998 at 100 mg/kg, SHP2i RMC-4550 at 30 mg/kg, 2 doses of a-PD-1 were administered to respective mice at 10 mg/kg. b) Harvested tumours were dissociated into a single cell suspension and red blood cell lysis (RBCL) was performed; CD45+ immune cells were then removed from all samples through a magnetic pulldown; eBFP+ KPAR1.3 KRAS G12C and Luc-eGFP+ KPAR1.3 KRAS G12D cells were then collected via flow cytometric sorting, subsequently, RNA was isolated,

libraries were generated from samples and NGS sequencing was performed. Image was created with BioRender.

The pulldown of CD45$^+$ cells to remove auto fluorescent immunocytes was successful, as the eBFP$^+$ gate remained clear when running the negative control of a tumour sample with untraduced KPAR1.3 cells (**Figure 5.14**). Hence, it was possible to submit both tumour cell fractions for RNA sequencing in this experiment.

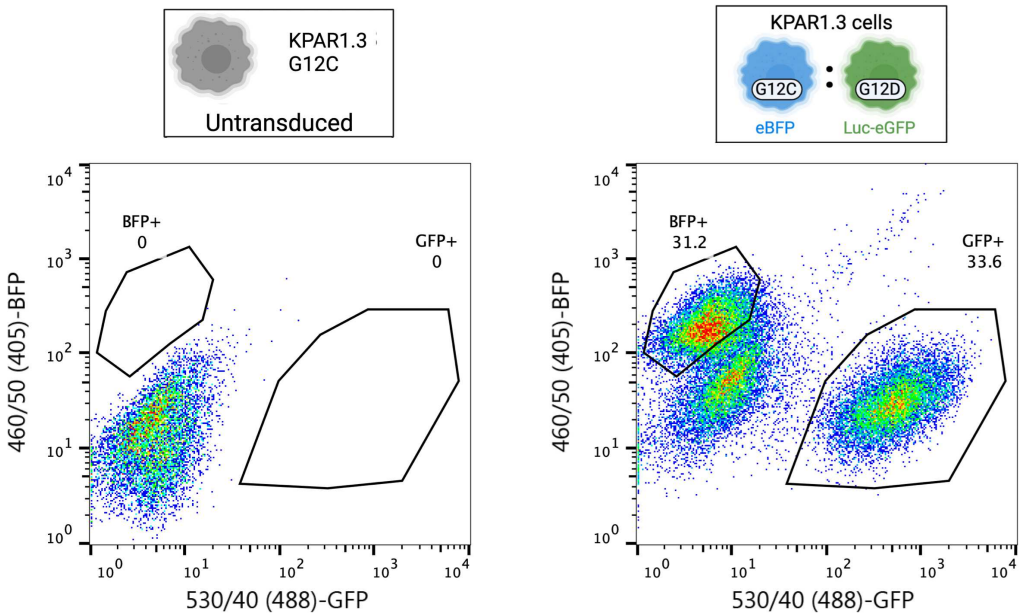


Figure 5.14 Flow cytometric gating for tumour cell sort. Left panel: Sample derived from a tumour established from un-transduced KPAR1.3 cells was used as negative control for setting up sorting gates. Right panel: Example of a sample derived from a tumour bearing mouse that was treated with KRASi RMC-4998. Tumour cells in BFP$^+$ or GFP$^+$ gates were sorted into separate tubes for RNA isolation.

Once samples were sequenced, initial raw data was again processed as described in **Figure 5.2**. Subsequently, initial read counts were again visualised and normalised via a calculated size factor. Of note, it appeared that one sample, “G12D_SHP2i_4”, had accumulated more reads, compared to other samples. This was cross-checked together with the Advanced sequencing facility as well as the Bioinformatics core at the Crick. It was concluded that this discrepancy in read counts likely occurred due to a pipetting inaccuracy during

library preparation, which was done using small sample volumes. This did, however, not compromise the experiment and was accounted for during read count normalisation, as visualised below.

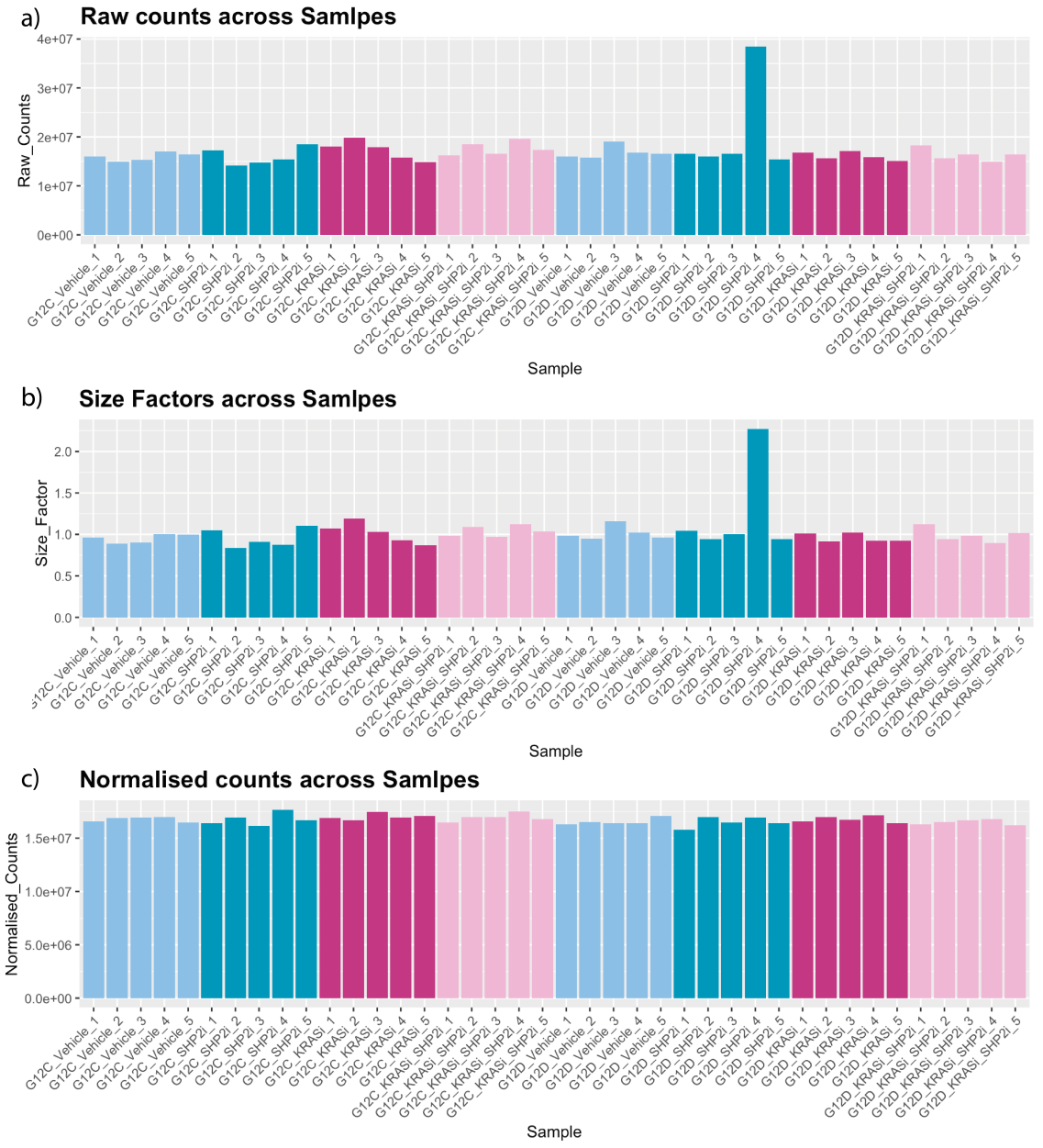


Figure 5.15 Read Count normalisation. a) Total raw counts for each sample. b) Computed size factor for each sample, used for read count normalisation. c) Normalised read counts across all samples.

As in the previous experiment, data was log-transformed and genes with low read counts were accounted for. Again, dispersion estimates were visualised to

assess the quality of the sequencing data. In brief, the resulting distribution of gene wise dispersion indicated a high quality of the sequencing data set.

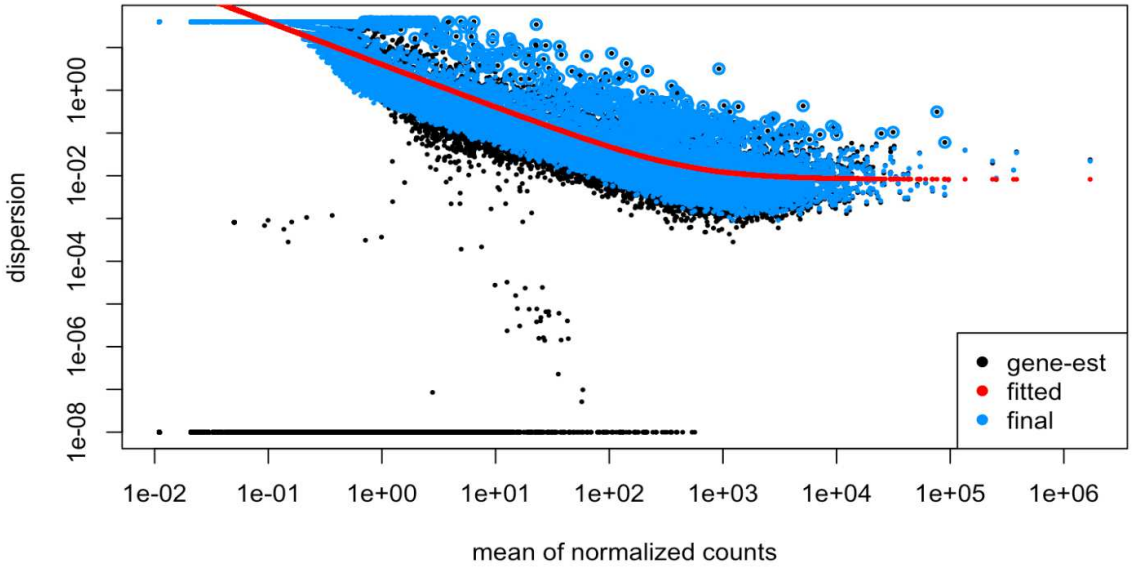


Figure 5.16 Dispersion estimates for each gene across samples. The dispersion of gene expression (y-axis) is plotted over the mean of normalised gene counts (x-axis). Each point in the plot is representative of an individual gene; the black dots indicate the initial maximum likelihood dispersion estimate. The red line is fitted as an estimated mean for the expected dispersion for genes with a certain number of read counts. Blue dots indicate adjusted dispersion values for individual genes. Genes with extremely high dispersion values, which are not regressed towards the mean are indicated as black dots surrounded by blue circles.

Next, PCA was performed to probe how samples of different genotypes and treatments would cluster together as well as to probe for any potential batch effects (**Figure 5.17**). This first revealed a clear segregation in gene expression between the two isogenic tumour cell lines (**Figure 5.17a**). Colouring the samples by their respective treatment groups, further implied that within each genotype, samples roughly clustered together by treatment groups (**Figure 5.17b**). Here, in the KPAR1.3 KRAS G12C cell-derived samples, the vehicle samples clustered further away from the treated samples, with the combination treated samples appearing the furthest away from the vehicle. However, samples of different treatment groups overall appeared to overlap in space, indicating that SHP2i and KRASi may induce similar effects on the tumour cells. In the G12D-mutant compartment, on the other hand, Vehicle- and KRASi-treated samples clustered closer together while samples treated with SHP2i,

alone or in combination, also clustered together, farther away on the axis of G12C derived samples. This indicated that the presence of the SHP2i may have induced a differing cell state in the G12D tumour cell compartment, either through tumour cell intrinsic or extrinsic effects.

Next, the data set was tested for potential batch effects relating to gender of the mice or the day the tumour cells were sorted. Due to the limited number of GH- mice available, the cohort for this experiment was made up of both, male and female mice. The mice were equally stratified into treatment groups, with samples from 2 female and 3 male mice submitted for each treatment group. We hypothesized that the gender of the mice should not exert an influence on the setting of this study. This is because first, the analysed tumour samples had not been induced endogenously, but were all derived from the same engrafted KPAR1.3 cell lines. Further, the KPAR1.3 cell line was derived from a female mouse and should hence be tolerated equally well by males and females, as both genders possess at least one X chromosome. To test this hypothesis, samples were coloured by gender on the PCA plot (**Figure 5.17c**). Indeed, it appeared that the gender of mice did not result in strong batch effects. Of course, any potential gender-related differences were still considered in the statistical model that was fitted to investigate differential gene expression between genotype and treatment groups. Next, as the sample preparation and sorting are time-consuming procedures, the samples were processed over two successive days. Of course, tumour sizes, treatment start- and end days, etc. were all taken into account to normalise experimental conditions. To assess whether there were still batch effects present through the different sort days, this was also visualised in the PCA plots (**Figure 5.17d**). Again, the day of the sort did not appear to play a significant role in sample clustering but was still considered when setting up the mathematical model for gene expression analysis between sample groups.

In the previous experiment, the Vehicle and KRASi treated samples in the KRAS G12D tumour cell-derived samples had not clustered together. However,

it is important to note that the PCA plot only show the axis of the first two principal components and samples may cluster differently when more variables, such as different genotypes, are introduced. Additionally, in this experiment, different treatment groups were investigated. Nonetheless, PCA plots visualising genotype-internal clustering were also generated to allow for an approximated comparison with the previous bRNA-seq experiment. This showed that vehicle samples still clustered separately from treated samples, which roughly overlapped with each other in the KRAS G12C-tumour cell compartment (**Figure 5.17e**). On the other hand, Vehicle- and KRASi-treated samples were now further separated from each other and even more separated from SHP2i-treated samples, which is a better reflection of the sample distribution of the first bRNA-seq experiment.

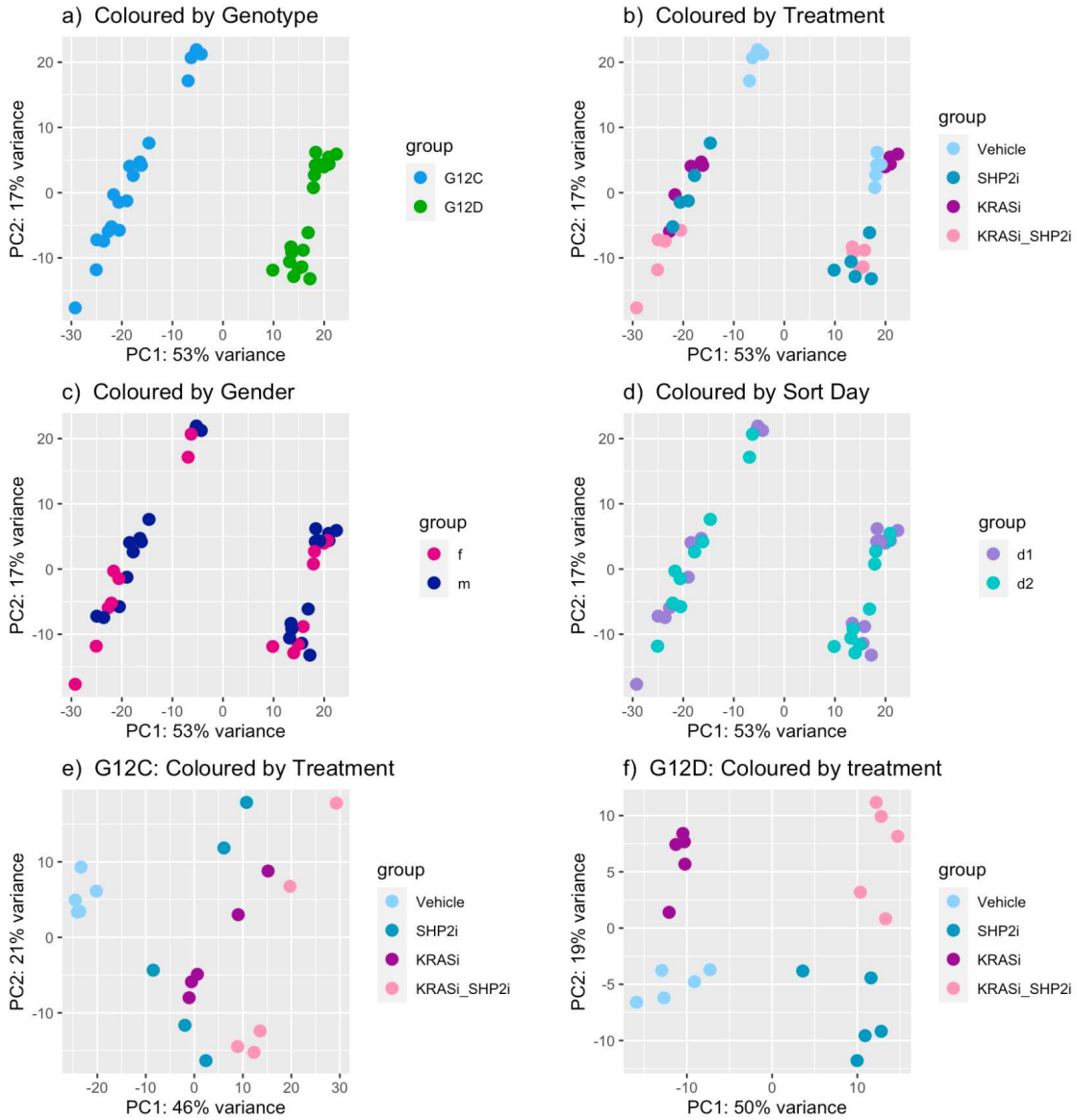


Figure 5.17 Principal component analysis of dataset. PCA-plots of the whole bRNA-seq datasets are shown coloured by a) Genotype, b) Treatment group, c) Gender of the mice, d) Sort day. Furthermore, PCA plots of subsetted datasets of e) KRAS G12C mutant tumour cell samples and f) KRAS G12D mutant tumour cell samples are shown, coloured by treatment group.

As in the previous experiment, differences in gene expression between pairwise compared sample groups were visualised employing MA plots (**Figure 5.18**).

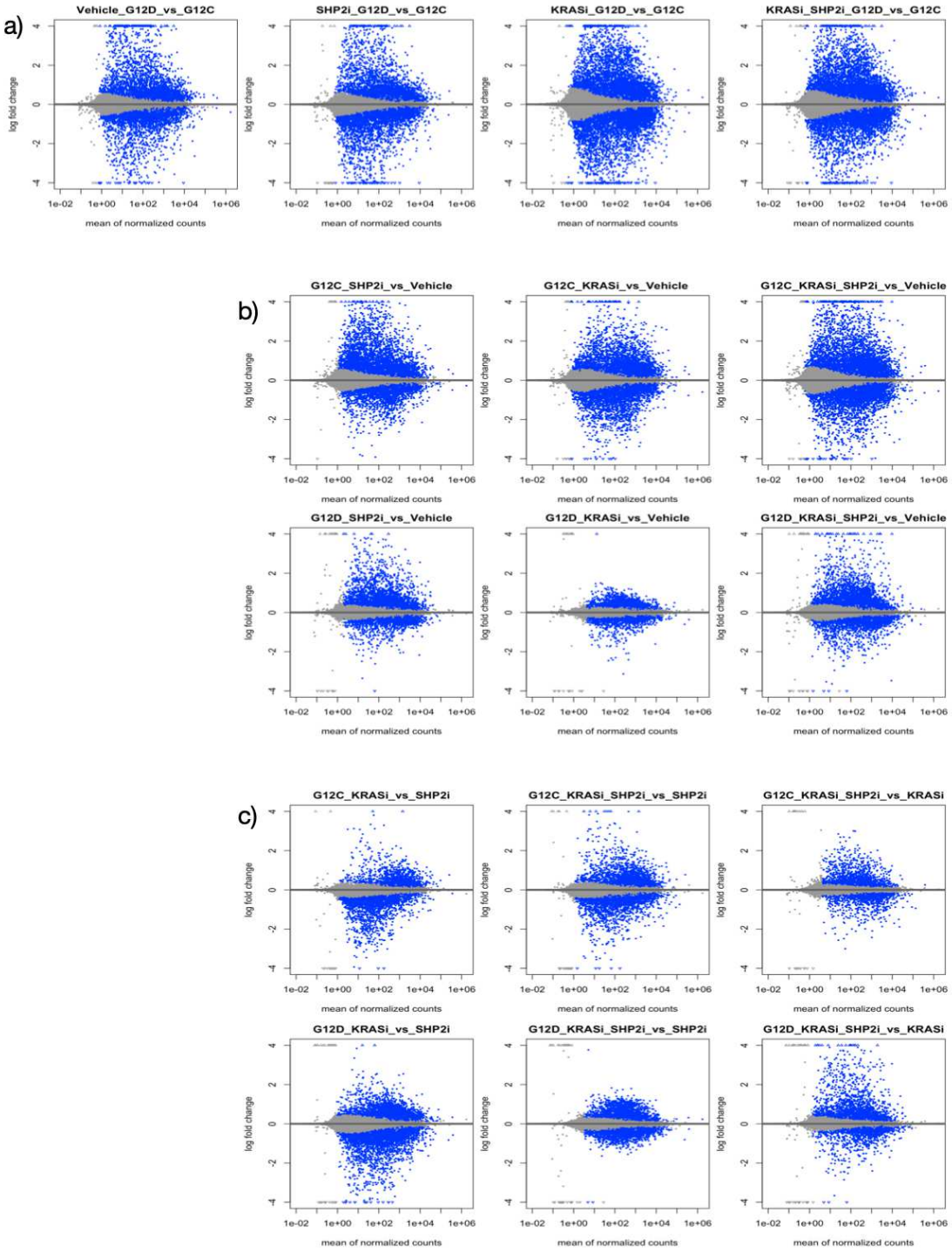


Figure 5.18 Differential gene expression between sample groups. MA-plots visualising the log2 fold changes over the mean expression of normalised gene counts. The later term in the respective plot titles is considered as "baseline" (set as 0 on x-axis). Data points on plot are coloured blue if padj ≤0.1. If data points fall out of the range of the defined y-axis they are plotted as triangles. KRASi (RMC-4998), SHP2i (RMC-4550). Differential gene expression is shown for comparison of different genotypes by treatment group (a); pairwise comparisons between treatment groups for KRAS G12C-derived (b), and G12D-derived (c) tumour cell samples.

To understand the potentially differing responses of KRAS G12C- and -G12D-mutant tumour cells to therapy exposure, gene expression of individual genes of interest were plotted across treatment groups. A few exemplary genes are shown below (**Figure 5.19**). Interestingly, KRAS expression was upregulated in KRAS G12C mutant samples which were treated with KRASi, indicating a potential compensatory mechanism. Etv4, Etv5, and Dusp6, targets of the KRAS signalling pathway, were downregulated in KRAS G12C-derived samples, especially so in the combination treated samples, indicative of an enhanced inhibition of the KRAS pathway. On the other hand, these genes appeared to be expressed at higher levels in the G12D-mutant samples that were treated with KRAS G12Ci as monotherapy. The lower panel shows gene expression for the transcripts of Cxcl9, Cxcl10, H2-K1, and interferon regulatory factor 1 (Irf1), which are indicative of an inflammatory response when expressed at elevated levels. Here Cxcl9 and Cxcl10 encode for chemokines, H2-K1 encodes for a subunit of the MHC-I complex and is hence indicative of antigen presentation, and Irf1 for a transcription factor positively regulating interferon responses. Treatment with the SHP2i appeared to increase their expression level in both KRAS G12C and G12D mutant tumour cell samples. However, with the present information it is not possible to conclude whether SHP2i induces a higher expression of these genes through cancer cell intrinsic effects or through increasing anti-tumour immunity and cytokine signalling in the TME.

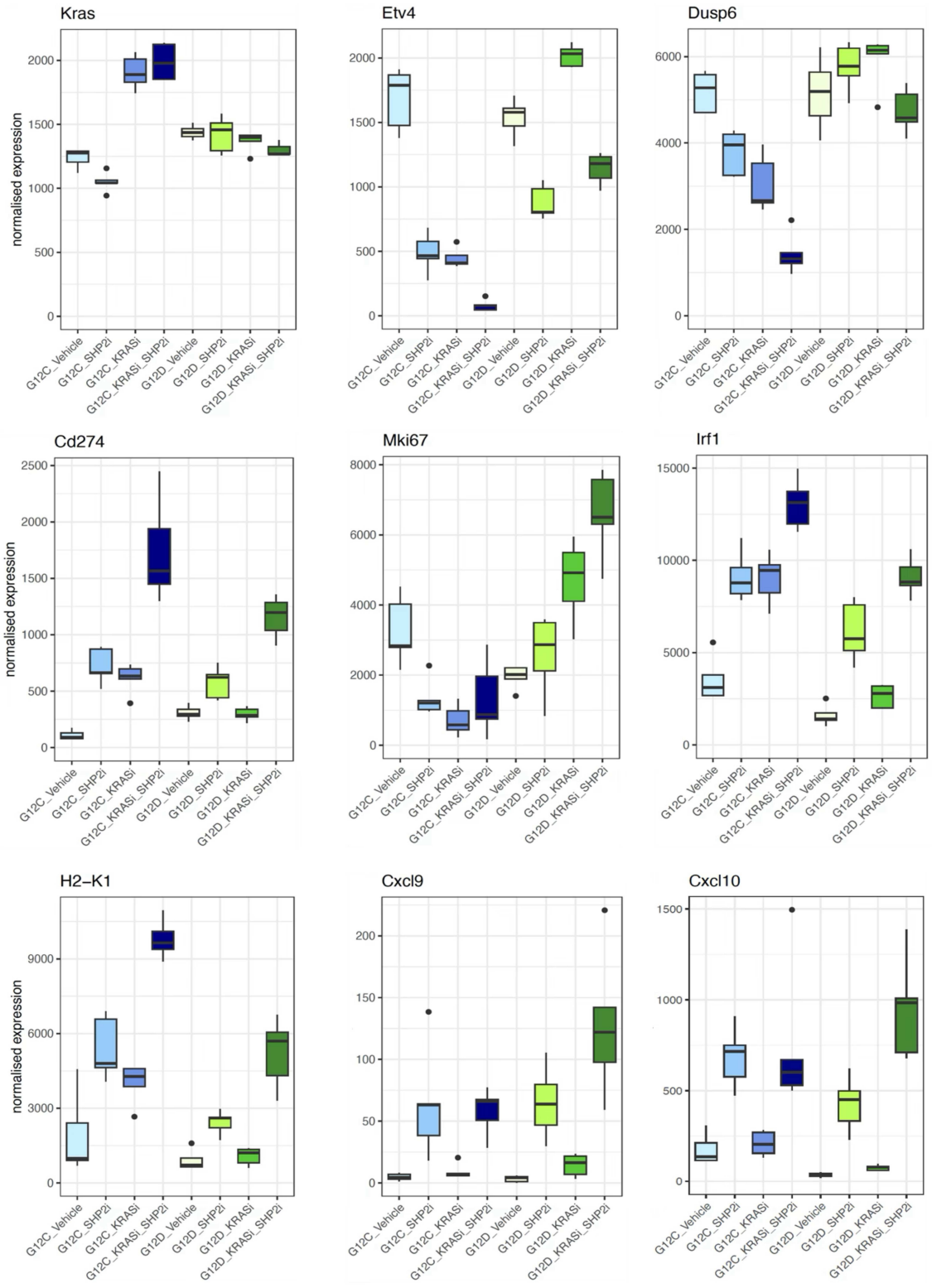


Figure 5.19 Individual gene expression by treatment group. Gene expression of selected target genes by treatment groups, Upper range of y-axis is not normalised across plots, due to differences in gene expression. KRAS G12C-derived samples are shown in blue, - G12D derived samples in green. Box plots display the median, shown as black line inside the box, coloured box itself visualises interquartile range, whiskers represent largest and smallest quartile and out layers are displayed as individual dots.

Next Gene set enrichment analysis was performed for pairwise comparisons between different treatment groups and vehicle samples for both genotypes (**Figure 5.20**). Interestingly, KRAS G12C-derived tumour cells, treated with either SHP2i, KRASi, or a combination of both showed a significant downregulation of proliferation associated signatures, as indicated, for example, by the MYC, E2F, and G2M hallmark sets. Simultaneously, several inflammation-associated signatures were enriched in inhibitor treated KRAS G12C-samples, compared to vehicle. In the KRAS G12D tumour cell-derived compartment, some proliferation signatures were enriched in samples treated with KRASi. This proliferative signature was more pronounced when choosing a more lenient padj value (not shown). The fact that this proliferative signature is less pronounced in this, compared to the previous experiment may be related to overall lower read counts, which in turn, is related to normalising the samples to a lower concentration to accommodate not pooling any individual samples in this experiment.

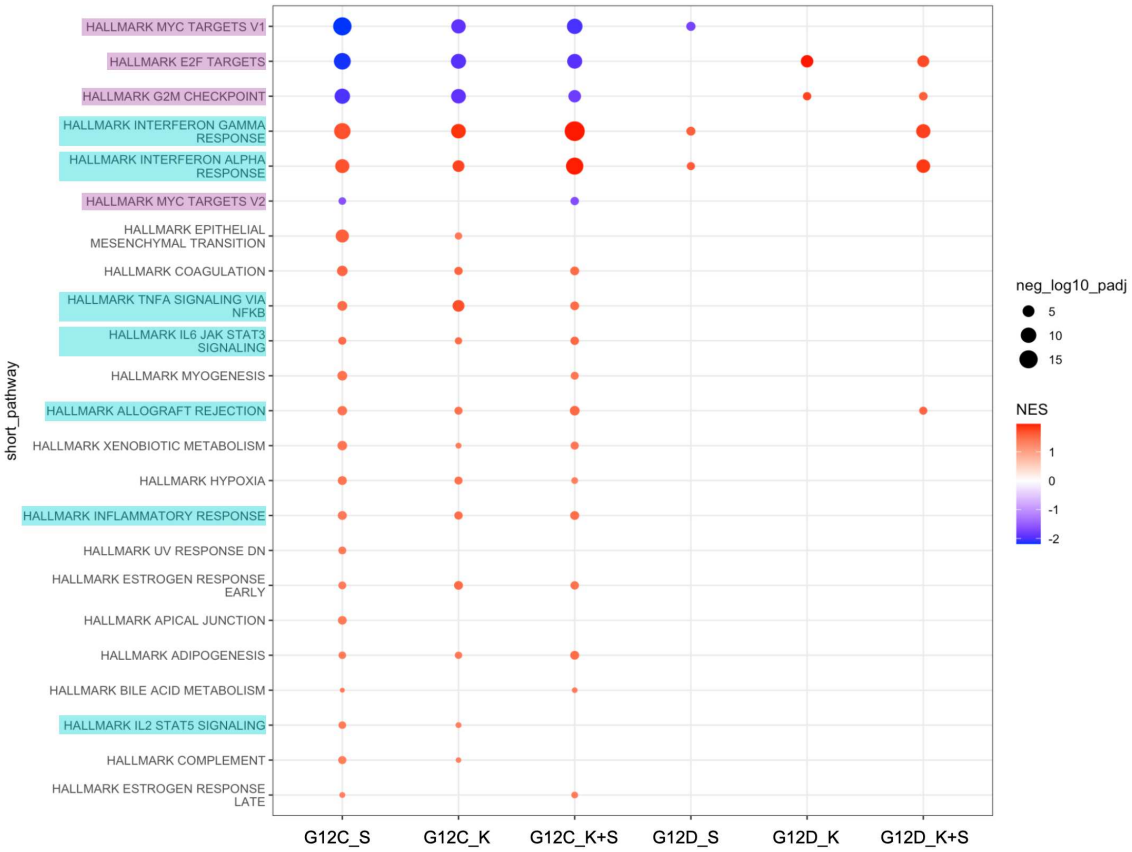


Figure 5.20 GSEA of primary treatment effects across genotypes. Overview of enriched gene sets across treatment groups, with normalised enrichment scores (NES) indicated by colour of respective dots, and respective adjusted p-values indicated by size of respective dots. For all comparisons, the vehicle groups of the respective genotypes are set as baseline and positively(red) or negatively (blue) differentially expressed gene sets are displayed. Only gene sets which had a padj of ≤ 0.05 in at least one of the compared treatment groups are shown. Along the y-axis, proliferation and/or cell cycle progression associated signatures are highlighted in mauve, inflammation associated signatures in green. Along the x-axis, isotype of KRAS-mutant KPAR1.3 tumour cells is indicated as either G12C or G12D; treatments are abbreviated as: SHP2 inhibitor RMC-4550 (S) and KRAS G12C inhibitor RMC-4998 (K).

GSEA was also performed to assess secondary treatment effects and synergy between treatment groups. This revealed that the combination treatment induced a stronger inflammatory response compared to single treatments for both tumour cell genotypes.

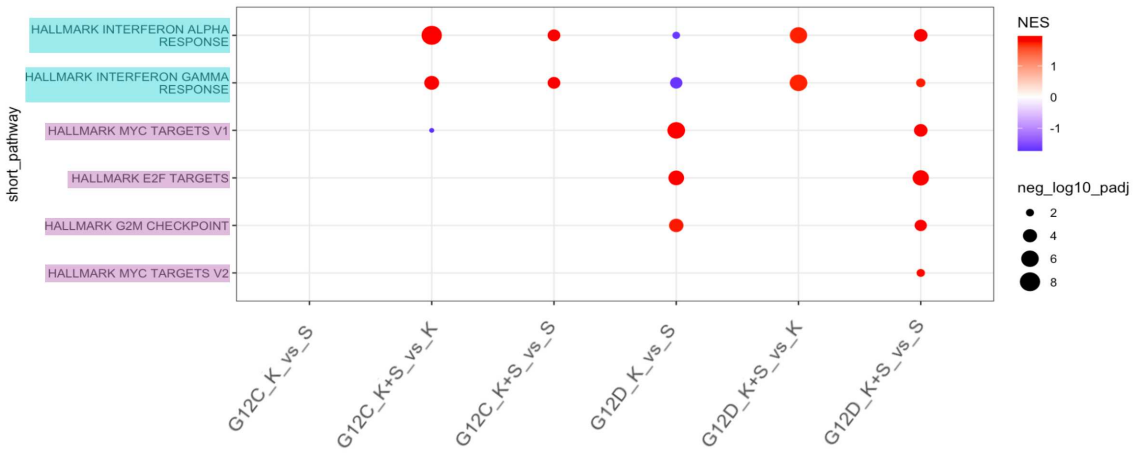


Figure 5.21 GSEA for secondary treatment effects. Overview of enriched gene sets comparing between treatment groups within each genotype, with normalised enrichment scores (NES) indicated by colour of respective dots and with respective adjusted p-values indicated by size of respective dots. For all comparisons, the later term in the tile of the x-axis was set as baseline and differentially enriched gene sets are displayed on the plot. Only gene sets which had a padj of ≤ 0.05 in at least one of the compared treatment groups are shown. Along the y-axis, proliferation and/or cell cycle progression associated signatures are highlighted in mauve, inflammation associated signatures in green. Abbreviation on x-axis:'G12C': KPAR1.3 KRAS G12C tumour cells, 'G12D': KPAR1.3 KRAS G12D tumour cells, 'K': RMC-4998 (KRASi), 'S': RMC-4550 (SHP2i). The first vertical gridline for "G12C_K_vs_S" is empty because no significant enrichment scores were achieved for any gene sets with the selected padj value.

As a proof of concept, the top 50 "leading edge genes", which contribute most to the enrichment score of a particular gene set, were selected for heatmap plots (**Figure 5.22**). Here, the comparison between vehicle and KRASi of the E2F target gene set were chosen because KRASi-treated G12C and G12D mutant tumour cells appeared to have opposite responses in the GSEA analysis visualised above (**Figure 5.20**). These heatmaps again signified the profound alterations in cancer cell-state signatures. In the G12C compartment, all inhibitor treatments resulted in the downregulation of proliferation signature-associated genes, while in the G12D tumour cells, only samples treated with KRASi displayed an increase in the expression of proliferation associated genes.

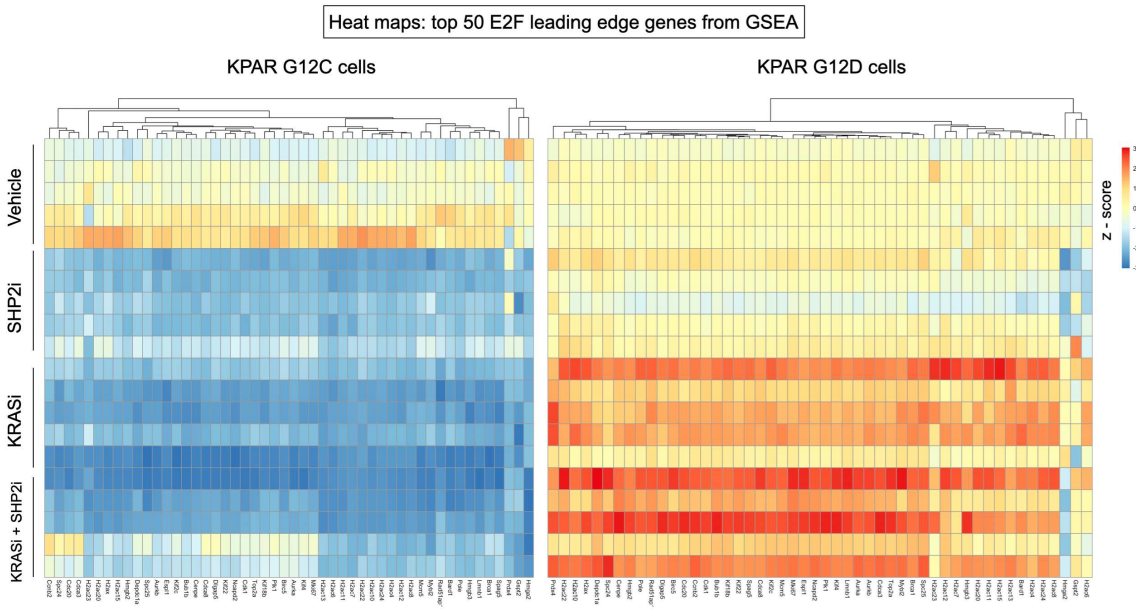


Figure 5.22 Heatmap of leading-edge genes for E2F gene set KRASi vs vehicle. Heatmaps for the same 50 leading edge genes of the E2F signature in the comparison between vehicle and KRASi for KRASG12C mutant (left) and KRASG12D mutant cancer cells (right). Here plotted for all treatment groups with SHP2i: RMC-4550 and KRASi: RMC-4998. The average of the 5 vehicle samples was taken to define a baseline for z-score calculations and was set to zero. A positive z-score (red) indicates increased expression of a gene while a negative z-score (blue) indicates decrease in expression, compared to the average expression across vehicle samples.

The two bRNA-seq experiments provided further insights as to why the KRAS G12D mutant cells proliferate at an accelerated rate in the presence of KRAS G12C inhibition. It further revealed that treatment synergy between KRASi and SHP2i can enhance inflammation associated signatures in both genotypes. However, it still remained unclear whether an increase in SHP2i-induced inflammatory signatures was caused through cancer cell intrinsic inhibition of KRAS signalling or external effects, exerted by enhanced anti-tumour immunity. Furthermore, RNA-seq does not provide unambiguous insights into the activation state of effector proteins in the KRAS-signalling cascade, such as the components of the MAPK or PI3K/AKT/mTOR pathways, as their activity is widely regulated through post-translational modifications. To address these questions, further in *vitro* assays with the isogenic KPAR1.3 cell lines were conducted to isolate cancer cell-intrinsic treatment responses.

5.3 Investigating cancer cell-intrinsic effects of oncogenic pathway inhibition

To further disentangle the effects that KRASi and SHP2i exert in a cancer cell intrinsic manner in contrast to effects caused by enhanced antitumour immunity in the TME, a series of in *vitro* assays were conducted. Here, the effects of SHP2 inhibition in KRAS G12D mutant cancer cells was of particular interest. The G12D mutant KRAS protein is less dependent on upstream reactivation, compared to the G12C mutant variant, due to differing protein-intrinsic properties (**Figure 1.2**). Mice engrafted with KPAR1.3 KRAS G12D-derived tumours did not appear to respond to SHP2i, in terms of tumour regression during treatment (**Figure 4.2**). However in the subsequent RNA-seq experiments, SHP2i did appear to alter the cell state of respective tumour cells (**Figure 5.17**, **Figure 5.19**).

To better understand the inhibitor response rates of KRAS G12C and G12D mutant KPAR1.3 cells, a series of viability assays was conducted employing SHP2i RMC-4550 as well as KRASi Adagrasib. Of note, the extent of drug responses in cell culture can depend on culture media composition. The supplemented serum contains additional hormone and growth factors, as well as a source of proteins, vitamins and other trace elements, such as inorganic salts[305]. Adding FCS to cell cultures, may thus contribute to mimicking physiological conditions for cancer cells to grow and proliferate. Moreover, this may also aid cancer cells in bypass signalling to circumvent the targeted inhibition of an oncogenic signalling node. Hence, reducing the serum concentration may help to isolate the effects of respective drugs. Further, FCS-low media may be more representative of the tumour core, which is often hypoxic and nutrient depleted. To understand the full range of treatment-responses, viability assays were performed with culture media supplemented with different concentrations of FCS (**Figure 5.23a-c**).

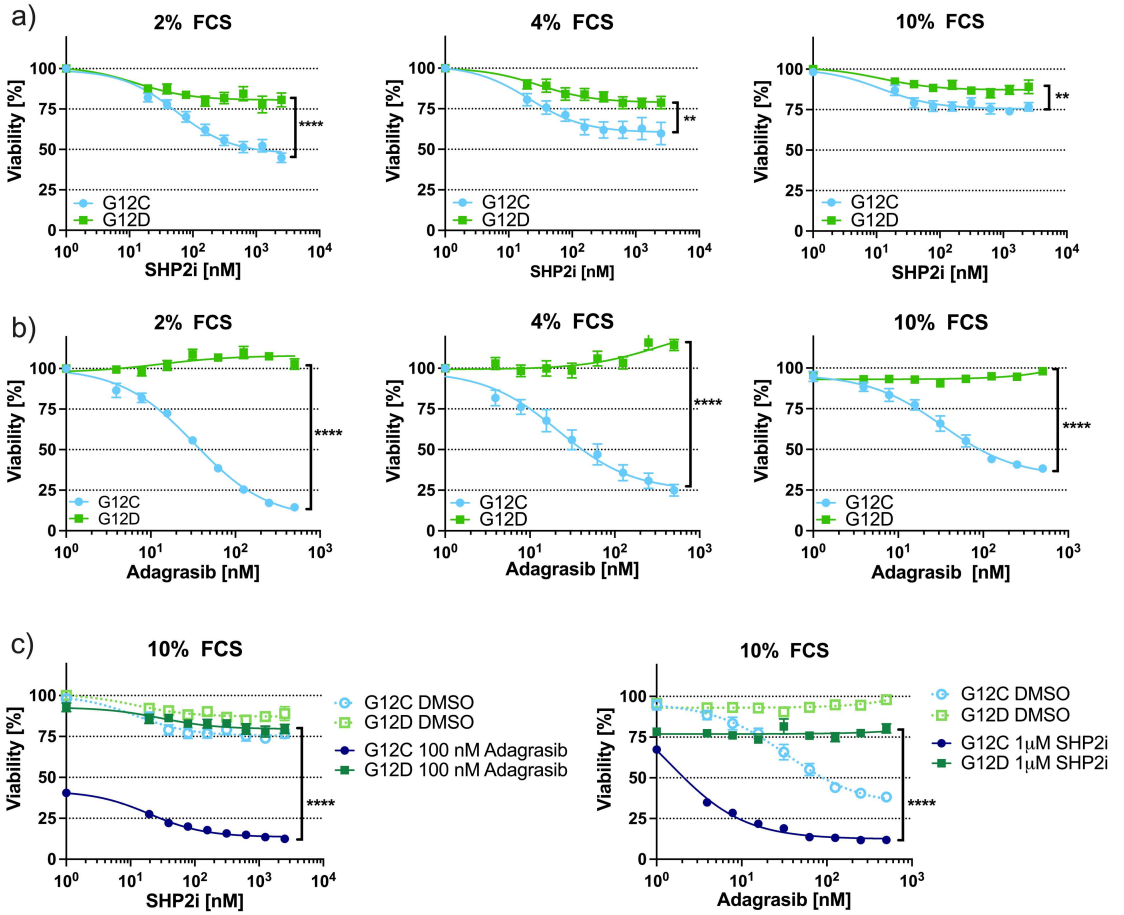


Figure 5.23 Viability assays of KRAS G12C- and G12D mutant cancer cells. eBFP$^+$ KRAS G12C or Luc-eGFP$^+$ KRAS G12D mutant KPAR1.3 cancer were treated with a) SHP2i RMC-4550or the b) KRAS G12C(OFF) inhibitor Adagrasib in culture media with indicated FCS concentrations. c) Treatment synergy between the two targeted inhibitors: in addition to the drug gradients, a fixed dose of either 100 nM Adagrasib (left) or 1 μM SHP2i (right) were added to all wells in the respective treatment group. As reference, the single inhibitor response curves from (a, b) are added as dotted lines. All experiments were performed as 3-4 independent biological experiments with 3 technical replicates each, dots show mean values and error bars indicate SEM. A two-way ANOVA test was performed to assess genotype-related differences in SHP2i-response between the KPAR1.3 KRAS G12C or G12D mutant cell lines.

First, the results of these assays indicate that KRAS G12C mutant cancer cells respond more to SHP2 inhibition compared to G12D mutant cancer cells at all serum concentrations, with the extent of inhibitor response decreasing when more FCS was added to the medium. As expected, KRAS G12D mutant cancer cells did not respond to Adagrasib. The response of KRAS G12C mutant KPAR cells, on the other hand, was more profound and also depended on the concentration of FCS in the media. To test for possible treatment synergy

between Adagrasib and SHP2i within the cancer cells, further combination treatment viability assays were performed, using media containing 10% FCS, (**Figure 5.23d**). Viability experiments showed that in G12C cells, combination of SHP2i plus KRASi enhanced the inhibition of cell proliferation. Whereas, as expected, no combination effect was observed in the G12D cells.

Next, the extent to which SHP2 inhibition affects the activation of effector proteins downstream in the oncogenic KRAS signalling pathway in G12C or G12D mutant cancer cells was investigated. As the regulation of oncogenic signalling networks is a dynamic process, time course assays were performed to capture drug responses with temporal resolution. Here KPAR1.3 KRAS G12C or G12D mutant cancer cells were treated with SHP2i for 6h, 24h, or 48h and a '0h' DMSO-vehicle time point was also included to establish a baseline. Here, cells were either cultured in 10% FCS- or 2% FCS-containing media. Next, the protein fraction of the cultured cells was isolated, with protease- and phosphatase inhibitors added to the lysis buffer to avoid altering the proteome post sample isolation. Western blots were then run to interrogate activation of effector proteins downstream of KRAS, positively indicated by phosphorylation status of respective protein sites. The effector signalling proteins investigated here included Erk, a signalling protein of the MAP-kinase pathway, Akt, a signalling protein with a role in the Pi3K–mTOR axis, and S6, a ribosomal protein a ribosomal protein downstream of several S6-kinases, which can be indicative of mTOR signalling activities in this experimental setting.

In both, KRAS G12C and G12D mutant KPAR1.3 samples cultured in 10% (**Figure 5.24a**) or 2% (**Figure 5.24b**) FCS-containing media, the investigated effector signalling proteins appeared to exist largely in their inactive conformation after 6h of SHP2i. However, a rebound was observed for the 24 h and 48 h timepoints. This rebound of effector proteins in their active conformation was even enhanced compared to baseline expression in the DMSO control for the proteins Akt and S6, indicating a potential compensation mechanism.

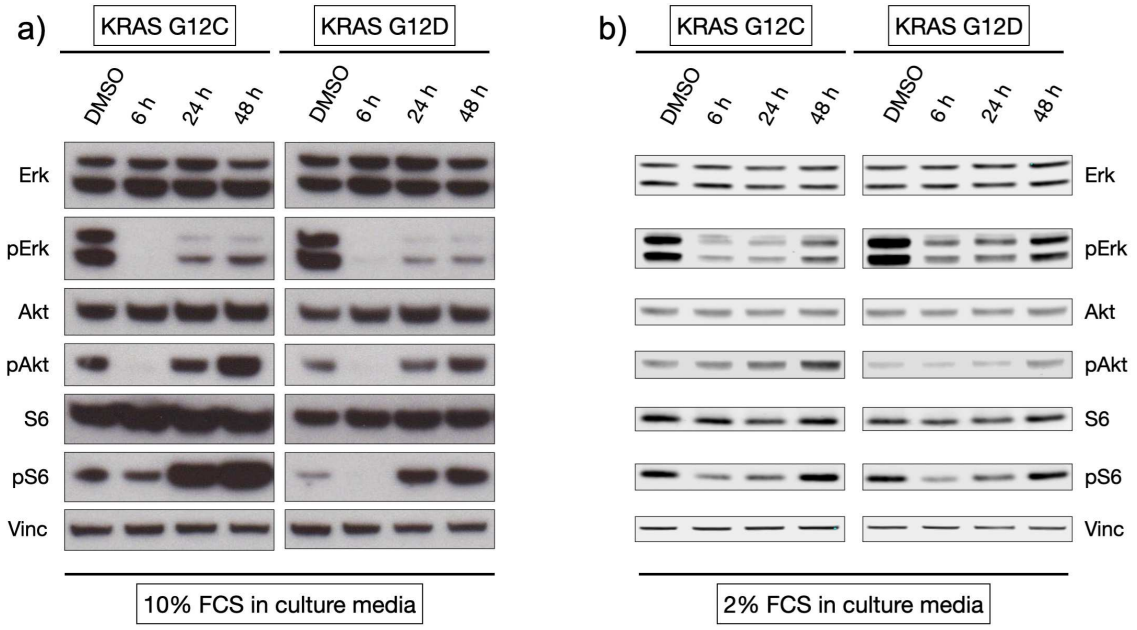


Figure 5.24 Western blots of SHP2i time course assays. Western blots analysis of vinculin (expression control) Akt/pAkt, Erk/pErk, S6/pS6 expression in time-course experiment. Cells were treated in culture with 1 µM SHP2i (RMC-4550) for indicated time points or DMSO as negative control. 'KRAS G12C': KPAR1.3 KRAS G12C mutant cancer cells, 'KRAS G12D': KPAR1.3 KRAS G12D mutant cancer cells. Experiment was performed in a) media containing 10% FCS with n = 3, one representative western blot is shown and b) 2% FCS containing media with n = 2, one representative western blot is shown. The Western blots in (b) were performed with the kind help of Sareena Rana from our research group and Isabel Rafalin, a visiting student.

In viability assays as well as in *vivo* treatment experiments, KRAS G12D mutant cancer cells appeared to respond less to SHP2i compared to G12C mutant cells (**Figure 4.2, Figure 5.23**), although cells still presented with significantly inhibited oncogenic to SHP2i at the 6 h time point. Therefore, it was tested whether the expression of transcriptional targets downstream of oncogenic KRAS signalling was also affected. Here, matching RNA samples, which had also been collected during the time course assays, were used to run qRT-PCRs.

On the RNA level, it again appeared that cancer cells overall responded less to SHP2i in culture media containing 10% FCS (**Figure 5.25a**), compared to 2% FCS (**Figure 5.25b**). This was in accordance with the observations from the

previously conducted viability assays (**Figure 5.23**). For both culture conditions, a trend was observed in which KRAS G12C mutant cancer cells presented with lower expression of respective target genes compared to their matched KRAS G12D mutant counterpart for each timepoint. This would be consistent with the findings that the KRAS G12C mutant proteins are more dependent on upstream activation compared to the KRAS G12D mutant isoform[53,55,56,60,61]. In contrast to the corresponding Western blots (**Figure 5.24**), where a rebound in signalling protein phosphorylation was observed as a trend, the expression of downstream signalling targets was still downregulated at the 24 h and 48 h time points, compared to the vehicle control. This might imply that the increase of phosphorylated signalling proteins observed in the Western blots are not sufficient to rescue expression of downstream transcriptional targets.

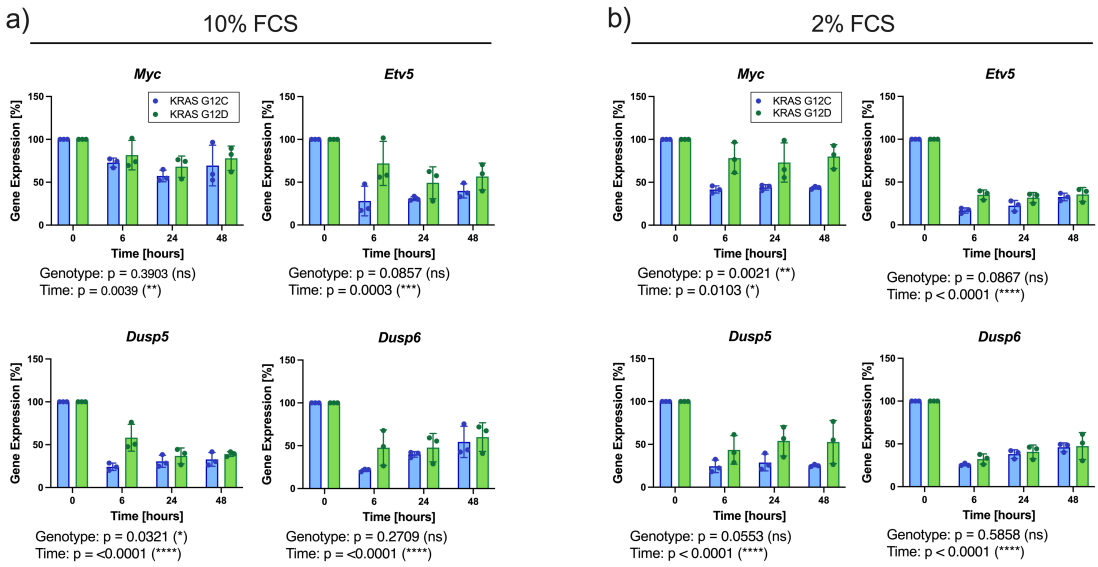


Figure 5.25 qPCR analysis of SHP2i time course assays on KRAS signalling transcriptional targets. Relative expression level of transcripts for *Myc*, *Etv5*, *Dusp5* and *Dusp6* in matched KRAS G12C or -G12D mutant KPAR1.3 cancer cell samples, treated with 1 µM SHP2i (RMC-4550) for indicated time points or DMSO as negative control. 'KRAS G12C': KPAR1.3 KRAS G12C mutant cancer cells, 'KRAS G12D': KPAR1.3 KRAS G12D mutant cancer cells. qPCR analysis was performed for n=3 independent biological replicates with tr=2 technical replicates. Dots in the bar graphs indicate mean expression of technical replicates + SD, samples were normalised to vehicle control. A two-way ANOVA test was performed to assess response difference between the two different cancer cell genotypes (KRAS G12C or G12D) as well as over different time points. Experiment was performed in a) culture media containing 10% FCS or b) 2% FCS. The qPCRs were performed with the kind help of Sareena Rana from our research group and Isabel Rafalin, a visiting student.

It is known that oncogenic KRAS signalling can supress cancer cell intrinsic stress responses, to initiate or in response to an anti-tumour immune response[136], for example, by decreasing expression of antigen presentation machinery or supressing IFN-γ responses. In the bRNA-seq data sets, the addition of SHP2i therapy was associated with an increase in inflammatory signatures in both KRAS G12C and G12D mutant tumour cells. However, it remained unclear whether this alteration in cancer cell state was induced through cancer cell intrinsic alleviation of oncogenic signalling mediated immune suppression or through pressures induced by SHP2i-enhanced anti-tumour immunity. Hence, we also ran qPCR analysis on targets associated with an inflammatory response in the samples collected for the time course assays (**Figure 5.26**). So far, this has only been done with 3 independent replicates for the cDNA isolated from samples that were cultured in media containing 10% FCS. However, the samples cultured in media containing 2% FCS will also be assessed. The targets analysed in this assay included the transcripts for H2-K1 and B2M genes, which encode for components of the antigen presentation machinery MHC-I complex. The STAT1 and STAT2 genes are part of the JAK/STAT signalling pathway and key regulators of IFN type 1 and 3 responses[306]. The interferon-regulatory factor (IRF)1, -7, and -9 transcripts encode for proteins belonging to a family of transcription factors known to regulate interferon responses which act downstream of the IFN- γ receptor. [307] PD-L1 expression, on the other hand, is associated with inducing T cell exhaustion, when aberrantly expressed on cancer cells. As an overall trend, it was observed that the expression of genes promoting inflammation were slightly elevated, although this was not significant for all of the targets. However, treatment induced changes in expression of inflammation associated genes appeared to be less pronounced in in *vitro* assays compared the observations made in the bRNA-seq data. Moreover, as a trend, expression of inflammation associated genes appeared to be more elevated in KRAS G12C compared to G12D mutant cancer cells, which might be due to more extensive

inhibitory effects of the SHP2i. On the other hand, PD-L1 expression also appeared to be upregulated at the 24 h and 48 h time points. Implying a potential dual role in the SHP2i-mediated regulation of inflammation response.

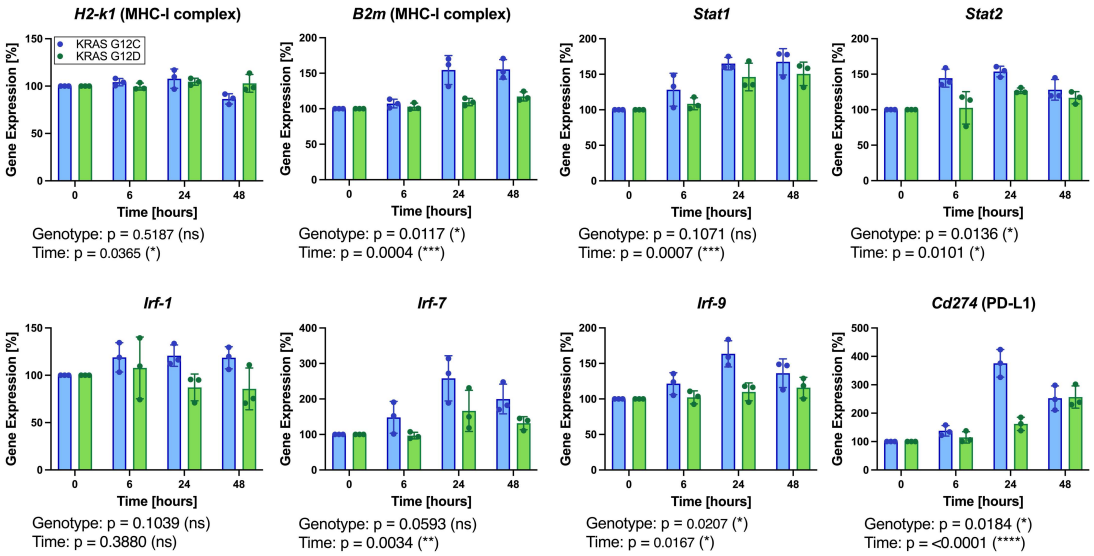


Figure 5.26 qPCR analysis of SHP2i time course assays on inflammation-associated transcriptional targets. Relative expression levels of transcripts for genes associated with an inflammatory signature in matched KRAS G12C or G12D mutant KPAR1.3 cancer cell samples, treated with 1 µM SHP2i (RMC-4550) for indicated time points or DMSO as negative control. 'KRAS G12C': KPAR1.3 KRAS G12C mutant cancer cells, 'KRAS G12D': KPAR1.3 KRAS G12D mutant cancer cells. qPCR analysis was performed for n=3 independent biological replicates with tr=2 technical replicates. Dots in the bar graphs indicate mean expression of technical replicates + SD, samples were normalised to vehicle control. A two-way ANOVA test was performed to assess response difference between the two different cancer cell isotypes (KRAS G12C or G12D) as well as over different time points. Experiment was performed in culture media containing 10% FCS. The scale on the y-axis was not normalised for all the targets, due to the wide range of expression changes between transcript targets. The qPCRs were performed with the kind help of Sareena Rana from our research group.

Overall, investigating therapy induced changes in the cancer cell compartment provided several additional insights. First, the increase in proliferation in the KPAR1.3 KRAS G12D mutant tumour cells during KRASi treatment appeared to be mediated through several signalling networks, including MYC- and E2F-mediated target gene sets. Moreover, this proliferative signature was also maintained in the dual combination treated samples. This could imply that the generation of CRs in these groups relied on immune mediated elimination of cancer cells, rather than direct treatment-mediated cancer cell killing. However,

although these experiments provided additional mechanistic insights as to how the increase in proliferation is mediated in the KRAS G12D mutant tumour sub-population, the underlying causes of this phenomenon have not yet been identified and may require further investigation.

Secondly, responses to anti-cancer therapies tended to correlate with an increase in inflammatory response signatures in the RNA-seq data and, to a moderate extent, also in corresponding in *vitro* assays with SHP2i. The time course assays investigating how SHP2i influences expression of inflammatory signature genes for samples cultured in media containing reduced FCS have not yet been analysed. It is possible that changes in inflammatory state of the cancer cells would be more pronounced in these samples. Furthermore, the expression of additional inflammatory signature targets that were identified through the RNA-sequencing experiments, should be validated. However, as changes in inflammatory response were only moderate in these in *vitro* assays, it might also imply that SHP2i indirectly induces additional pro-inflammatory effects on the tumour cell compartment in *vivo* through enhancing anti-tumour immunity. Together, these findings provide a rational for exploiting the therapeutic window in which the targeted inhibitors alleviate oncogenic KRAS signalling mediated immune suppression in the majority of the tumour mass, thereby allowing for the establishment of enhanced anti-tumour immunity.

Chapter 6. Investigating therapy-induced alterations in TME immune cell composition and architecture

We hypothesized the combination therapy schemes were able to foster the development of an adaptive immune response and immune memory in immune competent mice, capable of targeting KRAS G12Ci-resistant cancer cells This is remarkable, considering that KRAS G12D cells retain their proliferative phenotype, even when exposed to combination treatments. Therefore, the underlying mechanisms governing the development of effective anti-tumour immunity and elimination of KRASi-resistant tumour sub-populations was further investigated. Here, immune compromised murine models were used to disentangle the contribution of therapy combinations to bolstering adaptive anti-tumour immunity. The serum of treated mice was then probed for the presence of a humoral immune response in the form of tumour cell-specific antibodies. Furthermore, a combination of different omics-based approaches was employed to analyse the composition and structural organisation of the immune compartment in the local TME. This included spectral flow cytometry, where a 36-plex ab was used to conduct immune phenotyping of the TME. Additionally, tdLNs across treatment groups had also been collected to probe for potential signs of a central coordination of anti-tumour immune response. Further, multiplex imaging of tissue sections across treatment groups, employing a 7-plex ab was also performed, to gain further insights into therapy-induced changes in TME architecture.

6.1 Investigating the contribution of the adaptive anti-tumour immunity in elimination of KRASi-resistant sub-populations

We first aimed to confirm that adaptive anti-tumour immunity contributed to the elimination of KRASi-resistant tumour cell subpopulations on a systemic level. For this, an immune compromised version of the GH-mouse strain was generated, which was achieved by crossing GH mice with $Rag1^{-/-}$ C57BL/6J mice ($Rag1^{-/-}$ GH-mice). The resulting strain lacks an adaptive immune compartment, because the loss of the Rag1 enzyme compromises the genomic V(D)J recombination process, necessary for the generation of antigen-specific B and T cells[72]. Over two generations, the $Rag1^{-/-}$ GH strain was also selectively crossed to retain its albino fur coat to facilitate IVIS scanning.

In previous survival experiments, treatment combinations were tested in immune competent mice co-engrafted with 99.96% $eBFP^{+}$ KRAS G12C tumour cells and 0.04% of Luc-eGFP KRAS G12D cancer cells (**Figure 4.3**). This experimental setting was now repeated in the $Rag1^{-/-}$ GH strain, with the omission of a-PD-1 therapy. It is known that PD-1 can be expressed on a variety of immune cells, including immunocytes of the innate immune compartment, such as NK cells[308], and tumour associated macrophages[309,310]. However, it is believed that CPI-based therapies act mainly through enhancing T cell responses[311-313]. Hence, for ethical reasons as well as the limited number of mice that were available, it was decided to focus on the combination of SHP2i RMC-4550 and KRAS G12Ci RMC-4998. Mice in this experiment were treated for two consecutive weeks, to match the therapy schedule that immune competent mice had initially received for this dual combination**.**

Following the tumour growth over time revealed that SHP2i and KRASi, either alone or in combination did induce tumour regression during the treatment period (**Figure 6.1a**). However, all mice relapsed after the treatment period had

ended and no complete responders were observed. IVIS scans further indicated that, similar to previous experiments, the addition of KRASi resulted in an outgrowth of the KRAS G12D mutant tumour subpopulation (**Figure 6.1b**). However, compared to previous experiments, this observation was made in all combination-treated $Rag1^{-/-}$ mice. Interestingly, plotting the probability of survival, stratified by treatment group (**Figure 6.1c**), visualised that the combination treatment provided less of a survival advantage, in contrast to immune competent mice (**Figure 4.4c, Figure 4.6a**). As an additional readout, flow cytometric analysis of tumours was performed when mice reached an experimental endpoint, as well as of a few representative tumours at the end of treatment, to capture the fraction of KRAS G12D mutant cancer cells present in the tumour mass (**Figure 6.1c**). This implied that after tumours grew back, the percentage of KRAS G12D cells within all live cancer cells varied between mice within the same treatment group (**Figure 6.1d**). Indicating that both, remaining KRAS G12C mutant or G12D mutant cancer cells could contribute to the tumour mass.

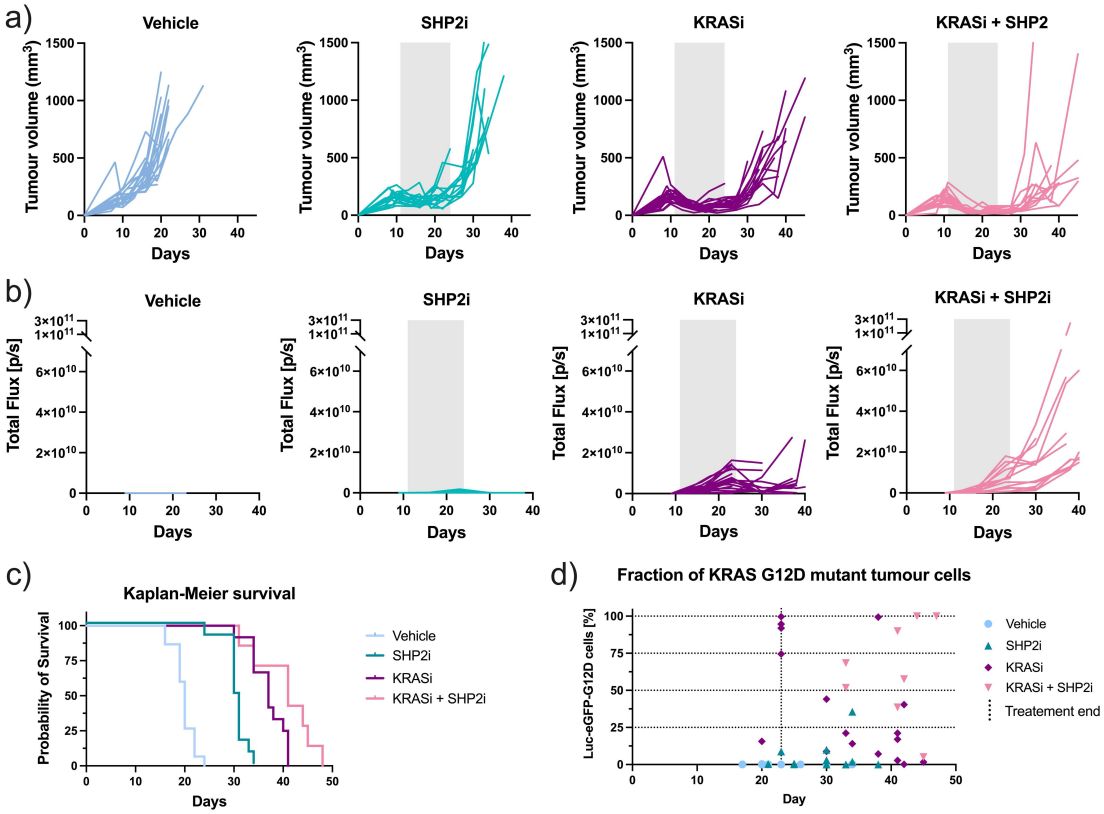


Figure 6.1 Assessing therapy effects in Rag1$^{-/-}$ GH-mice. Rag1$^{-/-}$ GH-mice were treated 2 weeks, whereat 12 doses of the oral drugs KRAS G12C(ON)i RMC-4998 (100 mg/kg; indicated as KRASi) or SHP2 inhibitor RMC-4550 (30 mg/kg; indicated as SHP2i) were administered (grey area on plots). Graphs show the results of n=2 independent biological replicates of this experiment. a) Tumour volume over time of individual tumours by treatment group. b) Photon flux per second, measured via IVIS scans, indicative of the abundance of KPAR1.3 KRAS G12D cells over time. c) Probability of survival, stratified by treatment group. d) Fraction of Luc-eGFP KRAS G12D mutant tumour cells out of all tumour cells, assessed through flow cytometric analysis; each dot represents an individual tumour of the respective treatment group; tumours isolated at the end of treatment are indicated by dotted vertical line.

Next, to further disentangle the contribution of individual cell types of the adaptive immune response, we performed selective depletion experiments in immune competent glowing head mice. Tumours were engrafted as in previous experiments and either stratified into a vehicle control group or were treated with the KRASi (RMC-4998) + SHP2i (RMC-4550) combination treatment. Mice receiving the combination treatment were then further subdivided into three groups, for two of which either CD8^{+} T cells or CD20^{+} B cells were depleted for the duration of the treatment period, by injecting the indicated immunocyte-depleting antibodies. This allows to isolate the contribution of individual cell

subpopulations within the adaptive immune compartment to the elimination of cancer cells. In this experiment, there were 4/12 CR in the KRASi + SHP2i treatment group, 1/12 CR in the KRASi + SHP2i + a-CD20 group and 1/10 CR in KRASi + SHP2i + a-CD8 treatment group (**Figure 6.2a**). This suggests that both CD8 T cells and B cells play a role in the generation of CRs. Complementary IVIS scans indicated that during the treatment period KRAS G12D mutant tumour cells overall proliferated less in this experiment (**Figure 6.2b**) compared to the previous experiment with $Rag1^{-/-}$ GH mice (**Figure 6.1b**). GH-mice treated with KRASi + SHP2i with only one type of adaptive immune cell depleted also survived longer on average (**Figure 6.2c**), compared to the $Rag1^{-/-}$ GH mice treated with the same combination (**Figure 6.1c**). Complete responder mice were then re-challenged by injecting KRAS G12D mutant KPAR1.3 cancer cells in the opposite flank. Neither the mouse from B cell, nor the $CD8^{+}$ T cell depletion groups were able to immune reject the secondary tumour. While two mice from the KRASi + SHP2i group remained tumour free (**Figure 6.1d**). However, compared to naïve control mice, tumour growth of all previously treated mice appeared to be slower.

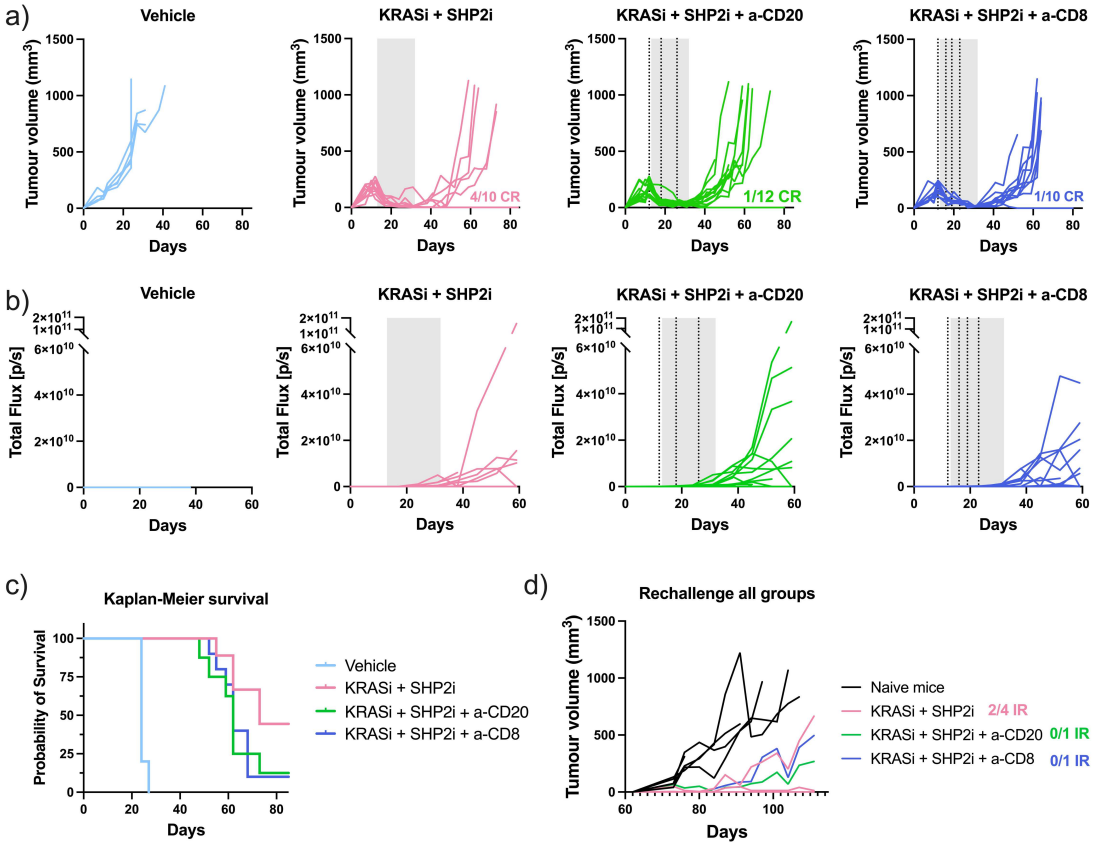


Figure 6.2 Selective depletion of immune cell populations. Immune competent GH-mice were stratified into vehicle or KRASi (RMC-4998; 100mg/kg) and SHP2i (RMC-4550; 30 mg/kg) combination treated mice. Here, mice received 18 doses of the combination treatment over three weeks via oral gavage. In two of the treated groups, CD8 T or B cells were depleted with respective depleting antibodies, as indicated by dotted vertical lines in respective graphs. For B cells, 3 doses of a-CD20 (10 mg/kg) were administered via tail vein; for CD8 T cells, 4 doses of an a-CD8 ab (12.5 mg/kg) were administered via intraperitoneal injection. a) Tumour growth over time for respective treatment groups. Complete responders (CR) indicated on respective graphs. b) Corresponding IVIS scans. c) Probability of survival over time by treatment group. d) Tumour growth of re-challenge experiment, proportion of mice which were able to immune-reject (IR) the repeated engraftment of cancer cells are indicated for respective previous treatment groups.

Comparing this experiment with the equivalent experiment performed in RAG1$^{-/-}$ GH mice may indicate that immune rejection of cancer cells is achieved through a combined effort of immune cell population within the adaptive immune compartment. Depleting an individual population of the adaptive immune compartment might compromise but not completely impair an adaptive immune response. CD4^{+} T cells were not depleted in this experiment, as these encompass a group of heterogenous populations with diverse and sometimes opposing functions. Hence, depleting this group of immunocytes might result in

ambiguous results. It may, however, be of interesting to deplete the $CD4^+$ subgroup of T-regulatory cells in the future because it had been discovered by our group that KRASi can also lead to increased Treg infiltration in the TME, which may hamper the development of an effective adaptive immune response [218]. From this section of experiments, it was concluded that immune-deficient mice are compromised in their ability to reject tumours containing drug-resistant sub-populations. The results of depleting individual immune cell populations of the adaptive immune compartment indicated that multiple types of immunocytes may contribute to an adaptive immune response. Moreover, there may be a certain degree of effector redundancy, with a partial adaptive immune response remaining intact even if only one immune subpopulation is depleted.

In initial immunohistochemical stainings of tumour sections across different treatment groups, only few B cells were detected within the TME of subcutaneous tumours (**Figure 6.3**). Here, tumour sections across treatment groups were stained for two B cell markers, CD19 and B220, to provide an overview of the B cells abundancy. The two markers were selected as CD19 is a marker highly specific to B cells but can get downregulated in differentiated plasma cells while B220 is expressed universally by B cells but can also be present on other particular sub-populations of immunocytes. Here a spleen was also included as positive staining control. Similar to the IF stainings, qPCRs conducted earlier in the project to probe for the presence of CD19 transcripts in subcutaneous KPAR1.3 tumour samples, did not detect a clear signal that would indicate the presence of B cells (not shown). As B cells can promote anti-tumour immunity through secretion of tumour cell specific antibodies, their abundance in the TME may not be a direct indication of their efficacy. However, due to the low B cell counts, it was initially still surprising that B cell depletion appeared to reduce the number of CRs.

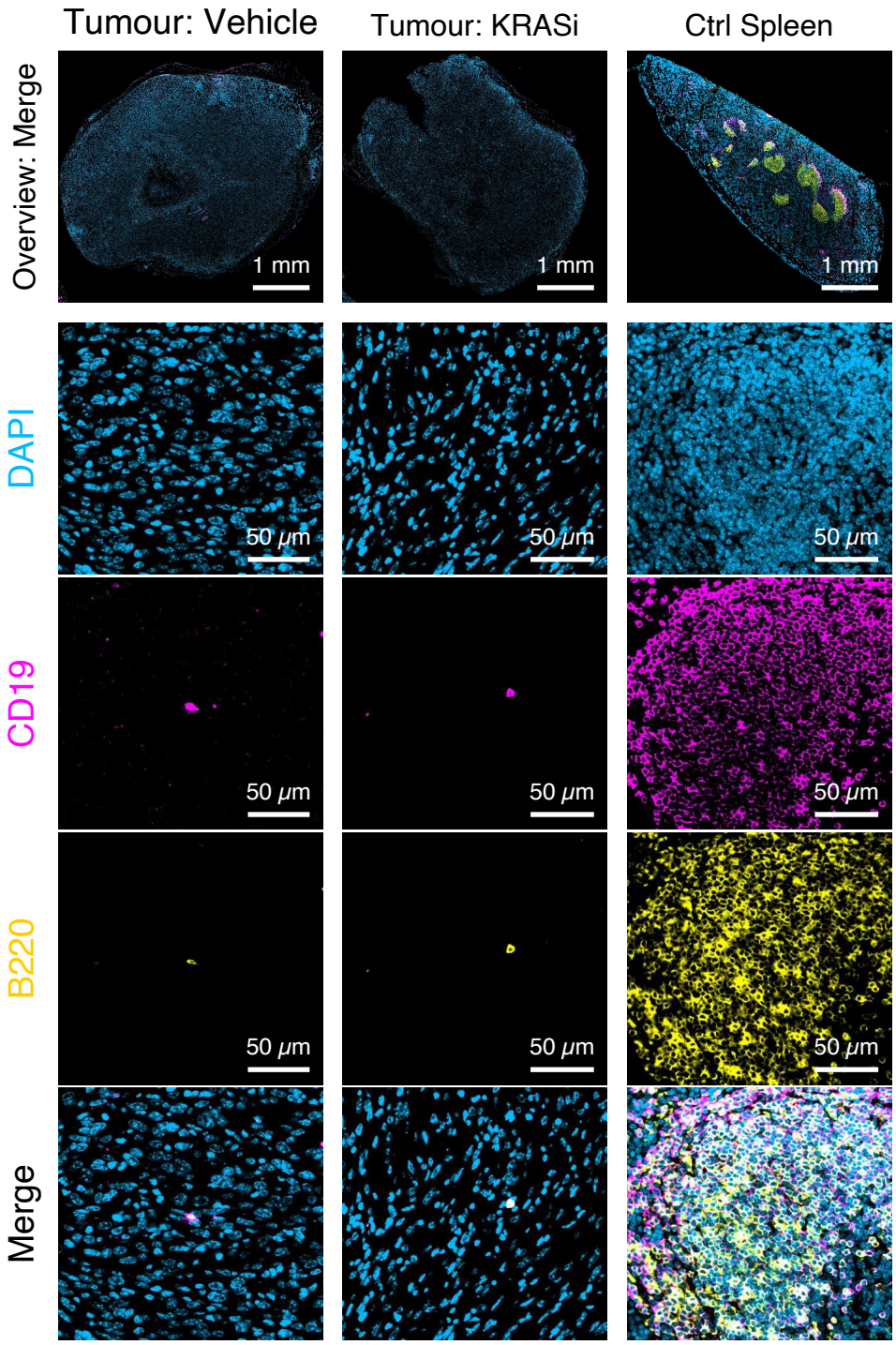


Figure 6.3 Immunohistochemical staining of B cells. Exemplary IF staining of B cells in subcutaneous KPAR1.3 tumours treated with either vehicle or KRAS G12C inhibitor RMC-4998 (100 mg/kg) for 6 days before sample collection. The spleen was derived from a C57BL/6 mouse and had kindly been provided by the experimental histopathology department.

Therefore, it was assessed whether B cells may contribute to anti-tumour immunity through a more systemic humoral response by secreting of tumour

cell specific abs. For this purpose, the serum samples of the end point experiment used to test for potential treatment-induced liver toxicities (**Figure 4.6**) were now employed to test for the presence of cancer cell specific antibodies. Here, small volumes of serum samples were used to stain cultured KPAR1.3 cells (**Figure 6.4**), to assess whether serum-residing abs had successfully opsonised the cancer cells. A Fc-region-specific, fluorophore-conjugated secondary ab was then added to samples, and mean fluorescent intensity (MFI) was subsequently quantified via flow cytometric analysis.

In this experiment, both KPAR1.3 KRAS G12C and G12D cancer cells were stained, to test whether serum-derived abs would have equal affinity to the two cancer cell isotypes. Moreover, the original untransduced KPAR1.3 cell lines were used for this investigation, to ensure that a potential B cell-mediated immune response was against the cancer cell antigens and not the artificially expressed reporter constructs. It was important to ensure that the detected fluorescent signal corresponded to a biological meaningful level of cancer cell opsonisation by serum abs. Hence, the median fluorescence intensity (MFI) was normalised to control samples, stained with serum from naïve mice, which had not been exposed to cancer cells before. This experiment revealed that tumour-cell specific abs were indeed present in the serum of KPAR1.3 tumour bearing mice. Comparing the matching MFIs for the two cancer cell isotypes within each individual serum sample, indicated that serum antibodies had similar affinity to tumour cells regardless of the specific KRAS mutation. This humoral response was also independent of the presence of reporter constructs. However, therapies did not appear to increase the serum titre of cancer cell specific antibodies, as serum obtained from vehicle mice appeared to contain similar concentrations to the treated groups.

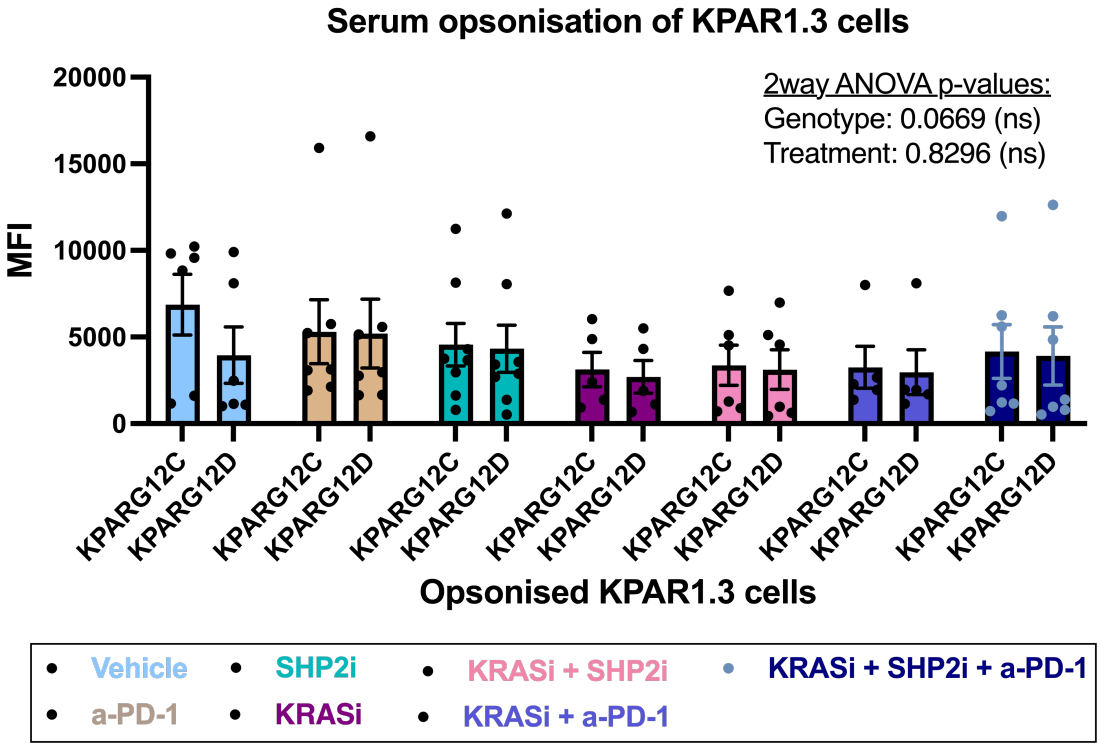


Figure 6.4 Cancer cell-specific abs in serum from experimental mice. Median fluorescent intensity (MFI) of serum-stained un-transduced KPAR1.3 KRAS G12C or G12D cancer cells assessed via flow cytometric analysis. All samples were normalised to the MFI of matching KPAR1.3 KRAS G12C or G12D cells, stained with serum from naïve mice. Results are coloured by treatment groups and segregated by genotype. Each dot indicates serum from one mouse, the height bars indicate mean across samples within each group and whiskers depict the SEM. 2way ANOVA test was performed, probing for overall significant differences between (I) MFI of stained KRAS G12C vs G12D mutant KPAR1.3 cell samples ('Genotype') and (II) MFI between treatment groups within each genotype ('Treatment'). This experiment was performed together with the help of Claire Pillsbury and the control serum from naïve mice was kindly provided by Panos Anastasiou.

The fact that the antibodies were able to bind both cancer cell isotypes might indicate that plasma B cells could play a systemic role in the bystander killing of KRAS G12Ci-resistant tumour cell sub-populations. However, it was unclear which specific antigens on cancer cells were recognised by the serum-derived abs. Our group previously described that the immunogenicity of the KPAR1.3 cell lines appeared to result from the aberrant expression of the Endogenous Murine Leukemia Virus 2 (EMV2) envelope glycoprotein [122]. In healthy somatic cells and under physiological conditions, the expression of these viral envelope proteins is supressed. However compromised regulation of gene expression and genomic instability in cancer cells can lead to anomalous expression of this

tumour-associated antigen. Jesse Boumelha and Alicia Alonso from our group had previously generated a KPAR1.3 Emv2 k.o. cell line to follow up on this discovery. This cell line was now employed to test whether the humoral response present in our preclinical murine model system was also targeting this viral envelope glycoprotein. Therefore, serum samples were again utilised to opsonise the original or Emv2 k.o. KPAR1.3 cells. This revealed that a majority of the humoral response appeared to be targeting Emv2. This phenotype did not appear to be altered significantly across therapy schemes, implying a universal role of the Emv2 protein in presenting an immunogenic, tumour-associated antigen target.

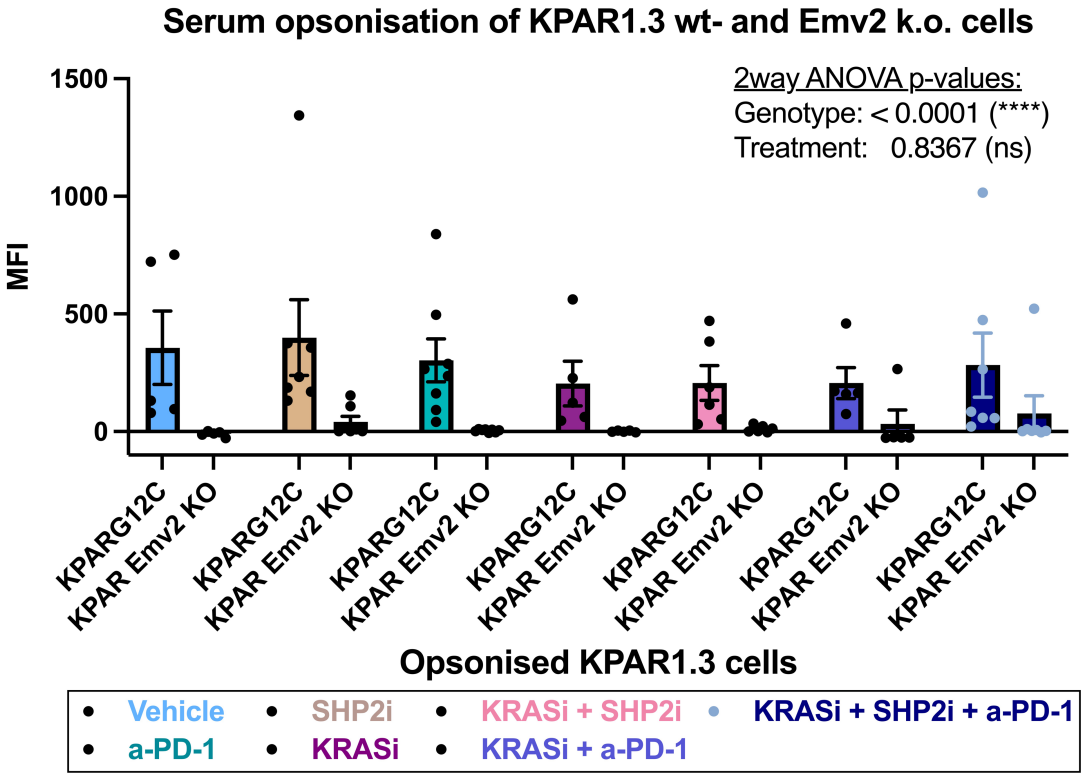


Figure 6.5 Testing for Emv2 specificity in serum antibodies. Median fluorescent intensity (MFI) of serum-stained, original or Emv2 k.o. KPAR1.3 cancer cells, assessed via flow cytometric analysis. All samples were normalised to the MFI of matching KPAR1.3 cells stained with serum from naïve mice. Results are coloured by treatment groups and segregated by respective cell line. Each dot indicates the serum of one mouse, the hight bars indicate mean of MFI across samples within each group and whiskers depict the SEM. 2way ANOVA test was performed, probing for overall significant differences between (I) MFI of stained original KPAR1.3 KRAS G12C vs KPAR1.3 Emv2 KO cell samples ('Genotype') and (II) MFI between treatment groups within each genotype ('Treatment'). This experiment was performed with the kind help of Alicia Alonso; the control serum sample from naïve mice had again kindly been provided by Panos Anastasiou.

These results suggest that even through few B cells were detected in the TME, their contribution to cancer cell killing could be through a more systemic humoral response whereat EMV2 expression in KPAR1.3 cells possibly contributed to their immunogenicity.

6.2 Immune phenotyping of the TME and tdLNS

In the previous series of experiments, the contribution of immunocyte populations within the adaptive immune compartment was assessed on a systemic level. However, we aimed to further isolate the underlying mechanisms governing the therapy-enhanced efficacy of an anti-tumour immune response. For this, a 36-plex ab panel for spectral flow cytometry was employed (**Table 2.9**) enabling extensive immune phenotyping of the TME. Additionally, tumour-adjacent tdLNs had also been collected from experimental mice of all treatment groups to probe for potential therapy-induced proximal coordination of an adaptive anti-tumour immune response. This panel allowed to identify immune subpopulation of both, innate and adaptive immunity via a broad array of lineage markers. It further provided insights into the cell state of respective immunocytes, such as their activation, proliferation, differentiation, and exhaustion status.

To set up this main study, several pilot flow cytometric experiments had been performed to assess optimal experimental parameters. This included the engrafted fraction of cancer cell subpopulations, length of treatment period before sample collection, establishment of a staining protocol, titration of antibodies, etc., which are not shown here. However, these initial tests had determined several factors and limitations for our main experiment. First, it was found that four days of treatment was too short to observe significant changes in immune cell composition in the TME. On the other hand, treating for 5 days or more resulted in too little material for immune phenotyping of triple

combination-treated samples, as tumour size had regressed too much. Letting tumours grow larger before the start of treatment, to compensate for sample loss in the triple combination treatment group with KRAS G12Ci + SHP2i + a-PD1 had likely resulted in an overall more “cold” TME phenotype and again no significant treatment induced changes were observed in the immune compartment. Because of this, it was decided to treat mice for 6 days while tumours were still at a smaller volume, but to omit the triple combination treatment group.

In the final experimental parameters (**Figure 6.6**), eBFP^{+} KRAS G12C and Luc-eGFP^{+} G12D mutant cancer cells were co-engrafted with a fraction of 0.2% G12D cells. The increase in this fraction, compared to the 0.04% in survival experiments (**Chapter 4.3**), was decided on to allow for the potential detection of potential eGFP^{+} CD45 cells in sufficient frequency. When tumours reached an average volume of ~340 mm^{3}, respective mice were treated with 6 doses of KRASi RMC-4998, SHP2i RMC-4550 and 2 doses of a-PD-1. Tumours, as well as adjacent tdLNs were then harvested and processed to create a single cell suspension, whereat red blood cells had been removed. Samples were then stained with the immune phenotyping ab panel as described in **methods chapter 2.8.3** and analysed on a spectral flow cytometer. The sample processing for this large experiment was done with the amazing support of our research team members and the data analysis was done with the kind help of Claire Pillsbury.

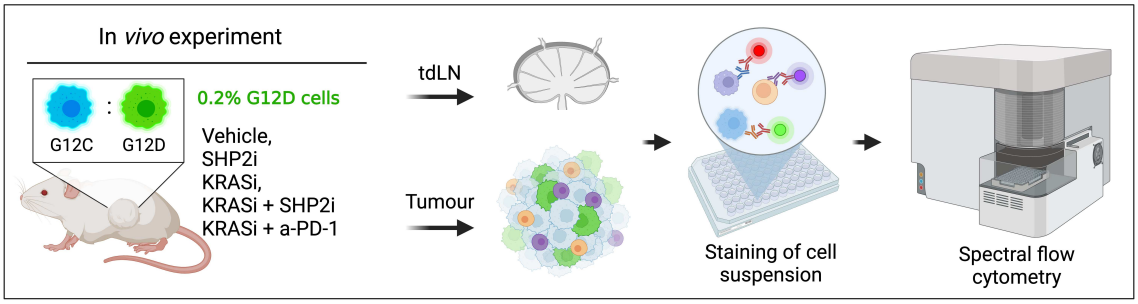


Figure 6.6 Experimental workflow for immune phenotyping. Overview of experimental set up for flow cytometric immune phenotyping of tumours and tdLNs across treatment groups. Mice were engrafted with 99.8% eBFP^{+} KRAS G12C KPAR1.3 cells ('G12C') and 0.2% Luc-eGFP KRAS G12D KPAR1.3 cells ('G12D'). Once tumours reached an average volume of ~340 mm^3 mice received 6 doses of the oral drugs RMC-4998 (KRASi) at 100 mg/kg, RMC-4550 (SHP2i) at 30 mg/kg, and 2 doses of a-PD-1 at 10 mg/kg. Tumours and tdLNs were harvested, a single cell suspension was created and samples were stained in a 96 well plate format. Subsequently, fluorescence profiles of cells were assessed via spectral flow cytometry. Image created with Biorender.

For all the subsequent quantifications of cell populations and the assessment of their cell states, the same initial gating strategy was performed. Here, first, live cells populations were delineated, segregating them from debris and other adverse events appearing in the forward and side scatter channels. Next, doublets, and subsequently dead cells were gated out, thereby isolating the single-cell, live populations of interest for further analysis.

The first step of the subsequent analysis was to create an overview of the general proportions of cancer cells and immunocytes in the samples across treatment groups was generated. This revealed that the proportions of tumour cells in samples derived from therapy-receiving mice had significantly decreased compared to vehicle mice (**Figure 6.7a**). Within the tumour cell compartment, the fraction of the KRAS G12D mutant tumour cells was increased in tumour samples derived from mice that received KRASi treatment (**Figure 6.7b**), which is consistent with previous findings.

Of note, the true percentages of the KPAR1.3 KRAS G12C tumour cell fractions present at the day of sample collection may have been underestimated in this analysis due to sample processing and analysis. Because KPAR1.3 KRAS

G12C cells respond more to the anti-cancer therapies, cells of this population may have been more likely to disintegrate during tumour dissociation, because of the already elevated level of cell stress. Apoptotic cells had also been gated out during analysis of the spectral flow data, due to their higher auto-fluorescent profile, thereby further decreasing their presence in the final analysis.

In the immunocyte compartment, $CD45^+$ immunocytes increased in samples of treated tumours as a trend (**Figure 6.7c**). However, these changes were only significant in the comparison between vehicle and KRASi + a-PD-1 treated mice. This might be related to the increased variability in immune cell proportions in treated samples.

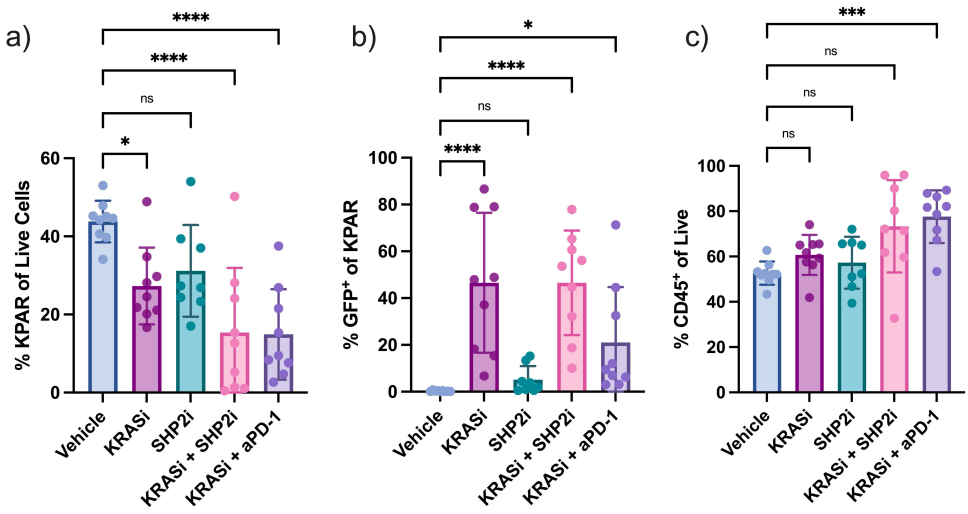


Figure 6.7 Overview of cancer cell and immunocyte proportions. For all plots, each dot represents one biological tumour sample, height of bars shows sample mean within each treatment group and whiskers indicate SD. One-way ANOVA test was performed, comparing vehicle samples with individual treatment groups, with significant p-values defined as: * $p \leq 0.05$, ** $p \leq 0.01$, *** $p \leq 0.001$, **** $p \leq 0.0001$. Percentages of positive cell counts are shown for a) Live tumour cells within all live cells, b) Luc-eGFP KRAS G12D KPAR1.3 tumour cells within all tumour cells, c) CD45 positive immunocytes within all live cells.

Next, the distribution of immune cell sub-types within each treatment group was quantified (**Figure 6.8**), which revealed treatment-induced changes in immune cell proportions. For example, an increase in T cell populations and DCs was observed in treated samples compared to vehicle, while the proportions of

Macrophage (MP) populations (segregated via their CD11c and CD11b expression status) in treated samples were decreased.

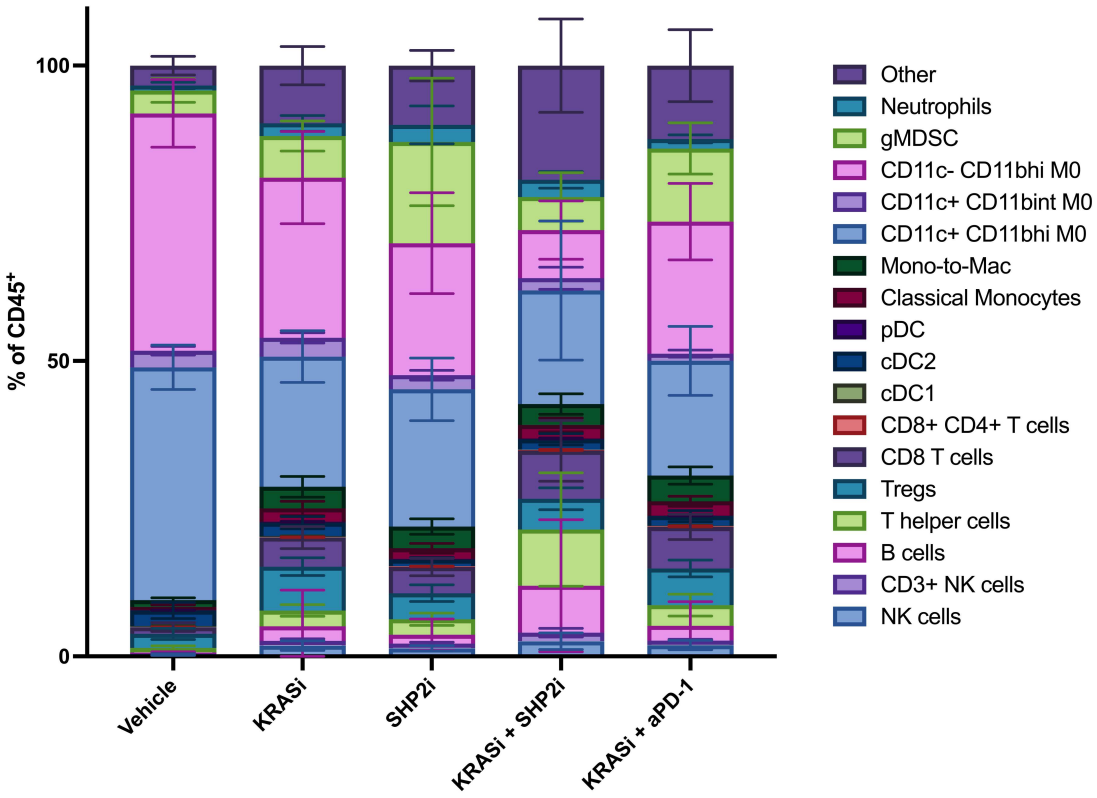


Figure 6.8 Immune sub-type classification by treatment group. Mean percentages of $CD45^+$ immune cell sub-types by treatment groups, whiskers indicate SD within each population across individual samples. Abbreviations from top to bottom: 'gMDSC': granulocytic monocyte derived suppressor cells; '$CD11c^-$ $CD11b^{hi}$ M0': mature macrophages; '$CD11c^+$ $CD11b^{int}$ M0': macrophages in the process of differentiation; '$CD11c^+$ $CD11b^{hi}$ M0': immature macrophages; 'Mono-to-Mac': a population of monocytes in transition-phase to differentiating macrophages; 'pDC': plasmacytoid dendritic cell; 'cDC2': conventional dendritic cell with alternative, type 2 polarisation; 'cDC1': conventional dendritic cell with type 1 polarisation; '$CD8^+$ $CD4^+$ T cells': a population of T cells which is double positive for both lineage markers; 'Tregs': T regulatory cells'; '$CD3^+$ NK cells': natural killer T cells; 'NK': natural killer cells.

After generating a general overview of the $CD45^+$ populations present in the TME, different immunocyte sub-populations were analysed in more detail to understand treatment induced changes in their abundancy and activation state. As initial in *vivo* experiments with immune compromised mice hinted at a contribution of adaptive anti-tumour immunity in bystander cell killing of KRAS G12D mutant tumour cells, these populations were analysed first. Quantifying

the proportions of T cell populations within all live $CD45^+$ cells, a significant increase in the abundance of $CD3^+$ T cells (**Figure 6.9a**), as well as $CD8^+$ T cells (**Figure 6.9b**) was observed in all treatment groups compared to vehicle. Further, proportions of T helper cells (**Figure 6.9c**) and $CD4^+$ $CD8^+$ double-positive T cells (**Figure 6.9d**) appeared to increase in treated samples as a trend, although this shift was not significant in some of the treatment groups compared to vehicle. In this experiment the proportion of the $CD4^+$ $CD8^+$ population was minute, with the highest recorded percentage being below 0.3% of all $CD45^+$ cells. Under physiological conditions, $CD4^+$ $CD8^+$ double positive T cells are typically found in the thymus, during their early stages of T cell development [72]. However, their existence among TILs has been confirmed across cancer types and it was hypothesized that they may even exert a certain degree of effector functions[314,315]. Their presence had also been confirmed across different murine lung cancer models by our group. On the other hand, the fraction of infiltrating Tregs were also increased (**Figure 6.9e**), especially in the presence of KRAS G12Ci which is consistent with previous findings in our group [218], hinting at a potential dual role of KRAS G12Ci-modulated T cell recruitment. However, when assessing the fraction of Tregs within all T lymphocytes present in the TME (**Figure 6.9f**), their overall proportions were lower in treated samples. Implying that the influx rate for cytotoxic $CD8^+$ T cells and other types of T helper cells was greater than that of Tregs.

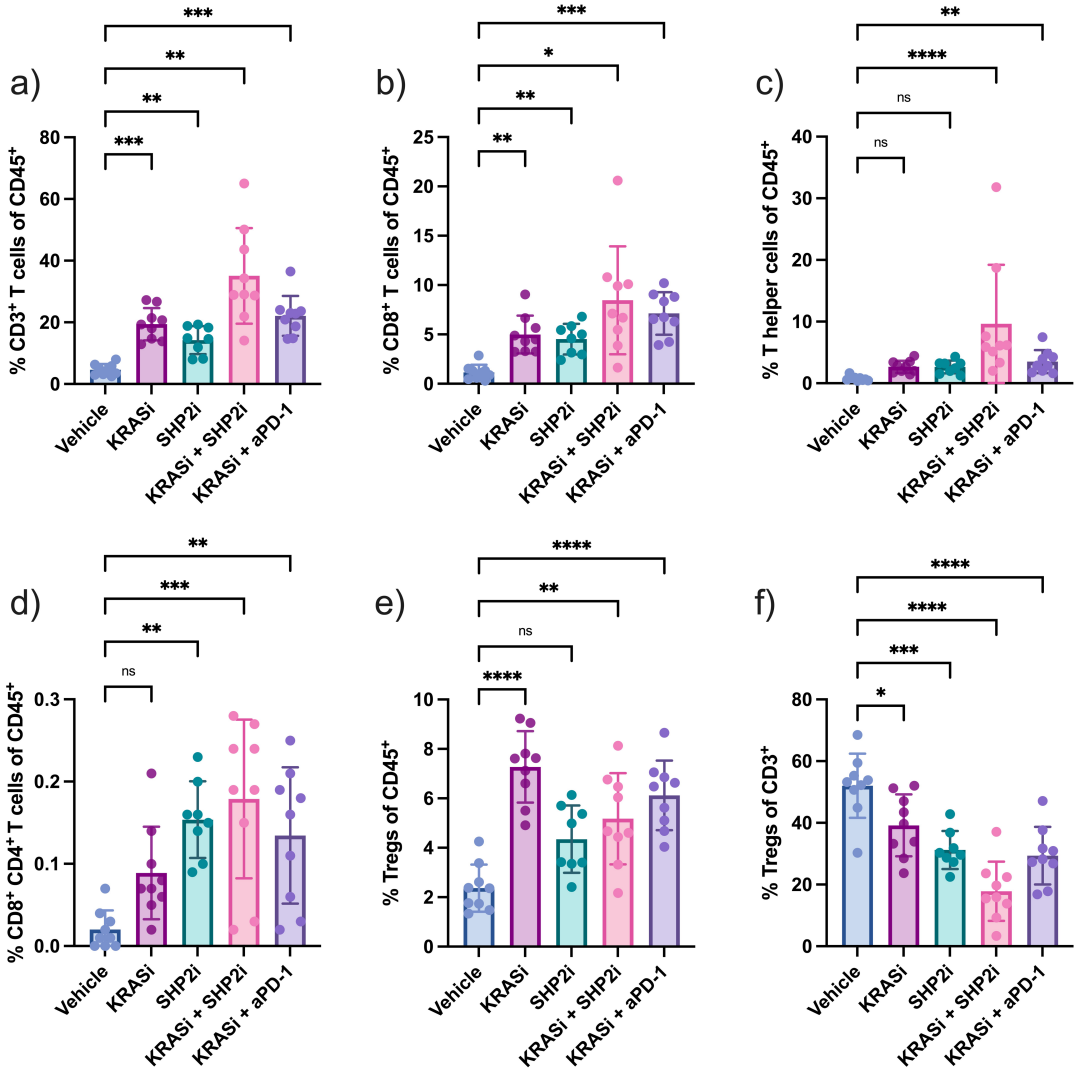


Figure 6.9 Proportions of T cell populations by treatment groups. Each dot is representative of an individual biological sample, hight of bars indicates mean percentages of TIL subtypes by treatment groups, whiskers indicate SD of sample means within each treatment group. One-way ANOVA test was performed, comparing vehicle samples with individual treatment groups with significant p-values defined as: * (1 star) indicative of $p \leq 0.05$, ** (2 stars) indicative of $p \leq 0.01$, *** (3 stars) indicative of $p \leq 0.001$, **** (4 stars) indicative of $p \leq 0.0001$. Percentages of T cell subpopulations are shown for a) $CD3^+$ T cells within all $CD45^+$ immunocytes, b) $CD8^+$ T cells within all $CD45^+$ immunocytes, c) $CD4^+$ T cells (encompassing different T helper cell subpopulations) within all CD45+ immunocytes, d) $CD8^+$ $CD4^+$ double-positive T cells within all $CD45^+$ immunocytes, e) Fraction of Tregs within all $CD45^+$ immunocytes (gated as fraction of $CD3^+$, $CD4^+$, and $Foxp3^+$ cells), f) Fraction of Tregs (with aforementioned gating strategy) within all TILs ($CD3^+$ T cells).

Surprisingly, analysing cell-state markers within the $CD8^+$ T cell compartment revealed an overall decrease in T cell activation (**Figure 6.10a**). This was determined via the expression of proliferation marker Ki67 or the combination of

$CD69^+/PD\text{-}1^+$ double positive status, CD69 being a T cell activation marker and PD-1 also indicative of T cell activation in this combination. Further, the $TIM3^+/LAG3^+$ double positive cells, which demarcate a population of terminally exhausted T cells that had previously likely induced an anti-tumorigenic activity, also appeared to have decreased in KRASi-treated samples[316,317]. A similar trend was observed for $CD4^+$ T helper cells (**Figure 6.10b**), with a reduction of Ki67 expression across all treated group as well as decreased expression of some activation and exhaustion markers. Here, the $TIM3^+/LAG3^+$ double-positive population appeared to be smaller in the sample groups KRASi or KRASi + SHP2i, although this was not significant. Lastly, the fraction of $Ki67^+$ Tregs was also significantly decreased in treated samples compared to vehicle control samples (**Figure 6.10c**). As anti-cancer drugs increase the number of apoptotic cancer cells and could alleviate immune suppression in the TME, it is possible that additional T cells were recruited to the tumour as a general site of inflammation. However, it is generally believed that only a small fraction of T cells in the TME expresses an antigen specific TCR, while the majority of T cells are recruited as unspecific bystander cells, whereat they could still fulfil certain indirect effector functions[110]. As T cells are quantified as relative fractions over CD45+ cells, it is still possible that more activated T cells were present in treated samples, but that this effect had been overshadowed by an increased influx of TILs.

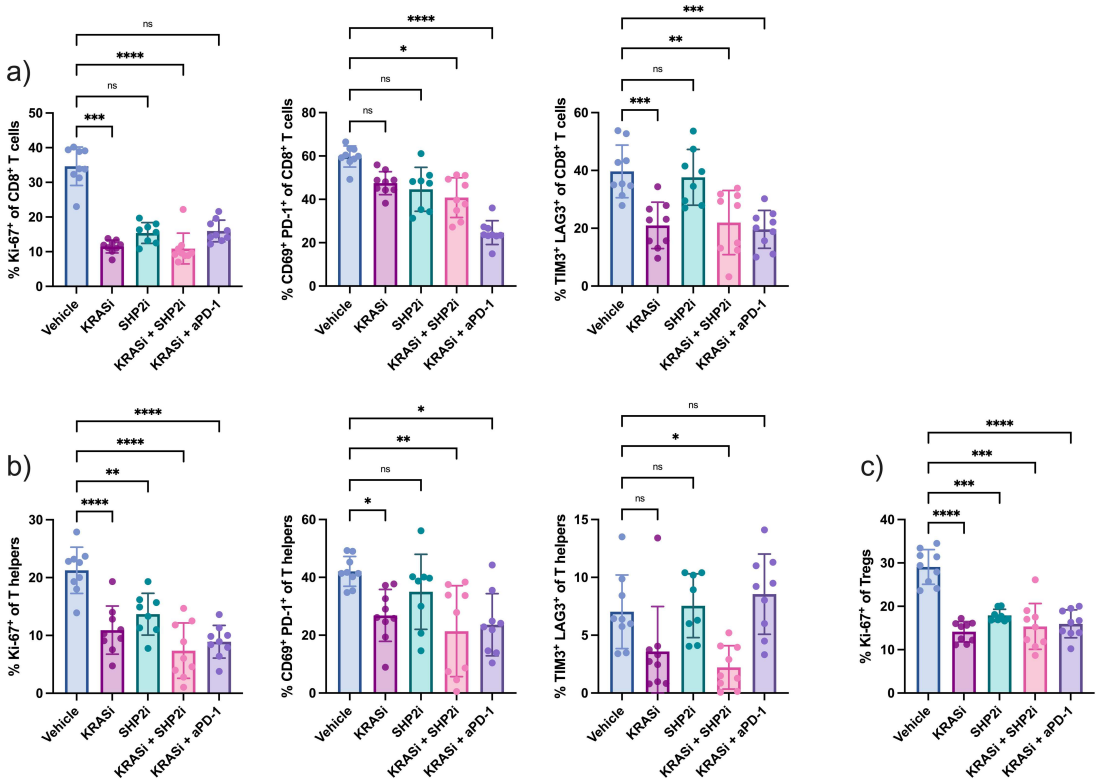


Figure 6.10 Activation status of T cell subpopulations. Each dot is representative of one biological tumour sample, height of bars indicates mean percentages of TIL subtypes by treatment groups, whiskers indicate SD of sample means within each treatment group. One-way ANOVA test was performed, comparing vehicle samples with individual treatment groups. Percentages of T cells positive for the activation markers indicated on the y-axis are show for a) $CD8^+$ T cells, b) $CD4^+$ T cells and c) Tregs (defined as $CD3^+$, $CD4^+$, and $Foxp3^+$ population).

Next, the role of other immunocytes of the lymphocyte lineage was investigated. First, the abundance of NK, NKT, and B cells were quantified as percentage of all within $CD45^+$ immunocytes (**Figure 6.11a**). Similar to T cell populations, it appeared that therapy schemes overall induced an increase in the influx of non-T lymphocytes. Assessing $Ki67^+$ expression as an indicator of proliferation status (**Figure 6.11b**) implied that the proliferating fraction in the NK cell compartment of treated samples was significantly decreased compared to vehicle tumours, which was also observed as a trend for NKT cells. On the other hand, the fraction of $Ki67^+$ B cells appeared to be slightly increased in treated samples, although this was not significant.

Unlike for cytotoxic T cells, NK and NKT cells do not require an antigen specific receptor to engage in an immune synapse with cancer cells and exert their effector functions. However, a main mechanism of action for these cells is to detect the aberrant downregulation of MHC-I molecules on cancer cells. As earlier experiments implied that the applied therapies induced an increase in MHC-I expression, it is possible that this may have hampered NK and NKT cell engagement.

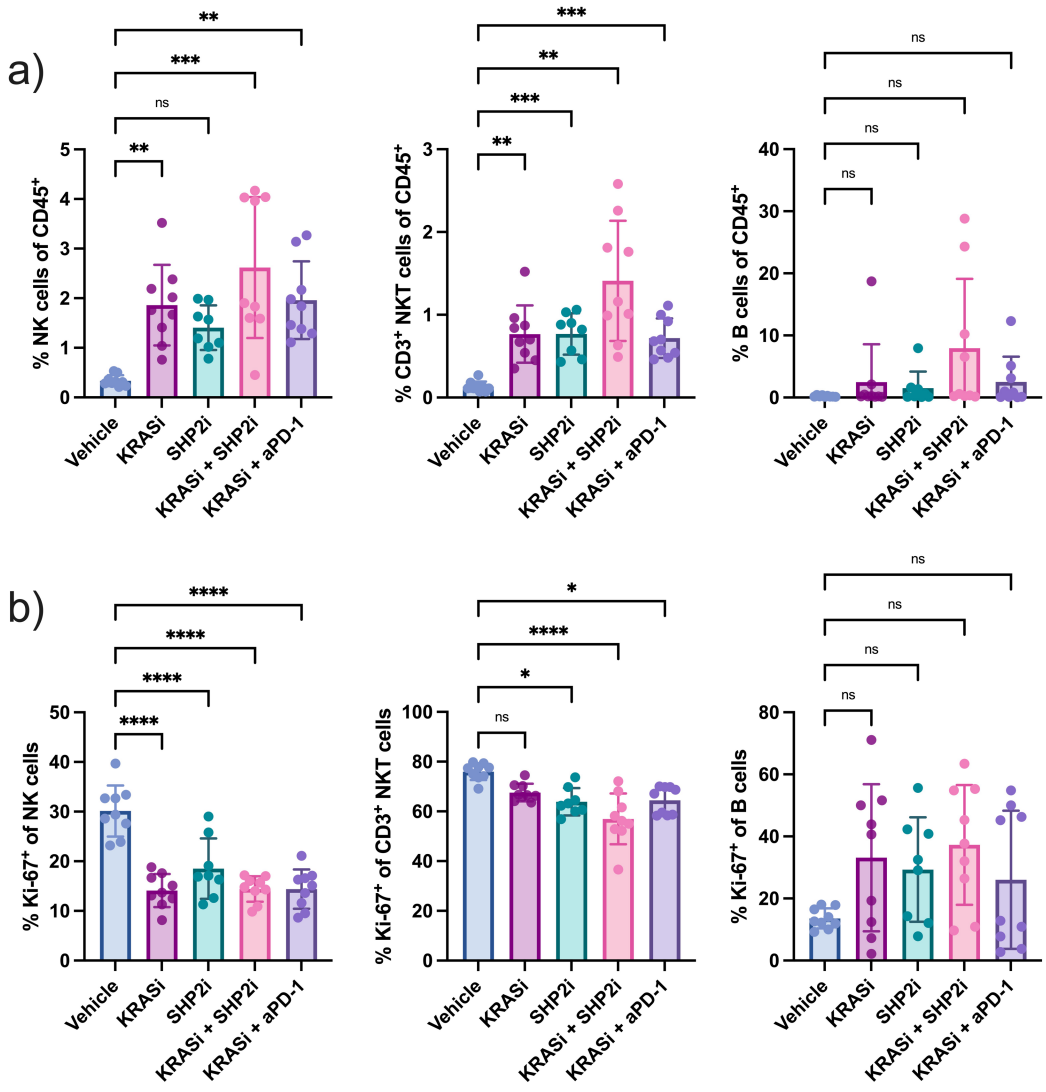


Figure 6.11 Analysis of non-T cell lymphocytes Each dot is representative of one biological tumour sample, height of bars indicates mean percentages of TIL subtypes by treatment groups, whiskers indicate SD of sample means within each treatment group. One-way ANOVA test was performed, comparing vehicle samples with individual treatment groups. a) Proportions of lymphocyte subpopulations as percentage of all $CD45^+$ cells shown for for (left to right) NK, NKT, and B cells as well as (b) their respective of $Ki67^+$ fractions,

Next, treatment-induced changes in the immune populations of the innate immune response were assessed. Here, alterations in the tumour infiltrating macrophage profiles were investigated first. Quantifying overall proportions of MPs (**Figure 6.12a**) within $CD45^+$ cells showed a significant decrease of the MP fraction in treated samples compared to vehicle control. Here, MPs were further subcategorised by their degree of functional differentiation, with $CD11c^+$ $CD11b^{hi}$ cells indicating immature MPs and $CD11c^-$ $CD11b^{hi}$ expression delineating mature MPs. This sub-classification revealed a significant decrease in both, immature MPs and fully differentiated MPs in tumours of treated mice compared to vehicle. This was particularly pronounced in samples from the KRASi + SHP2i combination. An additional strategy of stratifying MPs is by their polarisation, which can be indicative of their effector functions in the TME (**Figure 6.12b**). Here, M1-polarised macrophages are believed to exude an overall supportive role in anti-tumour immunity, while the presence of alternatively M2-polarised macrophages can hamper anti-tumour immunity. Assessing the proportions of these two polarisation types in mature $CD11c^-$ $CD11b^{hi}$ MPs, revealed both, a significant increase in M1-polarised MPs, and a decrease in alternatively activated M2 MPs in all treated samples. In immature $CD11c^+$ $CD11b^{hi}$ MPs a similar trend was observed. These findings indicate a treatment induced shift in MP populations in favour of fostering an effective anti-tumour immune response. To further investigate whether the M1 MPs might exert a role in providing co-stimulation to tumour infiltrating T cells, CD86 expression status was quantified (**Figure 6.12c**), confirming that treatments indeed induced a positive effect on MP-mediated co-stimulation of T cell effector functions.

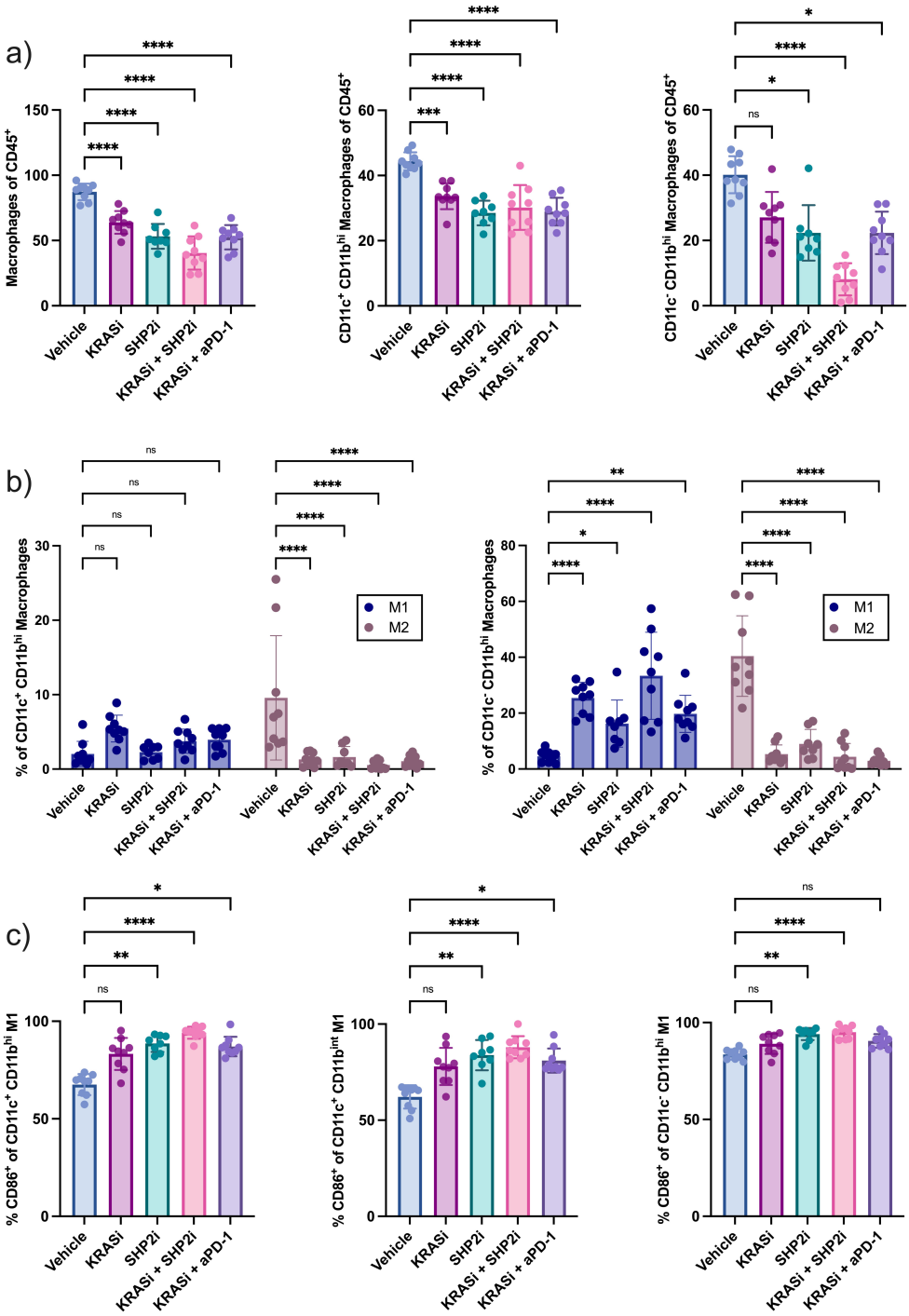


Figure 6.12 Analysis of tumour-infiltrating macrophage compartment. Each dot is representative of one biological tumour sample, height of bars indicates mean percentages of MP subtypes by treatment groups, whiskers indicate SD of sample means within each treatment group. One-way ANOVA test was performed, comparing vehicle samples with individual treatment groups. Plots show distribution of MP populations segregated by treatment groups. a) from left to right: Fraction of MP populations as fraction of $CD45^+$ compartment (I) all MPs, (II) immature MPs, and (III) mature MPs. b) Fractions of M1 or M2 polarised MPs (from left to right) (I) of mature MPs and (II) of immature MPs. c) Within the M1 polarised MP compartment, fraction of $CD86^+$ (marker for T cell co-stimulation) expressing MPs for (from left to right) (I) immature MPs (II) differentiating MPs (II) mature MPs.

Another cell type of interest in the category of APCs were DCs, which can also present with differently polarisation phenotypes. Conventional Dendritic Cells type 1 (cDC1), amongst other functions, play a crucial role in cross-presenting tumour cell specific antigens, predominantly to $CD8^+$ T cells, thereby priming and maintaining a functional cytotoxic T cell effector response. Plasmacytoid Dendritic Cells (pDCs) can also be involved in priming of T cell responses, however, their main function lays in producing large amounts of type I interferons, thereby taking on a dual role in supporting and hampering antitumour immunity. Conventional Dendritic Cells type 2 (cDC2) can also play a bivalent role by both, promoting and hindering anti-tumour immunity. For example, by predominantly cross-presenting tumour cell specific antigens predominantly to $CD4^+$ T cells via their MHC-II complex. This can lead to the activation of anti-tumour directed T helper cells but also Tregs. cDC2s can further be involved in expressing checkpoint inhibitory molecules or other immune-modulatory cytokines, which can promote T cell exhaustion.

Next, treatment-induced changes in the abundancy of different DC subtypes were assessed (**Figure 6.13a**). Interestingly, the addition of the SHP2i therapy resulted in a significant decrease of the fraction of cDC1s of $CD45^+$ cells in the TME. As a trend, a therapy-mediated increase in pDCs was observed and no clear therapy-induced changes were evident in the fraction of cDC2s. Furthermore, an overall increase in the expression of the costimulatory transmembrane protein CD86 was observed in treated samples compared to vehicle in all DC subtypes (**Figure 6.13b**). Moreover, quantifying MFI for PD-L1 expression in cDC2s revealed a treatment-induced increase in the expression of this checkpoint protein across treatment groups, thereby indicating a possible role in their contribution to accelerating T cell exhaustion.

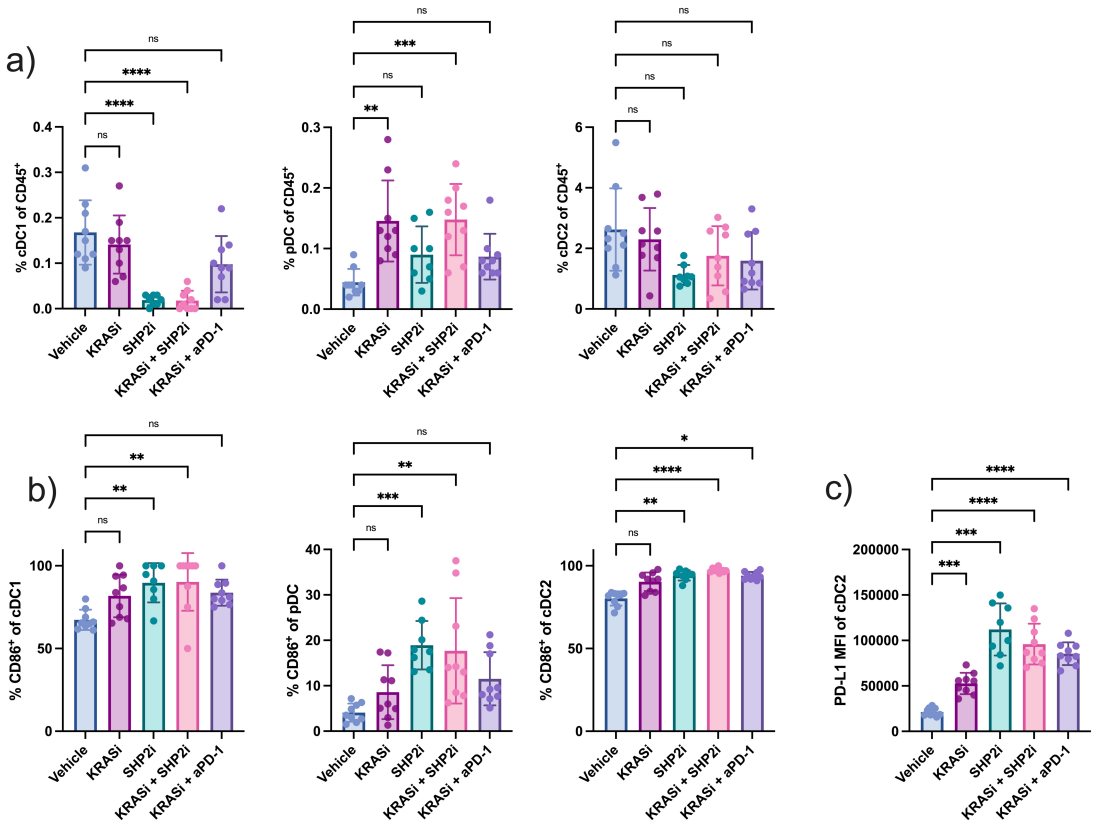


Figure 6.13 Analysis of tumour-infiltrating dendritic cells. Each dot is representative of one biological tumour sample, height of bars indicates mean percentages of DC subtypes by treatment groups, whiskers indicate SD of sample means within each treatment group. One-way ANOVA test was performed, comparing vehicle samples with individual treatment groups. Plots show distribution of DC populations segregated by treatment groups. a) Fraction of DC subpopulations of $CD45^+$ cells for (from left to right) (I) cDC1s, (II) pDCs, (III) cDC2s). b) Fraction of $CD86^+$ DCs for (from left to right) (I) cDC1s, (II) pDCs, (III) cDC2s. c) MFI for PD-L1 expression in cDC2s.

This in-depth immune phenotyping of the TME revealed that the employed therapy schemes indeed influence the immune cell composition as well as the cell-state of different immunocyte populations. Here, the anti-cancer treatments appear to exude both immune promoting and hampering effects. Importantly, however, these results indicate that treatments may promote the influx of TILs as well as the priming of a local anti-tumour immune response through enhanced APC-mediated cross-presentation of tumour-cell specific antigens to the adaptive immune compartment. However, this potential mechanistic axis of therapy-mediated promotion adaptive immunity will require further validation.

APC mediated priming of adaptive immunity can occur in both, the TME and tdLNs. Lymph nodes provide a compact infrastructure that can facilitate the antigen cross-presentation between APCs, T cells and B cells[72]. Moreover, the cancer cell compartment may emit immune suppressive cues in the local TME which may hinder the establishment of a functional adaptive immune response, while conditions in tdLNs may be more favourable. Indeed, it was observed during sample collection that tdLNs were often enlarged in treated mice, compared to the tdLNs of vehicle or naïve mice (not shown).

Flow cytometric analysis of the T cell compartment of the collected tdLNs did not reveal profound alterations of T cell subtype quantities, except for a significant increase of Tregs in the KRASi or SHP2i treated mice (**Figure 6.14a**). However, when assessing the activation state of $CD8^+$ cytotoxic T cells (**Figure 6.14b**), a significant increase in $PD\text{-}1^+$, and $TIM3^+/LAG3^+$ cytotoxic T cells was observed in the KRASi + a-PD-1 treatment group. Here, $CD8^+$ effector memory T cells ($CD62L^-/CD44^+$) were also increased. This is a group of memory T cells that can circulate peripheral tissues and is already differentiated, expressing a range of effector molecules[318].

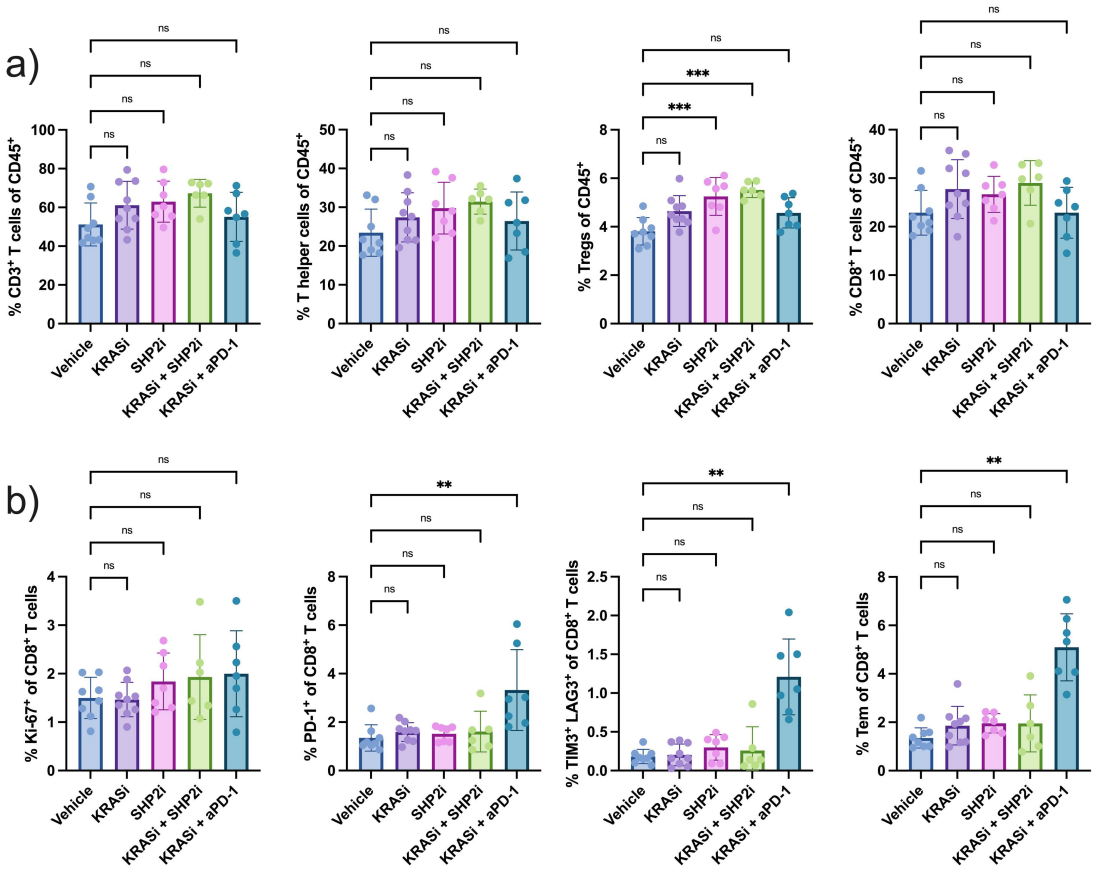


Figure 6.14 Analysis of T cell compartment in tdLNs. Each dot is representative of one biological tumour sample, height of bars indicates mean percentages of T cell subtypes by treatment groups, whiskers indicate SD of sample means within each treatment group. One-way ANOVA test was performed, comparing vehicle samples with individual treatment groups. a) Fraction of T cell subpopulations of $CD45^+$ cells in tdLNs for (from left to right) (I) all $CD3^+$ T cells, (II) $CD4^+$ T cells, (III) $CD4^+$ Treg cells (IV) $CD8^+$ T cells). b) Quantification of activation and exhaustion profiles as well as effector memory status (Tem) within $CD8^+$ T cell compartment.

Next, changes in the B cell compartment of tdLNs were assessed (**Figure 6.15**). Here, the proportion of B cells within lymph nodes did not appear to be altered in treated samples compared to vehicle and no significant changes for activation markers were observed. Here, exemplary plots are shown for proliferation marker Ki67, as well as MFIs for CD19, and MHC-II. Because CD19 is a part of the BCR signalling complex and MHC-II, can be indicative of antigen cross presentation to T helper cells, both of these components are expected to be downregulated in fully differentiated plasma cells. While MHC-II could be upregulated during early stages of B cell activation compared to naïve cells[319].

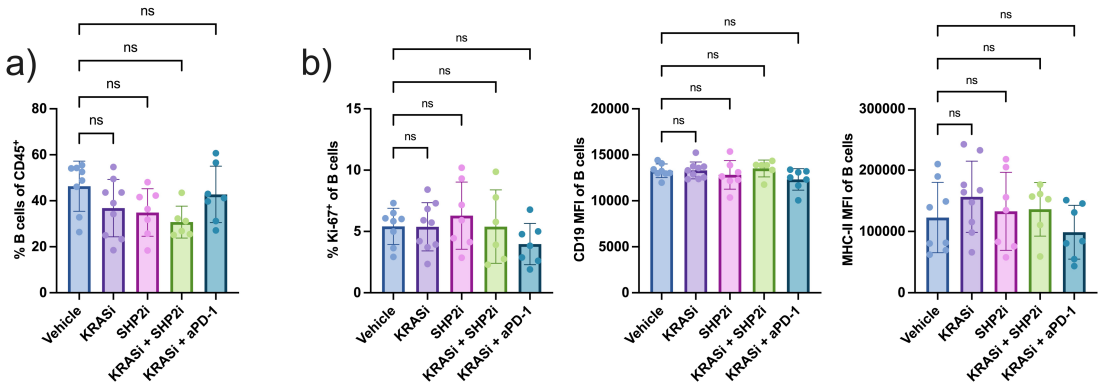


Figure 6.15 Analysis of B cell compartment in tdLNs. Each dot is representative of one biological tumour sample, height of bars indicates mean percentages of B cells by treatment groups, whiskers indicate SD of sample means within each treatment group. One-way ANOVA test was performed, comparing vehicle samples with individual treatment groups. a) Fraction of B cell subpopulations of $CD45^+$ cells in tdLNs. b) Quantification of functional B cell profiles.

Other types of immunocytes were also analysed, however, because no significant changes in immune cell composition or activation profile were found, this analysis is not shown here. The reason for not finding more changes in immune cell activation in tdLNs could be related to the treatment interval. In an earlier pilot experiment where mice had been treated for four days, no insightful significant changes in tdLNs had been found either (not shown). It is possible that a longer treatment interval would be required for the coordination of a proximal immune response. However, this would have compromised the collection of tumour samples. Unlike tumours, tdLNs are organs with a clearly defined structural layout with defined compartments and zones for the location of particular immunocyte subtypes. Hence, it is also possible that the physiological architecture of tdLN would constrain changes in immune cell subtype composition. An additional limitation for assessing treatment-induced changes in tdLN was that the absolute number of $CD45^+$ cells in individual tdLN was not recorded. During sample collection, we had observed that tdLNs from treated mice were often enlarged compared to tdLNs from vehicle or naïve mice. Hence, it was possible that, rather than changes in immune cell subtype composition, the absolute number of immunocytes in the enlarged lymph nodes may have been indicative of a treatment-induced immune response. However,

due to time constrains of this large protocol, sample sizes had been normalised through estimation of pellet sizes and this information was not available. In future experiments, the size of tdLNs after extraction should be recorded as well as cell counts before sample normalisation.

To further corroborate whether APCs which had phagocytosed cancer cell material, it would be intriguing to investigate whether they appeared as positive events in the $eGFP^+$ or $eBFP^+$ gates in the flow cytometric analysis. Because the majority of the engrafted tumour cells are $eBFP^+$ KPAR1.3 KRAS G12C cells and this isotype was also more likely to undergo drug-mediated apoptosis, it may have been statistically more likely to detect APCs that have phagocytosed $eBFP^+$ cancer cell material compared to $eGFP^+$ material. However, this hypothesis could not be fully verified with the current dataset due to the technical limitations of this experiment. eBFP inherently encompasses a dimmer fluorophore[298] and had mainly been selected above brighter yellow or red FP alternatives due to its high structural homology to eGFP. Unlike previous FACS experiments (**Figure 3.1c, Figure 5.14**), the protocol for spectral flow cytometry required fixation and permeabilization of the samples. This had quenched the fluorescence profile of the already dim eBFP fluorophore to a point where it was no longer detectable over the autofluorescence profile of the APCs. To visualise the FPs during flow cytometric analysis, an additional intracellular staining step for the FPs could have been introduced. However, because no suitable fluorophore-conjugated primary ab was available, this would have required a primary + secondary ab staining with additional washes. This, in turn, would have led to additional sample loss which could have compromised the quality of the acquired data set.

Hence, it was decided to omit analysis of eBFP expression in $CD45^+$ cells and instead focus on probing the presumably smaller fraction of $eGFP^+$ expressing $CD45^+$ cells. As expected, the number of $eGFP^+$ immunocytes was low and not all immunocyte subtypes could be unambiguously identified. Hence, the following data should be considered as preliminary and further experiments will

be necessary to corroborate these findings. The fraction of CD45$^+$ GFP$^+$ cells across treatment groups (**Figure 6.16a**) appeared to be representative of the fraction of GFP$^+$ cancer cells within all cancer cells (**Figure 6.7b**). Further analysing the subtype composition of GFP+ immunocytes revealed that the largest lineage-defined immune subtypes were MPs. Additionally, a large proportion of CD45$^+$ GFP$^+$ cells, labelled as “other” could not be assigned to a distinct subtype, as their profile of lineage and activation markers was ambiguous. This could also have been indicative of a higher autofluorescence profile, associated with an early stage of apoptosis and will require further investigation. It was further investigated which MPs were GFP$^+$, which indicated a mixed profile of immature- and mature subtypes, as well as a subpopulation which could not be unambiguously classified (**Figure 6.7b**).

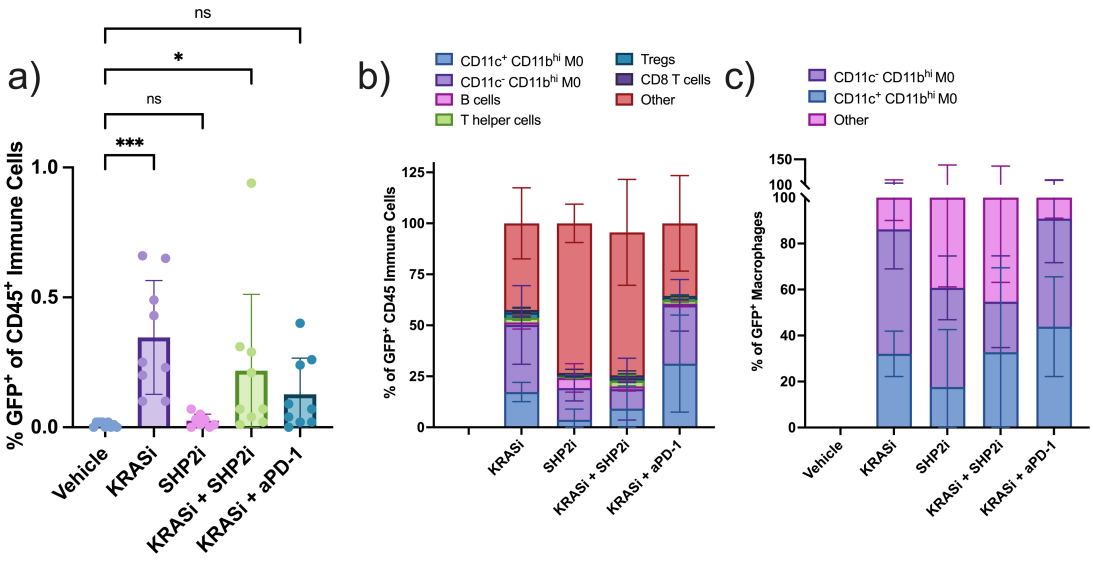


Figure 6.16 Analysis of GFP$^+$ immunocytes in the TME. Each dot is representative of one biological tumour sample, height of bars indicates mean percentages of GFP$^+$ immunocytes by treatment groups, whiskers indicate SD of sample means within each treatment group. a) GFP$^+$ immunocytes as percentage of all CD45$^+$ cells; one-way ANOVA test was performed, comparing vehicle samples with individual treatment groups. b) Percentages of immune cell subpopulations within the GFP$^+$ CD45$^+$ population. The vehicle group was excluded due to low cell counts. Additionally, a category of “other” was introduced, which was a group of immunocytes with a generally high autofluorescence profile, which could be indicative of an early apoptosis state c) Fraction of MP subpopulations within all GFP+ MPs.

As a proof of concept, it may be of interest to engraft GH-mice with tumours solely derived from eGFP-expressing KPAR1.3 KRAS G12C cells. Mice could then be treated with either vehicle or one of the combination therapies for subsequent flow cytometric analysis. This experimental design may facilitate the detection of APCs that have phagocytosed cancer cell material. If such immunocytes were found, they could further be isolated via flow cytometric sorting and placed in co-cultures with primed cytotoxic T cells and cancer cells to test whether they may bolster adaptive immunity through antigen presentation.

This immune phenotyping experiment revealed the complexity of therapy-induced remodelling of immune cell composition in the TME. It further unveiled a potentially bivalent role of the targeted anti-cancer treatments, which induced both, anti-tumour directed and potentially tumour-promoting alterations. Taken together with the findings of previous survival experiments, it is possible that therapies could increase APC effector functions of phagocytosing- and subsequently cross-presenting cancer cell-derived material to T cells. Thereby priming an adaptive immune response to recognise a pan-cancer cell archetype. Simultaneously, a therapy-mediated increase in T cell infiltration had also been observed which could enhance anti-tumour immunity through direct cancer cell killing or through bystander effects. On the other hand, the information that KRAS G12C inhibitors increases T reg infiltration could be clinically valuable for the development of further treatment strategies, for example, the introduction of Treg depleting antibodies.

6.3 Spatial analysis of the tumour microenvironment

A limitation of the immune phenotyping of the previous study is that it lacks insights into the spatial distribution of the TME and how different therapy schemes might influence tissue organisation. For example, it was previously discovered in our orthotopic murine lung cancer models, that T cells cluster

around the tumour borders in vehicle tumour but are able to infiltrate deeper into the tumour tissue once mice received KRASi treatment[217,218]. This shift would not have been evident from simply quantifying immune cell populations. To gain further insights into therapy-induced changes in tumour architecture, multiplexed immunohistochemistry of tumour sections across treatment groups was performed (**Figure 6.17**).

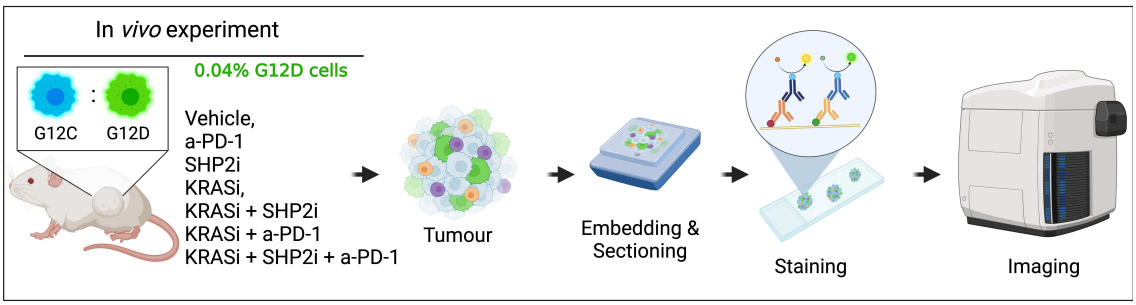


Figure 6.17 Overview of multiplex EHP workflow. Overview of experimental set up for spatial TME analysis of subcutaneous tumours across treatment groups. Mice were engrafted with 99.8% eBFP^{+} KRAS G12C KPAR1.3 cells ('G12C') and 0.04 Luc-eGFP KRAS G12D KPAR1.3 cells ('G12D'). Once tumours reached an average volume of ~185 mm^3 mice received 6 doses of the oral drugs RMC-4998 (KRASi) at 100 mg/kg, RMC-4550 (SHP2i) at 30 mg/kg, and 2 doses of a-PD-1 at 10 mg/kg. Tumours were then isolated, embedded, cut into 5 µm thin sections and were stained with an eight-antibody panel. Subsequently, tissue sections were imaged using an AxioScan slide scanner. Image created with BioRender.

Here, 0.04% Luc-eGFP-expressing KPAR1.3 KRAs G12D cells were engrafted together with 99.96% of eBFP KPAR1.3 KRAS G12C cancer cells. Thereby mimicking the ratio of drug resistant cells present in the initial survival experiments (**Figure 4.3, Figure 4.5**). In this experiment, we were able to create a panel with up to 8 markers. For this, we first included DAPI to demarcate nuclei for cell type identification. Next, CD4 and CD8 were included to gain insights into the distribution of TIL populations. We also wanted to identify KRAS G12C or G12D mutant tumour cell populations. Because of the high structural homology between eGFP and eBFP, there are no antibodies which could distinguish the two FPs. Hence, an anti-eBFP/eGFP ab was employed as a pan-cancer cell marker. Additionally, a luciferase-targeting ab was included to identify the Luc-eGFP KRAS G12D mutant tumour cells, which would appear as double-positive for the GFP/BFP and Luciferase staining's. To

gain insight into the cell state of cancer and T cells, Ki67 was included as a marker for proliferation and Casp3 was included to identify apoptotic cells.

Initially, PD-1 had also been included as a qualitative marker for assessing T cell state. However, the quality of staining for this marker was poor in the final experiment with a high background signal throughout the whole tumour sections and could hence not be included in the final analysis. It was suspected that this was caused by the extensive extracellular matrix structures present in the subcutaneous tumours which may have led to unspecific ab binding. Tissue sections had also been stained to assess the presence of fibroblasts and endothelial cells (not shown). However, this was not further pursued as no clear differences were visible between treatment groups. Moreover, it had been considered to include APC markers in the panel and preliminary stainings had been performed (not shown). However, it became evident in these pilots that a number of lineage markers would be necessary for unambiguous identification of any given APC population, which would have taken up too many channels of the 8 markers available for multiplex staining.

Intriguingly, the multiplex staining reveal a treatment-induced increase in T cell density for both, helper- and cytotoxic T cells. Representative images of whole tumour sections (**Figure 6.18**) as well as high resolution ROIs (**Figure 6.19**) are also shown. Although T cell densities varied within- and between tumours of the same treatment groups and T cell densities remain to be quantified. Of note, it is possible that the observed increase in T cell densities in treated tumours could, at least partially, be attributed treatment and/or immune mediated clearing of cancer cells, thereby bringing T cells closer together due to the decrease in tumour size. However, regardless of the cause, the increase in T cell density in itself has advantageous effects in asserting anti-tumorigenic functions.

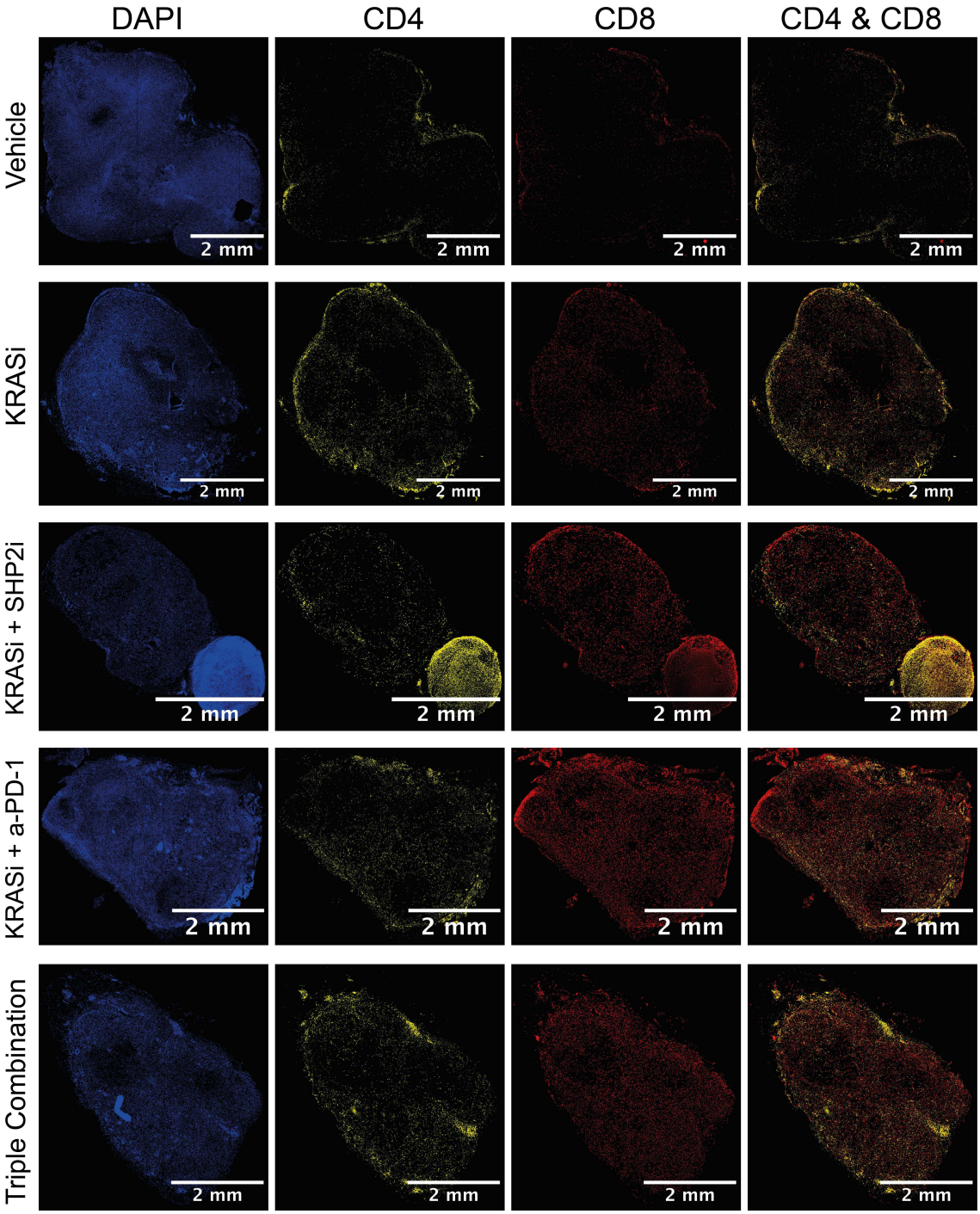


Figure 6.18 Overview of T cell staining on whole tumour sections. Representative images of T cell infiltration in tumours of different treatment groups. Stainings are shown for (from left to right): Nuclei (DAPI; blue), $CD4^+$ T cells (yellow), $CD8^+$ T cells (red), merge image of $CD4^+$ and $CD8^+$ T cells. Representative tumours are shown for the treatment groups of (from top to bottom): Vehicle, KRAS G12C inhibitor RMC-4998 (KRASi), SHP2 inhibitor RMC-4550 (SHP2i), the dual combinations of KRASi + SHP2i and KRASi + a-PD-1 as well as the triple combination of KRASi + SHP2i + a-PD1. The bulbous structure in the lower right corner of the tumour from the KRASi + SHP2i treatment group is a tdLN which had not been removed during sample preparation. Scale bars with a length of 2mm are indicated on individual images. This image was generated retaining high quality to allow zooming in for higher resolution.

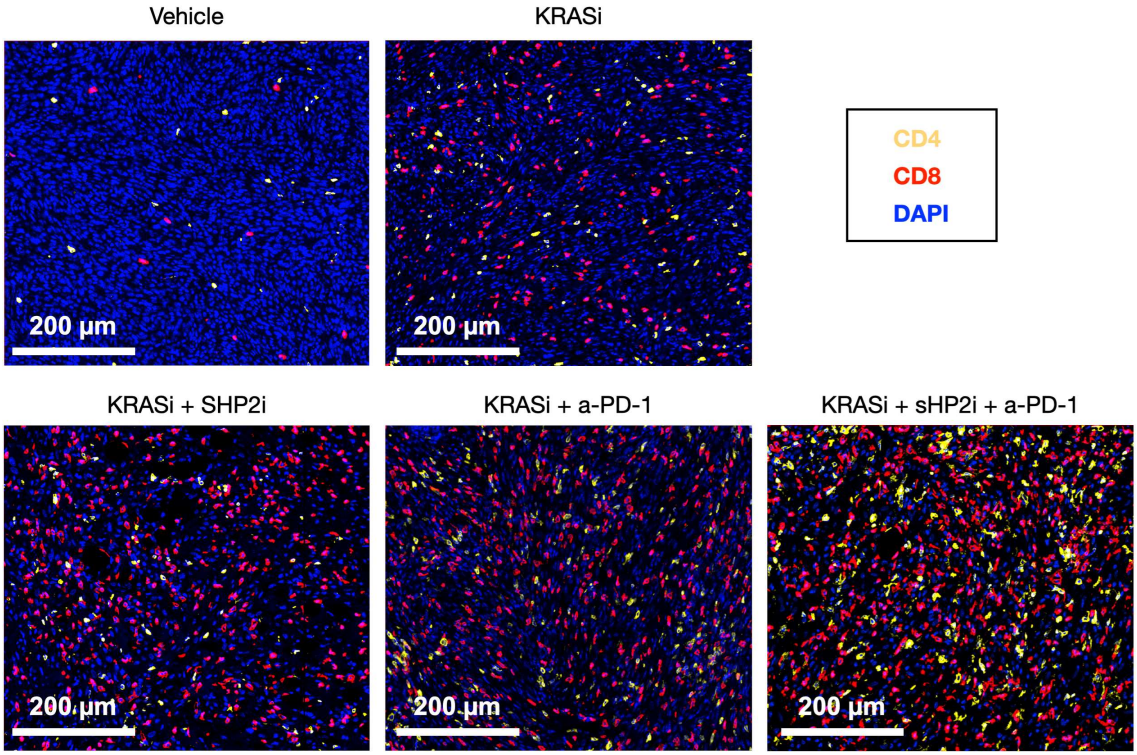


Figure 6.19 High resolution ROIs of T cell infiltration across treatment groups.

Representative ROIs of T cell infiltration in tumour sections of indicated treatment groups. Merged images of Nuclei (DAPI; blue), $CD4^+$ T cells (yellow), and $CD8^+$ T cells (red) are shown. Scale bars with a length of 200 µm are indicated on the individual images.

Overall, the observed treatment-induced increase in T cell counts correlated well with the previous immune phenotyping experiment. Although the PD-1 staining did not work well in this multiplex experiment, quantifying the fraction of $Ki67^+$ T cells across treatment groups provides another opportunity to probe for therapy-induced changes in the activation status of cytotoxic and helper T cells.

Separate from the multiplex experiment, tumours across all treatment groups were recently stained for the presence of tumour infiltrating Tregs. This revealed a possible increase in tumour infiltrating Tregs in KRASi-treated tumours (**Figure 6.20**). In vehicle tumours Tregs were observed around the outer perimeters but were barely observed to infiltrate deeper into the tumours, while in KRASi treated samples, Tregs were present throughout the tumours. This observation also appears to correlate well with the data obtained from the

immune phenotyping, however the Treg infiltration in this experiment remains to be quantified.

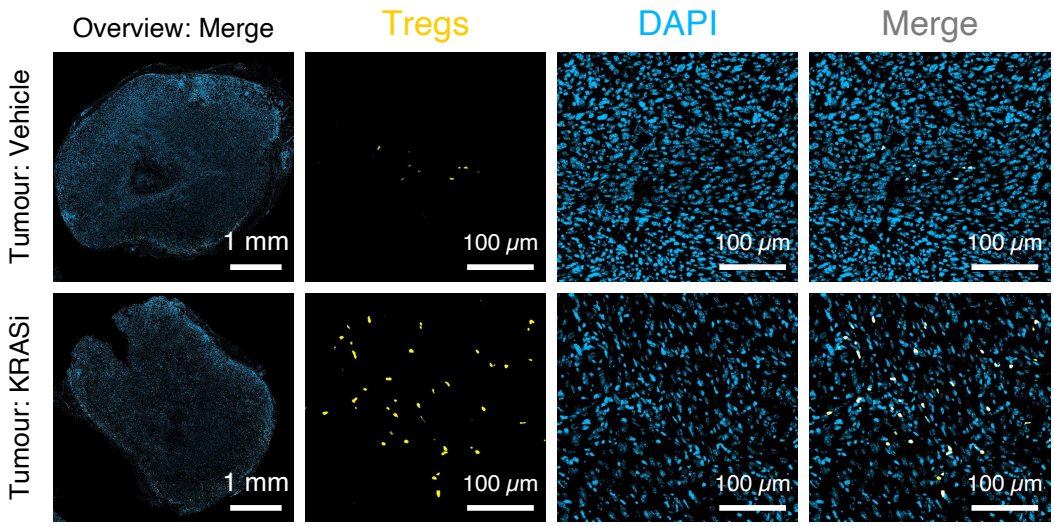


Figure 6.20 Exemplary images for tumour infiltrating Tregs. Representative images of vehicle or KRASi treated tumour sections stained for Foxp3 expression, which is indicative of tumour-infiltrating Tregs. DAPI was used to visualise nuclei of all cells. Scalebar is indicated for respective images. Scale bars with a length of 100 µm are indicated on the individual images.

Another notable treatment-induced change was the presence of KPAR1.3 KRAS G12D clusters present in KRASi treated samples, which were absent in Vehicle-, a-PD-1 -, and SHP2i-treated samples. Assessing the Ki67 status of these KRAS G12D mutant clusters, revealed that the majority of cells were positive for this marker, indicating they were actively proliferating (**Figure 6.21 and Figure 6.22**). This is in accordance previous findings of the KPAR1.3 KRAS G12D tumour cell subpopulation proliferating in KRASi treated samples, such as the proliferative signatures discovered in the bRNA-seq data or the increase in IVIS signal in respective survival experiments. In addition, it is possible that in samples treated with KRASi or SHP2i, KRAS G12C mutant cancer cells were less proliferative compared to G12D mutant cells, due to therapy-induced inhibition of oncogenic signalling. The triple therapy combination is not shown here, as the fraction of remaining cancer cells in the tumour samples was generally highly variable and no KPAR1.3 KRAS G12D clusters were found which exacerbated selecting a representative image.

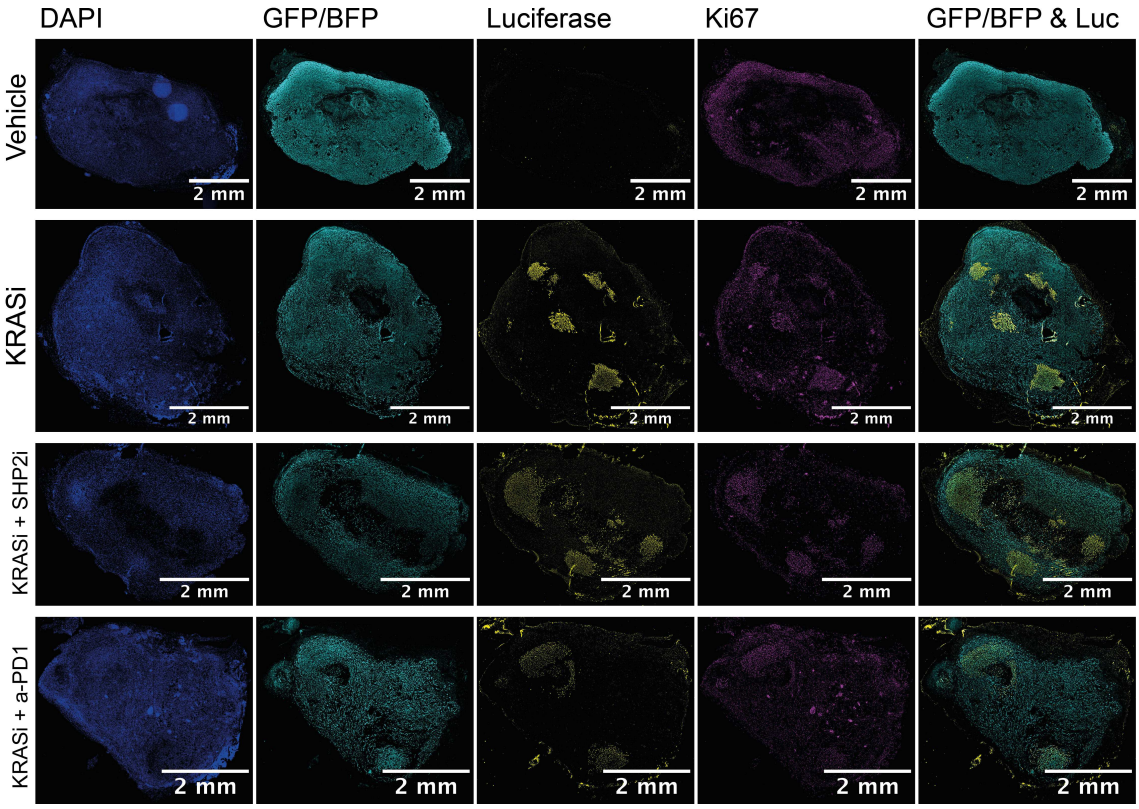


Figure 6.21 Tumour cell populations across treatment groups. Representative images of KPAR1.3 KRAS G12C- and G12D mutant tumour cell fractions and Ki67 expression across different treatment groups. Stainings are shown for (from left to right): Nuclei (DAPI; blue), all tumour cells (BFP/GFP, cyan), KRAS G12D mutant tumour cells (Luciferase, yellow), all proliferating cells (Ki67, magenta), merge of BFP/GFP and Luciferase stainings. Representative tumours are shown for the treatment groups of (from top to bottom): Vehicle, KRAS G12C inhibitor RMC-4998 (KRASi), the dual combinations of KRASi + SHP2 inhibitor RMC-4550 (SHP2i) and KRASi + a-PD-1. Scale bars have a length of 2mm are indicated on individual images. This image was generated retaining high quality to allow zooming in for higher resolution.

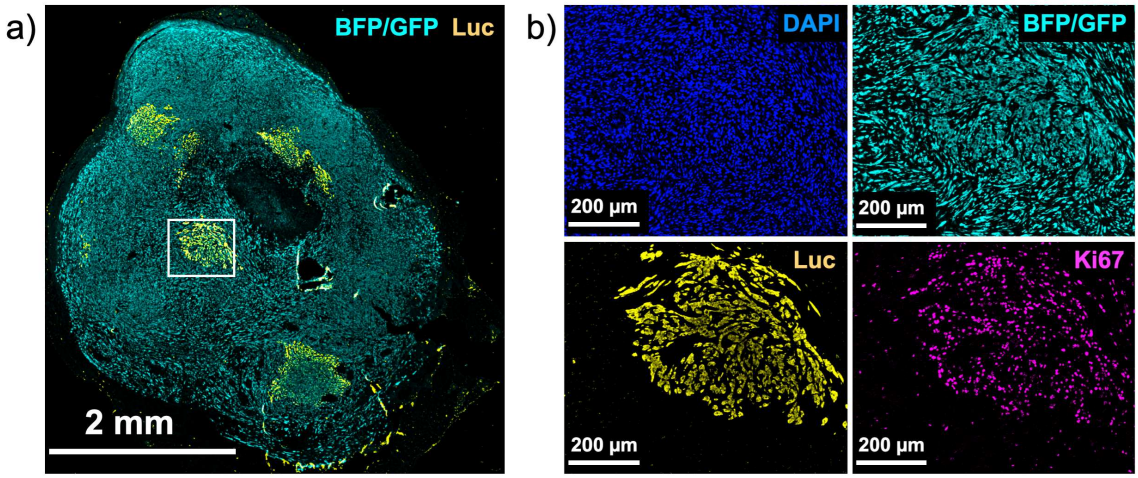


Figure 6.22 Exemplary ROI of a proliferating KPAR1.3 KRAS G12D cluster. a) Representative tumour section of a RMC-4998 treated tumour with merged stainings for BFP/GFP (cyan) as pan-cancer cell marker and Luciferase (Luc, yellow), demarcating KRAS G12D mutant KPAR1.3 cells. Scale bar has a length of 2mm and the white box highlights the ROI selected for the right panel. b) High resolution ROI of an exemplary KPAR1.3 KRAS G12D cluster. Stainings are shown for (I) nuclei (DAPI, blue), (II) all KPAR1.3 cancer cells (BFP/GFP, cyan), KPAR1.3 KRAS G12D cells (Luciferase (Luc), yellow), Ki67 (magenta). Scale bars with a length of 200 µm are indicated on the individual images.

Assessing apoptosis in the tumour cell compartment via Casp3 staining, revealed that there appeared to be at least two different sources for apoptotic events. First, larger tumours, especially in the Vehicle, a-PD-1 and SHP2i treatment groups sometimes had larger apoptotic areas located at the centre of the tumour (**Figure 6.23**). Consulting a histopathologist confirmed that these are likely necrotic cores resulting from limited nutrient and/or oxygen availability or the accumulation of toxic metabolic waste products in the centre of the tumour. The second occurrence of apoptosis in cancer cells occurred predominantly outside of the centre of tumours and presented as more singled out $Cas3^{+}$ cancer cells. Here, apoptosis may also have been triggered by treatments or anti-tumour immunity.

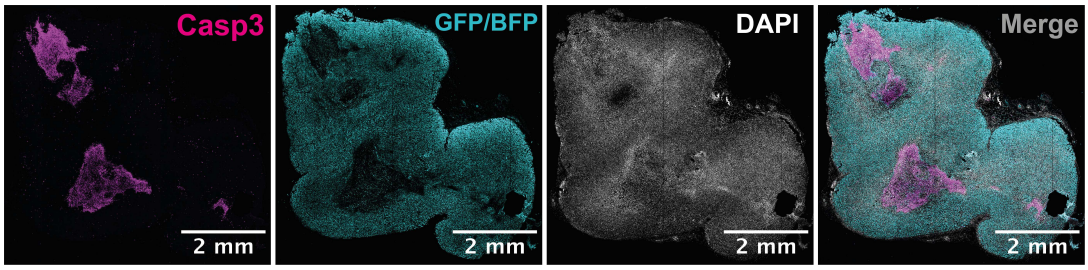


Figure 6.23 Visualisation of necrotic tumour cores. Representative images of a Vehicle tumour containing necrotic areas. Stainings are shown for (from left to right): Casp3 (magenta), all tumour cells (BFP/GFP, cyan), nuclei (DAPI, white), and merge of Casp3 and BFP/GFP stainings. Scale bars have a length of 2mm are indicated on individual images. This image was generated retaining high quality to allow zooming in for higher resolution.

To quantify the observations of the multiplex staining, a machine-learning based pipeline was developed with the kind help of KangBo Ng for accurate quantification of different cancer and immune cell populations for which the analysis is currently ongoing. An outline of the segmentation and quantification workflow is shown in (**Figure 6.24**). As several tumour sections were imaged on each objective slide, the areas of interest were first manually outlined (**Figure 6.24a**). Here, staining and tissue processing artefacts, such as wrinkles or rips in tissue sections had also been highlighted for subsequent exclusion to avoid introducing any falsifying data in the subsequent analysis. Additionally, necrotic cores were highlighted as they may later be considered separately when analysing apoptosis in the tumour cell compartment.

Next, a machine learning-based segmentation pipeline was established to segment the distinct cell types in the predefined areas of analysis (**Figure 6.24b**). Here, the initial step was to delineate the location of all the nuclei, which was necessary for several reasons. First, erythrocytes present in the TME, for example due to leaky vasculature, can appear as positive events in the respective imaging channels, due to the high autofluorescence of haemoglobin. However, as erythrocytes lack a nucleus, they can be disregarded by adding the condition that only cells with a nucleus are considered for quantification. Secondly, the eBFP, eGFP and luciferase expressed by cancer cells are located in the cytoplasm, not the plasma membrane. Hence, it is difficult to

define a precise outline of distinct cancer cells, which often cluster closely together. By considering the nuclei first, they can serve as pinpoints to quantify the number of cancer cells present in a certain area. Thirdly, although CD4 and CD8 are plasma membrane residing markers, T cells have a small diameter of only ~2-5 µm and are often asymmetric in shape, possibly due to their role of surveying their surrounding or forming immune synapses with other cell types. Hence, the CD8 and CD4 lineage markers can also take on shapes which are difficult to define without a nucleus as reference point. To define the location of individual cells and distinguish their outlines, a semantic segmentation approach was applied. Here, first, each pixel in the image is assigned as either being positive or negative for a given marker, using a random forest classification method[320]. Next, identities for each of the cell types were assigned by determining whether a threshold number of cell lineage marker-positive pixels were present within a defined perimeter of the nucleus. Subsequently, the same approach was employed to assign proliferation or apoptosis status to the defined cell types (**Figure 6.24c**). The next steps in this pipeline will be to quantify the cell counts for the different cell types and states within each tumour section (**Figure 6.24d**). Cell counts will then be normalised by the size of the analysed area as tumours of different treatment groups were of different proportions. This index can then be used to quantify therapy-induced changes in TIL densities within the TME and to investigate the fraction of actively proliferating T cells increased in treated samples. In the cancer cell compartment, the size and number of KRAS G12D-mutant cell clusters per tumour section in different groups can be analysed. Within the KRAS G12D mutant clusters, the fraction of $Ki67^+$ cancer cells will further be quantified. Additionally, after gating out necrotic cores, the number of $Casp3^+$ cancer cells across different treatment groups and isotypes can be quantified. In addition to quantifying different cell counts, the spatial information obtained in this multiplex staining experiment can also be considered. Here, a simplified neighbourhood analysis[321] could be performed, for example, to investigate how many T cells are in direct contact with individual tumour cells of different genotypes and across treatment groups. This approach could be extended to assess whether

clusters of KRAS G12D mutant tumour cells are more immune infiltrated in combination treated samples compared to tumours that had been treated with KRAS G12Ci as monotherapy.

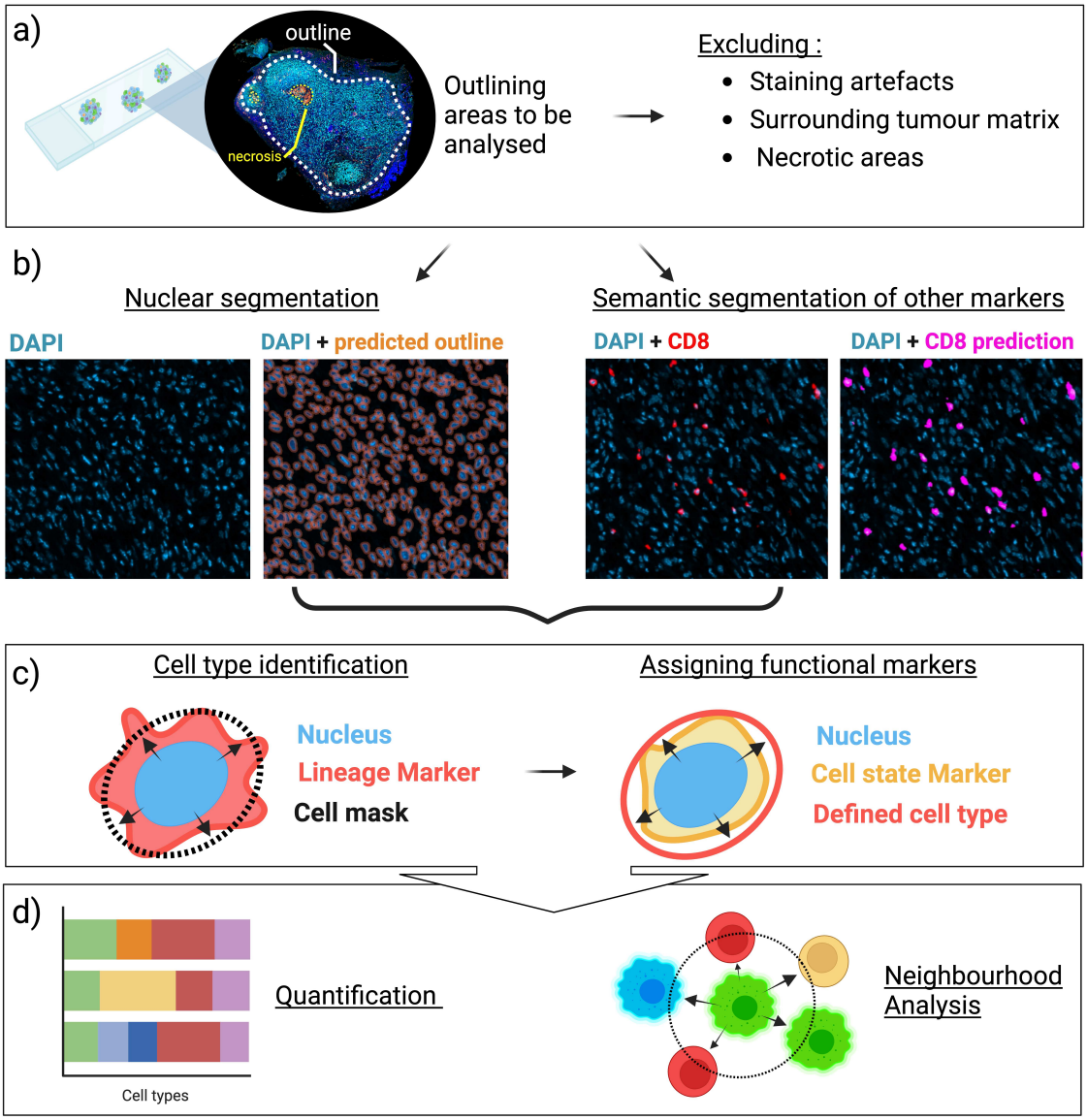


Figure 6.24 Outline of image analysis pipeline. a) Objective slide containing several tumour sections was imaged in one frame, ROIs within image were outlined (white outline) excluding staining artefacts and the matrix surrounding the tumour; necrotic areas were also demarcated as separate entities (yellow outlines); these areas were excluded for subsequent analysis. b) Left panel: exemplary ROI showing nuclear segmentation, right panel: exemplary ROI showing semantic segmentation of $CD8^+$ T cells. c) Schematic of subsequent steps. Left panel: cell type identification using the lineage markers of BFP/GBP and Luciferase for cancer cell as well as CD8 and CD4 to demarcate T cells. Right panel: Subsequently, defined cell types are assigned positive or negative values for the functional state markers Ki67 and Casp3. d) After cell type classification, respective populations can be quantified and tumour architecture can be explored employing neighbourhood analysis. Figure was created with BioRender. This pipeline was developed by KangBo Ng and tumours in (a) were outlined with the kind help of Sapta Mukherjee.

In this chapter, we were able to show that the employed treatments were indeed able to enhance adaptive anti-tumour immunity and induce changes in the tumour infiltrating immune compartment. On a systemic level, the adaptive immune compartment appeared to contribute to durable treatment responses, especially in mice which had received combination therapies. Here, both T cells and B cells appeared to contribute to enhanced anti-tumour immunity. Emv2 is likely contributing to the immunogenicity of this cancer cell line. In the future, it would be interesting to investigate whether the employed treatments assert similar effects on different murine cancer cell lines which do not express EMV2 or present with a more immunologically cold phenotype. Closer investigation of the immune cell composition in the TME uncovered that the employed therapies likely induced an increase in cytotoxic T cell infiltration as well as a shift in the polarisation of MP and DC populations to a more anti-tumour directed phenotype. On the other hand, it also highlighted the multifaceted, highly complex organisation of the immune compartment, with therapy schemes playing a dual role in remodulating anti-tumour immunity. For example, KRASi lead to a significant increase in tumour infiltrating Tregs while SHP2i lead to a decrease in the proportion of anti-tumour directed cDC1 population.

More experiments will be necessary to fully understand how the employed treatments affect anti-tumour immunity and how therapy schemes could be further optimised to potentiate the development of effective anti-tumour immunity able to recognise and eliminate both sensitive and resistant cells.

Chapter 7. Discussion

The newly developed KRAS G12C inhibitors hold the potential to create new treatment avenues for eligible cancer patients. However, in early clinical trials, it became evident that the majority of cancer patients that initially responded well to this therapy had developed treatment-resistance within months. Hence, employing this new line of drugs as monotherapy may not be sufficient to achieve durable responses. It had further been discovered that initially responsive tumours can evolve to bypass the inhibitor mechanism of action through myriad compensatory actions, which can compound the development of appropriate combination therapies.

In this project, we explored treatment strategies that can enhance the clinical efficacy of KRAS G12C inhibitors through combination therapies that further bolster anti-tumour immunity. As the immune system presents an equally dynamic and adaptable entity, we hypothesised that it may be possible to foster an adaptive anti-tumour immune response capable of recognising a pan-cancer cell archetype. Thereby enabling immune-mediated elimination of KRASi-resistant tumour subpopulations.

7.1 A rationale for the investigation of therapy combinations

In this study, we first established and validated an in *vivo* model system mimicking the development of KRASi-resistance, employing mechanisms observed in the clinic; through the acquisition of further point mutations in the KRAS G12C mutant oncoprotein, which prevent KRAS G12C inhibitors from effectively interacting with their target[236-240]. Here, reporter-traced, KPAR1.3 KRAS G12C or G12D mutant lung cancer cell lines were created. The reporters were designed to allow for the distinction of the two isogenic tumour cell populations through a wide range of omics-based techniques. Next a pre-

clinical murine model system with traced, co-engrafted KRAS G12C and G12D mutant tumour cells was optimised to study the efficacy of different therapy combinations.

Here, the glowing head mouse model was employed for in *vivo* experiments, because this strain is thought to be centrally tolerised towards the reporters eGFP and Luciferase. Through in silico modelling, we predicted that mice are likely equally tolerant towards eBFP due to the high structural similarity with eGFP. Of note, another publication by C. Grzelak et. al had found that no significant improvements in immune tolerance to reporter-traced cancer cell lines were detected when employing GH-mice[322]. Due to time constraints on this project, we had not performed extensive investigation whether the reporter expression in GH mice was more stable compared to standard C57BL/6J mice. Further experiments in GH mice could also be performed to assess whether the TME architecture, tumour growth, or therapy responses would differ when engrafting reporter-traced or untraced cell lines. However, regardless GH strain immune-tolerization towards the reporters, their albino fur coat still provides an advantage over using C57BL/6J mice, allowing for enhanced precision during IVIS scanning.

In initial experiments, we wanted to assess whether treating tumours derived from co-engrafted KRAS G12C and G12D mutant KPAR1.3 cell lines with Adagrasib would already be sufficient in enhancing anti-tumour immunity and enable rejection of the drug-resistant sub-population through alleviation of oncogenic-KRAS mediated immune suppression. However, it became evident that employing Adagrasib as monotherapy resulted in the rapid proliferation of the KRASi-resistant tumour sub-population. Here, mice relapsed within only two weeks of treatment, with the majority of the tumour mass being comprised of KRAS G12D mutant cells, even if they were engrafted with a starting ratio of only 0.01%. This observation may reflect the findings of the early clinical trials conducted with the KRAS G12C(OFF) inhibitors, where the majority of patients which initially responded well would become treatment resistant in a matter of

months [222,223,225,227,228,231]. It is further possible that treatment-mediated selection of resistant tumour populations could contribute to the development of cross-resistance to other therapy types, thereby potentially exacerbating the outcome of subsequent treatment responses to other anti-cancer drugs. For example, Haas et al demonstrated, in a pre-clinical model system for melanoma, that mice which had relapsed on MAPK inhibitors had also developed cross-resistance to immunotherapy [300]

Therefore, we hypothesised that it may provide a therapeutic advantage to instead simultaneously target distinct selective vulnerabilities in tumour cells by employing treatments that function through different modes of action. Here, lines of therapy which foster anti-tumour immunity may present a particularly promising approach. Indeed, we found that combining KRAS G12C inhibitor RMC-4998 with SHP2i RMC-4550 or the therapeutic ab a-PD-1, lead to enhanced therapy responses in our mouse model through treatment synergy. Here, durable complete responses were achieved when administering dual treatment combinations and therapy efficacy was further enhanced in the triple-combination of these drugs. Moreover, re-challenging complete responders by re-engrafting only the KRAS G12D mutant cancer cells on the opposite flank indicated that these mice had developed enhanced anti-tumour immunity. This could be attributed to an adaptive immune response, capable of recognising and targeting a pan-cancer cell archetype.

For mice which had relapsed after the end of the treatment period, IVIS scans, in conjunction with flow cytometric analysis of tumour cell composition implied that the bulk of some relapsed tumours was re-established from KRAS G12C mutant tumour cells which must have persisted during treatment. The study of Haas et al. had further suggested that therapy resistant tumour cells can form a protective niche for remaining treatment responsive cancer cells, thereby enabling them to persist during treatment intervals, which may explain the findings in our survival experiments. This finding could provide valuable insights

into the tumour cell population dynamics during the evolution of resistance towards targeted therapy.

Designing these survival experiments required large cohorts of mice, whereat several factors had to be taken into account due to the limited number of GH mice available. First, most experiments were performed in gender-mixed cohorts, which was accounted for by assigning equal numbers of male and female mice to each treatment group. This was possible because the original KPAR1.3 cell line was established from a female mouse, which possesses two X-chromosomes. Hence, it is at least likely that male mice, which are also in the possession of an X chromosome would not have an adverse immune reaction to this cell line based on sex-difference. RNA sequencing of the cancer cell compartment in our study implied that there were likely no significant sex differences relating to the overall treatment-induced cancer cell state. Employing mouse cohorts of mixed genders may even have provided an advantage to the clinical applicability of our results. As it was pointed out that the postulated findings of some pre-clinical studies may be subject to gender bias from employing predominantly male mice[323-326]. Similarly, conducting these larger pre-clinical studies sometimes necessitated the inclusion of mice across a slightly wider age range, between 7-12 weeks at the start of the experiment. If the older mice could not be matched equally across treatment groups due to odd numbers, experiment were always designed to be slightly biased against the stated hypothesis. Being able to generate complete responders in mice across a wider age-range in our experimental set up could also hint to the clinical effectiveness of the employed therapy schemes.

Another aspect contributing to treatment responses was the tumour size and fraction of drug-resistant cells at the start of treatment. Overall, it was observed that mice were more likely to become complete responders if tumours were either smaller or IVIS scans implied that a tumour encompassed a lower proportion of KRAS G12D-mutant tumour cells. This was again considered when making treatment groups. However, it is possible that this could have

affected the number of CRs generated between individual experiments. It is also likely that the therapy combinations would not be sufficient to generate durable responses if tumours were too large at the start of treatment, which may, on a larger scale, also impact on clinical implementations. Additionally, treatment duration affected therapy efficacy, with extended treatment periods generally yielding better responses.

For mimicking the emergence of a KRAS G12C inhibitor-resistant tumour subpopulation, two distinct mechanisms of drug resistance were explored. In the clinic, the acquisition of further mutations within the KRAS G12C mutant oncoprotein had been observed, which was imitated by employing the isogenic KRAS G12D mutant KPAR1.3 cell line. Secondly, a novel KPAR1.3 KRAS G12C^{res} cell line with increased resistance to KRASi was recently established in our group. This was achieved through further in *vivo* propagation of the parental cell line, with tumour bearing mice receiving intermittent KRASi treatment until they no longer responded. Investigation of the underlying mechanism conveying increased KRASi resistance revealed that this could be, at least in part, attributed to an EMT-like shift, which had previously also been observed in the clinic[235,246]. In our model system, we were able to show that the employed combination therapies were effective in achieving durable responses in mice harbouring tumours containing either of the KRASi-resistant subpopulations.

To further validate the impact of our findings, additional cell lines and different mechanisms of KRAS G12Ci resistance could be evaluated. For example, our group has recently established another KRASi-resistant KPAR1.3 KRAS G12C cell line by knocking out cyclophilin A, which is the chaperone required for the RMC-4998 mediated tri-complex formation. Furthermore, the KPAR1.3 cell lines are inherently immunogenic, as they had originally been derived from a lung tumour of an immune-compromised mouse and had hence not undergone complete immune editing. To grasp a wider scope of clinical cases, immunologically cold isogenic lung cancer cell lines should also be investigated in our model system. This could, for example, include the 3LL and KPB6 murine

lung cancer cell lines, which our group had found to give rise to more immunologically cold tumours[216]. Additionally, assessing how the loss of function for different TSGs in the cancer cell compartment synergises with oncogenic KRAS signalling in influencing therapy mediated immune modulation may be of interest. Other than TP53, commonly co-mutated TSGs in lung cancer patients include KEAP1 and STK11, which were found to have relatively poor response to checkpoint blockade.[229,327,328].

In order to interpret the clinical relevance of our findings, it is also imperative to take the multitude of species related differences into account. The saying *"the human is a bad model system for the mouse"* outlines the scientific disconnect which can arise in proclaiming cancer cures discovered in small rodents. For example, metabolic turnover can affect the efficacy and pharmacokinetics of therapies, while differences in immune, inflammatory, and tissue repair responses can affect observations related to immune-modulatory drugs. Moreover, differences in protein isotypes, redundancies in signalling circuits, hormone physiology, aging, circadian rhythm, activity levels, etc. may all affect treatment responses. Another important factor is resilience to therapy-related toxicities. Mice in this project had tolerated even the triple therapy combination of KRAS inhibitor RMC-4998, SHP2 inhibitor RMC-4550, and a-PD-1 well. On the other hand, patient data from clinical trials suggests that dual therapy combinations with KRAS G12C inhibitors, or ever single-agent treatments can coincide with high toxicity levels [226,229,329]. For example, in the "KRYSTAL1" phase 1 trial, NSCLC patients had received 600 mg of Adagrasib twice daily[228]. In this cohort, 44.8% of patients experienced adverse effects reaching grade 3 or higher, indicating severe side effects. After initial dose escalation phase of the "CodeBreaK100" clinical trial for Sotorasib [227], this drug was administered to NSCLC patients at 960 mg once daily[222]. Here, adverse treatment effects with grade 3 or higher were experienced by 20.6 % of individuals. Moreover, high toxicity profiles were observed in clinical trials assessing the efficacy of combining KRAS inhibitors with immunotherapeutic antibodies. Amgen's Codebreak 100/101 trial investigated treatment responses for combined

treatment of Sotorasib with checkpoint blockade Pembrolizumab or Atezolizumab. This clinical trial reported more incidences of grade 3 and 4 hepatotoxicities[301,330] compared to NSCLC patients treated with comparable doses of KRASG12Ci as monotherapy[226]. For Sotorasib, increased liver toxicity as well as non-liver adverse events were also observed in patients which had previously been treated with checkpoint inhibitors[331].

However, at least some of the KRAS G12C inhibitor-related adverse effects appear to be compound-specific. They may be related to unspecific binding of cysteine targeting warhead in the KRAS G12C(OFF) inhibitors[332]. Additionally, differences in pharmacokinetics may also influence toxicity levels. For example, the difference between Adagrasib and Sotorasib in the percentage of patients experiencing severe adverse effects may be related to the stability of respective compounds. Adagrasib was reported to have a plasma half-life of 23 h[228] while Sotorasib was less stable with a half-life of only 5.5 h+/- 1.8 h [227]. It was hypothesized that the extended half-life of Adagrasib may have contributed to an increase in hepatotoxicity related symptoms. It is possible that for this new class of oncogenic KRAS inhibitors higher doses may not coincide with the highest overall clinical benefit or even the best response rates. Lower doses might still have high efficacy but with less side effects [333,334], which may be related to off-targeting effects at maximal doses being higher. In the Codebreak 100/101 dose escalation trials, patients receiving lower doses of Sotorasib experienced high grade liver toxicities less frequently[330]. Similarly, the "KRYSTAL7 trial", investigated the therapeutic benefits of combining pembrolizumab (PD-1) with reduced concentrations for Adagrasib[229]. This combination therapy resulted in a response rates of 49%, with an overall manageable toxicity profile, which has resulted in the initiation of a larger phase 3 clinical trial[230]. In addition, next generation KRAS G12C inhibitors, which are currently in early pre-clinical or clinical testing [37], seem to present with less off-targeting and more favourable toxicity profiles for patients. For example, the KRAS G12Ci Divarasib (GDC-6036), that is currently in phase 1 clinical testing, [329] is showing decreased toxicities compared to first generation inhibitors and

increased median progression free survival. The G12C inhibitor Opnurasib (JDQ-443) from Novartis is also showing promising results, although the number of participants enrolled to the trial is still low[335].

Clinical toxicity profiles for the SHP2 inhibitor RMC-4550 or other related drugs are not yet publicly available and will likely determine how feasible future combination therapies with KRAS G12Ci will be. However, even if high toxicities of SHP2 inhibitors as monotherapy are reported, it might still be possible to achieve treatment synergy in administering SHP2i at lower doses in combination with next generation KRAS G12C inhibitors. By carefully adjusting the doses and treatment schedules of the individual drugs and further development of improved compounds, there may still be a therapeutic window to be exploited.

7.2 Therapy-induced alterations in the tumour cell compartment

We next investigated how therapy combinations contribute to the cell-state of KRAS G12C or G12D mutant tumour cells. We had hypothesized that this could include direct effects of the inhibitors acting on cancer cells signalling as well as responses to environmental cues. It was also of particular interest to understand why the KRAS G12D mutant tumour cells, that do not respond to G12Ci directly, appeared to increase their proliferation rate in response to this inhibitor in our model system.

In the KRAS G12C mutant tumour cell compartment, proliferation-associated signatures were significantly downregulated in both SHP2i and KRASi treated samples. Simultaneously gene sets relating to an inflammatory response were upregulated in response to treatment. It is possible that the treatment induced changes in the KRAS G12C mutant tumour cells would have been even more pronounced than what was captured in this experiment. This is because the

most treatment-responsive KRAS G12C mutant tumour cells may have already been eliminated during the initial in *vivo* treatment period or they may have been lost during sample processing, due to treatment-induced compromised cellular integrity. KRASi responsive cells may also have been gated out during flow cytometric sorting, if they had entered an early apoptotic stage. Overall however, the results of the bRNA-seq experiment are in congruence with previous findings of our group, indicating that KRAS G12C inhibitors can inhibit oncogenic KRAS signalling and enhance interferon responses in pre-clinical models of KRAS G12C mutant NSCLC[172].

Sequencing of the KRAS G12D mutant cells isolated from KRASi treated tumours revealed a shift in cell state towards a more proliferative phenotype, where a significant upregulation of gene sets relating to Myc signalling, E2F targets, and cell cycle progression was observed. This also held true for samples from mice which had received combination treatments of KRASi together with SHP2i or a-PD-1. For the KRAS G12D mutant tumour cell compartment, the RNA sequencing experiments provided insights as to how and through which transcriptional networks the increased proliferation was regulated, however, the underlying causes inducing this phenotype require further investigation. Here, different types of KRAS G12Ci-resistant tumour cell subpopulations could be employed in our model system to assess whether this proliferative signature is conserved across other types of drug-resistant subpopulations. To explore whether this proliferative signature may have been dependent on environmental cues, employing more in depth spatial omics techniques, such as SLIDE-sequencing[336], CosMx single cell imaging[337], imaging mass cytometry[338] could be considered.

In KRAS G12D mutant cells, inflammation-associated signatures were downregulated in samples isolated from mice which had received KRASi treatment as monotherapy or in combination with a-PD-1. However, in samples of mice which had received SHP2i treatment, either as monotherapy or in combination with KRASi, this phenotype was reversed. An array of in *vitro*

assays suggested that both internal and external factors may have contributed to the SHP2i-induced increase in these inflammatory signatures. Moreover, time course assays suggested a potential compensatory mechanism to SHP2i in both, KRAS G12C and G12D mutant cancer cells, through an increase in activated effector proteins downstream of oncogenic KRAS. However, further experiments would be necessary to draw any conclusions on this subject. This could include further in *vitro* co-culture assays with the two isogenic cell lines, matching the conditions from the in *vivo* bRNA-seq experiments, such as population fractions and treatment duration.

Understanding the underlying causes contributing to the rapid selection process of drug-resistant sub-populations may aid the identification of novel treatment rationales counteracting this development. For example, to inhibit cell cycle progression in KRASi-resistant cells, CDK4/6 inhibitors could be investigated[196,271]. Inhibiting the rapid outgrowth of drug-resistant subpopulations may aid the timely development of an adaptive immune response while the majority of the tumour mass remains KRASi responsive. CDK4/6 inhibitors may also convey the additional advantage of suppressing Treg activity[264]. Another potential approach to block the outgrowth KPAR1.3 KRAS G12D tumour subpopulation in treated samples may be to target Myc, which is a key regulator in mediating proliferation and survival signalling downstream of oncogenic signalling. Inhibiting Myc directly, was shown to successful in preventing tumour growth in oncogenic KRAS-driven murine lung cancer model[265] and Myc degradation similarly lead to increased tumour control[339,340]. However, as Myc also plays a universal role in maintaining homeostasis across healthy tissues and organs, treatment related toxicities may reduce the therapeutic window of potential inhibitors.

The subsequent histopathological multiplex staining of tumour tissue sections across treatment groups provided additional spatial information, showing that the outgrowth of the KPAR1.3 KRAS G12D mutant subpopulation in KRAS treated samples appeared to occur in clusters. This observation is different from

the initial stainings of tumours engrafted from KPAR1.3 KRAS G12C:G12D cells mixed at a 50:50 ratio, where the two cell types appeared to grow mostly in an interspersed pattern. It is possible that the observed clusters in treated samples originated from a single KPARG12D cell and are the result of localised, sub-clonal cell division. The formation of clusters of KRASi unresponsive cells could also have provided an immune-protective niche, as was hypothesised by Haas et al in a comparable preclinical model[300]. Depending on the causes for the outgrowth of drug-resistant cells, further treatment combinations targeting, for example, cancer cell metabolism or autophagy regulation could be considered.

Taken together, these findings could provide valuable insights into potential tumour cell population dynamics during therapy exposure as well as potential combination therapy rationales.

7.3 Contribution of anti-tumour immunity to achieve durable therapy responses

To understand how therapy mediated remodelling of the immune compartment may have contributed to the achievement of durable responses a series of in *vivo* experiments in immune compromised mice as well as immune phenotyping of the immune TME were conducted.

In $Rag1^{-/-}$ mice, which lack functional lymphocytes of the adaptive immune compartment, no complete responders were generated with KRASi as monotherapy or in combination with SHP2i. To further narrow down which populations within the adaptive immunity may contribute to immune-mediated cancer cell killing, either $CD8^{+}$ T cells or B cells were depleted from immune competent mice which had again been engrafted with the isogenic cancer cell lines. Here, fewer complete responders were observed in KRASi + SHP2i treated mice for both immune cell depletion groups. This may indicate a certain

degree of redundancy in the role of immune cell mediated cancer cell killing in different adaptive immune cell populations. When the CR mice were re-challenged, mice which had previously undergone immune cell depletion of either type were unable to immune-reject the reinjected cancer cells. Although the number of mice entering the re-challenge phase was too small to draw any definite conclusions, this might indicate that multiple types of immune cells contributing to anti-tumour immunity.

Initial immunohistopathological stainings for B cells in tumour sections as well as the immune phenotyping had indicated that only few B cells were generally present in the TME. However, probing the serum of mice across treatment groups for the presence of cancer cell specific antibodies revealed that B cells may further contribute to anti-tumour immunity through a systemic response. Here, tumour cell specific antibodies were able to opsonise the isogenic KPAR1.3 cancer cell lines equally well. The antigen mainly recognised by this humoral response appeared to be the endogenous retroviral protein EMV2. This finding may be clinically relevant, as it was discovered by K. Ng et al that this class of usually silenced proteins can also be aberrantly expressed in human cancer [122]. In their study, interrogating the TCGA and TRACERx sequencing repositories for human lung cancer uncovered that the aberrant expression of endogenous retroviral envelope glycoproteins (ERVEGPs) was present in a substantial proportion of cases. Testing serum samples of LUAD patients further revealed the presence of a humoral response towards ERVEGPs. Moreover, ICB therapy was found to overall improve this humoral response, indicating a therapeutic potential in harnessing its anti-tumorigenic effects.

In this project, it could be further explored whether the serum isolated from KPAR1.3 tumour bearing mice may hold a therapeutic potential. Here, it could be investigated whether treating mice that bear tumours of the mixed isogenic KPAR1.3 cell lines with a combination of KRASi and the aforementioned serum may enhance responses through treatment synergy. To further narrow down

whether the ab-producing B cells stem from the TME, tertiary lymphoid structures or adjacent tdLNs, samples from these tissues could be incubated in culture media and the supernatant tested for the presence of cancer-cell specific antibodies.

Next, the mechanisms underlying a therapy-enhanced anti-tumour immune response were studied by performing immune phenotyping of tumours and tdLNs across treatment groups with a 36-plex ab panel. This experiment highlighted the complex organisation of the immune compartment in the TME as well as the multifaceted therapy-induced effects on anti-tumour immunity. Our findings implied it was possible that alleviating oncogenic KRAS-induced immune suppression in the TME may have created more favourable conditions for the coordination of anti-tumour immunity. This is in congruence with numerous other studies, investigating KRASi-induced promotion of antitumour-immunity[136,172,197,216-218]. The results of our immune phenotyping experiment suggested an increase in the proportion of T cells was detected, as well as a shift in the polarisation towards more activated APCs. Further, an increase in GFP-positive macrophages had been observed in KRASi-treated samples. Together, this could imply that, due to increased immunogenic cell death induced by KRAS G12C inhibitors, APC may have increased phagocytosis of cancer cell material which might, in turn, have facilitated priming an adaptive immune response.

On the other hand, the increase in TILs after treatment did not coincide with an increase in their overall activation status. The decrease of activated T cells might appear counterintuitive. However, because the immunocyte subpopulations are quantified as relative fractions of their respective T cell subtypes, it is possible that more TILs get recruited to the TME as a general site of inflammation, for example, due to the increase in cell death in the tumour cell compartment and alleviation of immune suppression. It is speculated that only a small proportion of the newly recruited T cells would likely express a tumour antigen-specific TCR. The remaining TILs may act as bystander T cells,

although they may still be able to contribute to anti-tumour immunity through certain effector functions[110]. To gain further qualitative and quantitative insights into which $CD8^+$ or $CD4^+$ clonal T cell populations are enriched in the TME, single cell RNA sequencing together with TCR sequencing could be performed[341,342]. Using this approach, the activation profile of T cells that are clonally enriched in the TME could compared to non-enriched populations. This might elucidate whether T cell activation is restricted to T cells potentially expressing a cancer cell antigen specific TCR. It is also possible to perform spatially resolved TCR sequencing on tissue sections, thereby allowing to map out enriched T cell clonotypes, to assess their activation state and analyse which neighbouring cells they interact with[343]. To study the potential role of treatment-enhanced cytotoxic T cell mediated cancer cell killing on a more mechanistic level, a co-culture assay system could also be established. Towards the end of this project, we had attempted several experiments where $CD8^+$ T cells were isolated from the TME, tdLNs or the spleen. Here, naïve control mice were compared to tumour bearing mice which had either received vehicle or anti-cancer treatments. Subsequently, $CD8^+$ T cells were co-cultured with KRAS G12C or G12D mutant KPAR1.3 cancer cells. As readout, both, live-cell-imaging and flow cytometric analysis of appropriate lineage and activation markers were attempted to assess whether $CD8^+$ T cells derived from mice harbouring KPAR1.3 KRAS G12C mutant tumours would be able to eliminate KRAS G12D mutant cells in culture, confirming their role in bystander killing of drug-resistant tumour subpopulations. However, so far it has proven difficult to keep $CD8^+$ T cells alive in culture while avoiding their artificial activation through supplementation of growth factors and other stimulatory molecules which could obscure the in *vivo* treatment-related activation. We also attempted to establish co-cultures which contained APCs to enhance T cell function, however, these trials will require further technical optimisation. A more commonly used system for the perform co-culture assays between T cells and cancer cells involves the use of Ovalbumin (OVA)/ Ova Transgenic 1 (OT-1) mice[300,344,345]. Here, OVA serves as a model-antigen expressed by the cancer cells to be studied in combination with OT-1 transgenic mice which harbour a $CD8^+$ T cells with a

TCR specific for an OVA-derived peptide presented by the MHC-I complex. So far, we had decided against employing this model system to prevent the introduction of any artificial artefacts which may hamper the clinical impact of the findings in our model system. Alternative to the aforementioned co-culture systems, ELISpot assays with $CD8^+$ T cells, isolated from tumour bearing mice of different treatment groups, could be performed to probe for IFN-γ release[346,347].

To increase the fraction of cytotoxic T cells in the TME that actively perform effector functions, further treatment agents capable of alleviate tumour cell-induced immune suppression could be explored. For example, inhibiting CD73 may provide therapeutic benefits. It was shown across multiple cancer types, including lung cancer, that tumour cells can aberrantly upregulate expression of CD73, a cell-surface-residing ecto-5'-nucleotidase involved in conversion of adenosine monophosphate (AMP) to adenosine[174,175]. High levels of this metabolite in the interstitial space of tumours can promote immune suppression through multiple mechanisms, including the suppression of activation, proliferation, and cytokine production in T cells[175]. Another potential target may be Diacylglycerol kinases (DGKs), a group of enzymes that convert diacylglycerol (DAG) to phosphatidic acid (PA)[348]. In lymphocytes, accumulation of DAG can promote differentiation and effector functions [349,350]. Thus, DGK inhibition could further increase anti-tumour directed T cell, B cell and NK cell activities. Another approach to enhance cytotoxic T cell mediated cancer cell killing could be the employment of bivalent antibodies, also known as bispecific T cell engagers (BiTEs). This is based on proof of concept studies, showing that conjugates of oncogenic KRAS-derived peptides covalently bound to KRAS G12C(OFF) inhibitors can be presented on the MHC-I complex of cancer cells[351 352]. BITEs could be utilised to promote the formation of an immune synapse between cytotoxic T cells and tumour cells to enhance T cell mediated cancer cell killing. These conjugates between KRAS G12Ci and oncogenic KRAS derived peptides could potentially serve as neoantigens in APC-coordinated anti-tumour immunity, if they were cross presented. However,

these initial studies were only performed in *vitro* and would require further validation. It has also been demonstrated across different cancer models, including KPAR1.3-derived tumours, that oncogenic KRAS signalling can promote immune evasion through upregulation of Cox2 expression[176,177,353]. This is an enzyme involved in the synthesis of the prostaglandin E2 which can enhance immune-suppressive effects, including the inhibition of DC, NK, and $CD8^+$ T cell effector functions[354]. Hence, inhibiting Cox2 or targeting prostaglandin receptors on recipient cells may also produce beneficial immune modulatory effects[43]. An additional approach for enhancing a $CD8^+$ T cell effector response capable of eliminating KRASi-resistant subpopulations could include the identification of mutant-KRAS specific neoantigens[374,375] in conjunction with the development of anti-cancer vaccines[355-358 359]. Similarly, adoptive T cell transfer with cytotoxic T cells specific to oncogenic KRAS-derived neoantigens could be considered, which was recently successfully demonstrated in a cohort of KRAS mutant colorectal cancer patients[103].

In addition to favourable therapy-induced changes in immune cell composition, the findings of this immune phenotyping also revealed a potential bivalent role of KRASi in remodelling the immune compartment of the TME. For example, a KRASi-induced increase in tumour infiltrating Tregs had been observed, which could hamper therapy-mediated enhancement of anti-tumour immunity. This finding is in congruence with the preliminary Foxp3 immunohistochemical staining performed on the tumour sections across treatment groups in this project. It also coincides with previous studies of our group, where KRASi treatment led to an increase in Treg infiltration in orthotopic murine NSCLC models[172,197,218,219]. Understanding the full scope of therapy-mediated TME remodelling is essential for highlighting therapeutic windows for the development of enhanced treatment strategies. For example, KRAS G12C inhibitors could be combined with a therapeutic Treg-depleting ab, which was shown to potentiate anti-tumour immunity in one of our pre-clinical mouse models [218]. To counteract a treatment-induced influx of immature monocytes, combination therapies with CCL2 /CCR2 inhibitors could be explored. It was

shown by our group that lung tumour cells can be a main source of the monocyte-recruiting chemokine CCL2, thereby promoting an immunologically cold TME[360]. Moreover, tumour cells in KRAS-mutant lung cancer can inhibit APC effector functions through aberrant expression of CD47, which binds to Sirp1α which is mainly expressed by MPs[361]. Cancer immunotherapy targeting the CD47/SIRP1α axis through anti-CD47 inhibitors may help the restoration of their role in phagocytosis of cancer cell material and antigen-cross presentation[361,362]. This approach may be especially effective in combination with KRAS G12C inhibitors as it could further facilitate the uptake of cancer cell derived neoantigens after KRAS G12Ci induced cancer cell killing[363].

Not only can spectral flow cytometry be used to characterise therapy-induced changes in TME composition, but it also allows to track the phagocytosis of cancer cell material in APCs. Identification of these cells could aid the development of alternative strategies that potentiate bystander killing of drug-resistant tumour subpopulations. In future follow up experiments, it would be interesting to optimise a protocol for re-straining of the cancer cell derived FPs, to enable the detection of both, phagocytosed BFP and GFP within APCs. Alternatively, immuno-histochemical stainings of APC markers and BFP/GFP in the tumour sections across treatment groups could be performed to investigate this further. Additionally, potentially by extending the in *vivo* treatment period before sample collection, the presence of GFP/BFP$^+$ APCs in tdLNs could also be investigated, which may provide further insights into APC mediated cross-presentation of neoantigens. Moreover, mice could be engrafted with untraced KPAR1.3 KRAS G12C cells and treated with therapy combinations until tumours have regressed. Subsequently, T cells and APCs could be isolated from tdLNs for co-culture assays to test whether their potential of targeting untraced KPAR1.3 KRAS G12C- or G12D cells has increased. This way, the mechanism of priming an adaptive immune response that recognises a pan-cancer cell archetype, independent of reporter construct expression could be further corroborated.

Flow cytometric immune phenotyping encompasses the limitation of not providing spatial information about therapy-mediated remodelling of TME architecture. For example, our group had previously discovered that KRAS G12Ci in orthotopic lung tumour mouse models increased the TME infiltration depth of T cells, while these immunocytes were mostly restricted to the tumour perimeter in vehicle mice[217]. To gain further insights into treatment induced changes in TME architecture, multiplexed stainings of tumour sections across all treatment groups were performed. Analysis of the spatial organisation of infiltrating T cells, as well as the two isogenic tumour populations across treatment groups is ongoing. However, initial findings indicated an increased presence of $Ki67^{+}$ KPAR1.3 KRAS G12D tumour cell clusters in samples derived from KRASi-treated mice. An increase in T cells, infiltrating deeper into the tissue structures in tumours isolated from mice which received KRASi, had also been observed. A potential additional increase in T cell density was observed in combination treated samples, although this remains to be quantified. These tissue sections could also be utilised to probe for the presence of APCs that have phagocytosed cancer cell material. This could be achieved through combined IF staining of GFP/BFP together with appropriate APC lineage markers. If the presence of such MPs or DCs was detected, it could further be quantified whether their fraction was increased in treated samples and whether the number of T cells in their neighbourhoods was higher compared to vehicle tumours. The number of markers investigated in this experiment was not sufficient to fully isolate any mechanistic insights into immune cell interactions. As mentioned above, employing more comprehensive techniques for spatial analysis, such as IMC, SLIDE-sequencing or similar could provide more in-depth insights into the structural organisation between immunocytes as well as their neighbourhoods with cancer cells and other TME components.

To translate our results to a more clinically relevant setting, we had also worked on implementing an orthotopic mouse model for the engraftment of mixed KPAR1.3 KRAS G12C- and G12D mutant tumours. This aspect is especially

relevant for the investigation of treatment-induced effects on anti-tumour immunity. Our group had previously reported differences in immune cell composition as well as a-PD-1 responses between subcutaneous- and orthotopic tumours derived from the KPAR1.3 cell lines[294]. The challenge in establishing an orthotopic model for this system was to engraft single foci tumours in the lung with a reproducible fraction of KRASi-resistant G12D cells. Conventionally, the establishment of murine lung tumours can be achieved via tail vein injection of lung cancer cells. This is based on the premises that cancer cells are likely to get stuck in the thin lung capillaries which may subsequently facilitate engraftment. However, such tumours likely develop from a single cancer cell, so injecting a mix of KRAS G12C and G12D mutant cells via tail vein would not necessarily result in tumours comprised of both genotypes. Therefore, we tested a number of different approaches to engraft tumours directly into the lung. Of note, all the techniques described below were either performed on anaesthetised mice which received appropriate post-procedural care or were only attempted on cadavers.

One strategy, which is typically utilised for viral infections[364] or to administer other small particles [13] was to guide a narrow, flexible tube into the trachea and administer cancer cells in a small volume of liquid [365]. The advantage of this technique is that is non-invasive, compared to other subsequently described methods. However, cancer cells are less likely to engraft if they are not fixed in place and may also be exposed to additional immune surveillance across the epithelial linings of the lung. Further, this approach would not result in single foci tumours with a reproducible fraction of drug-resistant cells as the administered cancer cells would scatter across the lung lobes as mice are breathing during the procedure. Administering the cancer cells in matrigel might aid the engraftment of orthotopic tumours, however, as small volumes of matrigel can solidify rapidly, it may clog the trachea. Further, if a tumour should engraft in the central airway, it may lead to the rapid a respiratory obstruction and pose a health risk for mice. Ishiwata et al. published an approach of inserting a bent probe deeper into one of the bronchi branching out from the

trachea[366]. However, this research group had spent years developing specialised imaging equipment and corresponding software to visually guide a probe into one of the bronchi. Practise with cadavers revealed that attempting this approach without visual guidance held the risk of injuring the very delicate lining of the bronchi.

We also attempted to establish lung tumours by directly injecting cancer cells into the lung, for which different protocols were assessed. In general, inserting a needle into the lung is a challenging procedure. First, there is an inherent risk of causing pneumothorax, should the pleural membrane spanning the lung lobes sustain any puncture damage during the injection. Secondly, as the lung is a highly vascularised organ, inserting a needle may cause a haemorrhage which, in turn, can cause pulmonary edema or thrombosis. Moreover, injecting too shallowly may lead to tumours engrafting in the pleural cavity or body wall, while inserting the needle too far may cause a cardiac puncture or lead to cancer cells being injected into the general circulatory, in turn leading to harmful metastasis. As the mice continue a breathing motion during the procedure, the injection depth of the needle is subject to how far expanded the lung lobes are at any given moment. Leaving the needle in the lung for any extended period of time might also increase the damage caused by the needle through the breathing motion of the mice. To make this procedure safer, we first attempted ultrasound guided injections, where a small probe is placed on the chest of a mouse to visualise the lung before injecting cancer cells through the lateral ribcage. However, this technique relies on sound waves being reflected by tissue matter, but lungs are mostly filled with air which made visualisation of the needle position ambiguous, among other challenges.

Another research group had published protocols in which anaesthetised mice were directly injected through the skin and lateral rib cage, without additional guidance or invasive procedures [300,367]. For this technique, injection depth needed to be precisely controlled, especially when injecting into the left lobe which had a narrow margin due to the close proximity to the heart. To achieve

consistent injection depth, we had designed special adaptors together with the kind help of the mechanical engineering STP at the Francis Crick Institute. However, as our mice had different genders and ages, it was still difficult to find the appropriate injection depth. It was crucial not to nudge the needle against the ribs as this may blunt the needle tip and increase the risk of pneumothorax. Additionally, because this approach did not allow visualisation of the lung lobes it was not possible to monitor for injury until the mice recovered from anaesthesia. When we asked the authors about these risks, they had advised us that it was normal to lose approximately 20% of mice due to short- or long-term side effects caused by this procedure. They had mostly utilised this technique for small-scale studies, requiring few mice with focal tumours. However, for our preclinical studies with larger treatment cohorts this did not seem feasible or ethical.

Another approach was pioneered by Rita Pedrosa (to our knowledge the protocol remains unpublished as of now), where a small skin incision was made above the lateral rib cage to visualise the ribs and lung. As the parietal pleura is transparent, it was possible to clearly see the lungs under the rib cage and allowed for a more accurate injection. Employing this approach, together with the kind help of the surgery team at our institute, several treatment and survival experiments with mixed tumours had been performed. However, a risk of mice falling ill rapidly as a result of this procedure remained and mice sometimes had to be culled early due to procedure-related health issues. In initial experiments, it became evident that moving our experimental system to an orthotopic context would require considerable optimisation to assess experimental parameters such as appropriate number of cells to inject, fraction of KPAR1.3 KRAS G12D cells, ideal starting point for treatment, treatment duration, etc. As our studies require larger cohorts and we did not want to cause unnecessary suffering in mice, this line of experiments was not further perused. In the future, developing a save and reproducible procedure for orthotopic engraftment of single foci lung tumours would enable further investigation of immune contribution to cancer cell killing in a more clinically relevant setting.

Further investigation across a broader spectrum of resistance mechanisms as well as cancer types will be necessary to assess the true clinical applicability of our findings. Isolating mechanisms of immune-mediated bystander killing of drug-resistant subpopulations in greater depth may provide meaningful clinical insights. Moreover, being able to obtain matched, pre- and post-treatment samples from KRAS G12Ci treated patients or consulting applicable publicly available human NSCLC sequencing data sets could provide further insights into KRASi mediated TME remodelling. Nonetheless, taken together our findings indicate a potential rationale for administering KRAS G12C inhibitors in combination with either SHP2 inhibitors or a-PD-1/a-PD-L1 immunotherapeutic abs to elicit durable treatment responses.

7.4 Concluding remarks

Tremendous scientific strides and medical advances have improved the quality of life for myriad patients. Here, the newly developed KRAS G12C inhibitors as well as the next generation RAS inhibitors open a new avenue for treating the most frequently mutated oncogene in human cancer. However, how to effectively employ this new class of inhibitors, achieve durable responses and avoid the development of secondary treatment resistance requires further investigation. Cancer is a highly complex and dynamic disease, capable of evolving to evade selection pressures such as anti-tumour immunity and clinical treatments. Hence, employing static therapy regimes without sufficient prognostic insights may exacerbate malignity over time, while leaving patients at the losing end of an immune-oncological tug-of-war. However, the immune system likewise presents a formidable and adaptable regiment that can contest a mutable malignancy. Hence, understanding the underlying mechanisms of harnessing effective anti-tumour immunity is a particularly auspicious avenue in helping the patient’s immune system to fight back.

In this study we were able to demonstrate that administration of KRASi in combination with therapy agents improving anti-tumour immunity may be a promising approach to enhance treatment efficacy. Further, this approach was able to combat the development of drug resistance, likely through enhanced adaptive immunity, capable of recognising a pan-cancer archetype. To investigate the underlying mechanisms governing therapy-enhanced anti-tumour immunity and remodelling of TME architecture, we employed a combination of different omics-based approaches. This functional characterisation of the layout and cell-state of anti-tumour immunity provided insights into underlying mechanisms governing the development of effective anti-tumour immunity. Understanding the nature of the employed therapy combinations on TME organisation may elucidate further strategies for combinations with KRAS G12C inhibitors that allow to revive or replace an exhausted immune response.

Combining targeted inhibitors with lines of immunotherapy may not only promote the emergence of synergy but may further allow the drugs to complement each other's strong points. As targeted therapy lines often results in drastic, but short-lived effects, while checkpoint inhibitors can achieve durable responses across cancer types[368,369], but only a subset of patients respond. Before developing resistance towards KRAS G12C inhibitors, most patients were found to present with a favourable initial treatment response. Our study suggests that during this period, oncogenic KRAS-mediated immune suppression may be alleviated in the TME. We were further able to demonstrate that this initial phase may provide a therapeutic window for combination therapies which further bolster anti-tumour immunity, thereby potentiating the efficacy of the newly developed KRAS G12C inhibitors and enabling the development of effective treatment responses with durable immune memory (**Figure 7.1**).

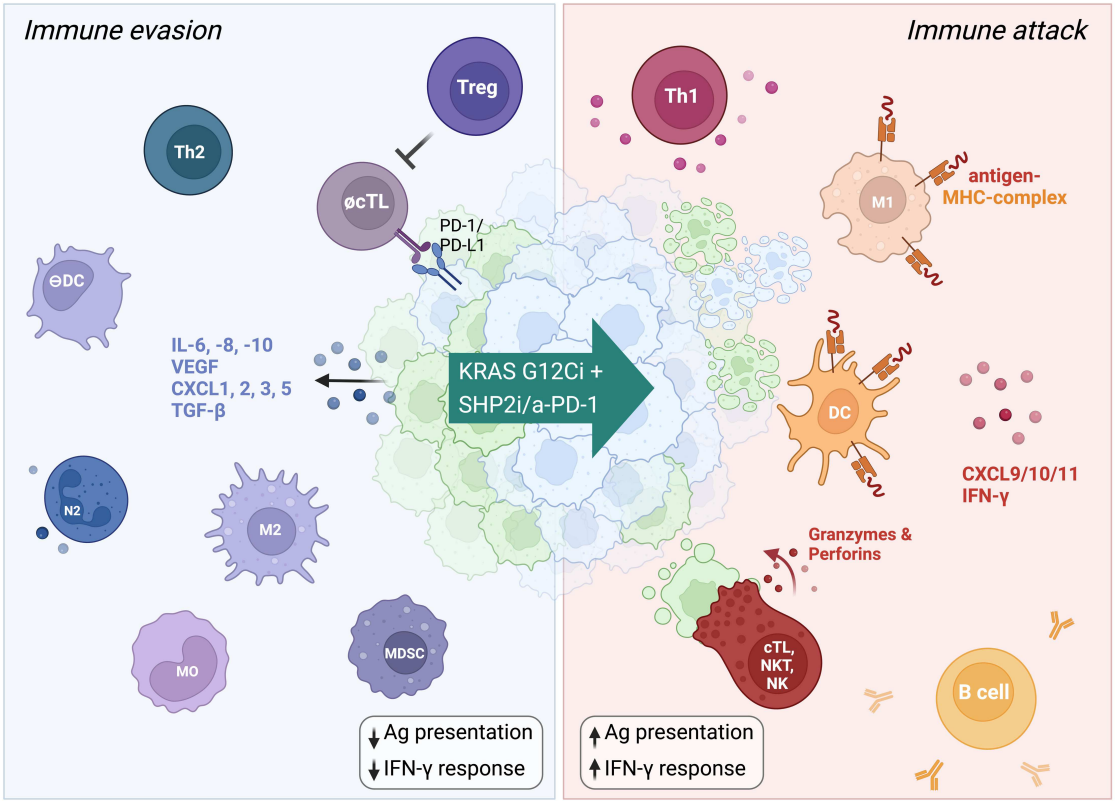


Figure 7.1 Combination therapies remodel TME and stimulate anti-tumour immunity.

Schematic of project rationale. Cell type abbreviations in left panel: Treg: T regulatory cell, ⃠cTL: exhausted $CD8^+$ cytotoxic T lymphocyte, Th2: $CD4^+$ T helper cell with subtype 2, (-) DC: inhibitory subtypes of dendritic cells, N2: type-2 polarised neutrophil, M2: M2 polarised macrophage, MO: Monocyte, MDSC: myeloid-derived suppressor cell. Right panel: Th1: $CD4^+$ T helper cell, M1: M1 polarised macrophage, DC: dendritic cell, cTL: $CD8^+$ cytotoxic T lymphocyte, NKT: natural killer T cell, NK: natural killer cell. Figure was adapted from Molina et al. 2024 and created with BioRender.

Reference List

1 Bray, F., Laversanne, M., Weiderpass, E., Soerjomataram, I. The ever-increasing importance of cancer as a leading cause of premature death worldwide. *Cancer* **127**, 3029-3030 (2021). https://doi.org:10.1002/cncr.33587

2 Sung, H., Ferlay, J., Siegel, R. L., Laversanne, M., Soerjomataram, I., Jemal, A., Bray, F. Global Cancer Statistics 2020: GLOBOCAN Estimates of Incidence and Mortality Worldwide for 36 Cancers in 185 Countries. *CA Cancer J Clin* **71**, 209-249 (2021). https://doi.org:10.3322/caac.21660

3 Soerjomataram, I., Bray, F. Planning for tomorrow: global cancer incidence and the role of prevention 2020-2070. *Nat Rev Clin Oncol* **18**, 663-672 (2021). https://doi.org:10.1038/s41571-021-00514-z

4 Bray, F., Laversanne, M., Sung, H., Ferlay, J., Siegel, R. L., Soerjomataram, I., Jemal, A. Global cancer statistics 2022: GLOBOCAN estimates of incidence and mortality worldwide for 36 cancers in 185 countries. *CA Cancer J Clin* **74**, 229-263 (2024). https://doi.org:10.3322/caac.21834

5 Siegel, R. L., Miller, K. D., Wagle, N. S. & Jemal, A. Cancer statistics, 2023. *CA Cancer J Clin* **73**, 17-48 (2023). https://doi.org:10.3322/caac.21763

6 Siegel, R. L., Giaquinto, A. N. & Jemal, A. Cancer statistics, 2024. *CA Cancer J Clin* **74**, 12-49 (2024). https://doi.org:10.3322/caac.21820

7 Schabath, M. B. & Cote, M. L. Cancer Progress and Priorities: Lung Cancer. *Cancer Epidemiol Biomarkers Prev* **28**, 1563-1579 (2019). https://doi.org:10.1158/1055-9965.EPI-19-0221

8 Kratzer, T. B., Bandi, P., Freedman, N. D., Smith, R. A., Travis, W. D., Jemal, A., Siegel, R. L. Lung cancer statistics, 2023. *Cancer* **130**, 1330-1348 (2024). https://doi.org:10.1002/cncr.35128

9 Dubey, A. K., Gupta, U., Jain, S. Epidemiology of lung cancer and approaches for its prediction: a systematic review and analysis. *Chin J Cancer* **35**, 71 (2016). https://doi.org:10.1186/s40880-016-0135-x

10 Akhtar, N. & Bansal, J. G. Risk factors of Lung Cancer in nonsmoker. *Curr Probl Cancer* **41**, 328-339 (2017). https://doi.org:10.1016/j.currproblcancer.2017.07.002

11 Malhotra, J., Malvezzi, M., Negri, E., La Vecchia, C. & Boffetta, P. Risk factors for lung cancer worldwide. *Eur Respir J* **48**, 889-902 (2016). https://doi.org:10.1183/13993003.00359-2016

12 Wong, M. C. S., Lao, X. Q., Ho, K. F., Goggins, W. B. & Tse, S. L. A. Incidence and mortality of lung cancer: global trends and association with socioeconomic status. *Sci Rep* **7**, 14300 (2017). https://doi.org:10.1038/s41598-017-14513-7

13 William Hill, E. L. L., Clare E. Weeden, Claudia Lee, Marcellus Augustine, Kezhong Chen, Feng-Che Kuan, Fabio Marongiu, Edward J. Evans Jr, David A. Moore, Felipe S. Rodrigues, Oriol Pich, Bjorn Bakker, Hongui Cha, Renelle Myers, Febe van Maldegem, Jesse Boumelha, Selvaraju Veeriah, Andrew Rowan, Cristina Naceur-Lombardelli, Takahiro Karasaki, Monica Sivakumar, Swapnanil De, Deborah R. Caswell, TRACERx Consortium, …Charles Swanton. Lung adenocarcinoma promotion by air pollutants. *Nature* **616**, 159-167 (2023). https://doi.org:10.1038/s41586-023-05874-3

14 Julian R. Molina, P. Y., Stephen D. Cassivi, Steven E. Schild, and Alex A. Adjei. Non–Small Cell Lung Cancer: Epidemiology, Risk Factors, Treatment, and Survivorship. *Mayo Clin Proc* **83**, 584–594 (2008). https://doi.org:10.4065/83.5.584

15 Niemira, M., Collin, F., Szalkowska, A., Bielska, A., Chwialkowska, K., Reszec, J., Niklinski, J., Kwasniewski, M., Kretowski, A. Molecular Signature of Subtypes of Non-Small-Cell Lung Cancer by Large-Scale Transcriptional Profiling: Identification of Key Modules and Genes by Weighted Gene Co-Expression Network Analysis (WGCNA). *Cancers (Basel)* **12** (2019). https://doi.org:10.3390/cancers12010037

16 Nooreldeen, R., Bach, H. Current and Future Development in Lung Cancer Diagnosis. *Int J Mol Sci* **22** (2021). https://doi.org:10.3390/ijms22168661

17 Michelle Chan-Seng-Yue, J. C. K., Gavin W. Wilson, Karen Ng, Eugenia Flores Figueroa, Grainne M. O'Kane, Ashton A. Connor, Robert E. Denroche, Robert C. Grant, Jessica McLeod, Julie M. Wilson, Gun Ho Jang, Amy Zhang, Anna Dodd, Sheng-Ben Liang, Ayelet Borgida, Dianne Chadwick, Sangeetha Kalimuthu, Ilinca Lungu, John M. S. Bartlett, Paul M. Krzyzanowski, Vandana Sandhu, Hervé Tiriac, Fieke E. M. Froeling, …Faiyaz Notta. Transcription phenotypes of pancreatic cancer are driven by genomic events during tumor evolution. *Nat Genet* **52**, 231-240 (2020). https://doi.org:10.1038/s41588-019-0566-9

18 Peixoto, R. D., Speers, C., McGahan, C. E., Renouf, D. J., Schaeffer, D. F., Kennecke, H. F. Prognostic factors and sites of metastasis in unresectable locally advanced pancreatic cancer. *Cancer Med* **4**, 1171-1177 (2015). https://doi.org:10.1002/cam4.459

19 Miller, M. & Hanna, N. Advances in systemic therapy for non-small cell lung cancer. *BMJ* **375**, n2363 (2021). https://doi.org:10.1136/bmj.n2363

20 Shiravand, Y., Khodadadi, F., Kashani, S. M. A., Hosseini-Fard, S. R., Hosseini, S., Sadeghirad, H., Ladwa, R., O'Byrne, K., Kulasinghe, A. Immune Checkpoint Inhibitors in Cancer Therapy. *Curr Oncol* **29**, 3044-3060 (2022). https://doi.org:10.3390/curroncol29050247

21 Onoi, K., Chihara, Y.,Uchino, J.,Shimamoto, T.,Morimoto, Y., Iwasaku, M., Kaneko, Y.,Yamada, T., Takayama, K. Immune Checkpoint Inhibitors for Lung Cancer Treatment: A Review. *J Clin Med* **9** (2020). https://doi.org:10.3390/jcm9051362

22 Sharma, P., Goswami, S., Raychaudhuri, D. ,Siddiqui, B. A., Singh, P., Nagarajan, A., Liu, J., Subudhi, S. K., Poon, C., Gant, K. L., Herbrich, S. M., Anandhan, S., Islam, S., Amit, M., Anandappa, G., Allison, J. P. Immune checkpoint therapy-current perspectives and future directions. *Cell* **186**, 1652-1669 (2023). https://doi.org:10.1016/j.cell.2023.03.006

23 Musaelyan, A. A., Moiseyenko, F. V., Emileva, T. E., Oganesyan, A. P., Oganyan, K. A., Urtenova, M. A., Odintsova, S. V., Chistyakov, I. V., Degtyarev, A. M., Akopov, A. L., Imyanitov, E. N., Orlov, S. V. Clinical predictors of response to single-agent immune checkpoint inhibitors in chemotherapy-pretreated non-small cell lung cancer. *Mol Clin Oncol* **20**, 32 (2024). https://doi.org:10.3892/mco.2024.2730

24 Majeed, U., Manochakian, R., Zhao, Y. & Lou, Y. Targeted therapy in advanced non-small cell lung cancer: current advances and future trends. *J Hematol Oncol* **14**, 108 (2021). https://doi.org:10.1186/s13045-021-01121-2

25 Imyanitov, E. N., Iyevleva, A. G. & Levchenko, E. V. Molecular testing and targeted therapy for non-small cell lung cancer: Current status and perspectives. *Crit Rev Oncol Hematol* **157**, 103194 (2021). https://doi.org:10.1016/j.critrevonc.2020.103194

26 Wang, M., Herbst, R. S. & Boshoff, C. Toward personalized treatment approaches for non-small-cell lung cancer. *Nat Med* **27**, 1345-1356 (2021). https://doi.org:10.1038/s41591-021-01450-2

27 Alduais, Y., Zhang, H., Fan, F., Chen, J. & Chen, B. Non-small cell lung cancer (NSCLC): A review of risk factors, diagnosis, and treatment. *Medicine (Baltimore)* **102**, e32899 (2023). https://doi.org:10.1097/MD.0000000000032899

28 Rathod, L. S., Dabhade, P. S. & Mokale, S. N. Recent progress in targeting KRAS mutant cancers with covalent G12C-specific inhibitors. *Drug Discov Today* **28**, 103557 (2023). https://doi.org:10.1016/j.drudis.2023.103557

29 Passiglia, F., Listi, A., Castiglia, M., Perez, A., Rizzo, S.. Bazan, V., Russo, A. EGFR inhibition in NSCLC: New findings.... and opened questions? *Crit Rev Oncol Hematol* **112**, 126-135 (2017). https://doi.org:10.1016/j.critrevonc.2017.02.009

30 Gristina, V., La Mantia, M., Iacono, F., Galvano, A., Russo, A., Bazan, V. The Emerging Therapeutic Landscape of ALK Inhibitors in Non-Small Cell Lung Cancer. *Pharmaceuticals (Basel)* **13** (2020). https://doi.org:10.3390/ph13120474

31 Peng, L., Zhu, L., Sun, Y., Stebbing, J., Selvaggi, G., Zhang, Y., Yu, Z. Targeting ALK Rearrangements in NSCLC: Current State of the Art. *Front Oncol* **12**, 863461 (2022). https://doi.org:10.3389/fonc.2022.863461

32 Liu, W. J., Du, Y., Wen, R., Yang, M., Xu, J. Drug resistance to targeted therapeutic strategies in non-small cell lung cancer. *Pharmacol Ther* **206**, 107438 (2020). https://doi.org:10.1016/j.pharmthera.2019.107438

33 Shaw, A. N. H. a. A. T. Resistance looms for KRASG12c inhibitors. *Nature MediciNe* **26**, 164-170 (2020). https://doi.org:10.1038/s41591-020-0765-z

34 Ian A. Prior, P. D. L., and Carla Mattos. A Comprehensive Survey of Ras Mutations in Cancer. *Cancer Resarch* (2010). https://doi.org:10.1158/0008-5472.CAN-11-2612

35 Prior, I. A., Hood, F. E. & Hartley, J. L. The Frequency of Ras Mutations in Cancer. *Cancer Res* **80**, 2969-2974 (2020). https://doi.org:10.1158/0008-5472.CAN-19-3682

36 Molina-Arcas, M., Samani, A. & Downward, J. Drugging the Undruggable: Advances on RAS Targeting in Cancer. *Genes (Basel)* **12** (2021). https://doi.org:10.3390/genes12060899

37 Molina-Arcas, M. & Downward, J. Exploiting the therapeutic implications of KRAS inhibition on tumor immunity. *Cancer Cell* **42**, 338-357 (2024). https://doi.org:10.1016/j.ccell.2024.02.012

38 Gimple, R. C., Wang, X. RAS: Striking at the Core of the Oncogenic Circuitry. *Front Oncol* **9**, 965 (2019). https://doi.org:10.3389/fonc.2019.00965

39 Pantsar, T. The current understanding of KRAS protein structure and dynamics. *Comput Struct Biotechnol J* **18**, 189-198 (2020). https://doi.org:10.1016/j.csbj.2019.12.004

40 Punekar, S. R. V., V. Neel, B. G. Wong, K. K. The current state of the art and future trends in RAS-targeted cancer therapies. *Nat Rev Clin Oncol* (2022). https://doi.org:10.1038/s41571-022-00671-9

41 Downward, J. Targeting RAS signalling pathways in cancer therapy. *Nat Rev Cancer* **3**, 11-22 (2003). https://doi.org:10.1038/nrc969

42 Pylayeva-Gupta, Y., Grabocka, E. & Bar-Sagi, D. RAS oncogenes: weaving a tumorigenic web. *Nat Rev Cancer* **11**, 761-774 (2011). https://doi.org:10.1038/nrc3106

43 Morstein, J., Shrestha, R., Van, Q. N., Lopez, C. A., Arora, N., Tonelli, M., Liang, H., Chen, D., Zhou, Y., Hancock, J. F., Stephen, A. G., Turbyville, T. J., Shokat, K. M. Direct Modulators of K‐Ras−Membrane Interactions. *ACS Chem Biol* **18**, 2082-2093 (2023). https://doi.org:10.1021/acschembio.3c00413

44 Eisenberg, S. & Henis, Y. I. Interactions of Ras proteins with the plasma membrane and their roles in signaling. *Cell Signal* **20**, 31-39 (2008). https://doi.org:10.1016/j.cellsig.2007.07.012

45 Giehl, K. Oncogenic Ras in tumour progression and metastasis. *Biological Chemistry* **386** (2005). https://doi.org:10.1515/BC.2005.025

46 Ruth Nussinov, G. W., Chung-Jung Tsai, Hyunbum Jang, Shaoyong Lu, Avik Banerjee, Jian Zhang, Vadim Gaponenko. Calmodulin and PI3K Signaling in KRAS Cancers. *Trends in cancer* **3**, P214-224 (2017). https://doi.org:10.1016/j.trecan.2017.01.007

47 Nussinov, R., Muratcioglu, S., Tsai, C. J., Jang, H., Gursoy, A., Keskin, O. The Key Role of Calmodulin in KRAS-Driven Adenocarcinomas. *Mol Cancer Res* **13**, 1265-1273 (2015). https://doi.org:10.1158/1541-7786.MCR-15-0165

48 Pupo, E., Avanzato, D., Middonti, E., Bussolino, F. & Lanzetti, L. KRAS-Driven Metabolic Rewiring Reveals Novel Actionable Targets in Cancer. *Front Oncol* **9**, 848 (2019). https://doi.org:10.3389/fonc.2019.00848

49 Laura S Harrington, G. M. F., Richard F Lamb. Restraining PI3K: mTOR signalling goes back to the membrane. *Trends Biochem Sci* **30**, 35-42 (2005). https://doi.org:10.1016/j.tibs.2004.11.003

50 Rodrik-Outmezguine, V. S., Chandarlapaty, S., Pagano, N. C., Poulikakos, P. I., Scaltriti, M., Moskatel, E., Baselga, J., Guichard, S., Rosen, N. mTOR kinase inhibition causes feedback-dependent biphasic regulation of AKT signaling. *Cancer Discov* **1**, 248-259 (2011). https://doi.org:10.1158/2159-8290.CD-11-0085

51 Takano, A., Usui, I., Haruta, T., Kawahara, J., Uno, T., Iwata, M., Kobayashi, M. Mammalian target of rapamycin pathway regulates insulin signaling via subcellular redistribution of insulin receptor substrate 1 and integrates nutritional signals and metabolic signals of insulin. *Mol Cell Biol* **21**, 5050-5062 (2001). https://doi.org:10.1128/MCB.21.15.5050-5062.2001

52 Carracedo, A., Ma, L., Teruya-Feldstein, J., Rojo, F., Salmena, L., Alimonti, A., Egia, A., Sasaki, A. T., Thomas, G., Kozma, S. C., Papa, A., Nardella, C., Cantley, L. C., Baselga, J., Pandolfi, P. P. Inhibition of mTORC1 leads to MAPK pathway activation through a PI3K-dependent feedback loop in human cancer. *J Clin Invest* **118**, 3065-3074 (2008). https://doi.org:10.1172/JCI34739

53 Hunter, J. C., Manandhar, A., Carrasco, M. A., Gurbani, D., Gondi, S., Westover, K. D. Biochemical and Structural Analysis of Common Cancer-Associated KRAS Mutations. *Mol Cancer Res* **13**, 1325-1335 (2015). https://doi.org:10.1158/1541-7786.MCR-15-0203

54 Han, Z., Zhou, D., Wang, J., Jiang, B., Liu, X. Reflections on drug resistance to KRAS(G12C) inhibitors and gene silencing/editing tools for targeting mutant KRAS in cancer treatment. *Biochim Biophys Acta Rev Cancer* **1877**, 188677 (2022). https://doi.org:10.1016/j.bbcan.2022.188677

55 Moore, A. R., Rosenberg, S. C., McCormick, F. & Malek, S. RAS-targeted therapies: is the undruggable drugged? *Nat Rev Drug Discov* **19**, 533-552 (2020). https://doi.org:10.1038/s41573-020-0068-6

56 Ostrem, J. M. & Shokat, K. M. Direct small-molecule inhibitors of KRAS: from structural insights to mechanism-based design. *Nat Rev Drug Discov* **15**, 771-785 (2016). https://doi.org:10.1038/nrd.2016.139

57 Haigis, K. M. KRAS Alleles: The Devil Is in the Detail. *Trends Cancer* **3**, 686-697 (2017). https://doi.org:10.1016/j.trecan.2017.08.006

58 Parikh, K., Banna, G., Liu, S. V., Friedlaender, A., Desai, A., Subbiah, V., Addeo, A. Drugging KRAS: current perspectives and state-of-art review. *J Hematol Oncol* **15**, 152 (2022). https://doi.org:10.1186/s13045-022-01375-4

59 Patricelli, M. P., Janes, M. R., Li, L. S., Hansen, R., Peters, U., Kessler, L. V., Chen, Y., Kucharski, J. M., Feng, J., Ely, T., Chen, J. H., Firdaus, S. J., Babbar, A., Ren, P., Liu, Y. Selective Inhibition of Oncogenic KRAS Output with Small Molecules Targeting the Inactive State. *Cancer Discov* **6**, 316-329 (2016). https://doi.org:10.1158/2159-8290.CD-15-1105

60 Mariyam Zuberi, I. K., John P. O'Bryan. Inhibition of RAS: proven and potential vulnerabilities. *Biochem Soc Trans* **48**, 1831–1841 (2021). https://doi.org:10.1042/BST20190023.

61 Ostrem, J. M., Peters, U., Sos, M. L., Wells, J. A. & Shokat, K. M. K-Ras(G12C) inhibitors allosterically control GTP affinity and effector interactions. *Nature* **503**, 548-551 (2013). https://doi.org:10.1038/nature12796

62 Swann, J. B. & Smyth, M. J. Immune surveillance of tumors. *J Clin Invest* **117**, 1137-1146 (2007). https://doi.org:10.1172/JCI31405

63 Junttila, M. R. & de Sauvage, F. J. Influence of tumour micro-environment heterogeneity on therapeutic response. *Nature* **501**, 346-354 (2013). https://doi.org:10.1038/nature12626

64 Anderson, N. M. & Simon, M. C. The tumor microenvironment. *Curr Biol* **30**, R921-R925 (2020). https://doi.org:10.1016/j.cub.2020.06.081

65 Cui, A., Huang, T., Li, S., Ma, A., Perez, J. L., Sander, C., Keskin, D. B., Wu, C. J., Fraenkel, E., Hacohen, N. Dictionary of immune responses to cytokines at single-cell resolution. *Nature* **625**, 377-384 (2024). https://doi.org:10.1038/s41586-023-06816-9

66 Barar, J. & Omidi, Y. Dysregulated pH in Tumor Microenvironment Checkmates Cancer Therapy. *Bioimpacts* **3**, 149-162 (2013). https://doi.org:10.5681/bi.2013.036

67 Brahimi-Horn, M. C., Chiche, J. & Pouyssegur, J. Hypoxia and cancer. *J Mol Med (Berl)* **85**, 1301-1307 (2007). https://doi.org:10.1007/s00109-007-0281-3

68 John C. Castle, M. U., Simarjot Pabla, Robert B. Stein and Jennifer S. Buell. Mutation-Derived Neoantigens for Cancer Immunotherapy. *Frontiers in Immunology* **10** (2019). https://doi.org:10.3389/fimmu.2019.01856

69 Aguade-Gorgorio, G. & Sole, R. Genetic instability as a driver for immune surveillance. *J Immunother Cancer* **7**, 345 (2019). https://doi.org:10.1186/s40425-019-0795-6

70 Gerard, C. L., Delyon, J., Wicky, A., Homicsko, K., Cuendet, M. A., Michielin, O. Turning tumors from cold to inflamed to improve immunotherapy response. *Cancer Treat Rev* **101**, 102227 (2021). https://doi.org:10.1016/j.ctrv.2021.102227

71 Fearon, J. A. J. a. D. T. T cell exclusion, immune privilege, and the tumor microenvironment. *science* **348** (2015). https://doi.org:10.1126/science.aaa4971

72 Kenneth M. Murphy, C. W., Leslie J. Berg. Janeway's Immunobiology. **10th Edition** (2022).

73 Cornel, A. M., Mimpen, I. L. & Nierkens, S. MHC Class I Downregulation in Cancer: Underlying Mechanisms and Potential Targets for Cancer Immunotherapy. *Cancers (Basel)* **12** (2020). https://doi.org:10.3390/cancers12071760

74 Taylor, B. C. & Balko, J. M. Mechanisms of MHC-I Downregulation and Role in Immunotherapy Response. *Front Immunol* **13**, 844866 (2022). https://doi.org:10.3389/fimmu.2022.844866

75 Dhatchinamoorthy, K., Colbert, J. D. & Rock, K. L. Cancer Immune Evasion Through Loss of MHC Class I Antigen Presentation. *Front Immunol* **12**, 636568 (2021). https://doi.org:10.3389/fimmu.2021.636568

76 Gasser, S. & Raulet, D. H. Activation and self-tolerance of natural killer cells. *Immunol Rev* **214**, 130-142 (2006). https://doi.org:10.1111/j.1600-065X.2006.00460.x

77 Paul, S. & Lal, G. The Molecular Mechanism of Natural Killer Cells Function and Its Importance in Cancer Immunotherapy. *Front Immunol* **8**, 1124 (2017). https://doi.org:10.3389/fimmu.2017.01124

78 Woo, S. R., Corrales, L. & Gajewski, T. F. Innate immune recognition of cancer. *Annu Rev Immunol* **33**, 445-474 (2015). https://doi.org:10.1146/annurev-immunol-032414-112043

79 Sanseviero, E. NK Cell-Fc Receptors Advance Tumor Immunotherapy. *J Clin Med* **8** (2019). https://doi.org:10.3390/jcm8101667

80 Kaltenmeier, C., Simmons, R. L., Tohme, S. & Yazdani, H. O. Neutrophil Extracellular Traps (NETs) in Cancer Metastasis. *Cancers (Basel)* **13** (2021). https://doi.org:10.3390/cancers13236131

81 Rigoni, A., Colombo, M. P. & Pucillo, C. Mast cells, basophils and eosinophils: From allergy to cancer. *Semin Immunol* **35**, 29-34 (2018). https://doi.org:10.1016/j.smim.2018.02.001

82 Poto, R., Gambardella, A. R., Marone, G., Schroeder, J. T., Mattei, F., Schiavoni, G., Varricchi, G. Basophils from allergy to cancer. *Front Immunol* **13**, 1056838 (2022). https://doi.org:10.3389/fimmu.2022.1056838

83 Simon, S. C. S., Utikal, J. & Umansky, V. Opposing roles of eosinophils in cancer. *Cancer Immunol Immunother* **68**, 823-833 (2019). https://doi.org:10.1007/s00262-018-2255-4

84 Khazaie, K., Blatner, N. R., Khan, M. W., Gounari, F., Gounaris, E., Dennis, K., Bonertz, A., Tsai, F. N., Strouch, M. J., Cheon, E., Phillips, J. D., Beckhove, P., Bentrem, D. J. The significant role of mast cells in cancer. *Cancer Metastasis Rev* **30**, 45-60 (2011). https://doi.org:10.1007/s10555-011-9286-z

85 Johanna Verneau, C. S.-F., Cheng-Ming Sun. Dendritic cells in the tumor microenvironment: prognostic and theranostic impact. *Seminars in Immunology, Elsevier* **48** (2020). https://doi.org:10.1016/j.smim.2020.101410.

86 Ji, Z. Z., Chan, M. K., Chan, A. S., Leung, K. T., Jiang, X., To, K. F., Wu, Y., Tang, P. M. Tumour-associated macrophages: versatile players in the tumour microenvironment. *Front Cell Dev Biol* **11**, 1261749 (2023). https://doi.org:10.3389/fcell.2023.1261749

87 Mempel, T. R., Lill, J. K. & Altenburger, L. M. How chemokines organize the tumour microenvironment. *Nat Rev Cancer* **24**, 28-50 (2024). https://doi.org:10.1038/s41568-023-00635-w

88 Nagarsheth, N., Wicha, M. S. & Zou, W. Chemokines in the cancer microenvironment and their relevance in cancer immunotherapy. *Nat Rev Immunol* **17**, 559-572 (2017). https://doi.org:10.1038/nri.2017.49

89 Zhou Y, F. M., Zhang G, Liang WC, Lin W, Wu Y, Piskol R, Ridgway J, McNamara E, Huang H, Zhang J, Oh J, Patel JM, Jakubiak D, Lau J, Blackwood B, Bravo DD, Shi Y, Wang J, Hu HM, Lee WP, Jesudason R, Sangaraju D, Modrusan Z, Anderson KR, Warming S, Roose-Girma M, Yan M. . Blockade of the Phagocytic Receptor MerTK on Tumor-Associated Macrophages Enhances P2X7R-Dependent STING Activation by Tumor-Derived cGAMP. *Immunity* **52**, 357-373 e359 (2020). https://doi.org:10.1016/j.immuni.2020.01.014

90 Blander, J. M. MerTK Blockade Fuels Anti-tumor Immunity. *Immunity* **52**, 212-214 (2020). https://doi.org:10.1016/j.immuni.2020.01.015

91 Sharonov, G. V., Serebrovskaya, E. O., Yuzhakova, D. V., Britanova, O. V. & Chudakov, D. M. B cells, plasma cells and antibody repertoires in the tumour

microenvironment. *Nat Rev Immunol* **20**, 294-307 (2020). https://doi.org:10.1038/s41577-019-0257-x
92 Weinberg, R. A. The Biology of Cancer—3rd International Student Edition. *WW Norton & Co* (2023).
93 Gardner, A. & Ruffell, B. Dendritic Cells and Cancer Immunity. *Trends Immunol* **37**, 855-865 (2016). https://doi.org:10.1016/j.it.2016.09.006
94 Musumeci, A., Lutz, K., Winheim, E. & Krug, A. B. What Makes a pDC: Recent Advances in Understanding Plasmacytoid DC Development and Heterogeneity. *Front Immunol* **10**, 1222 (2019). https://doi.org:10.3389/fimmu.2019.01222
95 Macri, C., Pang, E. S., Patton, T. & O'Keeffe, M. Dendritic cell subsets. *Semin Cell Dev Biol* **84**, 11-21 (2018). https://doi.org:10.1016/j.semcdb.2017.12.009
96 Swiecki, M. & Colonna, M. Unraveling the functions of plasmacytoid dendritic cells during viral infections, autoimmunity, and tolerance. *Immunol Rev* **234**, 142-162 (2010). https://doi.org:10.1111/j.0105-2896.2009.00881.x
97 Swiecki, M., Gilfillan, S., Vermi, W., Wang, Y. & Colonna, M. Plasmacytoid dendritic cell ablation impacts early interferon responses and antiviral NK and CD8(+) T cell accrual. *Immunity* **33**, 955-966 (2010). https://doi.org:10.1016/j.immuni.2010.11.020
98 Heesters, B. A., Myers, R. C. & Carroll, M. C. Follicular dendritic cells: dynamic antigen libraries. *Nat Rev Immunol* **14**, 495-504 (2014). https://doi.org:10.1038/nri3689
99 Storni, T. & Bachmann, M. F. On the role of APC-activation for in vitro versus in vivo T cell priming. *Cell Immunol* **225**, 1-11 (2003). https://doi.org:10.1016/j.cellimm.2003.09.001
100 Hwang, J. R., Byeon, Y., Kim, D., Park, S. G. Recent insights of T cell receptor-mediated signaling pathways for T cell activation and development. *Exp Mol Med* **52**, 750-761 (2020). https://doi.org:10.1038/s12276-020-0435-8
101 Adams, N. M., Grassmann, S. & Sun, J. C. Clonal expansion of innate and adaptive lymphocytes. *Nat Rev Immunol* **20**, 694-707 (2020). https://doi.org:10.1038/s41577-020-0307-4
102 Leidner, R., Sanjuan Silva, N., Huang, H., Sprott, D., Zheng, C., Shih, Y. P., Leung, A., Payne, R., Sutcliffe, K., Cramer, J., Rosenberg, S. A., Fox, B. A., Urba, W. J., Tran, E. Neoantigen T-Cell Receptor Gene Therapy in Pancreatic Cancer. *N Engl J Med* **386**, 2112-2119 (2022). https://doi.org:10.1056/NEJMoa2119662
103 Tran, E., Robbins, P. F., Lu, Y. C., Prickett, T. D., Gartner, J. J., Jia, L., Pasetto, A., Zheng, Z., Ray, S., Groh, E. M., Kriley, I. R., Rosenberg, S. A. T-Cell Transfer Therapy Targeting Mutant KRAS in Cancer. *N Engl J Med* **375**, 2255-2262 (2016). https://doi.org:10.1056/NEJMoa1609279
104 Wang, Q. J., Yu, Z., Griffith, K., Hanada, K., Restifo, N. P., Yang, J. C. Identification of T-cell Receptors Targeting KRAS-Mutated Human Tumors. *Cancer Immunol Res* **4**, 204-214 (2016). https://doi.org:10.1158/2326-6066.CIR-15-0188
105 Raskov, H., Orhan, A., Christensen, J. P. & Gogenur, I. Cytotoxic CD8(+) T cells in cancer and cancer immunotherapy. *Br J Cancer* **124**, 359-367 (2021). https://doi.org:10.1038/s41416-020-01048-4
106 Poncette, L., Bluhm, J. & Blankenstein, T. The role of CD4 T cells in rejection of solid tumors. *Curr Opin Immunol* **74**, 18-24 (2022). https://doi.org:10.1016/j.coi.2021.09.005
107 Speiser, D. E., Chijioke, O., Schaeuble, K. & Munz, C. CD4(+) T cells in cancer. *Nat Cancer* **4**, 317-329 (2023). https://doi.org:10.1038/s43018-023-00521-2
108 Heidi Braumüller, T. W., Ellen Brenner, Sonja Aßmann, Matthias Hahn, Mohammed Alkhaled, Karin Schilbach, Frank Essmann, Manfred

Kneilling, Christoph Griessinger, Felicia Ranta, Susanne Ullrich, Ralph Mocikat, Kilian Braungart, Tarun Mehra, Birgit Fehrenbacher, Julia Berdel, Heike Niessner, Friedegund Meier, Maries van den Broek, Hans-Ulrich Häring, Rupert Handgretinger, Leticia Quintanilla-Martinez, Falko Fend, ⋯ Martin Röcken. T-helper-1-cell cytokines drive cancer into senescence. *Nature* **494**, 361-365 (2013). https://doi.org:10.1038/nature11824

109 Thomas Kammertoens, C. F., Ainhoa Arina, Christian Idel, Dana Briesemeister, Michael Rothe, Andranik Ivanov, Anna Szymborska, Giannino Patone, Severine Kunz, Daniel Sommermeyer, Boris Engels, Matthias Leisegang, Ana Textor, Hans Joerg Fehling, Marcus Fruttiger, Michael Lohoff, Andreas Herrmann, Hua Yu, Ralph Weichselbaum, Wolfgang Uckert, Norbert Hübner, Holger Gerhardt, Dieter Beule, …Thomas Blankenstein. Tumour ischaemia by interferon-gamma resembles physiological blood vessel regression. *Nature* **545**, 98-102 (2017). https://doi.org:10.1038/nature22311

110 Meier, S. L., Satpathy, A. T. & Wells, D. K. Bystander T cells in cancer immunology and therapy. *Nat Cancer* **3**, 143-155 (2022). https://doi.org:10.1038/s43018-022-00335-8

111 Wouter Scheper, S. K., Lorenzo F. Fanchi, Carsten Linnemann, Gavin Bendle, Marije A. J. de Rooij, Christian Hirt, Riccardo Mezzadra, Maarten Slagter, Krijn Dijkstra, Roelof J. C. Kluin, Petur Snaebjornsson, Katy Milne, Brad H. Nelson, Henry Zijlmans, Gemma Kenter, Emile E. Voest, John B. A. G. Haanen & Ton N. Schumacher. Low and variable tumor reactivity of the intratumoral TCR repertoire in human cancers. *Nat Med* **25**, 89-94 (2019). https://doi.org:10.1038/s41591-018-0266-5

112 Baolin Liu, X. H., Kaichao Feng, Ranran Gao, Zhiqiang Xue, Sujie Zhang, Yuanyuan Zhang6, Emily Corse, Yi Hu, Weidong Han and Zemin Zhang. Temporal single-cell tracing reveals clonal revival and expansion of precursor exhausted T cells during anti-PD-1 therapy in lung cancer. *NATURE CANCER* (2021). https://doi.org:10.1038/s43018-021-00292-8

113 Laumont, C. M., Banville, A. C., Gilardi, M., Hollern, D. P. & Nelson, B. H. Tumour-infiltrating B cells: immunological mechanisms, clinical impact and therapeutic opportunities. *Nat Rev Cancer* **22**, 414-430 (2022). https://doi.org:10.1038/s41568-022-00466-1

114 Heath, W. R., Kato, Y., Steiner, T. M. & Caminschi, I. Antigen presentation by dendritic cells for B cell activation. *Curr Opin Immunol* **58**, 44-52 (2019). https://doi.org:10.1016/j.coi.2019.04.003

115 Teillaud, J. L. & Dieu-Nosjean, M. C. Intratumoral plasma cells: More than a predictive marker of response to anti-PD-L1 treatment in lung cancer? *Cancer Cell* (2022). https://doi.org:10.1016/j.ccell.2022.02.008

116 Schumacher, T. N. & Thommen, D. S. Tertiary lymphoid structures in cancer. *Science* **375**, eabf9419 (2022). https://doi.org:10.1126/science.abf9419

117 Sautes-Fridman, C., Lawand, M., Giraldo, N. A., Kaplon, H., Germain, C., Fridman, W. H., Dieu-Nosjean, M. C. Tertiary Lymphoid Structures in Cancers: Prognostic Value, Regulation, and Manipulation for Therapeutic Intervention. *Front Immunol* **7**, 407 (2016). https://doi.org:10.3389/fimmu.2016.00407

118 Dieu‐Nosjean, M. C., Giraldo, Nicolas A., Kaplon, Hélène, Germain, Claire, Fridman, Wolf Herman, Sautès‐Fridman, Catherine. Tertiary lymphoid structures, drivers of the anti‐tumor responses in human cancers. *Immunological Reviews* **271**, 260-275 (2016). https://doi.org:10.1111/imr.12405

119 Beth A. Helmink, S. M. R., Jianjun Gao, Shaojun Zhang, Rafet Basar, Rohit Thakur, Keren Yizhak, Moshe Sade-Feldman, Jorge Blando, Guangchun

Han, Vancheswaran Gopalakrishnan, Yuanxin Xi, Hao Zhao, Rodabe N. Amaria, Hussein A. Tawbi, Alex P. Cogdill, Wenbin Liu, Valerie S. LeBleu, Fernanda G. Kugeratski, Sapna Patel, Michael A. Davies, Patrick Hwu, Jeffrey E. Lee, Jeffrey E. Gershenwald, …Jennifer A. Wargo. B cells and tertiary lymphoid structures promote immunotherapy response. *Nature* **577**, 549-555 (2020). https://doi.org:10.1038/s41586-019-1922-8

120 Florent Petitprez, A. d. R., Emily Z. Keung, Tom Wei-Wu Chen, Cheng-Ming Sun, Julien Calderaro, Yung-Ming Jeng, Li-Ping Hsiao, Laetitia Lacroix, Antoine Bougoüin, Marco Moreira, Guillaume Lacroix, Ivo Natario, Julien Adam, Carlo Lucchesi, Yec′ han Laizet, Maud Toulmonde, Melissa A. Burgess, Vanessa Bolejack, Denise Reinke, Khalid M. Wani, Wei-Lien Wang, Alexander J. Lazar, Christina L. Roland, ⋯Wolf H. Fridman. B cells are associated with survival and immunotherapy response in sarcoma. *Nature* **577**, 556-560 (2020). https://doi.org:10.1038/s41586-019-1906-8

121 Rita Cabrita, M. L., Adriana Sanna, Marco Donia, Mathilde Skaarup Larsen, Shamik Mitra, Iva Johansson, Bengt Phung, Katja Harbst, Johan Vallon-Christersson, Alison van Schoiack, Kristina Lövgren, Sarah Warren, Karin Jirström, Håkan Olsson, Kristian Pietras, Christian Ingvar, Karolin Isaksson, Dirk Schadendorf, Henrik Schmidt, Lars Bastholt, Ana Carneiro, Jennifer A. Wargo, Inge Marie Svane & Göran Jönsson. Tertiary lymphoid structures improve immunotherapy and survival in melanoma. *Nature* **577**, 561-565 (2020). https://doi.org:10.1038/s41586-019-1914-8

122 Kevin W. Ng, J. B., Katey S. S. Enfield, Jorge Almagro, Hongui Cha, Oriol Pich, Takahiro Karasaki, David A. Moore, Roberto Salgado, Monica Sivakumar, George Young, Miriam Molina-Arcas, Sophie de Carné Trécesson, Panayiotis Anastasiou, Annika Fendler, Lewis Au, Scott T. C. Shepherd, Carlos Martínez-Ruiz, Clare Puttick, James R. M. Black, Thomas B. K. Watkins, Hyemin Kim, Seohee Shim, Nikhil Faulkner, TRACERx Consortium, CAPTURE Consortium, …George Kassiotis. Antibodies against endogenous retroviruses promote lung cancer immunotherapy. *Nature* (2023). https://doi.org:10.1038/s41586-023-05771-9

123 Fenton, S. E., Saleiro, D. & Platanias, L. C. Type I and II Interferons in the Anti-Tumor Immune Response. *Cancers (Basel)* **13** (2021). https://doi.org:10.3390/cancers13051037

124 Han, J., Khatwani, N., Searles, T. G., Turk, M. J. & Angeles, C. V. Memory CD8(+) T cell responses to cancer. *Semin Immunol* **49**, 101435 (2020). https://doi.org:10.1016/j.smim.2020.101435

125 Schluns, K. S. & Lefrancois, L. Cytokine control of memory T-cell development and survival. *Nat Rev Immunol* **3**, 269-279 (2003). https://doi.org:10.1038/nri1052

126 Megan A. Coopera, b., Julie M. Elliotta, Peter A. Keyela, Liping Yanga, Javier A. Carreroc, and Wayne M. Yokoyamaa. Cytokine-induced memory-like natural killer cells. *PNAS* **106**, 1915–1919 (2009). https://doi.org:10.1073 pnas.0813192106

127 Rizwan Romee, M. R., Melissa M. Berrien-Elliott, Julia A. Wagner, Brea A. Jewell, Timothy Schappe, Jeffrey W. Leong, Sara Abdel-Latif, Stephanie E. Schneider, Sarah Willey, Carly C. Neal, Liyang Yu, Stephen T. Oh, Yi-Shan Lee, Arend Mulder, Frans Claas, Megan A. Cooper, Todd A. Fehniger. Cytokine-induced memory-like natural killer cells exhibit enhanced responses against myeloid leukemia. *Sci Transl Med* **8**, 357ra123 (2016). https://doi.org:10.1126/scitranslmed.aaf2341

128 Cerwenka, A. & Lanier, L. L. Natural killer cell memory in infection, inflammation and cancer. *Nat Rev Immunol* **16**, 112-123 (2016). https://doi.org:10.1038/nri.2015.9
129 Mortezaee, K. Immune escape: A critical hallmark in solid tumors. *Life Sci* **258**, 118110 (2020). https://doi.org:10.1016/j.lfs.2020.118110
130 Wellenstein, M. D. & de Visser, K. E. Cancer-Cell-Intrinsic Mechanisms Shaping the Tumor Immune Landscape. *Immunity* **48**, 399-416 (2018). https://doi.org:10.1016/j.immuni.2018.03.004
131 Sundaram, G. M., Quah, S. & Sampath, P. Cancer: the dark side of wound healing. *FEBS J* **285**, 4516-4534 (2018). https://doi.org:10.1111/febs.14586
132 Meng, X., Zhong, J., Liu, S., Murray, M. & Gonzalez-Angulo, A. M. A new hypothesis for the cancer mechanism. *Cancer Metastasis Rev* **31**, 247-268 (2012). https://doi.org:10.1007/s10555-011-9342-8
133 Chen, S., Crabill, G. A., Pritchard, T. S., McMiller, T. L., Wei, P., Pardoll, D. M., Pan, F., Topalian, S. L. Mechanisms regulating PD-L1 expression on tumor and immune cells. *J Immunother Cancer* **7**, 305 (2019). https://doi.org:10.1186/s40425-019-0770-2
134 Zheng, Y., Fang, Y. C. & Li, J. PD-L1 expression levels on tumor cells affect their immunosuppressive activity. *Oncol Lett* **18**, 5399-5407 (2019). https://doi.org:10.3892/ol.2019.10903
135 Shi, Y. Regulatory mechanisms of PD-L1 expression in cancer cells. *Cancer Immunol Immunother* **67**, 1481-1489 (2018). https://doi.org:10.1007/s00262-018-2226-9
136 van Maldegem, F. & Downward, J. Mutant KRAS at the Heart of Tumor Immune Evasion. *Immunity* **52**, 14-16 (2020). https://doi.org:10.1016/j.immuni.2019.12.013
137 Terry R. Medler, T. C., and Lisa M. Coussens. Immune Response to Cancer Therapy: Mounting an Effective Antitumor Response and Mechanisms of Resistance. *Trends in Cancer* **1** (2015).
138 Xu C, J. G., Wu H, Cui W, Wang YH, Manne RK, Wang G, Zhang W, Zhang X, Han F, Cai Z, Pan BS, Hsu CC, Liu Y, Zhang A, Long J, Zou H, Wang S, Ma X, Duan J, Wang B, Liu W, Lan H, Xiong Q, Xue G, Chen Z, Xu Z, Furth ME, Haigh Molina S, Lu Y, Xie D, Bian XW, Lin HK. SIRPgamma-expressing cancer stem-like cells promote immune escape of lung cancer via Hippo signaling. *J Clin Invest* **132** (2022). https://doi.org:10.1172/JCI141797
139 Alausa, A., Lawal, K. A., Babatunde, O. A., Obiwulu, E. N. O., Oladokun, O. C., Fadahunsi, O. S., Celestine, U. O., Moses, E. U., Akaniro, I. R., Adegbola, P. I. Overcoming immunotherapeutic resistance in PDAC: SIRPalpha-CD47 blockade. *Pharmacol Res* **181**, 106264 (2022). https://doi.org:10.1016/j.phrs.2022.106264
140 Nishikawa, H. & Sakaguchi, S. Regulatory T cells in tumor immunity. *Int J Cancer* **127**, 759-767 (2010). https://doi.org:10.1002/ijc.25429
141 Giovanna Borsellino, M. K., Diletta Di Mitri, Alexander Sternjak, Adamo Diamantini, Raffaella Giometto, Sabine Höpner, Diego Centonze, Giorgio Bernardi, Maria Luisa Dell'Acqua, Paolo Maria Rossini, Luca Battistini, Olaf Rötzschke, Kirsten Falk. Expression of ectonucleotidase CD39 by Foxp3+ Treg cells: hydrolysis of extracellular ATP and immune suppression. *Blood* **110**, 1225-1232 (2007). https://doi.org:10.1182/blood-2006-12-064527
142 Law, A. M. K., Valdes-Mora, F. & Gallego-Ortega, D. Myeloid-Derived Suppressor Cells as a Therapeutic Target for Cancer. *Cells* **9** (2020). https://doi.org:10.3390/cells9030561
143 Dysthe, M., Parihar, R. Myeloid-Derived Suppressor Cells in the Tumor Microenvironment. In: Birbrair, A. (eds) Tumor Microenvironment. Advances in

Experimental Medicine and Biology. *Springer, Cham.* **1224**, pp 117–140 (2020). https://doi.org:10.1007/978-3-030-35723-8_8

144 Gabrilovich, D. I. Myeloid-Derived Suppressor Cells. *Cancer Immunol Res* **5**, 3-8 (2017). https://doi.org:10.1158/2326-6066.CIR-16-0297

145 Cendrowicz, E., Sas, Z., Bremer, E. & Rygiel, T. P. The Role of Macrophages in Cancer Development and Therapy. *Cancers (Basel)* **13** (2021). https://doi.org:10.3390/cancers13081946

146 Liu, J., Geng, X., Hou, J. & Wu, G. New insights into M1/M2 macrophages: key modulators in cancer progression. *Cancer Cell Int* **21**, 389 (2021). https://doi.org:10.1186/s12935-021-02089-2

147 Zeng XY, X. H., Yuan J, Jiang XY, Yong JH, Zeng D, Dou YY, Xiao SS. M2-like tumor-associated macrophages-secreted EGF promotes epithelial ovarian cancer metastasis via activating EGFR-ERK signaling and suppressing lncRNA LIMT expression. *Cancer Biol Ther* **20**, 956-966 (2019). https://doi.org:10.1080/15384047.2018.1564567

148 Lu Gao, F.-q. W., Hui-min Li, Jie-gang Yang, Jian-Gang Ren, Ke-fei, He, Bing Liu, Wei Zhang, Yi-Fang Zhao. CCL2/EGF positive feedback loop between cancer cells and macrophages promotes cell migration and invasion in head and neck squamous cell carcinoma. *Oncotarget* **7**, 87037-87051 (2016). https://doi.org:10.18632

149 Saito, Y., Komori, S., Kotani, T., Murata, Y. & Matozaki, T. The Role of Type-2 Conventional Dendritic Cells in the Regulation of Tumor Immunity. *Cancers (Basel)* **14** (2022). https://doi.org:10.3390/cancers14081976

150 Peng, Q., Qiu, X., Zhang, Z., Zhang, S., Zhang, Y., Liang, Y., Guo, J., Peng, H., Chen, M., Fu, Y. X., Tang, H. PD-L1 on dendritic cells attenuates T cell activation and regulates response to immune checkpoint blockade. *Nat Commun* **11**, 4835 (2020). https://doi.org:10.1038/s41467-020-18570-x

151 Demkow, U. Neutrophil Extracellular Traps (NETs) in Cancer Invasion, Evasion and Metastasis. *Cancers (Basel)* **13** (2021). https://doi.org:10.3390/cancers13174495

152 Antuamwine, B. B., Bosnjakovic, R., Hofmann-Vega, F., Wang, X., Theodosiou, T., Iliopoulos, I., Brandau, S. N1 versus N2 and PMN-MDSC: A critical appraisal of current concepts on tumor-associated neutrophils and new directions for human oncology. *Immunol Rev* **314**, 250-279 (2023). https://doi.org:10.1111/imr.13176

153 Tiwari, A., Oravecz, Tamas, Dillon, Laura A., Taliano, Antoine, Audoly, Laurent, Fridman, Wolf Hervé, Clifton, Guy Travis. Towards a consensus definition of immune exclusion in cancer. *Frontiers in Immunology* **14** (2023). https://doi.org:10.3389/fimmu.2023.1084887

154 Mortezaee, K. & Majidpoor, J. The impact of hypoxia on immune state in cancer. *Life Sci* **286**, 120057 (2021). https://doi.org:10.1016/j.lfs.2021.120057

155 Coelho MA, d. C. T. S., Rana S, Zecchin D, Moore C, Molina-Arcas M, East P, Spencer-Dene B, Nye E, Barnouin K, Snijders AP, Lai WS, Blackshear PJ, Downward J. Oncogenic RAS Signaling Promotes Tumor Immunoresistance by Stabilizing PD-L1 mRNA. *Immunity* **47**, 1083-1099 e1086 (2017). https://doi.org:10.1016/j.immuni.2017.11.016

156 Nan Chen, W. F., Zhong Lin, Peijian Peng, Juan Wang, Jianhua Zhan, Shaodong Hong, Jiaxing Huang, Lin Liu, Jin Sheng, Ting Zhou, Ying Chen, Hongyu Zhang & Li Zhang. KRAS mutation-induced upregulation of PD-L1 mediates immune escape in human lung adenocarcinoma. *Cancer Immunology, Immunotherapy* **66**, 1175-1187 (2017). https://doi.org:10.1007/s00262-017-2005-z

157 Liu, H., Liang, Z., Cheng, S., Huang, L., Li, W., Zhou, C., Zheng, X., Li, S., Zeng, Z., Kang, L. Mutant KRAS Drives Immune Evasion by Sensitizing Cytotoxic T-Cells to Activation-Induced Cell Death in Colorectal Cancer. *Adv Sci (Weinh)* **10**, e2203757 (2023). https://doi.org:10.1002/advs.202203757

158 Kim, M. J. & Ha, S. J. Differential Role of PD-1 Expressed by Various Immune and Tumor Cells in the Tumor Immune Microenvironment: Expression, Function, Therapeutic Efficacy, and Resistance to Cancer Immunotherapy. *Front Cell Dev Biol* **9**, 767466 (2021). https://doi.org:10.3389/fcell.2021.767466

159 Sukhbir Kaur, J. S. I., David D. Roberts. CD47 (Cluster of Differentiation 47). *Atlas Genet Cytogenet Oncol Haematol.* **25**, 83–102 (2021). https://doi.org:10.3109/10409238.2015.1014024

160 Hu, H., Cheng, R., Wang, Y., Wang, X., Wu, J., Kong, Y., Zhan, S., Zhou, Z., Zhu, H., Yu, R., Liang, G., Wang, Q., Zhu, X., Zhang, C. Y., Yin, R., Yan, C., Chen, X. Oncogenic KRAS signaling drives evasion of innate immune surveillance in lung adenocarcinoma by activating CD47. *J Clin Invest* **133** (2023). https://doi.org:10.1172/JCI153470

161 Steele CW, K. S., Leach JDG, Bailey P, Upstill-Goddard R, Rishi L, Foth M, Bryson S, McDaid K, Wilson Z, Eberlein C, Candido JB, Clarke M, Nixon C, Connelly J, Jamieson N, Carter CR, Balkwill F, Chang DK, Evans TRJ, Strathdee D, Biankin AV, Nibbs RJB, Barry ST, Sansom OJ, Morton JP. CXCR2 Inhibition Profoundly Suppresses Metastases and Augments Immunotherapy in Pancreatic Ductal Adenocarcinoma. *Cancer Cell* **29**, 832-845 (2016). https://doi.org:10.1016/j.ccell.2016.04.014

162 Wenting Liao, M. J. O., Adam T. Boutin, Xiaoying Shang, Di Zhao, Prasenjit Dey, Jiexi L Guocan Wang, Zhengdao Lan, Jun Li, Ming Tang, Shan Jiang, Xingdi Ma, Peiwen Chen, Riham Katkhuda, Krittiya Korphaisarn, Deepavali Chakravarti, AndrewChang, Ronald A. DePinho. KRAS-IRF2 Axis Drives Immune Suppression and Immune Therapy Resistance in Colorectal Cancer. *Cancer cell* **35**, 559-572.e557 (2019). https://doi.org:10.1016/j.ccell.2019.02.008

163 Ji H, H. A., Mariani TJ, Perera S, Kim CB, Padera R, Tonon G, McNamara K, Marconcini LA, Hezel A, El-Bardeesy N, Bronson RT, Sugarbaker D, Maser RS, Shapiro SD, Wong KK. K-ras activation generates an inflammatory response in lung tumors. *Oncogene* **25**, 2105-2112 (2006). https://doi.org:10.1038/sj.onc.1209237

164 Sparmann, A. & Bar-Sagi, D. Ras-induced interleukin-8 expression plays a critical role in tumor growth and angiogenesis. *Cancer Cell* **6**, 447-458 (2004). https://doi.org:10.1016/j.ccr.2004.09.028

165 Pylayeva-Gupta, Y., Lee, K. E., Hajdu, C. H., Miller, G. & Bar-Sagi, D. Oncogenic Kras-induced GM-CSF production promotes the development of pancreatic neoplasia. *Cancer Cell* **21**, 836-847 (2012). https://doi.org:10.1016/j.ccr.2012.04.024

166 Hamarsheh, S., Gross, O., Brummer, T., Zeiser, R. Immune modulatory effects of oncogenic KRAS in cancer. *Nat Commun* **11**, 5439 (2020). https://doi.org:10.1038/s41467-020-19288-6

167 Zehua Zhu , A. R. A., Travis J Cohoon, Thanh U Barbie, Yu Imamura, Shenghong Yang, Susan E Moody, Rhine R Shen, Anna C Schinzel, Tran C Thai, Jacob B Reibel, Pablo Tamayo, Jason T Godfrey, Zhi Rong Qian, Asher N Page, Karolina Maciag, Edmond M Chan, Whitney Silkworth, Mary T Labowsky, Lior Rozhansky, Jill P Mesirov, William E Gillanders, Shuji Ogino, Nir Hacohen, Suzanne Gaudet, Michael J Eck, Jeffrey A Engelman, Ryan B Corcoran, Kwok-Kin Wong, William C Hahn, David A Barbie. Inhibition of KRAS-driven

tumorigenicity by interruption of an autocrine cytokine circuit. *Cancer Discov* **4**, 452-465 (2014). https://doi.org:10.1158/2159-8290.CD-13-0646

168 Caetano, M. S., Zhang, H., Cumpian, A. M., Gong, L., Unver, N., Ostrin, E. J., Daliri, S., Chang, S. H., Ochoa, C. E., Hanash, S., Behrens, C., Wistuba,, II, Sternberg, C., Kadara, H., Ferreira, C. G., Watowich, S. S., Moghaddam, S. J. IL6 Blockade Reprograms the Lung Tumor Microenvironment to Limit the Development and Progression of K-ras-Mutant Lung Cancer. *Cancer Res* **76**, 3189-3199 (2016). https://doi.org:10.1158/0008-5472.CAN-15-2840

169 Massague, J. & Sheppard, D. TGF-beta signaling in health and disease. *Cell* **186**, 4007-4037 (2023). https://doi.org:10.1016/j.cell.2023.07.036

170 Zdanov S, M. M., Abu Eid R, Adamson-Fadeyi S, Wilson W, Qian J, Carnie A, Tarasova N, Mkrtichyan M, Berzofsky JA, Whiteside TL, Khleif SN. Mutant KRAS Conversion of Conventional T Cells into Regulatory T Cells. *Cancer Immunol Res* **4**, 354-365 (2016). https://doi.org:10.1158/2326-6066.CIR-15-0241

171 Kortlever, R. M., Sodir, N. M., Wilson, C. H., Burkhart, D. L., Pellegrinet, L., Brown Swigart, L., Littlewood, T. D., Evan, G. I. Myc Cooperates with Ras by Programming Inflammation and Immune Suppression. *Cell* **171**, 1301-1315 e1314 (2017). https://doi.org:10.1016/j.cell.2017.11.013

172 Edurne Mugarza, F. v. M., Jesse Boumelha, Christopher Moore, Sareena Rana, & Miriam Llorian Sopena, P. E., Rachel Ambler, Panayiotis Anastasiou, Pablo Romero-Clavijo, Karishma Valand, Megan Cole, Miriam Molina-Arcas, Julian Downward. Therapeutic KRASG12C inhibition drives effectiveinterferon-mediated antitumor immunity in immunogenic lung cancers. *Scientiffic advances* **8** (2022). https://doi.org:10.1126/sciadv.abm8780

173 Muthalagu N, M. T., Raffo-Iraolagoitia X, Wiesheu R, Whyte D, Hedley A, Laing S, Kruspig B, Upstill-Goddard R, Shaw R, Neidler S, Rink C, Karim SA, Gyuraszova K, Nixon C, Clark W, Biankin AV, Carlin LM, Coffelt SB, Sansom OJ, Morton JP, Murphy DJ. Repression of the Type I Interferon Pathway Underlies MYC- and KRAS-Dependent Evasion of NK and B Cells in Pancreatic Ductal Adenocarcinoma. *Cancer Discov* **10**, 872-887 (2020). https://doi.org:10.1158/2159-8290.CD-19-0620

174 Han, Y., Lee, T., He, Y., Raman, R., Irizarry, A., Martin, M. L., Giaccone, G. The regulation of CD73 in non-small cell lung cancer. *Eur J Cancer* **170**, 91-102 (2022). https://doi.org:10.1016/j.ejca.2022.04.025

175 Chiarella, A. M., Ryu, Y. K., Manji, G. A. & Rustgi, A. K. Extracellular ATP and Adenosine in Cancer Pathogenesis and Treatment. *Trends Cancer* **7**, 731-750 (2021). https://doi.org:10.1016/j.trecan.2021.04.008

176 Boumelha J, d. C. A., Bah N, Cha H, de Carné Trécesson S, Rana S, Tomaschko M, Anastasiou P, Mugarza E, Moore C, Goldstone R, East P, Litchfield K, Lee SH, Molina-Arcas M, Downward J. . CRISPR/Cas9 screen identifies KRAS-induced COX-2 as a driver of immunotherapy resistance in lung cancer. *BioRxiv* (2023). https://doi.org:10.1101/2023.04.13.536740

177 Pelly VS, M. A., Roelofsen LM, Bonavita E, Bell CR, Hutton C, Blanco-Gomez A, Banyard A, Bromley CP, Flanagan E, Chiang SC, Jørgensen C, Schumacher TN, Thommen DS, Zelenay S. . Anti-Inflammatory Drugs Remodel the Tumor Immune Environment to Enhance Immune Checkpoint Blockade Efficacy. *Cancer Discov* **11**, 2602-2619 (2021). https://doi.org:10.1158/2159-8290.CD-20-1815

178 Huang, L., Guo, Z., Wang, F. & Fu, L. KRAS mutation: from undruggable to druggable in cancer. *Signal Transduct Target Ther* **6**, 386 (2021). https://doi.org:10.1038/s41392-021-00780-4

179 Liu, S., Liu, T., Jiang, J., Guo, H. & Yang, R. p53 mutation and deletion contribute to tumor immune evasion. *Front Genet* **14**, 1088455 (2023). https://doi.org:10.3389/fgene.2023.1088455

180 Skoulidis F, B. L., Diao L, Papadimitrakopoulou VA, Tong P, Izzo J, Behrens C, Kadara H, Parra ER, Canales JR, Zhang J, Giri U, Gudikote J, Cortez MA, Yang C, Fan Y, Peyton M, Girard L, Coombes KR, Toniatti C, Heffernan TP, Choi M, Frampton GM, Miller V, Weinstein JN, Herbst RS, Wong KK, Zhang J, Sharma P, Mills GB, Hong WK, Minna JD, Allison JP, Futreal A, Wang J, Wistuba II, Heymach JV. Co-occurring genomic alterations define major subsets of KRAS-mutant lung adenocarcinoma with distinct biology, immune profiles, and therapeutic vulnerabilities. *Cancer Discov* **5**, 860-877 (2015). https://doi.org:10.1158/2159-8290.CD-14-1236

181 Jiehui Deng, A. T., Igor Dolgalev, Ting Chen, Jie Li, Antonio Marzio, John T. Poirier, David H. Peng, Mirna Bulatovic, Subhadip Mukhopadhyay, Heather Silver, Eleni Papadopoulos, Val Pyon, Cassandra Thakurdin, Han Han, Fei Li, Shuai Li, Hailin Ding, Hai Hu, Yuanwang Pan, Vajira Weerasekara, Baishan Jiang, Eric S. Wang, Ian Ahearn, …Kwok-Kin Wong. ULK1 inhibition overcomes compromised antigen presentation and restores antitumor immunity in LKB1 mutant lung cancer. *Nat Cancer* **2**, 503-514 (2021). https://doi.org:10.1038/s43018-021-00208-6

182 Koyama S, A. E., Li YY, Aref AR, Skoulidis F, Herter-Sprie GS, Buczkowski KA, Liu Y, Awad MM, Denning WL, Diao L, Wang J, Parra-Cuentas ER, Wistuba II, Soucheray M, Thai T, Asahina H, Kitajima S, Altabef A, Cavanaugh JD, Rhee K, Gao P, Zhang H, Fecci PE, Shimamura T, Hellmann MD, Heymach JV, Hodi FS, Freeman GJ, Barbie DA, Dranoff G, Hammerman PS, Wong KK. STK11/LKB1 Deficiency Promotes Neutrophil Recruitment and Proinflammatory Cytokine Production to Suppress T-cell Activity in the Lung Tumor Microenvironment. *Cancer Res* **76**, 999-1008 (2016). https://doi.org:10.1158/0008-5472.CAN-15-1439

183 Kitajima S, I. E., Guo S, Yoshida R, Campisi M, Sundararaman SK, Tange S, Mitsuishi Y, Thai TC, Masuda S, Piel BP, Sholl LM, Kirschmeier PT, Paweletz CP, Watanabe H, Yajima M, Barbie DA. Suppression of STING Associated with LKB1 Loss in KRAS-Driven Lung Cancer. *Cancer Discov* **9**, 34-45 (2019). https://doi.org:10.1158/2159-8290.CD-18-0689

184 Cristescu R, M. R., Ayers M, Albright A, Murphy E, Yearley J, Sher X, Liu XQ, Lu H, Nebozhyn M, Zhang C, Lunceford JK, Joe A, Cheng J, Webber AL, Ibrahim N, Plimack ER, Ott PA, Seiwert TY, Ribas A, McClanahan TK, Tomassini JE, Loboda A, Kaufman D. Pan-tumor genomic biomarkers for PD-1 checkpoint blockade-based immunotherapy. *Science* **362** (2018). https://doi.org:10.1126/science.aar3593

185 Marzio, A., Kurz, E., Sahni, J. M., Di Feo, G., Puccini, J., Jiang, S., Hirsch, C. A., Arbini, A. A., Wu, W. L.. Pass, H. I., Bar-Sagi, D.,. Papagiannakopoulos, T., Pagano, M. EMSY inhibits homologous recombination repair and the interferon response, promoting lung cancer immune evasion. *Cell* **185**, 169-183 e119 (2022). https://doi.org:10.1016/j.cell.2021.12.005

186 Manasi K. Mayekar, D. R. C., Natalie I. Vokes, Emily K. Law, Wei Wu, William Hill, Eva Gronroos, Andrew Rowan, Maise Al Bakir, Caroline E. McCoach, Collin M. Blakely, Nuri Alpay Temiz, Ai Nagano, D. Lucas Kerr, Julia K. Rotow, View ProfileFranziska Haderk, Michelle Dietzen, Carlos Martinez Ruiz, Bruna Almeida, Lauren Cech, Beatrice Gini, Joanna Przewrocka, Chris Moore, Miguel Murillo, Bjorn Bakker, Brandon Rule, Cameron Durfee, Shigeki Nanjo, Lisa Tan, Lindsay K. Larson, Prokopios P. Argyris, William L. Brown, Johnny Yu, Carlos Gomez, Philippe Gui, Rachel I. Vogel, Elizabeth A. Yu, Nicholas J. Thomas,

Subramanian Venkatesan, Sebastijan Hobor, Su Kit Chew, Nnennaya Kanu, Nicholas McGranahan, Eliezer M. Van Allen, Julian Downward, Reuben S. Harris, Trever G. Bivona, Charles Swanton. Targeted cancer therapy induces APOBEC fuelling the evolution of drug resistance. *bioRxiv preprint* (2020). https://doi.org:10.1101/2020.12.18.423280

187 Luis M. Cortez, A. L. B., Madeline A. Dennis, Christopher D. Collins, Alexander J. Brown, Debra Mitchell, Tony M. Mertz, Steven A. Roberts. APOBEC3A is a prominent cytidine deaminase
in breast cancer. *PLoS Genet* **15**, e1008545 (2019). https://doi.org:10.1371/journal.pgen.1008545

188 Burns, M. B., Temiz, N. A. & Harris, R. S. Evidence for APOBEC3B mutagenesis in multiple human cancers. *Nat Genet* **45**, 977-983 (2013). https://doi.org:10.1038/ng.2701

189 Sonja M. Wörmann, A. Z., Fredrik I. Thege, Robert W. Cowan, Dhwani N. Rupani, Runsheng Wang, Sara L. Manning, Chris Gates, Weisheng Wu, Rena Levin-Klein, Kimal I. Rajapakshe, Meifang Yu, Asha S. Multani, Ya'an Kang, Cullen M. Taniguchi, & Katharina Schlacher, M. D. B., Matthew H. G. Katz, Michael P. Kim, Jason B. Fleming, Steven Gallinger, Ravikanth Maddipati, Reuben S. Harris, Faiyaz Notta, Susan R. Ross, Anirban Maitra, and Andrew D. Rhim. APOBEC3A drives deaminase domain-independent chromosomal instability to promote pancreatic cancer metastasis. *NATuRE CANCER* **2**, 1338–1356 (2021). https://doi.org:10.1038/s43018-021-00268-8

190 John Maciejowski, A. C., Alexandra Dananberg, Kevan Chu, Eleonore Toufektchan, Leszek J. Klimczak, Dmitry A. Gordenin, Peter J. Campbell, Titia de Lange. APOBEC3-dependent kataegis and TREX1-driven chromothripsis during telomere crisis. *Nature Genetics* **52**, 884–890 (2020). https://doi.org:10.1038/s41588-020-0667-5

191 Subramanian Venkatesan, M. A., Clare Puttick, Haoran Zhai, Deborah R. Caswell, Wei-Ting Lu, Michelle Dietzen, Panagiotis Galanos, Konstantinos Evangelou, Roberto Bellelli, Emilia L. Lim, Thomas B.K. Watkins, Andrew Rowan, Vitor H. Teixeira, Yue Zhao, Haiquan Chen, Bryan Ngo, Lykourgos-Panagiotis Zalmas, Maise Al Bakir, Sebastijan Hobor, Eva Grönroos, Adam Pennycuick, Ersilia Nigro, Brittany B. Campbell, William L. Brown, Ayse U. Akarca, Teresa Marafioti, Mary Y. Wu, Michael Howell, Simon J. Boulton, Cosetta Bertoli, Tim R. Fenton, Robertus A.M. de Bruin, Apolinar Maya-Mendoza, Eric Santoni-Rugiu, Robert E. Hynds, Vassilis G. Gorgoulis, Mariam Jamal-Hanjani,Nicholas McGranahan, Reuben S. Harris, Sam M. Janes, Jirina Bartkova, Samuel F. Bakhoum, Jiri Bartek, Nnennaya Kanu, and Charles Swanton1,2,26 on behalf of the TRACERx Consortium. Induction of APOBEC3 Exacerbates DNA Replication Stress and Chromosomal Instability in Early Breast and Lung Cancer Evolution. *CANCER DISCOVERY* **2456** (2021). https://doi.org:10.1158/2159-8290.CD-20-0725

192 Joseph C.F. Ng, J. Q., Anita Grigoriadis, Michael H. Malim and & Fraternali, F. Pan-cancer transcriptomic analysis dissects immune and proliferative functions of APOBEC3 cytidine deaminases. *Nucleic Acids Research* **47**, 1178–1194 (2019). https://doi.org:10.1093/nar/gky1316

193 Nagasaka, M., Li, Y., Sukari, A., Ou, S. I., Al-Hallak, M. N., Azmi, A. S. KRAS G12C Game of Thrones, which direct KRAS inhibitor will claim the iron throne? *Cancer Treat Rev* **84**, 101974 (2020). https://doi.org:10.1016/j.ctrv.2020.101974

194 Muller, M. P., Jeganathan, S., Heidrich, A., Campos, J. & Goody, R. S. Nucleotide based covalent inhibitors of KRas can only be efficient in vivo if they

bind reversibly with GTP-like affinity. *Sci Rep* **7**, 3687 (2017). https://doi.org:10.1038/s41598-017-03973-6

195 Ryan, M. B., Fece de la Cruz, F., Phat, S., Myers, D. T., Wong, E., Shahzade, H. A., Hong, C. B., Corcoran, R. B. Vertical Pathway Inhibition Overcomes Adaptive Feedback Resistance to KRAS(G12C) Inhibition. *Clin Cancer Res* **26**, 1633-1643 (2020). https://doi.org:10.1158/1078-0432.CCR-19-3523

196 Hallin J, E. L., Hargis L, Calinisan A, Aranda R, Briere DM, Sudhakar N, Bowcut V, Baer BR, Ballard JA, Burkard MR, Fell JB, Fischer JP, Vigers GP, Xue Y, Gatto S, Fernandez-Banet J, Pavlicek A, Velastagui K, Chao RC, Barton J, Pierobon M, Baldelli E, Patricoin EF 3rd, Cassidy DP, Marx MA, Rybkin II, Johnson ML, Ou SI, Lito P, Papadopoulos KP, Jänne PA, Olson P, Christensen JG. The KRAS(G12C) Inhibitor MRTX849 Provides Insight toward Therapeutic Susceptibility of KRAS-Mutant Cancers in Mouse Models and Patients. *Cancer Discov* **10**, 54-71 (2020). https://doi.org:10.1158/2159-8290.CD-19-1167

197 Jude Canon, K. R., Anne Y. Saiki, Christopher Mohr, Keegan Cooke, Dhanashri Bagal, Kevin Gaida, Tyler Holt, Charles G. Knutson, Neelima Koppada, Brian A. Lanman, Jonathan Werner, Aaron S. Rapaport, Tisha San Miguel, Roberto Ortiz, Tao Osgood, Ji-Rong Sun, Xiaochun Zhu, John D. McCarter, Laurie P. Volak, Brett E. Houk, Marwan G. Fakih, Bert H. O'Neil, Timothy J. Price, …J. Russell Lipford. The clinical KRAS(G12C) inhibitor AMG 510 drives anti-tumour immunity. *Nature* **575**, 217-223 (2019). https://doi.org:10.1038/s41586-019-1694-1

198 Christopher J. Schulze, K. J. S., Yulei Zhao, Yu C. Yang, Jim Cregg, Dongsung Kim, Aidan Tomlinson, Tiffany J. Choy, Zhican Wang, Ben Sang, Yasin Pourfarjam, Jessica Lucas, Antonio Cuevas-Navarro, Carlos Ayala Santos, Alberto Vides, Chuanchuan Li, Abby Marquez, Mengqi Zhong, Vidyasiri Vemulapalli, Caroline Weller, Andrea Gould, Daniel M. Whalen, Anthony Salvador, Anthony Milin, Mae Saldajeno-Concar, Nuntana Dinglasan, Anqi Chen, Jim Evans, John E. Knox, Elena S. Koltun, Mallika Singh, Robert Nichols, David Wildes, Adrian L. Gill, Jacqueline A. M. Smith, and Piro Lito. Chemical remodeling of a cellular chaperone to target the active state of mutant KRAS. *Science*, 794-799 (2023). https://doi.org:10.1126/science.adg9652

199 Jänne, P. A., Bigot, F., Papadopoulos, K., Eberst, L., Sommerhalder, D., Lebellec, L., Voon, P.J., Pellini, B., Kalinka, E., Arbour, K. Abstract PR014: Preliminary safety and anti-tumor activity of RMC-6291, a first-in-class, tri-complex KRASG12C(ON) inhibitor, in patients with or without prior KRASG12C(OFF) inhibitor treatment. *Mol. Cancer Therapeut.* **22** (2023). https://doi.org:10.1158/1535-7163.TARG-23-PR014

200 Singhal, A., Li, B. T. & O'Reilly, E. M. Targeting KRAS in cancer. *Nat Med* **30**, 969-983 (2024). https://doi.org:10.1038/s41591-024-02903-0

201 Zhang, Z., Morstein, J., Ecker, A. K., Guiley, K. Z. Shokat, K. M. Chemoselective Covalent Modification of K-Ras(G12R) with a Small Molecule Electrophile. *J Am Chem Soc* **144**, 15916-15921 (2022). https://doi.org:10.1021/jacs.2c05377

202 Zhang, Z., Guiley, K. Z. & Shokat, K. M. Chemical acylation of an acquired serine suppresses oncogenic signaling of K-Ras(G12S). *Nat Chem Biol* **18**, 1177-1183 (2022). https://doi.org:10.1038/s41589-022-01065-9

203 Jill Hallin, V. B., Andrew Calinisan, David M. Briere, Lauren Hargis, Lars D. Engstrom, Jade Laguer, James Medwid, Darin Vanderpool, Ella Lifset, David Trinh, Natalie Hoffman, Xiaolun Wang, J. David Lawson, Robin J. Gunn, Christopher R. Smith, Nicole C. Thomas, Matthew Martinson, Alex Bergstrom, Francis Sullivan, Karyn Bouhana, Shannon Winski, Leo He, Julio Fernandez-Banet, …James G. Christensen. Anti-tumor efficacy of a potent and

selective non-covalent KRAS(G12D) inhibitor. *Nat Med* **28**, 2171-2182 (2022). https://doi.org:10.1038/s41591-022-02007-7

204 Chirnomas, D., Hornberger, K. R. & Crews, C. M. Protein degraders enter the clinic - a new approach to cancer therapy. *Nat Rev Clin Oncol* **20**, 265-278 (2023). https://doi.org:10.1038/s41571-023-00736-3

205 Dongsung Kim, L. H., Dorothea Rudolph, Yulei Zhao, Jark Böttcher, Alberto Vides, Carlos I. Ayala-Santos, Yasin Pourfarjam, Antonio Cuevas-Navarro, Jenny Y. Xue, Andreas Mantoulidis, Joachim Bröker, Tobias Wunberg, Otmar Schaaf, Johannes Popow, Bernhard Wolkerstorfer, Katrin Gabriele Kropatsch, Rui Qu, Elisa de Stanchina, Ben Sang, Chuanchuan Li, Darryl B. McConnell, Norbert Kraut & Piro Lito. Pan-KRAS inhibitor disables oncogenic signalling and tumour growth. *Nature* **619**, 160-166 (2023). https://doi.org:10.1038/s41586-023-06123-3

206 Johannes Popow, W. F., Andreas Gollner, Christiane Kofink, Gerhard Fischer, Melanie Wurm, David Zollman, Andre Wijaya, Nikolai Mischerikow, Carina Hasenoehrl, Polina Prokofeva, Heribert Arnhof, Silvia Arce-Solano, Sammy Bell, Georg Boeck, Emelyne Diers, Aileen B. Frost, Jake Goodwin-Tindall, Jale Karolyi-Oezguer, Shakil Khan, Theresa Klawatsch, Manfred Koegl, Roland Kousek, Barbara Kratochvil, Katrin Kropatsch, Arnel A. Lauber, Ross McLennan, Sabine Olt, Daniel Peter, Oliver Petermann, Vanessa Roessler, Peggy Stolt-Bergner, Patrick Strack, Eva Strauss, Nicole Trainor, Vesna Vetma, Claire Whitworth, Siying Zhong, Jens Quant, Harald Weinstabl, Bernhard Kuster, Peter Ettmayer, Alessio Ciulli. Targeting cancer with small molecule pan-KRAS degraders. *bioRxiv preprint* (2023). https://doi.org:10.1101/2023.10.24.563163

207 Matthew Holderfield, B. J. L., Jingjing Jiang, Aidan Tomlinson, Kyle J. Seamon, Alessia Mira, Enrico Patrucco, Grace Goodhart, Julien Dilly, Yevgeniy Gindin, Nuntana Dinglasan, Yingyun Wang, Lick Pui Lai, Shurui Cai, Lingyan Jiang, Nicole Nasholm, Nataliya Shifrin, Cristina Blaj, Harshit Shah, James W. Evans, Nilufar Montazer, Oliver Lai, Jade Shi, Ethan Ahler, …Mallika Singh. Concurrent inhibition of oncogenic and wild-type RAS-GTP for cancer therapy. *Nature* **629**, 919-926 (2024). https://doi.org:10.1038/s41586-024-07205-6

208 Arbour, K. C., Punekar, S., Garrido-Laguna, I., Hong, D. S., Wolpin, B., Pelster, M. S., Barve, M., Starodub, A., Sommerhalder, D., Chang, S., Zhang, Y., Salman, Z., Wang, X., Gustafson, C., Spira, A. I. 652O Preliminary clinical activity of RMC-6236, a first-in-class, RAS-selective, tri-complex RAS-MULTI(ON) inhibitor in patients with KRAS mutant pancreatic ductal adenocarcinoma (PDAC) and non-small cell lung cancer (NSCLC). *Annals of Oncology* **34** (2023). https://doi.org:10.1016/j.annonc.2023.09.1838

209 Jiang J, J. L., Maldonato BJ, Wang Y, Holderfield M, Aronchik I, Winters IP, Salman Z, Blaj C, Menard M, Brodbeck J, Chen Z, Wei X, Rosen MJ, Gindin Y, Lee BJ, Evans JW, Chang S, Wang Z, Seamon KJ, Parsons D, Cregg J, Marquez A, Tomlinson ACA, Yano JK, Knox JE, Quintana E, Aguirre AJ, Arbour KC, Reed A, Gustafson WC, Gill AL, Koltun ES, Wildes D, Smith JAM, Wang Z, Singh M. . Translational and Therapeutic Evaluation of RAS-GTP Inhibition by RMC-6236 in RAS-Driven Cancers. *Cancer Discov* **14**, 994-1017 (2024). https://doi.org:10.1158/2159-8290.CD-24-0027

210 Julian Downward, J. D. G., Patricia H. Warne, Sydonia Rayter & Doreen A. Cantrell Stimulation of p21ras upon T-cell activation. *Nature* **346**, pages719–723 (1990).

211 Linda Graziadei, K. R. D. B.-S. Co-capping of ras proteins with surface immunoglobulins in B lymphocytes. *nature* **347**, 396–400 (1990). https://doi.org:10.1038/347396a0

212 Boumelha J, d. C. T. S., Law EK, Romero-Clavijo P, Coelho MA, Ng KW, Mugarza E, Moore C, Rana S, Caswell DR, Murillo M, Hancock DC, Argyris PP, Brown WL, Durfee C, Larson LK, Vogel RI, Suárez-Bonnet A, Priestnall SL, East P, Ross SJ, Kassiotis G, Molina-Arcas M, Swanton C, Harris R, Downward J. An Immunogenic Model of KRAS-Mutant Lung Cancer Enables Evaluation of Targeted Therapy and Immunotherapy Combinations. *Cancer Res* **82**, 3435-3448 (2022). https://doi.org:10.1158/0008-5472.CAN-22-0325

213 David M. Briere, S. L., Andrew Calinisan, Niranjan Sudhakar, Ruth Aranda, Lauren Hargis, David H. Peng, Jiehui Deng, Lars D. Engstrom, Jill Hallin, Sole Gatto, Julio Fernandez-Banet, Adam Pavlicek, Kwok-Kin Wong, James G. Christensen, Peter Olson. The KRASG12C Inhibitor MRTX849 Reconditions the Tumor Immune Microenvironment and Sensitizes Tumors to Checkpoint Inhibitor Therapy. *Mol Cancer Ther* **20**, 975-985 (2021). https://doi.org:10.1158/1535-7163.MCT-20-0462

214 Kemp SB, C. N., Markosyan N, Sor R, Kim IK, Hallin J, Shoush J, Quinones L, Brown NV, Bassett JB, Joshi N, Yuan S, Smith M, Vostrejs WP, Perez-Vale KZ, Kahn B, Mo F, Donahue TR, Radu CG, Clendenin C, Christensen JG, Vonderheide RH, Stanger BZ. Efficacy of a Small-Molecule Inhibitor of KrasG12D in Immunocompetent Models of Pancreatic Cancer. *Cancer Discov* **13**, 298-311 (2023). https://doi.org:10.1158/2159-8290.CD-22-1066

215 Ischenko, I., D'Amico, S., Rao, M., Li, J., Hayman, M. J., Powers, S., Petrenko, O., Reich, N. C. KRAS drives immune evasion in a genetic model of pancreatic cancer. *Nat Commun* **12**, 1482 (2021). https://doi.org:10.1038/s41467-021-21736-w

216 Panayiotis Anastasiou, C. M., Sareena Rana, Andrea de Castro, Mona Tomaschko, Jesse Boumelha, Edurne Mugarza, Cristina Blaj, Sophie de Carné, Robert Goldstone, Jacqueline A.M. Smith, Elsa Quintana, Miriam Molina-Arcas and Julian Downward Combining RASG12C(ON) inhibitor with SHP2 inhibition sensitises immune excluded lung tumours to immune checkpoint blockade: a strategy for turning cold tumours hot. *bioRxiv preprint* (2024). https://doi.org:doi.org/10.1101/2024.01.15.575765

217 Febe van Maldegem, K. V., Megan Cole, Harshil Patel, Mihaela Angelova, Sareena Rana, Emma Colliver, Katey Enfield, Nourdine Bah, Victoria Siu Kwan Tsang, Edurne Mugarza, Christopher Moore, Philip Hobson, Dina Levi, Miriam Molina-Arcas, Charles Swanton, Julian Downward. Characterisation of tumour immune microenvironment remodelling following oncogene inhibition in preclinical studies using an optimised imaging mass cytometry workflow. *bioRxiv preprint* (2021). https://doi.org:10.1101/2021.02.02.429358

218 Megan Cole, P. A., Claudia Lee, Chris Moore, Edurne Mugarza, Martin Jones, Karishma Valand, Sareena Rana, Emma Colliver, Mihaela Angelova, Katey S.S. Enfield, Alastair Magness, Asher Mullokandov, Gavin Kelly, Tanja D. de Gruijl, Miriam Molina-Arcas, Charles Swanton, Julian Downward, Febe van Maldegem. Spatial proteomic analysis of a lung cancer model reveals regulatory T cells attenuate KRAS-G12C inhibitor-induced immune responses. *bioRxiv* (2024). https://doi.org:10.1101/2024.04.11.588725

219 Febe van Maldegem, K. V., Megan Cole, Harshil Patel, Mihaela Angelova, Sareena Rana, Emma Colliver, Katey Enfield, Nourdine Bah, Victoria Siu Kwan Tsang, Edurne Mugarza, Christopher Moore, Philip Hobson, Dina Levi, Miriam Molina-Arcas, Charles Swanton, Julian Downward. Characterisation of tumour microenvironment remodelling following oncogene inhibition in preclinical studies with imaging mass cytometry. *Nat Commun* **12**, 5906 (2021). https://doi.org:10.1038/s41467-021-26214-x

220 Krishnan K Mahadevan, K. M. M., Valerie S LeBleu, Sujuan Yang, Hengyu Lyu, Bingrui Li, Amari M Sockwell, Michelle L Kirtley, Sami J Morse, Barbara A Moreno Diaz, Michael P Kim, Ningping Feng, Anastasia M Lopez, Paola A Guerrero, Hikaru Sugimoto, Kent A Arian, Haoqiang Ying, Yasaman Barekatain, Patience J Kelly, Anirban Maitra, Timothy P Heffernan, Raghu Kalluri. Oncogenic Kras (G12D) specific non-covalent inhibitor reprograms tumor microenvironment to prevent and reverse early pre-neoplastic pancreatic lesions and in combination with immunotherapy regresses advanced PDAC in a CD8 (+) T cells dependent manner. *bioRxiv* (2023). https://doi.org:10.1101/2023.02.15.528757

221 Lucile Vanhersecke, M. B., Jean-Philippe Guégan, Christophe Rey, Antoine Bougouin, Sophie Cousin, Sylvestre Le Moulec, Benjamin Besse, Yohann Loriot, Mathieu Larroquette, Isabelle Soubeyran, Maud Toulmonde, Guilhem Roubaud, Simon Pernot, Mathilde Cabart, François Chomy, Corentin Lefevre, Kevin Bourcier, Michèle Kind, Ilenia Giglioli, Catherine Sautès-Fridman, Valérie Velasco, Félicie Courgeon, Ezoglin Oflazoglu, …Antoine Italiano. Mature tertiary lymphoid structures predict immune checkpoint inhibitor efficacy in solid tumors independently of PD-L1 expression. *Nat Cancer* **2**, 794-802 (2021). https://doi.org:10.1038/s43018-021-00232-6

222 Strickler JH, S. H., George TJ, Yaeger R, Hollebecque A, Garrido-Laguna I, Schuler M, Burns TF, Coveler AL, Falchook GS, Vincent M, Sunakawa Y, Dahan L, Bajor D, Rha SY, Lemech C, Juric D, Rehn M, Ngarmchamnanrith G, Jafarinasabian P, Tran Q, Hong DS. Sotorasib in KRAS p.G12C-Mutated Advanced Pancreatic Cancer. *N Engl J Med* **388**, 33-43 (2023). https://doi.org:10.1056/NEJMoa2208470

223 Bekaii-Saab, T. S., Yaeger, R., Spira, A. I., Pelster, M. S., Sabari, J. K., Hafez, N., Barve, M., Velastegui, K., Yan, X., Shetty, A., Der-Torossian, H., Pant, S. Adagrasib in Advanced Solid Tumors Harboring a KRAS(G12C) Mutation. *J Clin Oncol* **41**, 4097-4106 (2023). https://doi.org:10.1200/JCO.23.00434

224 Fakih MG, S. L., Esaki T, Modest DP, Lopez-Bravo DP, Taieb J, Karamouzis MV, Ruiz-Garcia E, Kim TW, Kuboki Y, Meriggi F, Cunningham D, Yeh KH, Chan E, Chao J, Saportas Y, Tran Q, Cremolini C, Pietrantonio F. . Sotorasib plus Panitumumab in Refractory Colorectal Cancer with Mutated KRAS G12C. *N Engl J Med* **389**, 2125-2139 (2023). https://doi.org:10.1056/NEJMoa2308795

225 Yaeger R, W. J., Pelster MS, Spira AI, Barve M, Ou SI, Leal TA, Bekaii-Saab TS, Paweletz CP, Heavey GA, Christensen JG, Velastegui K, Kheoh T, Der-Torossian H, Klempner SJ. . Adagrasib with or without Cetuximab in Colorectal Cancer with Mutated KRAS G12C. *N Engl J Med* **388**, 44-54 (2023). https://doi.org:10.1056/NEJMoa2212419

226 Skoulidis, F., Li, B. T., Dy, G. K., Price, T. J., Falchook, G. S., Wolf, J., Italiano, A., Schuler, M., Borghaei, H., Barlesi, F., Kato, T., Curioni-Fontecedro, A., Sacher, A., Spira, A., Ramalingam, S. S., Takahashi, T., Besse, B., Anderson, A., Ang, A., Tran, Q., Mather, O., Henary, H., Ngarmchamnanrith, G., Friberg, G., Velcheti, V., Govindan, R. Sotorasib for Lung Cancers with KRAS p.G12C Mutation. *N Engl J Med* **384**, 2371-2381 (2021). https://doi.org:10.1056/NEJMoa2103695

227 David S Hong, M. G. F., John H Strickler, Jayesh Desai, Gregory A Durm, Geoffrey I Shapiro, Gerald S Falchook, Timothy J Price, Adrian Sacher, Crystal S Denlinger, Yung-Jue Bang, Grace K Dy. John C Krauss, Yasutoshi Kuboki, James C Kuo, Andrew L Coveler, Keunchil Park, Tae Won Kim, Fabrice Barlesi, Pamela N Munster, Suresh S Ramalingam, Timothy F Burns, Funda Meric-Bernstam, Haby Henary, Jude Ngang, Gataree Ngarmchamnanrith, June Kim, Brett E Houk, Jude Canon, J Russell Lipford, Gregory Friberg, Piro Lito,

Ramaswamy Govindan, Bob T Li. KRASG12C Inhibition with Sotorasib in Advanced Solid Tumors. *N Engl J Med* **13**, 1207–1217 (2020). https://doi.org:10.1056/NEJMoa1917239

228 Ou, S. I., Janne, P. A., Leal, T. A., Rybkin,, II, Sabari, J. K., Barve, M. A., Bazhenova, L. A., Johnson, M. L., Velastegui, K. L., Cilliers, C., Christensen, J. G., Yan, X., Chao, R. C., Papadopoulos, K. P. First-in-Human Phase I/IB Dose-Finding Study of Adagrasib (MRTX849) in Patients With Advanced KRAS(G12C) Solid Tumors (KRYSTAL-1). *J Clin Oncol*, JCO2102752 (2022). https://doi.org:10.1200/JCO.21.02752

229 Janne, P. A., Riely, G. J., Gadgeel, S. M., Heist, R. S., Ou, S. I., Pacheco, J. M., Johnson, M. L., Sabari, J. K., Leventakos, K., Yau, E., Bazhenova, L., Negrao, M. V., Pennell, N. A., Zhang, J., Anderes, K., Der-Torossian, H., Kheoh, T., Velastegui, K., Yan, X.,,, Christensen, J. G., Chao, R. C., Spira, A. I. Adagrasib in Non-Small-Cell Lung Cancer Harboring a KRAS(G12C) Mutation. *N Engl J Med* (2022). https://doi.org:10.1056/NEJMoa2204619

230 Garassino, M. C., Theelen, W. S. M. E., Jotte, R., Laskin, J.. de, Marinis, F., Aguado, C., Badin, F. B., Chmielewska, I., Hochmair, M. J., Lu, S., Nadal, E., Ostoros, G., Felip, E., Spira, A. I., Lane, C. M., He, J., Chao, R., Jänne, P. A. LBA65 KRYSTAL-7: Efficacy and safety of adagrasib with pembrolizumab in patients with treatment-naïve, advanced non-small cell lung cancer (NSCLC) harboring a KRASG12C mutation. *Annals of Oncology* **34**, S1309-S1310 (2023). https://doi.org:10.1016/j.annonc.2023.10.066

231 Adrianus Johannes de Langen, M. L. J., Julien Mazieres, Anne-Marie C Dingemans, Giannis Mountzios, Miklos Pless, Jürgen Wolf, Martin Schuler, Hervé Lena, Ferdinandos Skoulidis, Yasuto Yoneshima, Sang-We Kim, Helena Linardou, Silvia Novello, Anthonie J van der Wekken, Yuanbin Chen, Solange Peters, Enriqueta Felip, Benjamin J Solomon, Suresh S Ramalingam, Christophe Dooms, Colin R Lindsay, Carlos Gil Ferreira, Normand Blais, Cynthia C Obiozor, Yang Wang, Bhakti Mehta, Tracy Varrieur, Gataree Ngarmchamnanrith, Björn Stollenwerk, David Waterhouse*, Luis Paz-Ares*, for the CodeBreaK 200 Investigators†. Sotorasib versus docetaxel for previously treated non-small-cell lung cancer with KRAS(G12C) mutation: a randomised, open-label, phase 3 trial. *Lancet* **401**, 733-746 (2023). https://doi.org:10.1016/S0140-6736(23)00221-0

232 Pasi A. Jänne, F. B., Kyriakos Papadopoulos, Lauriane Eberst, David Sommerhalder, Loic Lebellec, Pei Jye Voon, Bruna Pellini, Ewa Kalinka, Kathryn Arbour, Benjamin Herzberg, Valentina Boni, Stephanie Bordenave, Hyun Woo Lee, Sai I. Ou, Jonathan W. Riess, Joseph T. Beck, Mariano Ponz-Sarvise, Paolo Antonio Ascierto, Yoon Ji Choi, Daniel Tan, Michelle Yang, Lei Bao, Rakesh Raman, Luxi Yang, Yunming Mu, Sofia Wong, Richa Dua, Melissa Johnson. Preliminary Safety and Anti-Tumor Activity of RMC-6291, a First-in-Class, Tri-Complex KRASG12C(ON) Inhibitor, in Patients With or Without Prior KRASG12C(OFF) Inhibitor Treatment. *ENA poster presentation (unpublished)* (2023).

233 Zhang, J., Zhang, J., Liu, Q., Fan, X. X., Leung, E. L., Yao, X. J., Liu, L. Resistance looms for KRAS G12C inhibitors and rational tackling strategies. *Pharmacol Ther* **229**, 108050 (2022). https://doi.org:10.1016/j.pharmthera.2021.108050

234 Liu, J. K., R. Tang, D. The KRAS-G12C inhibitor: activity and resistance. *Cancer Gene Ther* (2021). https://doi.org:10.1038/s41417-021-00383-9

235 Zhang, Y., Liu, L., Pei, J., Ren, Z., Deng, Y., Yu, K. Tissue factor overexpression promotes resistance to KRAS-G12C inhibition in non-small cell

lung cancer. *Oncogene* **43**, 668-681 (2024). https://doi.org:10.1038/s41388-023-02924-y

236 Noritaka Tanaka, J. J. L., Chendi Li, Meagan B. Ryan, Junbing Zhang, Lesli A., Kiedrowski, A. G. M., Mohammed U. Syed, Katerina A. Fella, Mustafa Sakhi, Islam, Baiev, D. J., Justin F. Gainor, Samuel J. Klempner, Jochen K. Lennerz, Giulia & Siravegna, L. B.-P., Aaron N. Hata, Rebecca S. Heist, Ryan B. Corcoran. Clinical acquired resistance to KRASG12C inhibition through a novel KRAS switch-II pocket mutation and polyclonal alterations converging on RAS-MAPK reactivation. *Author Manuscript* (2021). https://doi.org:10.1158/2159-8290.CD-21-0365

237 M.M. Awad, S. L., I.I. Rybkin, K.C. Arbour, J. Dilly, V.W. Zhu, M.L. Johnson, R.S. Heist, T. Patil, G.J. Riely, J.O. Jacobson, X. Yang, N.S. Persky, D.E. Root, K.E. Lowder, H. Feng, S.S. Zhang, K.M. Haigis, Y.P. Hung, L.M. Sholl, B.M. Wolpin, J. Wiese, J. Christiansen, J. Lee, A.B. Schrock, L.P. Lim, K. Garg, M. Li, L.D. Engstrom, L. Waters, J.D. Lawson, P. Olson, P. Lito, S.-H.I. Ou, J.G. Christensen, P.A. Jänne, and A.J. Aguirre. Acquired Resistance to KRAS(G12C) Inhibition in Cancer. *N Engl J Med* **384**, 2382-2393 (2021). https://doi.org:10.1056/NEJMoa2105281

238 Zhao, Y., Murciano-Goroff, Y. R., Xue, J. Y., Ang, A., Lucas, J., Mai, T. T., Da Cruz Paula, A. F., Saiki, A. Y., Mohn, D.chanta, P., Sisk, A. E., Arora, K. S., Roy, R. S., Kim, D., Li, C. Lim, L. P., Li, M., Bahr, A., Loomis, B. R., de Stanchina, E., Reis-Filho, J. S., Weigelt,, B., Berger, M., Riely, G., Arbour, K. C., Lipford, J. R., Li,, B. T., Lito, P. Diverse alterations associated with resistance to KRAS(G12C) inhibition. *Nature* **599**, 679-683 (2021). https://doi.org:10.1038/s41586-021-04065-2

239 Takamasa Koga, D. K. S., Toshio Fujino , Shuta Ohara, Akira Hamada, Masaya Nishino, Masato Chiba, Masaki Shimoji, Toshiki Takemoto, Takeo Aritab Michael Gmachl Marco H.Hofmann, Junichi Soh, Tetsuya Mitsudomi. KRAS Secondary Mutations That Confer Acquired Resistance to KRAS G12C Inhibitors, Sotorasib and Adagrasib, and Overcoming Strategies: Insights From In Vitro Experiments. *Journal of Thoracic Oncology* **16**, 1321-1332 (2021). https://doi.org:10.1016/j.jtho.2021.04.015Get

240 Vaclova, T., Chakraborty, A., Sherwood, J., Ross, S., Carroll, D., Barrett, J. C., Downward, J., de Bruin, E. C. Concomitant KRAS mutations attenuate sensitivity of non-small cell lung cancer cells to KRAS G12C inhibition. *Sci Rep* **12**, 2699 (2022). https://doi.org:10.1038/s41598-022-06369-3

241 Xue, J. Y., Zhao, Y., Aronowitz, J., Mai, T. T., Vides, A., Qeriqi, B., Kim, D., Li, C., de Stanchina, E., Mazutis, L., Risso, D., Lito, P. Rapid non-uniform adaptation to conformation-specific KRAS(G12C) inhibition. *Nature* **577**, 421-425 (2020). https://doi.org:10.1038/s41586-019-1884-x

242 Ryan, M. B., Coker, O., Sorokin, A.. Fella, K., Barnes, H., Wong, E., Kanikarla, P., Gao, F.. Zhang, Y., Zhou, L., Kopetz, S., Corcoran, R. B. KRAS(G12C)-independent feedback activation of wild-type RAS constrains KRAS(G12C) inhibitor efficacy. *Cell Rep* **39**, 110993 (2022). https://doi.org:10.1016/j.celrep.2022.110993

243 Shinichiro Suzuki, K. Y., Takeshi Teramura, Toshiyuki Takehara, Ryoji Kato, Hitomi Sakai, Koji Haratani, Junko Tanizaki, Hisato Kawakami, Hidetoshi Hayashi, Kazuko Sakai, Kazuto Nishio, and Kazuhiko Nakagawa. KRAS Inhibitor Resistance in MET-Amplified KRASG12C Non–Small Cell Lung Cancer Induced By RAS- and Non–RAS-Mediated Cell Signaling Mechanisms. *Clin Cancer Res* **27**, 5697-5707 (2021). https://doi.org:10.1158/1078-0432.CCR-21-0856

244 Tsai, Y. S., Woodcock, M. G., Azam, S. H., Thorne, L. B., Kanchi, K. L., Parker, J. S., Vincent, B. G., Pecot, C. V. Rapid idiosyncratic mechanisms of clinical resistance to KRAS G12C inhibition. *J Clin Invest* **132** (2022). https://doi.org:10.1172/JCI155523

245 Solanki, H. S., Welsh, E. A., Fang, B., Izumi, V., Darville, L., Stone, B., Franzese, R., Chavan, S., Kinose, F., Imbody, D., Koomen, J. M., Rix, U., Haura, E. B. Cell Type-specific Adaptive Signaling Responses to KRAS(G12C) Inhibition. *Clin Cancer Res* **27**, 2533-2548 (2021). https://doi.org:10.1158/1078-0432.CCR-20-3872

246 Yuta Adachi, K. I., Yuko Hayashi, Ryo Kimura, Tuan Zea Tan, Rui Yamaguchi and Hiromichi Ebi. Epithelial-to-Mesenchymal Transition is a Cause of Both Intrinsic and Acquired Resistance to KRAS G12C Inhibitor in KRAS G12C–Mutant Non–Small Cell Lung Cancer. *CLINICAL CANCER RESEARCH* (2020). https://doi.org:10.1158/1078-0432.CCR-20-2077

247 Muzumdar, M. D., Chen, P. Y., Dorans, K. J., Chung, K. M., Bhutkar, A., Hong, E., Noll, E. M., Sprick, M. R., Trumpp, A., Jacks, T. Survival of pancreatic cancer cells lacking KRAS function. *Nat Commun* **8**, 1090 (2017). https://doi.org:10.1038/s41467-017-00942-5

248 Chen, P. Y. M., M. D. Dorans, K. J., Robbins, R., Bhutkar, A., Del Rosario, A., Mertins, P., Qiao, J., Schafer, A. C., Gertler, F., Carr, S., Jacks, T. Adaptive and Reversible Resistance to Kras Inhibition in Pancreatic Cancer Cells. *Cancer Res* **78**, 985-1002 (2018). https://doi.org:10.1158/0008-5472.CAN-17-2129

249 Atish Mohanty, A. N., Saumya Srivastava, Jeff Jones, Brett Lomenick, Sharad S. Singhal, Linlin Guo, Hyejin Cho, Aimin Li, Amita Behal, Tamara Mirzapoiazova, Erminia Massarelli, & Marianna Koczywas, L. D. A., TonyaWalser, Victoria Villaflor, Stanley Hamilton, sa Mambetsariev, Martin Sattler, Mohd W. Nasser, Maneesh Jain, Surinder K. Batra, Raffaella Soldi, Sunil Sharma, Marwan Fakih, Saswat Kumar Mohanty, Avijit Mainan, Xiwei Wu, Yihong Chen, Yanan He, Tsui-Fen Chou, Susmita Roy, John Orban, Prakash Kulkarni, Ravi Salgia. Acquired resistance to KRAS G12C small-moleculeinhibitors via genetic/nongenetic mechanisms in lung cancer. *Science Advances* **9** (2023). https://doi.org:10.1126/sciadv.ade3816

250 Johnson, C. W., Haigis, K. M. All Roads Lead to Rome: YAP/TAZ Activity Influences Efficacy of KRASG12C Inhibitors. *Cancer Res* **83**, 4005-4007 (2023). https://doi.org:10.1158/0008-5472.CAN-23-3547

251 Adachi, Y., Kimura, R., Hirade, K., Yanase, S., Nishioka, Y., Kasuga, N., Yamaguchi, R., Ebi, H. Scribble mis-localization induces adaptive resistance to KRAS G12C inhibitors through feedback activation of MAPK signaling mediated by YAP-induced MRAS. *Nat Cancer* **4**, 829-843 (2023). https://doi.org:10.1038/s43018-023-00575-2

252 Thijs J. Hagenbeek, J. R. Z., Marc Hafner, Rana Mroue, Jennifer A. Lacap, Nicole M. Sodir, Cameron L. Noland, Shervin Afghani, Ayush Kishore, Kamakoti P. Bhat, Xiaosai Yao, Stephen Schmidt, Saundra Clausen, Micah Steffek, Wendy Lee, Paul Beroza, Scott Martin, Eva Lin, Rina Fong, Paola Di Lello, Marta H. Kubala, Michelle N.-Y. Yang, Jeffrey T. Lau, Emily Chan, …Anwesha Dey. An allosteric pan-TEAD inhibitor blocks oncogenic YAP/TAZ signaling and overcomes KRAS G12C inhibitor resistance. *Nat Cancer* **4**, 812-828 (2023). https://doi.org:10.1038/s43018-023-00577-0

253 Hanahan, D. & Weinberg, R. A. Hallmarks of cancer: the next generation. *Cell* **144**, 646-674 (2011). https://doi.org:10.1016/j.cell.2011.02.013

254 Molina-Arcas, M. Development of combination therapies to maximize the impact of KRAS-G12C inhibitors in lung cancer. *SCIENCE TRANSLATIONAL MEDICINE* **11** (2019).

255 Carmine Fedele, S. L., Kai Wen Teng , Connor J.R. Foster , David Peng , Hao Ran, Paolo Mita, Mitchell J. Geer, Takamitsu Hattori, Akiko Koide, Yubao Wang, Kwan Ho Tang, Joshua Leinwand, Wei Wang, Brian Diskin, Jiehui Deng, Ting Chen, Igor Dolgalev, Ugur Ozerdem, George Miller , Shohei Koide, Kwok-Kin Wong, Benjamin G. Neel SHP2 inhibition diminishes KRASG12C cycling and promotes tumor microenvironment remodeling. *J Exp Med* **1**, e20201414 (2020). https://doi.org:10.1084/jem.20201414

256 Sodir, N. M., Pathria, G., Adamkewicz, J. I., Kelley, E. H., Sudhamsu, J., Merchant, M., Chiarle, R.. Maddalo, D. SHP2: A Pleiotropic Target at the Interface of Cancer and Its Microenvironment. *Cancer Discov* **13**, 2339-2355 (2023). https://doi.org:10.1158/2159-8290.CD-23-0383

257 Nichols, R. J., Haderk, F., Stahlhut, C., Schulze, C. J., Hemmati, G., Wildes, D., Tzitzilonis, C., Mordec, K., Marquez, A., Romero, J., Hsieh, T., Zaman, A., Olivas, V., McCoach, C., Blakely, C. M., Wang, Z., Kiss, G., Koltun, E. S., Gill, A. L., Singh, M., Goldsmith, M. A., Smith, J. A. M., Bivona, T. G. RAS nucleotide cycling underlies the SHP2 phosphatase dependence of mutant BRAF-, NF1- and RAS-driven cancers. *Nat Cell Biol* **20**, 1064-1073 (2018). https://doi.org:10.1038/s41556-018-0169-1

258 LaRochelle, J. R., Fodor, M., Vemulapalli, V., Mohseni, M., Wang, P., Stams, T., LaMarche, M. J., Chopra, R., Acker, M. G., Blacklow, S. C. Structural reorganization of SHP2 by oncogenic mutations and implications for oncoprotein resistance to allosteric inhibition. *Nat Commun* **9**, 4508 (2018). https://doi.org:10.1038/s41467-018-06823-9

259 Romero, C., Lambert, L. J., Sheffler, D. J., De Backer, L. J. S., Raveendra-Panickar, D., Celeridad, M., Grotegut, S.. Rodiles, S., Holleran, J., Sergienko, E., Pasquale, E. B., Cosford, N. D. P., Tautz, L. A cellular target engagement assay for the characterization of SHP2 (PTPN11) phosphatase inhibitors. *J Biol Chem* **295**, 2601-2613 (2020). https://doi.org:10.1074/jbc.RA119.010838

260 Pandey, G., Mazzacurati, L., Rowsell, T. M., Horvat, N. P., Amin, N. E., Zhang, G., Akuffo, A. A., Colin-Leitzinger, C. M., Haura, E. B., Kuykendall, A. T., Zhang, L., Epling-Burnette, P. K., Reuther, G. W. SHP2 inhibition displays efficacy as a monotherapy and in combination with JAK2 inhibition in preclinical models of myeloproliferative neoplasms. *Am J Hematol* **99**, 1040-1055 (2024). https://doi.org:10.1002/ajh.27282

261 Drilon A, S. M., Johnson ML, Yap TA, Gadgeel S, Nepert D, Feng G, Reddy MB, Harney AS, Elsayed M, Cook AW, Wong CE, Hinklin RJ, Jiang Y, Brown EN, Neitzel NA, Laird ER, Wu WI, Singh A, Wei P, Ching KA, Gaudino JJ, Lee PA, Hartley DP, Rothenberg SM. SHP2 Inhibition Sensitizes Diverse Oncogene-Addicted Solid Tumors to Re-treatment with Targeted Therapy. *Cancer Discov* **13**, 1789-1801 (2023). https://doi.org:10.1158/2159-8290.CD-23-0361

262 Hofmann MH, G. M., Ramharter J, Savarese F, Gerlach D, Marszalek JR, Sanderson MP, Kessler D, Trapani F, Arnhof H, Rumpel K, Botesteanu DA, Ettmayer P, Gerstberger T, Kofink C, Wunberg T, Zoephel A, Fu SC, Teh JL, Böttcher J, Pototschnig N, Schachinger F, Schipany K, Lieb S, Vellano CP, O'Connell JC, Mendes RL, Moll J, Petronczki M, Heffernan TP, Pearson M, McConnell DB, Kraut N. BI-3406, a Potent and Selective SOS1-KRAS Interaction Inhibitor, Is Effective in KRAS-Driven Cancers through Combined MEK Inhibition. BI-3406, a Potent and Selective SOS1-KRAS Interaction Inhibitor, Is Effective in KRAS-Driven Cancers through Combined MEK Inhibition. *Cancer Discov* **11**, 142-157 (2021). https://doi.org:10.1158/2159-8290.CD-20-0142

263 Chapman, P. B., Solit, D. B. & Rosen, N. Combination of RAF and MEK inhibition for the treatment of BRAF-mutated melanoma: feedback is not encouraged. *Cancer Cell* **26**, 603-604 (2014). https://doi.org:10.1016/j.ccell.2014.10.017

264 Brown WS, M. P., Nemirovsky O, Awrey S, Chafe SC, Schaeffer DF, Li J, Renouf DJ, Stanger BZ, Dedhar S. . Overcoming Adaptive Resistance to KRAS and MEK Inhibitors by Co-targeting mTORC1/2 Complexes in Pancreatic Cancer. *Cell Rep Med* **1**, 100131 (2020). https://doi.org:10.1016/j.xcrm.2020.100131

265 Soucek, L. W., J. R., Sodir, N. M., Masso-Valles, D., Serrano, E., Karnezis, A. N. Swigart, L. B., Evan, G. I. Inhibition of Myc family proteins eradicates KRas-driven lung cancer in mice. *Genes Dev* **27**, 504-513 (2013). https://doi.org:10.1101/gad.205542.112

266 Ernst SM, H. M., van der Horst TE, Paats MS, Heijboer FWJ, Aerts JGJV, Dumoulin DW, Cornelissen R, von der Thüsen JH, de Bruijn P, Hoop EO, Mathijssen RHJ, Koolen SLW, Dingemans AC. Hepatotoxicity in patients with non-small cell lung cancer treated with sotorasib after prior immunotherapy: a comprehensive clinical and pharmacokinetic analysis. *EBioMedicine* **102**, 105074 (2024). https://doi.org:10.1016/j.ebiom.2024.105074

267 Chour A, D. J., Mascaux C, Zysman M, Bigay-Game L, Swalduz A, Gounant V, Cortot A, Darrason M, Fallet V, Auclin E, Basse C, Tissot C, Decroisette C, Bombaron P, Giroux-Leprieur E, Odier L, Brosseau S, Creusot Q, Gueçamburu M, Meersseman C, Rochand A, Costantini A, Gaillard CM, Wasielewski E, Girard N, Cadranel J, Lafitte C, Lebossé F, Duruisseaux M. . Brief Report: Severe Sotorasib-Related Hepatotoxicity and Non-Liver Adverse Events Associated With Sequential Anti-Programmed Cell Death (Ligand)1 and Sotorasib Therapy in KRASG12C-Mutant Lung Cancer. *Thorac Oncol.* **18**, 1408-1415 (2023). https://doi.org:10.1016/j.jtho.2023.05.013

268 Luo, J., Solimini, N. L. & Elledge, S. J. Principles of cancer therapy: oncogene and non-oncogene addiction. *Cell* **136**, 823-837 (2009). https://doi.org:10.1016/j.cell.2009.02.024

269 Conan G. Kinsey, S. A. C., Amelie M. Boespflug, Katrin P. Guillen, Mona Foth, Amanda Truong, Sophia S. Schuman, Jill E. Shea, Michael T. Seipp, Jeffrey T. Yap, Lance D. Burrell, David H. Lum, Jonathan R. Whisenant, G. Weldon Gilcrease III, Courtney C. Cavalieri, Kaitrin M. Rehbein, Stephanie L. Cutler, Kajsa E. Affolter, Alana L. Welm, Bryan E. Welm, Courtney L. Scaife, Eric L. Snyder & Martin McMahon. Protective autophagy elicited by RAF-->MEK-->ERK inhibition suggests a treatment strategy for RAS-driven cancers. *Nat Med* **25**, 620-627 (2019). https://doi.org:10.1038/s41591-019-0367-9

270 Kirsten L. Bryant, C. A. S., Daniel Zeitouni, Jennifer E. Klomp, Sen Peng, Andrey P. Tikunov, Venugopal Gunda, Mariaelena Pierobon, Andrew M. Waters, Samuel D. George, Garima Tomar, Björn Papke, G. Aaron Hobbs, Liang Yan, Tikvah K. Hayes, J. Nathaniel Diehl, Gennifer D. Goode, Nina V. Chaika, Yingxue Wang, Guo-Fang Zhang, Agnieszka K. Witkiewicz, Erik S. Knudsen, Emanuel F. Petricoin III, Pankaj K. Singh, …Channing J. Der. Combination of ERK and autophagy inhibition as a treatment approach for pancreatic cancer. *Nat Med* **25**, 628-640 (2019). https://doi.org:10.1038/s41591-019-0368-8

271 Goel S, D. M., Watt AC, BrinJones H, Sceneay J, Li BB, Khan N, Ubellacker JM, Xie S, Metzger-Filho O, Hoog J, Ellis MJ, Ma CX, Ramm S, Krop IE, Winer EP, Roberts TM, Kim HJ, McAllister SS, Zhao JJ. CDK4/6 inhibition triggers

anti-tumour immunity. *Nature* **548**, 471-475 (2017). https://doi.org:10.1038/nature23465

272 Chakraborty, A. KRASG12C inhibitor: combing for combination. *Biochem Soc Trans* **48**, 2691-2701 (2020). https://doi.org:10.1042/BST20200473

273 Tan, S., Li, D. & Zhu, X. Cancer immunotherapy: Pros, cons and beyond. *Biomed Pharmacother* **124**, 109821 (2020). https://doi.org:10.1016/j.biopha.2020.109821

274 Wang, Y., Wang, M., Wu, H. X. & Xu, R. H. Advancing to the era of cancer immunotherapy. *Cancer Commun (Lond)* **41**, 803-829 (2021). https://doi.org:10.1002/cac2.12178

275 Varade, J., Magadan, S. & Gonzalez-Fernandez, A. Human immunology and immunotherapy: main achievements and challenges. *Cell Mol Immunol* **18**, 805-828 (2021). https://doi.org:10.1038/s41423-020-00530-6

276 Reck, M., Rodriguez-Abreu, D., Robinson, A. G., Hui, R., Csoszi, T., Fulop, A., Gottfried, M., Peled, N., Tafreshi, A., Cuffe, S., O'Brien, M., Rao, S., Hotta, K., Leiby, M. A., Lubiniecki, G. M., Shentu, Y., Rangwala, R., Brahmer, J. R. Pembrolizumab versus Chemotherapy for PD-L1-Positive Non-Small-Cell Lung Cancer. *N Engl J Med* **375**, 1823-1833 (2016). https://doi.org:10.1056/NEJMoa1606774

277 Gandhi L, R.-A. D., Gadgeel S, Esteban E, Felip E, De Angelis F, Domine M, Clingan P, Hochmair MJ, Powell SF, Cheng SY, Bischoff HG, Peled N, Grossi F, Jennens RR, Reck M, Hui R, Garon EB, Boyer M, Rubio-Viqueira B, Novello S, Kurata T, Gray JE, Vida J, Wei Z, Yang J, Raftopoulos H, Pietanza MC, Garassino MC. Pembrolizumab plus Chemotherapy in Metastatic Non-Small-Cell Lung Cancer. *N Engl J Med* **378**, 2078-2092 (2018). https://doi.org:10.1056/NEJMoa1801005

278 Danish Memon, H. R., George Fromm, Jayon Lihm, Adam J. Schoenfeld, Jennifer L. Sauter, Jia Luo, Andrew Chow, Umesh K. Bhanot, Caroline McCarthy, Darwin Ye, Chad M. Vanderbilt, Cailian Liu, Mohsen Abu-Akeel, Andrew J. Plodkowski, Nicholas McGranahan, Marta Łuksza, Benjamin D. Greenbaum, Taha Merghoub, Andy J. Minn, Pedro Beltrao, Taylor H. Schreiber, Martin L. Miller, Matthew D. Hellmann. Clinical and molecular features of acquired resistance to immunotherapy in non-small cell lung cancer. *Cancer Cell* **42**, 209-224 e209 (2024). https://doi.org:10.1016/j.ccell.2023.12.013

279 Zhou, S. & Yang, H. Immunotherapy resistance in non-small-cell lung cancer: From mechanism to clinical strategies. *Front Immunol* **14**, 1129465 (2023). https://doi.org:10.3389/fimmu.2023.1129465

280 Sadeghirad, H., Bahrami, T., Layeghi, S. M., Yousefi, H., Rezaei, M., Hosseini-Fard, S. R., Radfar, P., Warkiani, M. E., O'Byrne, K., Kulasinghe, A. Immunotherapeutic targets in non-small cell lung cancer. *Immunology* **168**, 256-272 (2023). https://doi.org:10.1111/imm.13562

281 Marcos Rubio, A., Everaert, C., Van Damme, E., De Preter, K. & Vermaelen, K. Circulating immune cell dynamics as outcome predictors for immunotherapy in non-small cell lung cancer. *J Immunother Cancer* **11** (2023). https://doi.org:10.1136/jitc-2023-007023

282 Lahiri, A., Maji, A., Potdar, P. D., Singh, N., Parikh, P., Bisht, B., Mukherjee, A., Paul, M. K. Lung cancer immunotherapy: progress, pitfalls, and promises. *Mol Cancer* **22**, 40 (2023). https://doi.org:10.1186/s12943-023-01740-y

283 Suzanne L. Topalian, M. D., F. Stephen Hodi, M.D., Julie R. Brahmer, M.D., Scott N. Gettinger, M.D., David C. Smith, M.D., David F. McDermott, M.D., John D. Powderly, M.D., Richard D. Carvajal, M.D., Jeffrey A. Sosman, M.D., Michael B. Atkins, M.D., Philip D. Leming, M.D., David R. Spigel, M.D., Scott J.

Antonia, M.D., Ph.D., Leora Horn, M.D., Charles G. Drake, M.D., Ph.D., Drew M. Pardoll, M.D., Ph.D., Lieping Chen, M.D., Ph.D., William H. Sharfman, M.D., Robert A. Anders, M.D., Ph.D., Janis M. Taube, M.D., Tracee L. McMiller, M.S., Haiying Xu, B.A., Alan J. Korman, Ph.D., Maria Jure-Kunkel, Ph.D., Shruti Agrawal, Ph.D., Daniel McDonald, M.B.A., Georgia D. Kollia, Ph.D., Ashok Gupta, M.D., Ph.D., Jon M. Wigginton, M.D., and Mario Sznol, M.D. Safety, Activity, and Immune Correlates of Anti–PD-1 Antibody in Cancer. *The New England Journal of Medicine*, 2443-2454 (2012). https://doi.org:10.1056/NEJMoa1200690

284 Quintana, E., Schulze, C. J., Myers, D. R., Choy, T. J., Mordec, K., Wildes, D., Shifrin, N. T., Belwafa, A., Koltun, E. S., Gill, A. L., Singh, M., Kelsey, S., Goldsmith, M. A., Nichols, R., Smith, J. A. M. Allosteric Inhibition of SHP2 Stimulates Antitumor Immunity by Transforming the Immunosuppressive Environment. *Cancer Res* **80**, 2889-2902 (2020). https://doi.org:10.1158/0008-5472.CAN-19-3038

285 Wang, Y., Salvucci, O., Ohnuki, H., Tran, A. D., Ha, T., Feng, J. X., DiPrima, M., Kwak, H. Wang, D., Yu, Y., Kruhlak, M., Tosato, G. Targeting the SHP2 phosphatase promotes vascular damage and inhibition of tumor growth. *EMBO Mol Med* **13**, e14089 (2021). https://doi.org:10.15252/emmm.202114089

286 Xu, Z., Guo, C., Ye, Q., Shi, Y., Sun, Y., Zhang, J., Huang, J., Huang, Y., Zeng, C., Zhang, X., Ke, Y., Cheng, H. Endothelial deletion of SHP2 suppresses tumor angiogenesis and promotes vascular normalization. *Nat Commun* **12**, 6310 (2021). https://doi.org:10.1038/s41467-021-26697-8

287 Boumelha, J., Molina-Arcas, M. & Downward, J. Facts and Hopes on RAS Inhibitors and Cancer Immunotherapy. *Clin Cancer Res* **29**, 5012-5020 (2023). https://doi.org:10.1158/1078-0432.CCR-22-3655

288 Dall'Olio, F. G., Marabelle, A., Caramella, C., Garcia, C., Aldea, M., Chaput, N., Robert, C., Besse, B. Tumour burden and efficacy of immune-checkpoint inhibitors. *Nat Rev Clin Oncol* **19**, 75-90 (2022). https://doi.org:10.1038/s41571-021-00564-3

289 Tang KH, L. S., Khodadadi-Jamayran A, Jen J, Han H, Guidry K, Chen T, Hao Y, Fedele C, Zebala JA, Maeda DY, Christensen JG, Olson P, Athanas A, Loomis CA, Tsirigos A, Wong KK, Neel BG. Combined Inhibition of SHP2 and CXCR1/2 Promotes Antitumor T-cell Response in NSCLC. *Cancer Discov* **12**, 47-61 (2022). https://doi.org:10.1158/2159-8290.CD-21-0369

290 Liu, Q., Qu, J., Zhao, M., Xu, Q. & Sun, Y. Targeting SHP2 as a promising strategy for cancer immunotherapy. *Pharmacol Res* **152**, 104595 (2020). https://doi.org:10.1016/j.phrs.2019.104595

291 Pardoll, D. M. The blockade of immune checkpoints in cancer immunotherapy. *Nat Rev Cancer* **12**, 252-264 (2012). https://doi.org:10.1038/nrc3239

292 Weinreb, C., Rodriguez-Fraticelli, A., Camargo, F. D. & Klein, A. M. Lineage tracing on transcriptional landscapes links state to fate during differentiation. *Science* **367** (2020). https://doi.org:10.1126/science.aaw3381

293 Day, C. P., Carter, J., Bonomi, C., Esposito, D., Crise, B., Ortiz-Conde, B., Hollingshead, M., Merlino, G. Lentivirus-mediated bifunctional cell labeling for in vivo melanoma study. *Pigment Cell Melanoma Res* **22**, 283-295 (2009). https://doi.org:10.1111/j.1755-148X.2009.00545.x

294 Jesse Boumelha, S. d. C. T., Emily K. Law, Pablo Romero-Clavijo, Matthew A. Coelho, Kevin Ng, Edurne Mugarza, Christopher Moore, Sareena Rana, Deborah R. Caswell, Miguel Murillo, David C. Hancock, Prokopios P. Argyris, William L. Brown, Cameron Durfee, Lindsay K. Larson, Rachel I. Vogel, Alejandro Suárez Bonnet, Simon L. Priestnall, Philip East, Sarah J. Ross, George Kassiotis, Miriam Molina-Arcas, Charles Swanton, Reuben Harris,

Julian Downward. An immunogenic model of KRAS-mutant lung cancer for study of targeted therapy and immunotherapy combinations. *bioRxiv preprint* (2022). https://doi.org:10.1101/2020.12.22.423126

295 Day, C. P., Carter, J., Weaver Ohler, Z., Bonomi, C., El Meskini, R., Martin, P., Graff-Cherry, C., Feigenbaum, L., Tuting, T., Van Dyke, T., Hollingshead, M., Merlino, G. "Glowing head" mice: a genetic tool enabling reliable preclinical image-based evaluation of cancers in immunocompetent allografts. *PLoS One* **9**, e109956 (2014). https://doi.org:10.1371/journal.pone.0109956

296 Zaw Thin, M., Moore, C., Snoeks, T., Kalber, T., Downward, J., Behrens, A. Micro-CT acquisition and image processing to track and characterize pulmonary nodules in mice. *Nat Protoc* (2022). https://doi.org:10.1038/s41596-022-00769-5

297 Andersson, G., Denaro, M., Johnson, K., Morgan, P., Sullivan, A., Houser, S., Patience, C., White-Scharf, M. E., Down, J. D. Engraftment of retroviral EGFP-transduced bone marrow in mice prevents rejection of EGFP-transgenic skin grafts. *Mol Ther* **8**, 385-391 (2003). https://doi.org:10.1016/s1525-0016(03)00210-7

298 Day, R. N. & Davidson, M. W. The fluorescent protein palette: tools for cellular imaging. *Chem Soc Rev* **38**, 2887-2921 (2009). https://doi.org:10.1039/b901966a

299 Boedtkjer, E. & Pedersen, S. F. The Acidic Tumor Microenvironment as a Driver of Cancer. *Annu Rev Physiol* **82**, 103-126 (2020). https://doi.org:10.1146/annurev-physiol-021119-034627

300 Haas, L. *et al.* Acquired resistance to anti-MAPK targeted therapy confers an immune-evasive tumor microenvironment and cross-resistance to immunotherapy in melanoma. *Nat Cancer* **2**, 693-708 (2021). https://doi.org:10.1038/s43018-021-00221-9

301 Begum, P., Goldin, R. D., Possamai, L. A. & Popat, S. Severe Immune Checkpoint Inhibitor Hepatitis in KRAS G12C-Mutant NSCLC Potentially Triggered by Sotorasib: Case Report. *JTO Clin Res Rep* **2**, 100213 (2021). https://doi.org:10.1016/j.jtocrr.2021.100213

302 Toita, R., Kawano, T., Fujita, S., Murata, M. & Kang, J. H. Increased hepatic inflammation in a normal-weight mouse after long-term high-fat diet feeding. *J Toxicol Pathol* **31**, 43-47 (2018). https://doi.org:10.1293/tox.2017-0038

303 Harshil Patel, P. E., Jonathan Manning, Maxime U Garcia, Alexander Peltzer, Rickard Hammarén, Olga Botvinnik, Adam Talbot, Gregor Sturm, nf-core bot, Matthias Zepper, Denis Moreno, Pranathi Vemuri, Mahesh Binzer-Panchal, silviamorins, Lorena Pantano, Robert Syme, Gavin Kelly, Friederike Hanssen, … Christian Mertes. nf-core/rnaseq: nf-core/rnaseq v3.15.0 - Aluminium Axolotl. *Zenodo* **Version 3.15.0** (2024). https://doi.org:10.5281/zenodo.13691888

304 Love, M. I., Huber, W. & Anders, S. Moderated estimation of fold change and dispersion for RNA-seq data with DESeq2. *Genome Biol* **15**, 550 (2014). https://doi.org:10.1186/s13059-014-0550-8

305 Lee, D. Y. *et al.* Review of the Current Research on Fetal Bovine Serum and the Development of Cultured Meat. *Food Sci Anim Resour* **42**, 775-799 (2022). https://doi.org:10.5851/kosfa.2022.e46

306 Au-Yeung, N., Mandhana, R. & Horvath, C. M. Transcriptional regulation by STAT1 and STAT2 in the interferon JAK-STAT pathway. *JAKSTAT* **2**, e23931 (2013). https://doi.org:10.4161/jkst.23931

307 Yanai, H., Negishi, H. & Taniguchi, T. The IRF family of transcription factors: Inception, impact and implications in oncogenesis. *Oncoimmunology* **1**, 1376-1386 (2012). https://doi.org:10.4161/onci.22475

308 Quatrini, L. *et al.* The Immune Checkpoint PD-1 in Natural Killer Cells: Expression, Function and Targeting in Tumour Immunotherapy. *Cancers (Basel)* **12** (2020). https://doi.org:10.3390/cancers12113285

309 Lu, D. *et al.* Beyond T Cells: Understanding the Role of PD-1/PD-L1 in Tumor-Associated Macrophages. *J Immunol Res* **2019**, 1919082 (2019). https://doi.org:10.1155/2019/1919082

310 Gordon, S. R. *et al.* PD-1 expression by tumour-associated macrophages inhibits phagocytosis and tumour immunity. *Nature* **545**, 495-499 (2017). https://doi.org:10.1038/nature22396

311 Gide, T. N. *et al.* Distinct Immune Cell Populations Define Response to Anti-PD-1 Monotherapy and Anti-PD-1/Anti-CTLA-4 Combined Therapy. *Cancer Cell* **35**, 238-255 e236 (2019). https://doi.org:10.1016/j.ccell.2019.01.003

312 Ohaegbulam, K. C., Assal, A., Lazar-Molnar, E., Yao, Y. and Zang, X. Human cancer immunotherapy with antibodies to the PD-1 and PD-L1 pathway. *Trends in molecular medicine* **21**, 24-33 (2015). https://doi.org:10.1016/j.molmed.2014.10.009

313 Salmaninejad, A. *et al.* PD-1/PD-L1 pathway: Basic biology and role in cancer immunotherapy. *J Cell Physiol* **234**, 16824-16837 (2019). https://doi.org:10.1002/jcp.28358

314 Schad, S. E. *et al.* Tumor-induced double positive T cells display distinct lineage commitment mechanisms and functions. *J Exp Med* **219** (2022). https://doi.org:10.1084/jem.20212169

315 Desfrancois, J. *et al.* Double positive CD4CD8 alphabeta T cells: a new tumor-reactive population in human melanomas. *PLoS One* **5**, e8437 (2010). https://doi.org:10.1371/journal.pone.0008437

316 Blank, C. U. *et al.* Defining 'T cell exhaustion'. *Nat Rev Immunol* **19**, 665-674 (2019). https://doi.org:10.1038/s41577-019-0221-9

317 Catakovic, K., Klieser, E., Neureiter, D. & Geisberger, R. T cell exhaustion: from pathophysiological basics to tumor immunotherapy. *Cell Commun Signal* **15**, 1 (2017). https://doi.org:10.1186/s12964-016-0160-z

318 Parham, P. The Immune System. *Norton & Co* **Fifth International Student edition** (2021).

319 Calame, K. L., Lin, K. I. & Tunyaplin, C. Regulatory mechanisms that determine the development and function of plasma cells. *Annu Rev Immunol* **21**, 205-230 (2003). https://doi.org:10.1146/annurev.immunol.21.120601.141138

320 Belgiu, M. & Drăguţ, L. Random forest in remote sensing: A review of applications and future directions. *ISPRS Journal of Photogrammetry and Remote Sensing* **114**, 24-31 (2016). https://doi.org:10.1016/j.isprsjprs.2016.01.011

321 Jackson, H. W. *et al.* The single-cell pathology landscape of breast cancer. *Nature* **578**, 615-620 (2020). https://doi.org:10.1038/s41586-019-1876-x

322 Candice A. Grzelak, E. T. G., Emma E. Lederer, Kamya Rajaram, Jinxiang Dai, Ryann E. Shor, Andrea R. Lim, Jeanna Kim, Slobodan Beronja, Alister P.W. Funnell, and Cyrus M. Ghajar. Elimination of fluorescent protein immunogenicity permits modeling of metastasis in immune-competent settings. *Cancer Cell* **40** (2022). https://doi.org:10.1016/j.ccell.2021.11.004

323 Yoon, D. Y. *et al.* Sex bias exists in basic science and translational surgical research. *Surgery* **156**, 508-516 (2014). https://doi.org:10.1016/j.surg.2014.07.001

324 Beery, A. K. & Zucker, I. Sex bias in neuroscience and biomedical research. *Neurosci Biobehav Rev* **35**, 565-572 (2011). https://doi.org:10.1016/j.neubiorev.2010.07.002

325 Nunamaker, E. A. & Turner, P. V. Unmasking the Adverse Impacts of Sex Bias on Science and Research Animal Welfare. *Animals (Basel)* **13** (2023). https://doi.org:10.3390/ani13172792

326 Karp, N. A. & Reavey, N. Sex bias in preclinical research and an exploration of how to change the status quo. *Br J Pharmacol* **176**, 4107-4118 (2019). https://doi.org:10.1111/bph.14539

327 Skoulidis F, G. M., Greenawalt DM, Hellmann MD, Awad MM, Gainor JF, Schrock AB, Hartmaier RJ, Trabucco SE, Gay L, Ali SM, Elvin JA, Singal G, Ross JS, Fabrizio D, Szabo PM, Chang H, Sasson A, Srinivasan S, Kirov S, Szustakowski J, Vitazka P, Edwards R, Bufill JA, Sharma N, Ou SI, Peled N, Spigel DR, Rizvi H, Aguilar EJ, Carter BW, Erasmus J, Halpenny DF, Plodkowski AJ, Long NM, Nishino M, Denning WL, Galan-Cobo A, Hamdi H, Hirz T, Tong P, Wang J, Rodriguez-Canales J, Villalobos PA, Parra ER, Kalhor N, Sholl LM, Sauter JL, Jungbluth AA, Mino-Kenudson M, Azimi R, Elamin YY, Zhang J, Leonardi GC, Jiang F, Wong KK, Lee JJ, Papadimitrakopoulou VA, Wistuba II, Miller VA, Frampton GM, Wolchok JD, Shaw AT, Jänne PA, Stephens PJ, Rudin CM, Geese WJ, Albacker LA, Heymach JV. STK11/LKB1 Mutations and PD-1 Inhibitor Resistance in KRAS-Mutant Lung Adenocarcinoma. *Cancer Discov* **8**, 822-835 (2018). https://doi.org:10.1158/2159-8290.CD-18-0099

328 Arbour, K. C. *et al.* Effects of Co-occurring Genomic Alterations on Outcomes in Patients with KRAS-Mutant Non-Small Cell Lung Cancer. *Clin Cancer Res* **24**, 334-340 (2018). https://doi.org:10.1158/1078-0432.CCR-17-1841

329 Sacher, A. *et al.* Single-Agent Divarasib (GDC-6036) in Solid Tumors with a KRAS G12C Mutation. *N Engl J Med* **389**, 710-721 (2023). https://doi.org:10.1056/NEJMoa2303810

330 Li, B. T., Falchook, G. S., Durm, G. A., Burns, T. F., Skoulidis, F., Ramalingam, S. S., Spira, A., Bestvina, C. M., Goldberg, S. B., Veluswamy, R., Iams, W. T., Chiappori, A. A., Lemech, C. R., Meloni, A. R.. Ebiana, V., Dai, T., Gauto, D. M., Varrieur, T. L., Snyder, W. J., Govindan, R. CodeBreaK 100/101: First Report of Safety/Efficacy of Sotorasib in Combination with Pembrolizumab or Atezolizumab in Advanced KRAS p.G12C NSCLC. *Journal of Thoracic Oncology* **17**, S10-S11 (2022). https://doi.org:10.1016/j.jtho.2022.07.025

331 Chour, A. *et al.* Brief Report: Severe Sotorasib-Related Hepatotoxicity and Non-Liver Adverse Events Associated With Sequential Anti-Programmed Cell Death (Ligand)1 and Sotorasib Therapy in KRAS(G12C)-Mutant Lung Cancer. *J Thorac Oncol* **18**, 1408-1415 (2023). https://doi.org:10.1016/j.jtho.2023.05.013

332 Wang, Y. *et al.* Global profiling of AMG510 modified proteins identified tumor suppressor KEAP1 as an off-target. *iScience* **26**, 106080 (2023). https://doi.org:10.1016/j.isci.2023.106080

333 Moran-McCabe, K. & Burris, S. Eviction and the Necessary Conditions for Health. *N Engl J Med* **385**, 1443-1445 (2021). https://doi.org:10.1056/NEJMp2031947

334 Mirat Shah, M. D., Atiqur Rahman, Ph.D., Marc R. Theoret, M.D., and Richard Pazdur, M.D. The Drug-Dosing Conundrum in Oncology — When Less Is More. *N Engl J Med* **385**, 1445-1447 (2021). https://doi.org:10.1056/NEJMp2109826

335 O'Leary, C. *et al.* Targeted Therapies for Kirsten Rat Sarcoma (KRAS) G12C Mutant Metastatic Non-Small-Cell Lung Cancers. *Cancers (Basel)* **15** (2023). https://doi.org:10.3390/cancers15235582

336 Samuel G. Rodriques, R. R. S., Aleksandrina Goeva, Carly A. Martin, Evan Murray, Charles R. Vanderburg, Joshua Welch, Linlin M. Chen, Fei Chen, Evan Z. Macosko. Slide-seq: A scalable technology for measuring genome-wide

expression at high spatial resolution. *Science*, 1463–1467 (2019). https://doi.org:10.1126/science.aaw1219

337 Subcellular characterization of over 100 proteins in FFPE tumor biopsies with CosMx Spatial Molecular Imager. *Cancer Res* **82**, Abstract 3878 (2022). https://doi.org:10.1158/1538-7445.AM2022-3878

338 Ali, H. R. *et al.* Imaging mass cytometry and multiplatform genomics define the phenogenomic landscape of breast cancer. *Nature Cancer* **1**, 163-175 (2020).

339 Devon R. Blake, A. V. V., Richard G. Hodge, McKenzie P. Kline, Thomas S. K. Gilbert, Vikas Tyagi, Daowei Huang, Gabrielle C. Whiten, Jacob E. Larson, Xiaodong Wang, Kenneth H. Pearce, Laura E. Herring, Lee M. Graves, Stephen V. Frye, Michael J. Emanuele, Adrienne D. Cox, Channing J. Der. Application of a MYC degradation screen identifies sensitivity to CDK9 inhibitors in KRAS-mutant pancreatic cancer. *Science Signalling* **12** (2019). https://doi.org:10.1126/scisignal.aav7259

340 Vaseva, A. V. *et al.* KRAS Suppression-Induced Degradation of MYC Is Antagonized by a MEK5-ERK5 Compensatory Mechanism. *Cancer Cell* **34**, 807-822 e807 (2018). https://doi.org:10.1016/j.ccell.2018.10.001

341 Bolotin, D. A. *et al.* Next generation sequencing for TCR repertoire profiling: platform-specific features and correction algorithms. *Eur J Immunol* **42**, 3073-3083 (2012). https://doi.org:10.1002/eji.201242517

342 Pai, J. A. & Satpathy, A. T. High-throughput and single-cell T cell receptor sequencing technologies. *Nat Methods* **18**, 881-892 (2021). https://doi.org:10.1038/s41592-021-01201-8

343 Liu, S. *et al.* Spatial maps of T cell receptors and transcriptomes reveal distinct immune niches and interactions in the adaptive immune response. *Immunity* **55**, 1940-1952 e1945 (2022). https://doi.org:10.1016/j.immuni.2022.09.002

344 Clarke, S. R. *et al.* Characterization of the ovalbumin-specific TCR transgenic line OT-I: MHC elements for positive and negative selection. *Immunol Cell Biol* **78**, 110-117 (2000). https://doi.org:10.1046/j.1440-1711.2000.00889.x

345 Miyagawa, F., Gutermuth, J., Zhang, H. & Katz, S. I. The use of mouse models to better understand mechanisms of autoimmunity and tolerance. *J Autoimmun* **35**, 192-198 (2010). https://doi.org:10.1016/j.jaut.2010.06.007

346 Kalyuzhny, A. E. Handbook of ELISPOT, Chemistry and Biology of the ELISPOT Assay. *Humana Press* **302** (2005). https://doi.org:10.1385/1-59259-903-6:015

347 Slota, M., Lim, J. B., Dang, Y. & Disis, M. L. ELISpot for measuring human immune responses to vaccines. *Expert Rev Vaccines* **10**, 299-306 (2011). https://doi.org:10.1586/erv.10.169

348 Epand, R. M. *et al.* Diacylglycerol Kinase-epsilon: Properties and Biological Roles. *Front Cell Dev Biol* **4**, 112 (2016). https://doi.org:10.3389/fcell.2016.00112

349 Riese, M. J., Moon, E. K., Johnson, B. D. & Albelda, S. M. Diacylglycerol Kinases (DGKs): Novel Targets for Improving T Cell Activity in Cancer. *Front Cell Dev Biol* **4**, 108 (2016). https://doi.org:10.3389/fcell.2016.00108

350 Singh, B. K. & Kambayashi, T. The Immunomodulatory Functions of Diacylglycerol Kinase zeta. *Front Cell Dev Biol* **4**, 96 (2016). https://doi.org:10.3389/fcell.2016.00096

351 Hattori, T. *et al.* Creating MHC-Restricted Neoantigens with Covalent Inhibitors That Can Be Targeted by Immune Therapy. *Cancer Discov* **13**, 132-145 (2023). https://doi.org:10.1158/2159-8290.CD-22-1074

352 Zhang, Z. *et al.* A covalent inhibitor of K-Ras(G12C) induces MHC class I presentation of haptenated peptide neoepitopes targetable by immunotherapy.

Cancer Cell **40**, 1060-1069 e1067 (2022). https://doi.org:10.1016/j.ccell.2022.07.005

353 Zelenay, S. *et al.* Cyclooxygenase-Dependent Tumor Growth through Evasion of Immunity. *Cell* **162**, 1257-1270 (2015). https://doi.org:10.1016/j.cell.2015.08.015

354 Liu, B., Qu, L. & Yan, S. Cyclooxygenase-2 promotes tumor growth and suppresses tumor immunity. *Cancer Cell Int* **15**, 106 (2015). https://doi.org:10.1186/s12935-015-0260-7

355 Asimgil, H. *et al.* Targeting the undruggable oncogenic KRAS: the dawn of hope. *JCI Insight* **7** (2022). https://doi.org:10.1172/jci.insight.153688

356 Zhang, Y., Ma, J. A., Zhang, H. X., Jiang, Y. N., & Luo, W. H. Cancer vaccines: Targeting KRAS-driven cancers. *Expert Review of Vaccines* **19**, 163–173 (2020). https://doi.org:10.1080/14760584.2020.1733420

357 Wang, S. H., Cao, Z., Farazuddin, M., Chen, J., Janczak, K. W., Tang, S., Cannon, J., Baker, J. R., Jr. A novel intranasal peptide vaccine inhibits non-small cell lung cancer with KRAS mutation. *Cancer Gene Ther* **31**, 464-471 (2024). https://doi.org:10.1038/s41417-023-00717-9

358 Ramalingam, P. S. & Arumugam, S. Reverse vaccinology and immunoinformatics approaches to design multi-epitope based vaccine against oncogenic KRAS. *Med Oncol* **40**, 283 (2023). https://doi.org:10.1007/s12032-023-02160-0

359 Rojas, L. A. *et al.* Personalized RNA neoantigen vaccines stimulate T cells in pancreatic cancer. *Nature* **618**, 144-150 (2023). https://doi.org:10.1038/s41586-023-06063-y

360 Mugarza, E. *et al.* Therapeutic KRASG12C inhibition drives effective interferonmediated anti-tumour immunity in immunogenic lung cancers. *bioRxiv preprint* (2021). https://doi.org:10.1101/2021.10.18.464819

361 Mills, G. B. & Labrie, M. Enhancing anticancer activity of macrophages through rational drug combinations. *J Clin Invest* **134** (2024). https://doi.org:10.1172/JCI180512

362 Advani, R. *et al.* CD47 Blockade by Hu5F9-G4 and Rituximab in Non-Hodgkin's Lymphoma. *N Engl J Med* **379**, 1711-1721 (2018). https://doi.org:10.1056/NEJMoa1807315

363 Kyle Vaccaro, J. A., Troy W. Whitfield, Asaf Maoz, Sarah Reeves, José Velarde, Dian Yang, Nicole Phan, George W. Bell, Aaron N. Hata, and Kipp Weiskopf1. Targeted therapies prime oncogene-driven lung cancers for macrophage-mediated destruction. *bioRxiv* (2023). https://doi.org:10.1101/2023.03.03.531059

364 Galani, I. E., Triantafyllia, V., Eleminiadou, E. E. & Andreakos, E. Protocol for influenza A virus infection of mice and viral load determination. *STAR Protoc* **3**, 101151 (2022). https://doi.org:10.1016/j.xpro.2022.101151

365 Grit S. Herter-Sprie Houari Korideck, C. L. C., Jan M. Herter, Kevin Rhee, Ross I. Berbeco, David G. Bennett,w, Esra A. Akbay, David Kozono, Raymond H. Mak, G. Mike Makrigiorgos, Alec C. Kimmelman & Kwok-Kin Wong. Image-guided radiotherapy platform using single nodule conditional lung cancer mouse models. *Nature Communications* (2014). https://doi.org:10.1038/ncomms6870

366 Tsukasa Ishiwata, T. S., Alexander Gregor, Masato Aragaki, Yamato Motooka, Tomonari Kinoshita, Terunaga Inage, Nicholas Bernards, Hideki Ujiie1, Zhenchian Chen, Andrew Effat, Juan Chen, Gang Zheng4,5,6,7, Koichiro Tatsumi, Kazuhiro Yasufuku. A preclinical research platform to evaluate photosensitizers for transbronchial localization and phototherapy of lung cancer

using an orthotopic mouse model. *Translational Lung Cancer Research* **10**, 243-251 (2021). https://doi.org:10.21037/tlcr-20-813

367 Jeffrey J. Quinn, M. G. J., Ross A. Okimoto, Shigeki Nanjo, Michelle M. Chan, Nir Yosef, Trever G. Bivona, Jonathan S. Weissman. Single-cell lineages reveal the rates, routes, and drivers of metastasis in cancer xenografts. *Science*, Page numbers not final at time of first release (2021). https://doi.org:10.1126/science.abc1944

368 Sharma, P., Allison, J. P. Immune checkpoint targeting in cancer therapy: toward combination strategies with curative potential. *Cell* **161**, 205-214 (2015). https://doi.org:10.1016/j.cell.2015.03.030

369 Alesha A Thai, P. B. J. S., Prof Lecia V Sequist, Justin F Gainor, Rebecca S Heist. Lung cancer. *The Lancet* **398**, P535-554 (2021). https://doi.org:10.1016/S0140-6736(21)00312-3